Appendix B - Extracts from *Lamb et al*

Examples of disorders that may be treated include ... ***autoimmune diseases***. The spectrum of autoimmune disorders ranges from ***organ specific diseases*** (such as ***thyroiditis, insulitis, multiple sclerosis,iridocyclitis, uveitis, orchitis, hepatitis, Addison's disease, myasthenia gravis***) to ***systemic illnesses*** such as ***rheumatoid arthritis*** or ***lupus erythematosus***. Other disorders include *immune hyperreactivity*, such as ***allergic reactions***.

...Organ-specific autoimmune diseases include ***multiple sclerosis, insulin dependent diabetes mellitus, several forms of anemia (aplastic, hemolytic), autoimmune hepatitis. thyroiditis, insulitis,iridocyclitis, skleritis, uveitis, orchitis, myasthenia gravis, ...***

Systemic autoimmune diseases include: ... ***scleroderma and systemic sclerosis, sjogren's syndrom, undifferentiated connective tissue syndrome, antiphospholipid syndrome, different forms of vasculitis(polyarteritis nodosa, allergic granulomatosis andangiitis. Wegner's granulomatosis, Kawasaki disease, hypersensitivity vasculitis,Henoch-Schoenlein purpura. Behcet's Syndrome, Takayasuarteritis, Giant cell arteritis,Thrombangiitis obliterans)***, ...

A more extensive list of disorders includes: ... ***allergic reactions, asthma, ... collagen diseases ... reperfusion injury, cardiac arrest, ... vascular inflammatory disorders, ... other cardiopulmonary diseases, inflammation associated with peptic ulcer, ... other diseases of the gastrointestinal tract, ... other hepatic diseases, ... other glandular diseases, ... other renal and urologic diseases, ... other oto-rhino-laryngological diseases, ... other dermal diseases, ... other dental diseases, orchitis or epididimo-orchitis, infertility, orchidal trauma*** or ***other immunerelated testicular diseases, placental dysfunction, placental insufficiency, habitualabortion. eclampsia, pre-eclampsia ... optic neuritis, ... retinitis*** or ***cystoid macular oedema, sympathetic ophthalmia, ... acute ischaemic optic neuropathy, ... Parkinson's disease, complication and/or side effects from treatment of Parkinson's disease, AIDS-related dementia complex HIV-related encephalopathy, Devic's disease, Sydenham chorea, Alzheimer's disease*** and ***other degenerative diseases, conditions or disorders of the CNS,... myelitis, encephalitis, subacute sclerosing pan-encephalitis, encephalomyelitis, acute neuropathy, subacute neuropathy, chronic neuropathy, Guillaim-Barre syndrome, Sydenham chora, myasthenia gravis, pseudo-tumourcerebri, Down's Syndrome, Huntington's disease, amyotrophic lateral sclerosis, inflammatory components of CNS compression or CNS trauma or infections of the CNS, inflammatory components of muscular atrophies and dystrophies, ... septic shock, infectious diseases, inflammatory complications or side effects of surgery ... side effects of gene therapy, ...***

Volume 47(9): 1101–1109, 1999
The Journal of Histochemistry & Cytochemistry
http://www.jhc.org

REVIEW

Cytochemical Methods for the Detection of Apoptosis

Mark C. Willingham

Department of Pathology, Wake Forest University School of Medicine, Winston–Salem, North Carolina

KEY WORDS
apoptosis
TUNEL
ISNT
ISEL
cell death
caspases
blebbing
annexin V
in situ end-labeling
mitochondria
time-lapse microscopy
DNA cytochemistry
DNA fragmentation

SUMMARY Detection of apoptotic cell death in cells and tissues has become of paramount importance in many fields of modern biology, including studies of embryonic development, degenerative disease, and cancer biology. In addition to methods that employ biochemical analysis of large populations of cells, cytochemical methods have recently been extensively used both in individual cells and in tissues. Most of these methods exploit properties of dying cells that are more or less specific for the apoptotic process. However, considerable confusion exists over the interpretation of some of these methods and their usefulness in all settings. This review attempts to summarize the more recent advances in cytochemical detection of apoptosis and emphasizes some of the pitfalls that confuse the interpretation of results of these methods. (J Histochem Cytochem 47:1101–1109, 1999)

THE FIELD OF CELL DEATH RESEARCH has undergone an explosion of new knowledge over the past decade. The realization that programmed cell death operates by highly conserved ubiquitous mechanisms in cells, and that these events are pivotal in most important pathologic processes, has focused interest on cell death research. The need for histochemical and cytochemical methods to evaluate death of cells, especially in intact tissues, has led to the development of several techniques. These methods are now used extensively in the study of a wide variety of diseases and in the study of physiology and development. However, the interpretation and accuracy of these methods are not always clear. This topic has been comprehensively reviewed previously and the difficulties in interpretation of apoptosis have been highlighted (Wyllie et al. 1981; Wyllie 1992; Allen et al. 1997; Sanders 1997; Darzynkiewicz et al. 1998; Zhu and Chun 1998). This review attempts to build on these prior reviews by summarizing the methods that are currently available for in situ detection of cell death in light of more recent biochemical and morphological mechanisms, and to evaluate their accuracy and potential interpretation.

Cell Death

Cells can die by either of two major mechanisms: necrosis or apoptosis. Necrosis is the death of cells through external damage, usually mediated via destruction of the plasma membrane or the biochemical supports of its integrity. Such a death is analogous to "cell murder." The necrotic cell exhibits a swollen morphology and the plasma membrane lyses, releasing cytoplasmic components into the surrounding tissue spaces. This release of necrotic debris attracts inflammatory cells, leading to the tissue destruction characteristic of inflammation. The death of single cells by this mechanism might be resolvable in some tissues, but a large number of cells dying by necrosis usually results in inflammation and subsequent repair and scarring, leading to compromise and permanent alteration of tissue architecture. Necrosis can occur in a matter of seconds (Collins et al. 1997).

The other major form of cell death is based on the concept of programmed cell death. Programmed cell death is a paradigm in which cells contain a geneti-

Correspondence to: Dr. Mark Willingham, Dept. of Pathology, Medical Center Boulevard, Winston-Salem, NC 27157-1072.

Received for publication April 7, 1999; accepted April 23, 1999 (9R4940).

© The Histochemical Society, Inc.

0022-1554/99/$3.30

cally coded program of elements that lead to the death of cells. The biochemical and morphological events that effect this death usually lead to a unique and highly controlled series of events. The terminal events of this process are termed apoptosis (Kerr et al. 1972) [although it has been previously pointed out that some programmed cell death may not involve the mechanisms of apoptosis (reviewed by Sanders 1997)]. Apoptosis is a much slower series of events than necrosis, requiring from a few hours to several days, depending on the initiator. This form of cell death is more analogous to "cell suicide," in which death is the consequence of molecular signals contained within individual cells. The importance of this suicide mechanism was first delineated in studies of embryonic development. Subsequent studies have focused attention on apoptosis, however, in that the apoptotic mechanism is widely employed in tissue homeostasis and forms a major component of many pathological processes, from the response of cancer cells to chemoradiotherapy to the death of cells in neurodegenerative diseases. Although the genetically programmed nature of this pathway was emphasized by its role in development, the same terminal mechanisms become a permanent part of the cell machinery and can be activated by extrinsic signals that require no new gene expression. Therefore, most cells possess a preordained mechanism of death that awaits an appropriate trigger. The mechanics of this death are essentially the same, whether induced by new genetic signals or induced through external initiators. The manifestations of apoptosis, both biochemical and morphological, are unique and are completely different from those of necrosis.

The terminal events of apoptosis involve the activation of a specific series of cytoplasmic proteases, termed caspases. The activation of these self-catalytic caspases in the cytoplasm is tightly regulated. The initiators of apoptosis that set off this cascade of events leading to caspase activation are multiple, and two major pathways of initiation of this terminal pathway have been identified. One pathway involves so-called death receptors at the cell surface, a pathway that can directly activate upstream caspases in the cytoplasm. Another pathway involves the participation of mitochondria through the induction of leakiness of the external mitochondrial membrane, leading to the release of cytochrome c into the cytosol. These two pathways also intersect, in that the death receptor pathway can be amplified through mitochondrial damage. Downstream from these initiator mechanisms are terminal caspases that lead to the morphological and biochemical consequences of apoptosis.

The historical recognition that apoptotic cell death was a unique series of events was initially based on morphological evidence of changes in cell structures, especially the segmentation of nuclei. Other studies have shown that cells in tissue culture usually go through a unique series of surface morphological changes (e.g., Collins et al. 1997), as shown in Figure 1. Although the specific timing and the shape changes in cells vary from cell type to cell type, the overriding message that has evolved over the past decade is that apoptosis is a reflection of an extremely highly conserved mechanism that shows remarkable uniformity through a long evolution. This conclusion has allowed extrapolation from one species and one system to others, and from cell culture to intact tissue. The final mechanics of the apoptotic events are common but the initiating pathways into apoptosis are myriad and complex. In a sense, this makes the task of identifying apoptotic changes easier because they result in a common effector pathway, but the context in which they occur has to be interpreted with caution. Table 1 summarizes features of the apoptotic process that have been exploited for detection in individual cells, in mass cell cultures, and in tissues.

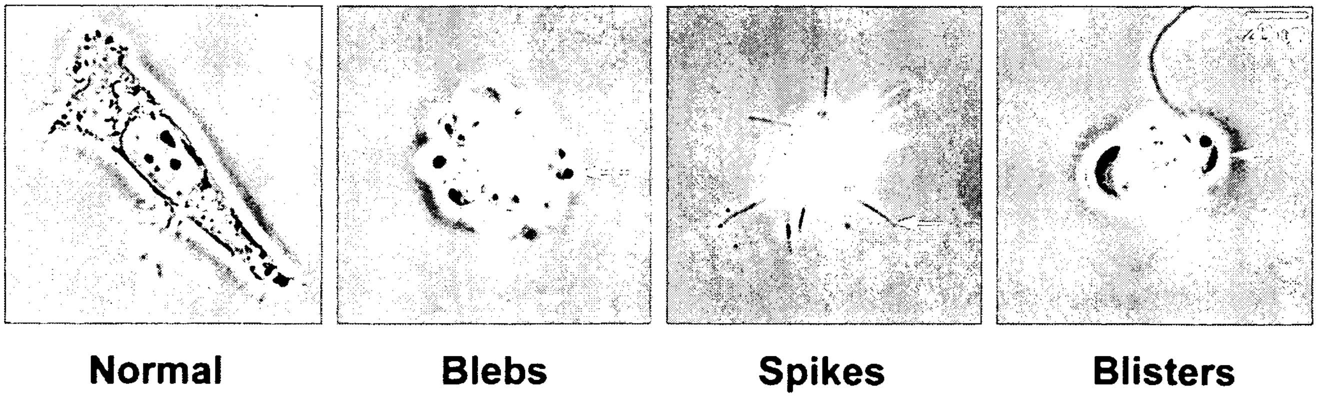

Figure 1 Surface morphological features of apoptotic cells in culture. These images demonstrate the hallmark sequential features (arrows) of apoptotic cells detected by phase-contrast microscopy, including blebs, echinoid spikes, and surface blisters. These images were generated using KB human carcinoma cells induced to go into apoptosis using ricin (Collins et al. 1997).

Table 1 Categories of cellular changes that form the basis of apoptosis assays

- Surface morphology and composition
  - Time-lapse surface morphology
  - Membrane permeability: impermeable dyes (PI), permeable DNA stains (DAPI, Hoechst)
  - Phospholipid externalization (Annexin V binding)
- Nuclear events and DNA cleavage
  - Nuclear morphology: segmentation of chromatin and nuclei
  - DNA cleavage by gels; large fragments and internucleosomal cleavage
  - DNA cleavage in situ; detection of strand breaks
    - In situ nick-translation (ISNT)
    - TUNEL (terminal transferase)
    - Anti-single-stranded DNA antibody
    - Hairpin oligos (double-stranded breaks)
- Cell dissolution (pre-GI peak) (apoptotic bodies containing DNA)
- Cytoplasmic biochemical activation events
  - Caspace cleavage products
  - Caspace activity (caged fluorophores, FRET)
  - PARP activity
  - Transglutaminase activity
  - Death antigens
- Mitochondrial function and integrity
  - Permeability transition (vital dyes)
  - Mitochondrial antigens (accessibility)
  - Metabolic activity
  - Cytochrome c release and alterations

Detection Methods in Individual Cells and in Tissues

Much of the knowledge about apoptosis mechanisms has derived from observations of isolated cells, such as tissue culture systems. However, the properties revealed in these assays are not always applicable to the study of intact tissues. For example, assays such as the binding of annexin V or the impermeability of propidium iodide depend on the ability to incubate intact impermeable cells with the reagent, a process not possible in fixed tissue sections. Assays based on the size of isolated cell fragments are not applicable to fixed tissue. The kinetic context related to the synchrony of apoptosis, the length of time necessary for the initiating event to lead to the changes that occur, and the removal of apoptotic cells in vivo through phagocytosis often make the assays of apoptosis that are useful in tissue culture less applicable to intact tissues. Furthermore, events that occur in individual cells can sometimes be implied from assays that are applicable only to the examination of large numbers of cells at one time. An analogy might be the ability to detect the low-level expression of products of specific transfected genes in mass culture through the use of sensitive enzyme assays (e.g., CAT assay) as opposed to the cytochemical identification of high levels of the specific protein product in a small number of individual cells (e.g., a GFP vector). These two approaches can sometimes yield conflicting results, often based on the heterogeneity or lack of synchrony of events in single cells vs the entire population. This has been a major point of confusion in the field of apoptosis.

Apoptosis Is Not Always Synchronous

A major and often unappreciated aspect of apoptotic cell death is that cells within a population may begin apoptosis at very different times after the addition of an initiator, and the length of the various stages of apoptotic morphological change can vary from cell to cell (Collins et al. 1997). For example, for apoptotic systems that depend on cell cycle alterations, the time from initial addition of an agent to the beginning of the first stages of apoptosis can be several days, and the actual completion of apoptosis to the point of cell lysis can require an additional day. The variability introduced can result in a highly asynchronous process. Some assays detect changes that occur early in the process, whereas other assays detect changes that occur only very late. Some changes are not stable and appear at one point in time, only to disappear as apoptosis progresses. Furthermore, the lysis that eventually occurs at the end of apoptosis is essentially the same membrane permeability event that occurs in necrosis, although the specific changes up to that point are very different. These problems point out the need for thoughtful analysis of the kinetics and synchrony within a system and the appropriate choice of assays that can detect those changes accurately.

Surface Morphological and Biochemical Changes

For tissue culture systems, a good point at which to start the analysis of apoptosis is the use of video time-lapse microscopy, a simple and clearly interpretable approach to defining the kinetics of apoptosis in cell culture (Fan et al. 1996; Pulkkinen et al. 1996; Collins et al. 1997). The usual sequence of morphological changes in adherent cultured cells are shown in Figure 1. These include the following: (a) a loss of adhesion to substratum, resulting in cell rounding; (b) a flurry of surface zeiotic blebbing, which may last for only a few hours (Laster and Mackenzie 1996); (c) shrinkage of the cell, with cessation of blebbing and other movements; (d) in some cells, the slow protrusion of elongated "echinoid spikes" from the cell surface (Collins et al. 1997); and (e) after a long delay of several hours, the "blistering" of the cell surface membrane with eventual lysis, similar to necrosis. Even these changes must be interpreted carefully, however, because some initiators (such as staurosporine) have profound effects on the motility mechanisms in cells, suppressing the normally dramatic series of surface morphological changes (Cartee et al. in press). The dynamic nature of the initial rounding and blebbing events makes them easy to spot in time-lapse recordings, and these events are a convenient point at which to designate the beginning of apoptosis. Unfortunately, evaluation of these events in intact tissue is not possible by this method.

Externalization of phosphatidylserine (PS) and phosphatidylethanolamine is a hallmark of the changes in the cell surface during apoptosis (Koopman et al. 1994; Martin et al. 1995; Emoto et al. 1997; Lecoeur et al. 1997; O'Brien et al. 1997; van Engeland et al. 1997). Annexin V binding can be used as a marker of PS externalization, using either microscopy or flow cytometry with fluorescently labeled annexin V (Zhang et al. 1997; van Engeland et al. 1998). These phospholipids are normally sequestered within the cell on the cytoplasmic face of the plasma membrane and other internal membranes. The exact reason for the appearance of PS on the external surface is not clear. In experiments to be presented elsewhere, we have examined this externalization and have found that annexin V binding appears to occur only on a minority of cells (less than one third in our system) during apoptosis. This occurs relatively early, just after the segmentation of nuclei (summarized in Figure 2). Other investigators have found similar labeling of subpopulations with annexin V (Boersma et al. 1996; Ferlini et al. 1997; Gatti et al. 1998). It is not clear why only a minority of cells show PS externalization during apoptosis, or whether they are in some way different from those that do not. However, it has been shown that inhibition of caspase activity also blocks the appearance of PS on the cell surface (Rimon et al. 1997). This suggests that the externalization of PS is caused by the same caspase activities that cause the other manifestations of apoptosis. Care must be exercised with the use of this assay, because the final lysis stage of apoptosis allows access to the PS that is normally inside all cells, creating a highly labeled cell fragment. Such labeling would also be evident in necrotic cells.

The permeability of the plasma membrane is also a central difference between necrosis and apoptosis. Large molecular weight DNA binding dyes, such as propidium iodide (PI), cannot enter intact cells because of their large size and, without permeabilization treatments, do not label apoptotic cells until the final lysis stage. On the other hand, smaller dyes, especially those that can attach to DNA, can label both apoptotic cells and normal cells. Using flow cytometry, one can distinguish apoptotic from necrotic cells as those that show internal DNA labeling with a small dye (such as DAPI, Hoechst 33342 or 33258, or calcein-AM), while not labeling with PI (Bussolati et al. 1995; Gatti et al. 1998). As cells generate apoptotic bodies that release some of their segmented nuclei, the strength of the internal DNA signal decreases, and this can be used as an assay of apoptotic progression. When the cell finally lyses and its membrane becomes permeable, then the larger-sized markers (such as PI) can label any DNA left within the cell. For microscopy, the altered morphology of nuclei selectively labeled with DNA-specific fluorescent dyes, such as DAPI or Hoechst dyes, can be a very easily interpreted assay for apoptosis.

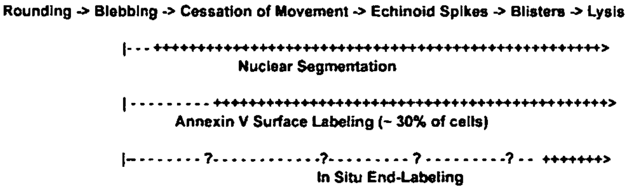
Rounding -> Blebbing -> Cessation of Movement -> Echinoid Spikes -> Blisters -> Lysis
Nuclear Segmentation
Annexin V Surface Labeling (~ 30% of cells)
In Situ End-Labeling

Figure 2 Apoptosis detection by in situ assays in the context of morphological changes. The appearance of positive signals during apoptosis for in situ end-labeling of DNA strand breaks is very dependent on technical details, including fixation conditions and pretreatment procedures. For some studies, positive cells appear early or even before other apoptotic features, whereas in other studies the positive signals occur only late in the process.

Nuclear Morphology Changes and DNA Changes May Not Be the Same

An early observation concerning apoptosis was that cells that entered apoptosis from nonmitotic parts of the cell cycle showed dramatic and characteristic changes in nuclear shape and organization. It is perhaps correct to say that the characteristic change in nuclear morphology is the most accurate indicator of the involvement of apoptosis in the death of a cell. This is true even in the face of the ironic observation that nuclear segmentation is not actually required for other aspects of apoptosis. That is, cells that have been enucleated still undergo the other changes associated with apoptosis (Schulze-Osthoff et al. 1994). This points to the cytoplasmic location of the effector systems of the apoptotic machinery. However, in cells that contain nuclei, the change in nuclear morphology is still an early and relatively unequivocal hallmark of apoptosis. This nuclear shape change occurs at an early point in the series of apoptotic morphological events, usually soon after the beginning of surface blebbing (Collins et al. 1997).

In addition to changes in nuclear morphology, loss of DNA integrity also characterizes apoptosis. It was assumed that these two events were in some way related, as they may be. However, there is no compelling reason necessarily to assume that they are. When DNA extracted from apoptotic cells was analyzed using gel electrophoresis, a characteristic internucleosomal "ladder" of DNA fragments was found. Larger DNA fragments have also been seen at earlier times in apoptotic cell cultures. These gel results have been used as a hallmark of apoptotic detection. However, such analysis requires the extraction of DNA from large numbers of cells. In addition, the apoptosis must be relatively synchronous for this analysis, a synchrony that is not always present. It has not been directly demonstrated that DNA fragments in this way in intact cells. That is, it is possible that the internucleosomal breaks in DNA occur after or during DNA extraction procedures because of the potential fragility of caspase-treated DNA in removing other components of chromatin structure. Furthermore, the detection of strand breaks may be so sensitive that only a small number of apoptotic cells may be needed in a population to produce a detectable signal. That is, the entry of the majority of cells into apoptosis might occur at a much later time point than the first detection of "ladders." Even so, these observations led to the development of in situ assays for the presence of single-strand or double-strand breaks in DNA. The interpretation and application of these methods have been somewhat controversial. Regardless of the specific methods used, the change in nuclear morphology often does not coincide with the appearance of detectable strand breaks in every cell.

The Terminology of DNA and Nuclear Changes in Apoptosis

Although many cytochemical methods are based on the detection of strand breaks or on the appearance of DNA fragments in gel electrophoresis, there is no reason to assume that nuclear morphological changes and detectable DNA strand breaks occur at the same time. As a point of terminology, there has been considerable confusion generated by the term "nuclear fragmentation." This term mixes the concepts of the generation of DNA fragments (DNA fragmentation) with the changes in nuclear shape. A better alternative, which I prefer, is the use of the term "nuclear segmentation." This describes the change in nuclear shape in which the normally round or oval nucleus segments into smaller, compact, homogeneous, variably sized chromatin masses, the characteristic change seen in apoptosis. This term does not imply any generation of DNA fragments or strand breaks but refers only to the shape of the nucleus. Because there is reason to believe that the shape and the DNA breaks may not necessarily be related in each cell, it appears better to use this more precise term to describe shape changes.

When Do DNA Strand Breaks Appear in Situ?

The major methods developed for detection of DNA strand breaks involve the detection of 3′-OH ends of single-stranded DNA (in situ end-labeling; ISEL). Addition of labeled nucleotides to these ends, either using *E. coli* polymerase (or its Klenow fragment) by in situ nick-translation (ISNT) (Figure 3) or using terminal transferase (TUNEL) (Modak and Bollum 1970,1972; Gavrieli et al. 1992; Hall et al. 1994; Tatton et al. 1998), allows the cytochemical demonstration of free DNA strand ends (Ansari et al. 1993; Fujita et al. 1997). Another method for detecting these single strand ends is the use of monoclonal antibody reactive with single-stranded DNA (Naruse et al. 1994; Frankfurt et al. 1996a,b). Such single strand ends are not specific for apoptosis and can also be seen in necrotic cells. Double strand breaks can be detected by other methods, such as the use of hairpin oligos (Didenko et al. 1998). A clear conclusion from the use of such methods, however, is that the preservation methods used to prepare cells can have dramatic effects on detection of strand breaks (Negoescu et al. 1996; Hikim et al. 1997; Labat-Moleur et al. 1998; Tateyama et al. 1998). False-positivity can be generated through nonapoptotic mechanisms (Kockx et al. 1998; Mizoguchi et al. 1998). On the other hand, inaccessibility of sites can prevent the detection of strand breaks (Nakamura et al. 1997). This has led to the use of protease treatment to unmask such inaccessible sites. This is somewhat ironic because the process to be detected is the consequence of endogenous protease activity. It has been suggested that exogenous protease may render sites in apoptotic cells accessible specifically because of the increased fragility of apoptotic DNA that has been affected by activated caspases in the cell. However, the impact of this exogenous protease treatment on the specificity of labeling is not clear. In some cases, methods have been sufficiently sensitive to detect DNA repair mechanisms that are independent of apoptosis. Depending on permeabilization and fixation protocols, some methods detect so-called preapoptotic nuclei in which strand breaks are detected but no nuclear morphological changes have occurred. In other cases, the positive detection of strand breaks does not correlate with individual cells that show nuclear segmentation. In other cases, detection of DNA strand breaks occurs only very late in the process, corresponding to the lytic stage at the end of apoptosis, far removed from the changes in nuclear morphology (Collins et al. 1997). Therefore, although these methods are useful, they are neither theoretically nor practically specific, as yet, for apoptosis. Many authors have pointed out the need for simultaneous interpretation of these in situ methods along with apoptotic nuclear shape changes. The major advantage of these methods, however, is that they are applicable to intact tissue sections directly.

Apoptotic Cells May Not "Live" Long In Vivo

Dying cells in vivo are removed from tissues by phagocytic cells, a process that emphasizes the usefulness of

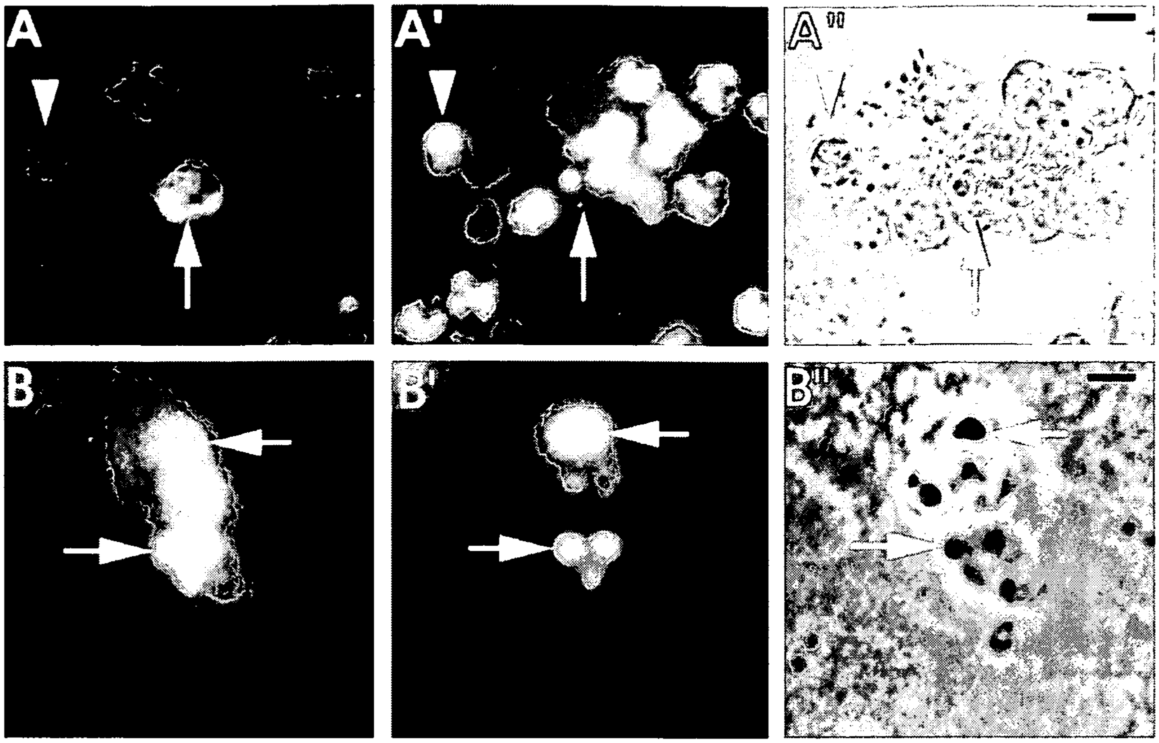

Figure 3 Detection of DNA strand breaks in apoptotic cells using ISNT. KB cells induced to enter apoptosis by ricin treatment were fixed, permeabilized with detergent, and labeled using in situ nick-translation (ISNT) with rhodamine fluorescence detection. Nuclear segments (A,B) demonstrate positive signals (arrows) indicative of DNA fragmentation late in the apoptotic process, whereas earlier nuclear segments show no detectable signal (A, arrowhead). (A,B) ISNT rhodamine; (A',B') DAPI; (A'',B'') phase-contrast. Bars: A'' = 12 μm; B'' = 6 μm.

the apoptotic mechanism for normal tissue remodeling. However, the removal of cells can occur with different efficiencies in different tissues. Massive apoptosis can overwhelm the phagocytic potential of a tissue, and virtually all apoptotic cells will remain for extended periods. In the case of limited apoptosis, however, phagocytic or other adjacent cells may remove the apoptotic remnants as rapidly as they are generated. Unlike cell culture, in which the cell remnants remain undisturbed, in vivo apoptosis may yield only a hint of an occasional cell remnant in a phagocytically active tissue. This problem makes in vivo measurements and interpretation of apoptosis by in situ cytochemical methods extremely difficult.

Other Biochemical Changes

Recent studies have revealed many other steps in the apoptotic machinery inside cells. Among these are the activation of caspases and the cleavage of specific caspase substrates. Incorporation of specific caspase substrates into living cells and the detection of cleavage products (e.g., using fluorescence resonance energy transfer) have been presented as new assays of apoptosis (Xu et al. 1998). Whether or not this will provide better insight into the process at the cytochemical level is not yet clear. My own experience with one of these substrates for caspase 3 (Phiphilux; OncoImmunin, College Park, MD) has been that the signal generated in cells appeared to occur only late in the apoptotic process (results not presented). The other aspect of these assays is that they would probably not be useful for intact tissues.

Methods for detection of activity of endogenous caspase substrates (such as PARP) have also been presented recently (Davis et al. 1998). On the other hand, a polyclonal affinity-purified antibody (CM-1) has been recently described that recognizes a cleaved subunit of caspase 3 (Srinivasan et al. 1998). With this antibody, apoptotic neurons could be selectively detected in cultures and in paraffin sections of mouse embryos. The point in the apoptotic process at which this antibody reaction can be detected was not precisely determined, and some cells appeared to undergo apoptosis without becoming reactive for this antibody. However, this approach may be a promising one for identification of apoptotic cells in intact tissues.

Another example of antibodies specific for caspase-generated cleavage products was a study describing an antibody specific for a caspase-generated fragment of actin, termed "fractin" (Yang et al. 1998). In this study, individual apoptotic neurons could be identified on the basis of their fractin content. Studies in vitro suggested a surprisingly rapid time course for the appearance of this fragment when colchicine was used as an apoptosis-inducing agent, perhaps more rapid than one would expect in most cells. Whether this reflects a cell type-specific sensitivity or changes that could occur in the context of morphological events independent of apoptosis will require further study. The authors suggested that fractin might reflect events involved in surface blebbing at the beginning of apoptosis. Blebbing itself, however, is also seen in other settings, so an important clarification will be whether this fragment appears selectively only in blebbing induced by apoptosis or whether it might also appear in other contexts independent of cell death. Even so, this type of approach may provide important insights into the design of new assays useful for tissue sections.

Transglutaminase activation is another biochemical change that has been proposed as an indicator of apoptosis, but whether or not this would be applicable to all systems is not yet clear (Kashima et al. 1997). Certain surface and intracellular antigens have been identified that are expressed as part of the apoptotic process, and these may in the future present new avenues for cytochemical assays.

Mitochondria have been implicated in the apoptotic pathway due to many death inducers, even those that act primarily through surface death receptors but are then amplified through mitochondrial damage. The primary event proposed as important for apoptotic induction is the leakiness of the external membrane of the mitochondrion, resulting in leakage of cytochrome c into the cytosol. This is different from the overall loss of membrane potential of the entire mitochondrion (the permeability transition) as measured by vital dyes such as rhodamine 123 or Mitotracker, but both events may occur in dying cells (Lemasters et al. 1998). Therefore, cytochemical detection of cytochrome c localization is a potential assay for apoptotic induction, although the amount necessary for apoptotic death (how many mitochondria must be leaky for death) is not yet clear. Furthermore, there is some evidence that this leakiness may be reversible, especially in cells in which caspases are inhibited. Antibodies have been identified that detect conformational changes in cytochrome c that appear during apoptosis, but the timing of this change, and whether this might be exploited as a general histochemical assay of apoptosis, is not yet completely clear (Jemmerson et al. 1999; Varkey et al. 1999). Measurements of the metabolic activity of mitochondria have also been used to measure cell death, but this would not necessarily be specific for apoptosis. Some internal antigens in mitochondria (Zhang et al. 1996; Koester et al. 1997) are inacessible in intact mitochondria that are well preserved by fixation. Therefore, the accessibility in apoptotic cells for these antigens in the cytosol (selectively detected using permeabilization with saponins) has also been presented as a potential assay for apoptosis, especially using flow cytometry (Koester et al. 1997). Although many of these methods deal with important mechanisms during the apoptotic process, they still are not easily applicable to detection of apoptotic cells in intact tissue sections.

Conclusions

This brief review emphasizes some of the recently employed cytochemical methods for the detection of apoptosis in cells. Unfortunately, there is no single assay that can be used blindly with perfect specificity and sensitivity. Ironically, the most specific assay is perhaps the oldest, the detection of nuclear shape changes in the early stages of apoptosis. In combination with other methods, this morphological interpretation usually allows a relatively accurate interpretation of apoptosis. For tissue sections, many investigators recommend labeling of DNA strand breaks (ISNT, TUNEL, anti-SS DNA) together with analysis of nuclear morphology. Although detection of DNA strand breaks is a cornerstone method for use in tissue sections, it requires care in interpretation, especially in the details of cell fixation, permeabilization, and processing. For cultured cells, a direct and easily interpretable assay for apoptosis is the observation of surface morphological features with time-lapse microscopy. For flow cytometry using DNA binding dyes, detection of apoptotic bodies as a pre-G_1 peak is a simple and rapid assay for large numbers of cells. Labeling of surface-exposed phosphatidylserine is a useful although imperfect method for both microscopy and flow cytometry. Perhaps the only comforting conclusion from these observations is that the mechanism of apoptotic death appears to be extremely highly conserved in eukaryotes. As a consequence, the development of new techniques will have to deal with the many facets of only a single, albeit complex, biological mechanism.

Acknowledgments

The author thanks Katherine Barrett for expert technical assistance, and Kristy K. Young and Jae A. Collins for help with the ISNT experiments shown in Figure 3.

Literature Cited

Allen RT, Hunter WJ, Agrawal DK (1997) Morphological and biochemical characterization and analysis of apoptosis. J Pharmacol Toxicol Methods 37:215–228

Ansari B, Coates BD, Greenstein BD, Hall PA (1993) In situ end labeling detects DNA strand breaks in apoptosis and other physiological and pathological states. J Pathol 170:1–8

Boersma AW, Nooter K, Oostrum RG, Stoter G (1996) Quantification of apoptotic cells with fluorescein isothiocyanate-labeled annexin V in Chinese hamster ovary cell cultures treated with cisplatin. Cytometry 24:123–130

Bussolati O, Belletti S, Uggeri J, Gatti R, Orlandini G, Dall'Asta V, Gazzola GC (1995) Characterization of apoptotic phenomena induced by treatment with L-asparaginase in NIH3T3 cells. Exp Cell Res 220:283-291

Cartee L, Kucera GL, Willingham MC (in press) Induction of apoptosis by gemcitabine in BG-1 human ovarian cancer cells compared with induction by staurosporine, paclitaxel and cisplatin. Apoptosis

Collins JA, Schandl CA, Young KK, Vesely J, Willingham MC (1997) Major DNA fragmentation is a late event in apoptosis. J Histochem Cytochem 45:923-934

Davis RE, Mysore V, Browning JC, Hsieh JC, Lu Q-AT, Katsikis PD (1998) In situ staining for poly (ADP-ribose) polymerase activity using an NAD analogue. J Histochem Cytochem 46:1279-1289

Darzynkiewicz Z, Bedner E, Traganos, F, Murakami T (1998) Critical aspects in the analysis of apoptosis and necrosis. Hum Cell 11:3-12

Didenko VV, Tunstead JR, Hornsby PJ (1998) Biotin-labeled hairpin oligonucleotides: probes to detect double-strand breaks in DNA in apoptotic cells. Am J Pathol 152:897-902

Emoto K, Toyama-Sorimachi N, Karasuyama H, Inoue K, Umeda M (1997) Exposure of phosphatidylethanolamine on the surface of apoptotic cells. Exp Cell Res 232:430-434

Fan W, Schandl CA, Cheng L, Norris JS, Willingham MC (1996) Gluococorticoids modulate taxol cytotoxicity in human solid tumor cells. Cell Pharmacol 3:343-348

Ferlini C, Kunkl A, Scambia G, Fattorossi A (1997) The use of Apostain in identifying early apoptosis. J Immunol Methods 205: 95-101

Frankfurt OS, Robb JA, Sugarbaker EV, Villa L (1996a) Monoclonal antibody to a single-stranded DNA is a specific and sensitive cellular marker of apoptosis. Exp Cell Res 226:387-397

Frankfurt OS, Robb JA, Sugarbaker EV, Villa L (1996b) Apoptosis in human breast and gastrointestinal carcinomas. Detection in histological sections with monoclonal antibody to single-stranded DNA. Anticancer Res 16:1979-1988

Fujita K, Ohyama H, Yamada T (1997) Quantitative comparison of in situ methods for detecting apoptosis induced by X-ray irradiation in mouse thymus. Histochem J 29:823-830

Gatti R, Belletti S, Orlandini G, Bussolati O, Dall'Asta V, Gazzola GC (1998) Comparison of annexin V and calcein-AM as early vital markers of apoptosis in adherent cells by confocal laser microscopy. J Histochem Cytochem 46:895-900

Gavrieli Y, Sherman Y, Ben-Sasson SA (1992) Identification of programmed cell death in situ via specific labeling of nuclear DNA fragmentation. J Cell Biol 119:493-501

Hall PA, Coates PJ, Ansari B, Hopwood D (1994) Regulation of cell number in the mammalian gastrointestinal tract: the importance of apoptosis. J Cell Sci 107:3569-3577

Hikim AO, Lue Y, Swerdloff RS (1997) Separation of germ cell apoptosis from toxin-induced cell death by necrosis using in situ end-labeling histochemistry after glutaraldehyde fixation. Tissue Cell 29:487-493

Jemmerson R, Liu J, Hausauer D, Kong-Peng L, Mondino A, Nelson RD (1999) A conformational change in cytochrome c of apoptotic and necrotic cells is detected by monoclonal antibody binding and mimicked by association of the native antigen with synthetic phospholipid vesicles. Biochemistry 38:3599-3609

Kashima K, Yokoyama S, Daa T, Nakayama I, Iwaki T (1997) Immunohistochemical study on tissue transglutaminase and copper-zinc superoxide dismutase in human myocardium: its relevance to apoptosis detected by the nick end labelling method. Virchows Arch 430:333-338

Kerr JFR, Wyllie AH, Currie AR (1972) Apoptosis: a basic biological phenomenon with wide-ranging implications in tissue kinetics. Br J Cancer 26:239-257

Kockx MM, Muhring J, Knaapen MWM, deMeyer GRY (1998) RNA synthesis and splicing interferes with DNA in situ end labeling techniques used to detect apoptosis. Am J Pathol 152: 885-888

Koester SK, Roth P, Mikulka WR, Schlossman SF, Zhang C, Bolton WE (1997) Monitoring early cellular responses in apoptosis is aided by the mitochondrial membrane protein-specific monoclonal antibody APO2.7. Cytometry 29:306-312

Koopman G, Reutelingsperger CP, Kuijten GA, Keehnen RM, Pasla ST, van Oers MH (1994) Annexin V for flow cytometric detection of phosphatidylserine expression on B cells undergoing apoptosis. Blood 84:1415-1420

Labat-Moleur F, Guillermet C, Lorimer P, Robert C, Lantuejoul S, Brambilla E, Negoescu A (1998) TUNEL apoptotic cell detection in tissue sections: critical evaluation and improvement. J Histochem Cytochem 46:327-334

Laster SM, Mackenzie JM (1996) Bleb formation and F-actin distribution during mitosis and tumor necrosis factor-induced apoptosis. Microsc Res Tech 34:272-280

Lecoeur H, Ledru E, Prevost MC, Pougeon ML (1997) Strategies for phenotyping apoptotic peripheral human lymphocytes comparing ISNT, annexin-V and 7-AAD cytofluorometric staining methods. J Immunol Methods 209:111-123

Lemasters JJ, Nieminen AL, Qian T, Trost LC, Elmore SP, Nishimura Y, Crowe RA, Cascio WE, Bradham CA, Brenner DA, Herman B (1998) The mitochondrial permeability transition in cell death: a common mechanism in necrosis, apoptosis and autophagy. Biochim Biophys Acta 1366:177-196

Martin SJ, Reutelingsperger CP, McGahon AJ, Rader JA, van Schie RC, LaFace DM, Green DR (1995) Early redistribution of plasma membrane phosphatidylserine is a general feature of apoptosis regardless of the initiating stimulus: inhibition by overexpression of Bcl-2 and Abl. J Exp Med 182:1545-1556

Mizoguchi M, Manabe M, Kawamura Y, Kondo Y, Ishidoh K, Kominami E, Watanabe K, Asaga H, Senshu T, Ogawa H (1998) Deimination of 70-kD nuclear protein during epidermal apoptotic events in vitro. J Histochem Cytochem 46:1303-1309

Modak SP, Bollum FJ (1970) Terminal lens cell differentiation. Exp Cell Res 62:421-432

Modak SP, Bollum FJ (1972) Detection and measurement of single-stranded breaks in nuclear DNA in fixed lens sections. Exp Cell Res 75:307-313

Nakamura M, Yagi H, Ishii T, Kayaba S, Soga H, Gotoh T, Ohsu S, Ogata M, Itoh T (1997) DNA fragmentation is not the primary event in glucocorticoid-induced thymocyte death in vivo. Eur J Immunol 27:999-1004

Naruse I, Keino H, Kawarada Y (1994) Antibody against single-stranded DNA detects both programmed cell death and drug-induced apoptosis. Histochemistry 101:73-78

Negoescu A, Lorimier P, Labat-Moleur F, Drouet C, Robert C, Guillermet C, Brambilla C, Brambilla E (1996) In situ apoptotic cell labeling by the TUNEL method: improvement and evaluation on cell preparations. J Histochem Cytochem 44:959-968

O'Brien IE, Reutelingsperger CP, Holdaway KM (1997) Annexin-V and TUNEL used in monitoring the progression of apoptosis in plants. Cytometry 29:28-33

Pulkkinen JO, Elomaa L, Joensuu H, Martikainen P, Servomaa K, Grenman R (1996) Paclitaxel-induced apoptotic changes followed by time-lapse video microscopy in cell lines established from head and neck cancer. J Cancer Res Clin Oncol 122:214-218

Rimon G, Bazenet CE, Philpott KL, Rubin LL (1997) Increased surface phosphatidylserine is an early marker of neuronal apoptosis. J Neurosci Res 48:563-570

Sanders EJ (1997) Methods for detecting apoptotic cells in tissues. Histol Histopathol 12:1169-1177

Schulze-Osthoff K, Walczak H, Droge W, Krammer PH (1994) Cell nucleus and DNA fragmentation are not required for apoptosis. J Cell Biol 127:15-20

Srinivasan A, Roth KA, Sayers RO, Shindler KS, Wong AM, Fritz LC, Tomaselli KJ (1998) In situ immunodetection of activated caspase-3 in apoptotic neurons in the developing nervous system. Cell Death Differ 5:1004-1016

Tateyama H, Tada T, Hattori H, Murase T, Li W-X, Eimoto T (1998) Effects of prefixation and fixation times on apoptosis detection by in situ end-labeling of fragmented DNA. Arch Pathol Lab Med 122:252-255

Tatton NA, Maclean-Fraser A, Tatton WG, Perl DP, Olanow CW (1998) A fluorescent double-labeling method to detect and confirm apoptotic nuclei in Parkinson's disease. Ann Neurol 44: S142-148

van Engeland M, Kuijpers HJK, Ramaekers FCS, Reutelingsperger CPM, Schutte B (1997) Plasma membrane alterations and cytoskeletal changes in apoptosis. Exp Cell Res 235:421-430

van Engeland M, Nieland LJ, Ramaekers FC, Schutte B, Reutelingsperger CP (1998) Annexin V-affinity assay: a review on an apoptosis detection system based on phosphatidylserine exposure. Cytometry 31:1-9

Varkey J, Chen P, Jemmerson R, Abrams JM (1999) Altered cytochrome c display precedes apoptotic cell death in Drosophila. J Cell Biol 144:701-710

Wyllie AH (1992) Apoptosis and the regulation of cell numbers in normal and neoplastic tissues: an overview. Cancer Metast Rev 11:95-103

Wyllie AH, Beattie GJ, Hargreaves AD (1981) Chromatin changes in apoptosis. Histochem J 13:681-692

Xu X, Gerald AL, Huang BC, Anderson DC, Payan DG, Luo Y (1998) Detection of programmed cell death using fluorescence energy transfer. Nucleic Acids Res 26:2034-2035

Yang F, Sun X, Beech W, Teter B, Wu S, Sigel J, Vinters HV, Frautschy SA, Cole GM (1998) Antibody to caspase-cleaved actin detects apoptosis in differentiated neuroblastoma and plaque-associated neurons and microglia in Alzheimer's disease. Am J Pathol 152:379-389

Zhang C, Ao Z, Seth A, Schlossman SF (1996) A mitochondrial membrane protein defined by a novel monoclonal antibody is preferentially detected in apoptotic cells. J Immunol 157:3980-3987

Zhang G, Gurtu V, Kain SR, Yan G (1997) Early detection of apoptosis using a fluorescent conjugate of annexin V. Biotechniques 23:525-531

Zhu L, Chun J (1998) Apoptosis Detection and Assay Methods. Natick, MA, Biotechniques Books, Eaton Publishing

The EMBO Journal Vol.20 No.9 pp.2214–2223, 2001

Patched1 interacts with cyclin B1 to regulate cell cycle progression

Elizabeth A.Barnes, Monica Kong, Vincent Ollendorff[1] and Daniel J.Donoghue[2]

Department of Chemistry and Biochemistry, Center for Molecular Genetics, University of California, San Diego, La Jolla, CA 92093-0367, USA

[1]Present address: INSERM U119, 27 Bd Lei Roure, 13009 Marseille, France

[2]Corresponding author
e-mail: ddonoghue@ucsd.edu

The initiation of mitosis requires the activation of M-phase promoting factor (MPF). MPF activation and its subcellular localization are dependent on the phosphorylation state of its components, cdc2 and cyclin B1. In a two-hybrid screen using a bait protein to mimic phosphorylated cyclin B1, we identified a novel interaction between cyclin B1 and patched1 (ptc1), a tumor suppressor associated with basal cell carcinoma (BCC). Ptc1 interacted specifically with constitutively phosphorylated cyclin B1 derivatives and was able to alter their normal subcellular localization. Furthermore, addition of the ptc1 ligand, sonic hedgehog (shh), disrupts this interaction and allows cyclin B1 to localize to the nucleus. Expression of ptc1 in 293T cells was inhibitory to cell proliferation; this inhibition could be relieved by coexpression of a cyclin B1 derivative that constitutively localizes to the nucleus and that could not interact with ptc1 due to phosphorylation-site mutations to Ala. In addition, we demonstrate that endogenous ptc1 and endogenous cyclin B1 interact *in vivo*. The findings reported here demonstrate that ptc1 participates in determining the subcellular localization of cyclin B1 and suggest a link between the tumor suppressor activity of ptc1 and the regulation of cell division. Thus, we propose that ptc1 participates in a G_2/M checkpoint by regulating the localization of MPF.

Keywords: basal cell carcinoma/cytoplasmic retention signal/G_2/M checkpoint/M-phase promoting factor/ nevoid basal cell carcinoma syndrome

Introduction

Entry into mitosis requires the activation of M-phase promoting factor (MPF), a universal cell cycle regulatory complex. At late G_2, MPF translocates to the nucleus where it is responsible for the phosphorylation of many nuclear substrates required for mitotic progression (Peter *et al.*, 1990; Yamashiro *et al.*, 1991; Verde *et al.*, 1992). The MPF complex consists of two proteins that are regulated separately (Pondaven *et al.*, 1989; Ducommun *et al.*, 1991; Li *et al.*, 1995; Borgne *et al.*, 1999). The Ser/Thr kinase cdc2, which is ubiquitously expressed throughout the cell cycle, undergoes activation at the G_2/M transition (Ducommun *et al.*, 1991; Krek and Nigg, 1991; Borgne and Meijer, 1996) as a result of dephosphorylation of Thr14 and Tyr15 and phosphorylation of Thr161 (Solomon *et al.*, 1990; Krek and Nigg, 1991; Norbury *et al.*, 1991). In contrast, cyclin B1 is temporally regulated and does not begin to accumulate until S phase. At G_2 phase, cyclin B1 protein reaches maximal levels and begins to enter the nucleus in a phosphorylation-dependent manner (Hagting *et al.*, 1998, 1999; Yang and Kornbluth, 1999).

An important aspect of cyclin B1 regulation involves the cytoplasmic retention signal (CRS) domain. Initially, the CRS domain was described as mediating the cytoplasmic retention of cyclin B1 (Pines and Hunter, 1994), but more recently it has been demonstrated that a phosphorylation-dependent nuclear export signal (NES) resides within the CRS (Toyoshima *et al.*, 1998; Yang *et al.*, 1998). When the NES of cyclin B1 is active, it facilitates rapid export of unphosphorylated cyclin B1 from the nucleus (Yang *et al.*, 1998; Yang and Kornbluth, 1999). Phosphorylation of serine residues within the CRS domain, beginning in late G_2, disrupts the NES function and allows for the nuclear accumulation of MPF to initiate the onset of mitosis (Yang *et al.*, 1998).

Previous studies in our laboratory identified four major sites of serine phosphorylation within the CRS of *Xenopus* cyclin B1 (residues S94, S96, S101 and S113) (Li *et al.*, 1995). In addition, mutation of these four Ser residues to Ala, mimicking an unphosphorylated state, substantially decreased MPF activity in *Xenopus* oocyte maturation assays. Conversely, substitution of Glu residues to mimic the phosphorylated state greatly increased MPF activity in the oocyte system (Li *et al.*, 1997). This study suggested that the localization of cyclin B1, and of active MPF, is regulated by phosphorylation within the CRS domain. Recently, it was demonstrated that UV-induced DNA damage prevents cyclin B1 from entering the nucleus or, alternatively, causes cyclin B1 to shuttle rapidly from the nucleus to the cytoplasm, thereby delaying mitosis until the damage can be repaired (Jin *et al.*, 1998; Toyoshima *et al.*, 1998). Thus, the regulation of cyclin B1 localization is a key factor involved in a G_2/M checkpoint control. In an effort to identify biologically relevant partners that may regulate the trafficking and localization of phosphorylated cyclin B1, we employed a yeast two-hybrid approach.

Surprisingly, this search for cyclin B1-interacting proteins identified ptc1, a 12-pass integral membrane protein recently characterized as the receptor for sonic hedgehog (shh), an important developmental morphogen (Chen and Struhl, 1996; Marigo *et al.*, 1996; Stone *et al.*, 1996; Goodrich and Scott, 1998). Ptc1 is a tumor suppressor frequently mutated in association with nevoid basal cell carcinoma syndrome (NBCCS) and basal cell

© European Molecular Biology Organization

carcinoma (BCC) (Chidambaram *et al.*, 1996; Gailani *et al.*, 1996; Hahn *et al.*, 1996b; Unden *et al.*, 1996). NBCCS is acquired through autosomal dominant inheritance and predisposes patients to BCC and associated medical problems (Gorlin, 1995). Despite the undisputed role of ptc1 in BCC development, the mechanism of ptc1 anti-proliferative and/or tumor suppressor function has not been clearly defined. In this report, we describe the novel interaction between cyclin B1 and ptc1, demonstrate that cyclin B1 localization is mediated by ptc1, and show that MPF activity can be regulated by ptc1. Our data support the existence of a G_2/M checkpoint where MPF is sequestered by ptc1 to prevent mitotic progression.

Results

Isolation of ptc1 from a yeast two-hybrid screen

In this study, we exploited a *Xenopus* cyclin B1 mutant with the four Ser phosphorylation sites in the CRS domain mutated to Glu, designed to mimic phosphoserine residues. Similarly, we utilized a mutant with the four Ser residues mutated to Ala to mimic an unphosphorylated state (Li *et al.*, 1997). These derivatives contain a tandem repeat of the CRS domain (CRS^{Ala}–CRS^{Ala} and CRS^{Glu}–CRS^{Glu}) (Figure 1A, a and b), based on previous observations that a minimum of 100 amino acids for the bait protein will enhance potential two-hybrid interactions (Kong *et al.*, 2000). Employing a yeast two-hybrid screen, a partial cDNA clone encoding ptc1 (residues 690–779) was identified in a mouse embryonic cDNA library as positively interacting with the CRS^{Glu}–CRS^{Glu} construct (Table I). This ptc1 cDNA clone did not interact with the CRS^{Ala}–CRS^{Ala} construct. The 90-amino acid-fragment of ptc1 identified from the screen represented a portion of the large intracellular loop (residues 690–736), a transmembrane segment (residues 737–755), and a portion of the second large extracellular loop (residues 756–779) (Figure 1A, e).

Ptc1 contains two large extracellular loops involved in binding shh and one large intracellular loop (Chen and Struhl, 1996; Marigo *et al.*, 1996; Stone *et al.*, 1996). A biologically relevant interaction of cyclin B1 with ptc1 would most likely involve the large intracellular loop, but not the transmembrane or extracellular domains, which should be inaccessible to cyclin B1. To confirm this, a synthetic gene encoding only the large intracellular loop of human ptc1 (consisting of residues 599–750) was assayed in the yeast two-hybrid system with the mutant CRS–CRS domains of cyclin B1 (Figure 1A, f). For both His$^-$ minimal media and β-gal liquid assays, this derivative of ptc1 exhibited interaction with only the CRS^{Glu}–CRS^{Glu} construct (Table I and data not shown). In addition, we

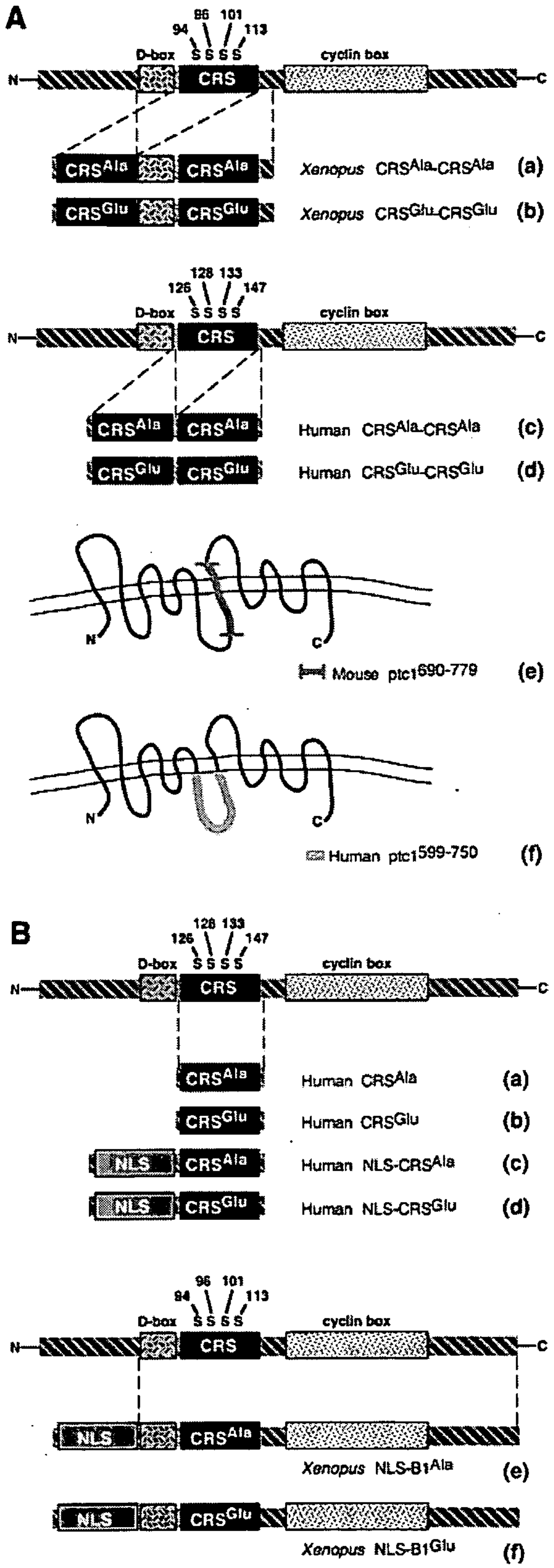

Fig. 1. (A) Schematic representation of cyclin B1 and patched1 constructs used in the yeast two-hybrid screen. (a–d) Cyclin B1 constructs containing a tandem repeat of the CRS domain. Ser residues (S) of the CRS domain were mutated to Ala or Glu to mimic the unphosphorylated or phosphorylated state of cyclin B1, respectively. (a and b) Constructs representing the *Xenopus laevis* CRS–CRS mutants with the destruction box (D-box) domain of cyclin B1 included. (c and d) Constructs representing the human CRS–CRS mutants. (e) Mouse ptc1 clone isolated from the two-hybrid screen. (f) Human ptc1 construct synthesized for further testing in the yeast two-hybrid system. (B) Schematic representation of cyclin B1 constructs used in mammalian cell studies. (a and b) Constructs representing the human CRS mutants. (c and d) Human CRS mutants with an appended NLS of *Xenopus* nucleoplasmin at the N-terminus. (e and f) Full-length *Xenopus* cyclin B1 derivatives with an appended NLS are represented.

Table I. Yeast two-hybrid interactions

Bait protein	Interacting protein	
	Mouse ptc1$^{(690–779)}$	Human ptc1$^{(599–750)}$
Xenopus CRS^{Ala}–CRS^{Ala}	–	–
Xenopus CRS^{Glu}–CRS^{Glu}	+	+
Human CRS^{Ala}–CRS^{Ala}	ND	–
Human CRS^{Glu}–CRS^{Glu}	ND	+
Lamin	–	–

ND, not determined.

examined whether the CRS domain of human cyclin B1 would interact with human ptc1 (Figure 1A, c and d). As before, we found that the large intracellular loop of human ptc1 interacts specifically with the human CRS^{Glu}–CRS^{Glu} construct (Table I). Thus, both the mouse ptc1 fragment and the human ptc1 intracellular loop were dependent upon the phosphorylation state of the CRS domain of cyclin B1 for binding. These results confirm that the large intracellular loop of ptc1 has the potential to interact with the phosphorylated CRS domain of cyclin B1 and, furthermore, that the intracellular portion of the original 90-amino-acid fragment of ptc1 isolated from the screen, corresponding to human ptc1 residues 704–750, is sufficient for this interaction.

The large intracellular loop of ptc1 and cyclin B1 interact in vivo

To determine whether the intracellular loop of ptc1 can bind to endogenous full-length cyclin B1, we transfected a glutathione *S*-transferase (GST)–ptc1 intracellular loop fusion construct specific for mammalian expression (GST–ptc1$^{599–750}$) into 293T cells. Mock-transfected cells were used as a negative control; in addition, a construct encoding GST protein alone was transfected into 293T cells as a negative control. Cell lysates were immunoprecipitated with cyclin B1 antiserum and interacting GST fusions were visualized by immunoblotting with GST antiserum (Figure 2A, upper panel). The GST–ptc1$^{599–750}$ fusion protein was found to bind specifically to endogenous cyclin B1 (Figure 2A, lane 3). As a control, the lower panel of Figure 2A demonstrates the presence of cyclin B1 in all samples as determined by immunoblotting. In addition, expression of the GST fusion proteins was examined in lysates by immunoblotting (Figure 2B, lanes 2 and 3). These results confirm that the large intracellular loop of ptc1 binds to full-length cyclin B1 *in vivo*.

Association between endogenous cyclin B1 and endogenous ptc1

The ptc1 transcript can be found in early embryonic tissues and in adult tissues as well, including brain, lung, kidney and liver (Goodrich *et al.*, 1996; Hahn *et al.*, 1996a). Therefore, to demonstrate an interaction between endogenous ptc1 and endogenous cyclin B1, we used human embryonic kidney 293T cells in a coimmunoprecipitation assay. Immunoprecipitation of endogenous ptc1 using a ptc1 antiserum, followed by immunoblotting using antiserum against cyclin B1, reveals the presence of cyclin B1 associated with ptc1 (Figure 3A, lower panel, lane 2). As a negative control and to demonstrate antibody specificity, lane 3 shows an anti-ptc1 immunoprecipitate in which a cognate ptc1 blocking peptide was pre-incubated with the antiserum. As a positive control, lane 1 demonstrates the presence of cyclin B1 and ptc1 in cell lysates (Figure 3A, lower and upper panels). These results indicate that endogenous ptc1 and endogenous cyclin B1 interact and can be recovered by coimmunoprecipitation.

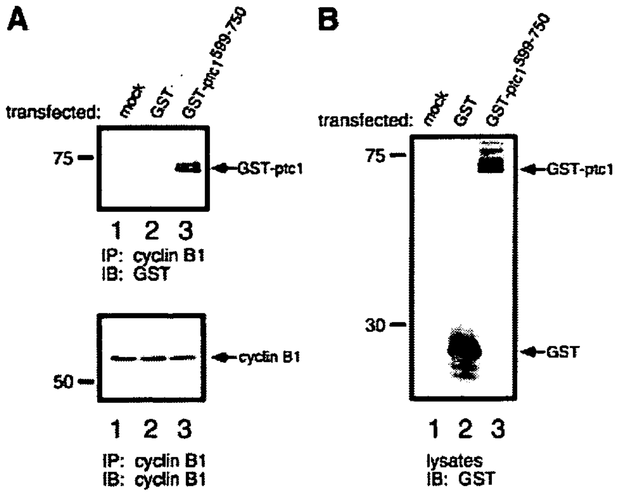

Fig. 2. Patched1 intracellular loop binds endogenous cyclin B1. (**A**) Mammalian GST fusion genes encoding either GST alone (GST) or GST fused to the intracellular loop of ptc1 (GST–ptc1$^{599–750}$) were transfected into 293T cells and immunoprecipitated with cyclin B1 antibody. Samples were analyzed by 10% SDS–PAGE and immunoblotted with mAb GST (upper panel) followed by mAb cyclin B1 (lower panel). (**B**) Expression of GST fusion proteins in lysates.

We then wished to examine whether exogenously expressed full-length ptc1 can also bind endogenous cyclin B1. Therefore, Myc–ptc1-transfected 293T cells were immunoprecipitated with cyclin B1 antiserum. As demonstrated in Figure 3B, cyclin B1 immunoprecipitates reveal an association with ptc1 (upper panel, lane 2). This interaction is specific, as addition of cyclin B1 blocking peptide abolishes the association (Figure 3B, upper panel, lane 3). As controls, the middle panel demonstrates the expression of cyclin B1 in these samples (Figure 3B, lanes 1 and 2), and the expression of Myc–ptc1 protein was confirmed by immunoblotting cell lysates (Figure 3B, lower panel, lanes 2 and 3). These results demonstrate that exogenously expressed ptc1 binds endogenous cyclin B1 *in vivo*.

Ptc1 binds to an activated MPF complex

To investigate whether ptc1 associates with cyclin B1 complexed to cdc2, we immunoprecipitated endogenous cdc2 from Myc–ptc1-transfected cells. As demonstrated in Figure 3C, cdc2 immunoprecipitates reveal an association with ptc1 (upper panel, lane 2). The middle panel demonstrates the expression of cyclin B1 complexed to cdc2 immunoprecipitates (Figure 3C, lanes 1 and 2). The lower panel shows the expression of cdc2 (Figure 3C, lanes 1 and 2). These results suggest that ptc1, cyclin B1 and cdc2 can be recovered in a complex *in vivo*. Alternatively, ptc1–cyclin B1 and ptc1–cdc2 complexes may exist independently.

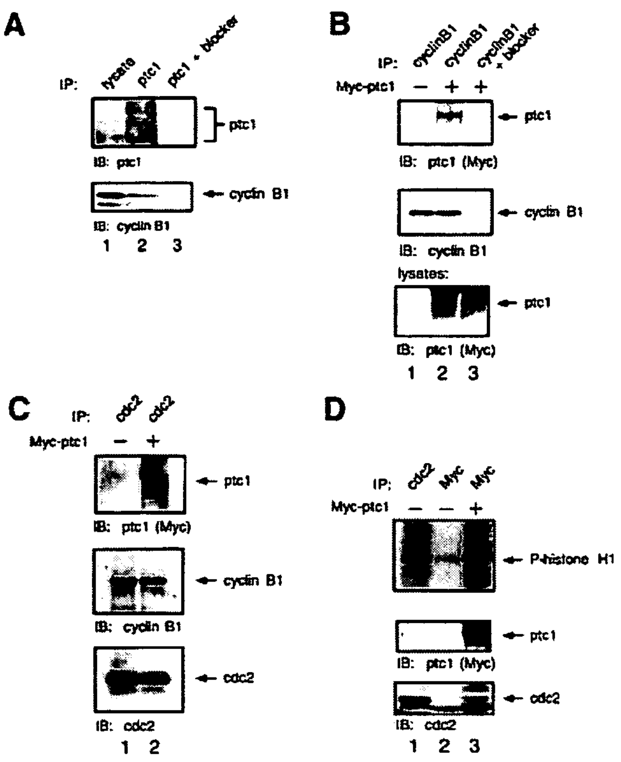

Fig. 3. Patched1 interacts with cyclin B1. (**A**) Endogenous ptc1 and endogenous cyclin B1 interact in 293T cells. Lysates were immunoprecipitated as indicated. Upper panel, immunoblot of ptc1 shows ptc1 in the lysate and immunoprecipitate. Lane 3 indicates the use of ptc1 blocking peptide to discriminate antibody specificity. Lower panel, immunoblot of cyclin B1 showing cyclin B1 in lysate and ptc1 immunoprecipitate, but not the peptide blocked lane. (**B**) Patched1 binds endogenous cyclin B1. 293T cells were transfected with Myc–ptc1, immunoprecipitated with cyclin B1 antibody and immunoblotted as indicated. Lane 3 indicates the use of cyclin B1 blocking peptide to discriminate antibody specificity. (**C**) Patched1, cyclin B1 and cdc2 form a complex. 293T cells were transfected with Myc–ptc1, immunoprecipitated with cdc2 antibody and immunoblotted as indicated. (**D**) Active MPF complex associates with patched1. 293T cells were transfected with Myc–ptc1 as indicated. Upper panel, lysates were immunoprecipitated and assayed for histone H1 kinase activity. Middle panel, anti-Myc immunoblot displaying expression of Myc–ptc1. Lower panel, anti-cdc2 immunoblot displaying the presence of cdc2 in lane 1 (positive control) and lane 3 (ptc1-transfected cells). The lower band represents the IgG band from mouse Myc antiserum as detected by mouse cdc2 antiserum.

One of several nuclear substrates for MPF is histone H1 protein (Pondaven *et al.*, 1989). Therefore, to determine whether ptc1 can interact with an active MPF complex, we examined histone H1 kinase activity associated with ptc1-transfected cells. As demonstrated in Figure 3D, histone H1 kinase activity was readily detected in association with immunoprecipitated Myc–ptc1 (upper panel, lane 3). As a positive control, cdc2 immunoprecipitates from mock-transfected cells also demonstrate the phosphorylation of histone H1 proteins (Figure 3D, upper panel, lane 1). As a negative control for histone H1 activity, mock-transfected cells were immunoprecipitated with Myc antiserum (Figure 3D, upper panel, lane 2). To confirm the presence of Myc–ptc1, immunoprecipitates were immunoblotted with Myc antiserum (Figure 3D, middle panel, lane 3). We also immunoblotted with cdc2 antiserum and confirmed that cdc2 is associated with Myc–ptc1 (Figure 3D, lower panel, lane 3). These data indicate that ptc1 interacts with active MPF, but the presence of cdc2 in ptc1 immunoprecipitates does not preclude the possibility that other cdks may also be associated with ptc1.

Ptc1 colocalizes with a cyclin B1 derivative that mimics phosphorylation of the CRS

As published previously, the localization of cyclin B1 is dependent on the phosphorylation state of the CRS domain (Li *et al.*, 1997). Extending these results, we constructed derivatives of the human cyclin B1 CRS domain (Figure 1B, a and b) and utilized indirect immunofluorescence studies to examine their subcellular localization. These experiments reveal that CRS$^{\mathrm{Ala}}$ localizes exclusively to the cytoplasm, while CRS$^{\mathrm{Glu}}$ is able to enter the nucleus (Figure 4A, a and c, respectively). Both of these constructs, when modified by appending a nuclear localization signal (NLS) from *Xenopus* nucleoplasmin, NLS–CRS$^{\mathrm{Ala}}$ and NLS–CRS$^{\mathrm{Glu}}$ (Figure 1B, c and d), localize constitutively to the nucleus (Figure 4A, e and g). To visualize Myc-tagged ptc1, ptc1 antiserum was used (Figure 4B, c). The punctate membrane staining of ptc1, as demonstrated in Figure 4B, is consistent with previous reports describing an atypical membrane localization for ptc1 (Stone *et al.*, 1996; Carpenter *et al.*, 1998).

Since endogenous ptc1 expression levels in COS-1 cells are low, we chose to cotransfect Myc-tagged ptc1 with either NLS–CRS construct to determine whether full-length ptc1 could alter their subcellular localization. NLS–CRS$^{\mathrm{Ala}}$ remained nuclear in the presence of Myc–ptc1 (Figure 4C, a, b and c). In contrast, NLS–CRS$^{\mathrm{Glu}}$ exhibited altered localization to the membrane when coexpressed with Myc–ptc1 (Figure 4C, d, e and f). Thus, these data suggest that ptc1 has the ability to recruit phosphorylated cyclin B1.

Ptc1 mediates the localization of a phosphorylated cyclin B1 derivative

To confirm that ptc1 can alter the localization of cyclin B1, cellular fractionation studies were performed to examine whether full-length ptc1 affects the localization of full-length cyclin B1. The *Xenopus* cyclin B1 derivative used in this study contained the four Ser phosphorylation sites in the CRS domain mutated to Glu with an appended NLS to target this protein to the nucleus (NLS–B1$^{\mathrm{Glu}}$) (Figure 1B, f). Cellular fractionation of NLS–B1$^{\mathrm{Glu}}$-transfected cells reveals nearly complete nuclear localization of this cyclin B1 derivative (Figure 5A, upper panel, lane 1). In contrast, cotransfection of NLS–B1$^{\mathrm{Glu}}$ with Myc–ptc1 results in predominantly cytoplasmic/plasma membrane localization of this nuclear-targeted cyclin B1 protein (Figure 5A, upper panel, lane 4). These results suggest that ptc1 inhibits phosphorylated cyclin B1 from entering the nucleus, and confirm the previous colocalization data discussed above (Figure 4C, d, e and f).

Since ptc1 is the receptor for sonic hedgehog (shh) and therefore an integral component of the hedgehog signaling pathway (Chen and Struhl, 1996; Goodrich and Scott, 1998), cells expressing both ptc1 and NLS–B1$^{\mathrm{Glu}}$ constructs were exposed to shh-N to determine whether this morphogen modulates the interaction between cyclin B1 and ptc1. The shh-N construct used in this study contains the first 197 amino acids of human shh protein, which have been shown to be sufficient for its interaction with ptc1

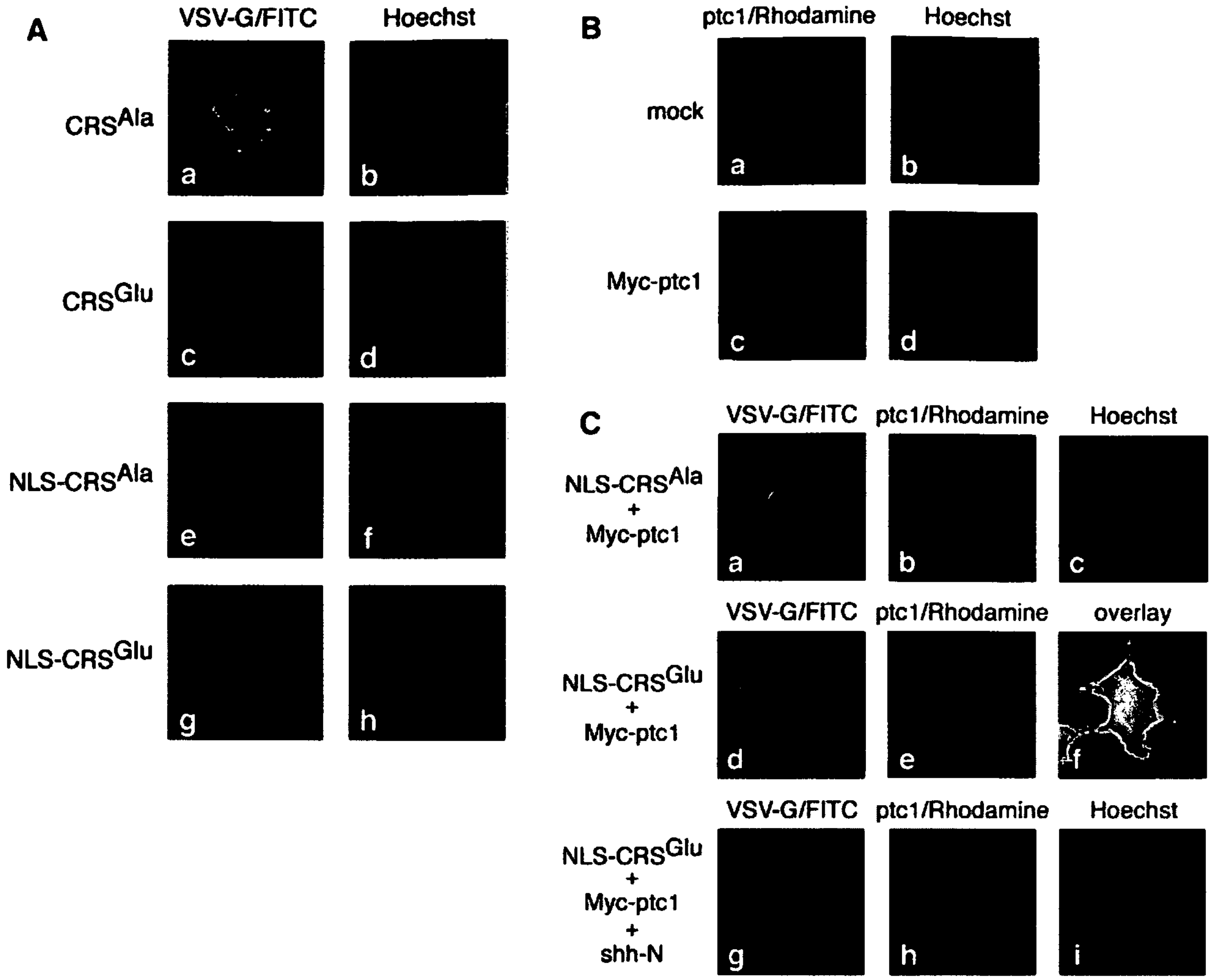

Fig. 4. Patched1 colocalizes with the CRS$^{\mathrm{Glu}}$ domain of cyclin B1 at the cell membrane. (**A**) Localization of human CRS and NLS–CRS constructs in COS-1 cells detected by immunofluorescence. (a) CRS$^{\mathrm{Ala}}$ construct expressed in cytoplasm. (c) CRS$^{\mathrm{Glu}}$ construct expressed in nucleus. (e and g) NLS–CRS$^{\mathrm{Ala}}$ and NLS–CRS$^{\mathrm{Glu}}$ constructs expressed in nucleus. (b, d, f and h) Nuclei detected with Hoechst dye. (**B**) Localization of Myc-tagged ptc1 in COS-1 cells detected by immunofluorescence. (a) Mock-transfected cell. (c) Myc–ptc1 expressed at membrane. (b and d) Nuclei detected with Hoechst dye. (**C**) Altered localization of NLS–CRS$^{\mathrm{Glu}}$ due to cotransfection of ptc1. (a) NLS–CRS$^{\mathrm{Ala}}$ remains nuclear in the presence of ptc1 expression (b). In contrast (d), NLS–CRS$^{\mathrm{Glu}}$ associates with the cell membrane due to ptc1 expression (e). (f) NLS–CRS$^{\mathrm{Glu}}$ and ptc1 colocalization. (g, h and i) Sonic hedgehog restores nuclear accumulation of NLS–CRS$^{\mathrm{Glu}}$. (g) NLS–CRS$^{\mathrm{Glu}}$ retains nuclear localization in the presence of ptc1 (h) with shh-N exposure. (c and i) Nuclei detected with Hoechst dye.

(Lee *et al.*, 1994; Marigo *et al.*, 1996; Stone *et al.*, 1996). Addition of shh-N to cotransfected cells altered the localization pattern of NLS–B1$^{\mathrm{Glu}}$, demonstrating an increase in nuclear accumulation of this cyclin B1 derivative (Figure 5A, lane 5). This suggests that shh-N inhibits the interaction between ptc1 and NLS–B1$^{\mathrm{Glu}}$, allowing cyclin B1 translocation to the nucleus. As a control, immunoblotting with Myc antiserum shows that ptc1 is expressed solely in the cytoplasmic/plasma membrane fraction (Figure 5A, middle panel, lanes 4 and 6). The lower panel indicates that the nuclear fractions are intact as demonstrated by nuclear histone protein expression (Figure 5A, lanes 1, 3 and 5). Figure 5B presents quantitation of localization data based on three independent cellular fractionation experiments, and demonstrates that 76% of NLS–B1$^{\mathrm{Glu}}$ is retained in the cytoplasm when ptc1 is present. With the addition of shh-N, only 24% of NLS–B1$^{\mathrm{Glu}}$ is retained in the cytoplasm. These results confirm by biochemical fractionation that ptc1 mediates the localization of phosphorylated cyclin B1 to the cytoplasmic/plasma membrane fraction of the cell, and that this localization can be altered by cellular exposure to shh.

In addition, to confirm the apparent subcellular redistribution of phosphorylated cyclin B1 due to shh exposure, we performed indirect immunofluorescence. Shh-N was added to COS-1 cells cotransfected with Myc–ptc1 and NLS–CRS$^{\mathrm{Glu}}$. As demonstrated in Figure 4C, shh-N addition restores the nuclear accumulation of NLS–CRS$^{\mathrm{Glu}}$ in cells overexpressing ptc1 (compare Figure 4C, g and d).

Ptc1 expression regulates cell proliferation

To examine the effects of ptc1 and cyclin B1 expression on cell cycle progression, cell proliferation assays were performed. The overexpression of ptc1 alone prevents cell growth, consistent with an anti-proliferative function (Figure 6A). Cells transfected with NLS–B1$^{\mathrm{Ala}}$ or NLS–

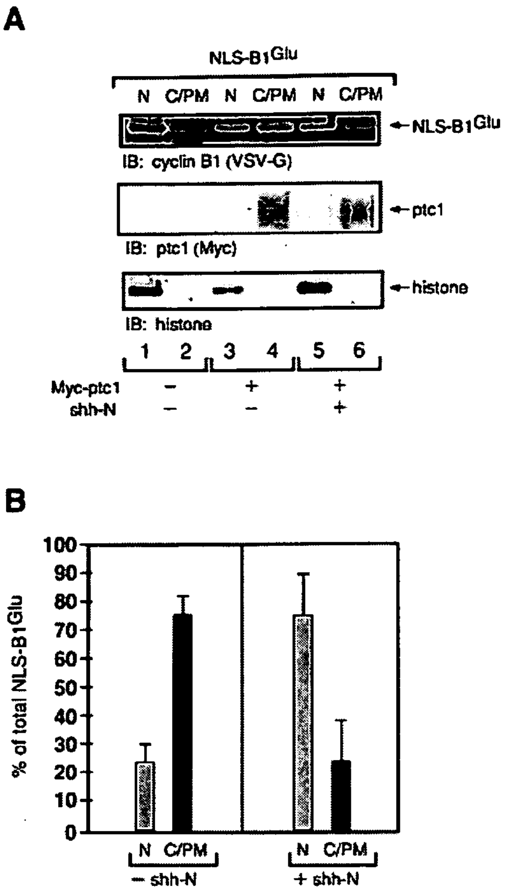

Fig. 5. Cyclin B1 localization mediated by patched1 expression and shh exposure. (**A**) Upper panel, expression of NLS-B1^{Glu} protein in cellular fractions. Middle panel, cytoplasmic/plasma membrane (C/PM) expression of ptc1 in cotransfected cells. Lower panel, nuclear (N) expression of endogenous histone proteins. (**B**) Quantitation of data presented in lanes 3–6 of (A) representing the average of three independent cellular fractionation experiments. The standard deviation is shown.

B1^{Glu} alone exhibited intermediate levels of proliferation, compared with mock-transfected cells (Figure 6A). These NLS-appended derivatives were used to ensure that even the non-phosphorylated derivative (NLS-B1^{Ala}) would still exhibit biological activity, due to the appended NLS (Li *et al.*, 1997). When ptc1 was coexpressed together with either NLS-B1^{Ala} or NLS-B1^{Glu}, we found that NLS-B1^{Ala}, but not NLS-B1^{Glu}, was able to restore cellular proliferation (Figure 6A). As a control for protein expression levels in all the samples, Figure 6B presents immunoblotting of cell lysates to detect Myc–ptc1 (upper panel) or cyclin B1 derivatives (lower panel).

Overexpression of mitotic cyclins increases cell cycle progression from G_2 to M, yet also leads to an increase in mitotic arrest (Murray *et al.*, 1989). We interpret the intermediate levels of proliferation observed as a reflection of these two conflicting roles. The mitotic index for the various cell populations is presented (Figure 6C). This bar graph demonstrates that the overexpression of NLS-B1^{Ala}, NLS-B1^{Glu} and coexpression of NLS-B1^{Ala} with ptc1 leads to an increase in the mitotic index for these samples even though their relative rates of proliferation are intermediate compared with mock-transfected cells. The mitotic index of cells expressing ptc1, or ptc1 plus NLS-B1^{Glu}, is significantly decreased, reflecting fewer cells in M phase. Taken together, these results strongly suggest that cell division is inhibited by the interaction of ptc1 with the derivative of cyclin B1 that mimics phosphorylation. The inhibitory effects of ptc1 on cell proliferation can be overcome by coexpression of NLS-B1^{Ala}, which is unable to interact with ptc1.

In addition, we investigated the physiological effect of shh addition on cell cycle progression. We found that cellular exposure to shh-N increased the cell number in all samples examined (Figure 6D). These data indicate that endogenous ptc1 can be affected by addition of shh-N. Also, cells overexpressing ptc1 respond similarly to exogenous shh-N, resulting in the promotion of cell growth. These results confirm that ptc1 inhibits cell division by interaction with phosphorylated cyclin B1, and that this inhibition can be relieved by shh cellular exposure.

Discussion

We have demonstrated a novel interaction between cyclin B1, the regulatory subunit of MPF and the tumor suppressor ptc1. Specifically, we show that the large intracellular loop of ptc1, containing amino acid residues 599–750, is sufficient for the interaction with cyclin B1. We also show that ptc1 is able to mediate the localization of phosphorylated cyclin B1. In addition, fractionation studies show that NLS-B1^{Glu} is expressed primarily in the cytoplasmic/plasma membrane fraction when ptc1 is present, indicating that ptc1 mediates the localization of phosphorylated cyclin B1. Taken together with the immunofluorescence data, these results confirm that ptc1 interacts with the phosphorylated CRS domain of cyclin B1 at the cell periphery, and also demonstrate a novel function for ptc1 that involves the release of phosphorylated cyclin B1 in response to shh stimulation. The presence of cdc2 as a constituent of a cyclin B1–ptc1 complex is demonstrated by histone H1 kinase and immunoprecipitation assays.

One model to account for these results is presented in Figure 7. In this model, an MPF–ptc1 complex inhibits cell growth. In this manner, ptc1 may function as a tumor suppressor at the G_2/M transition by binding phosphorylated cyclin B1, thereby delaying the nuclear events normally mediated by MPF activation. This model of regulation also suggests that stimulation of ptc1 by shh elicits the release of cyclin B1, allowing translocation of MPF to the nucleus and resumption of the cell cycle.

The ptc1 gene in vertebrates is essential for normal embryonic development and also functions as a tumor suppressor (Gailani *et al.*, 1996; Hahn *et al.*, 1996a; Johnson *et al.*, 1996). ptc1 inactivation has been found to underlie NBCCS and BCC development (Chidambaram *et al.*, 1996; Hahn *et al.*, 1996b; Unden *et al.*, 1997). NBCCS is an autosomal dominant syndrome characterized by developmental disorders and predisposition to BCC (Gorlin, 1995). BCC is the most common type of human cancer with 750 000 estimated cases per year in the United States alone (Gailani and Bale, 1997). ptc1 can form a complex with smoothened (smo), a 7-pass transmembrane protein and signaling component of the hedgehog pathway

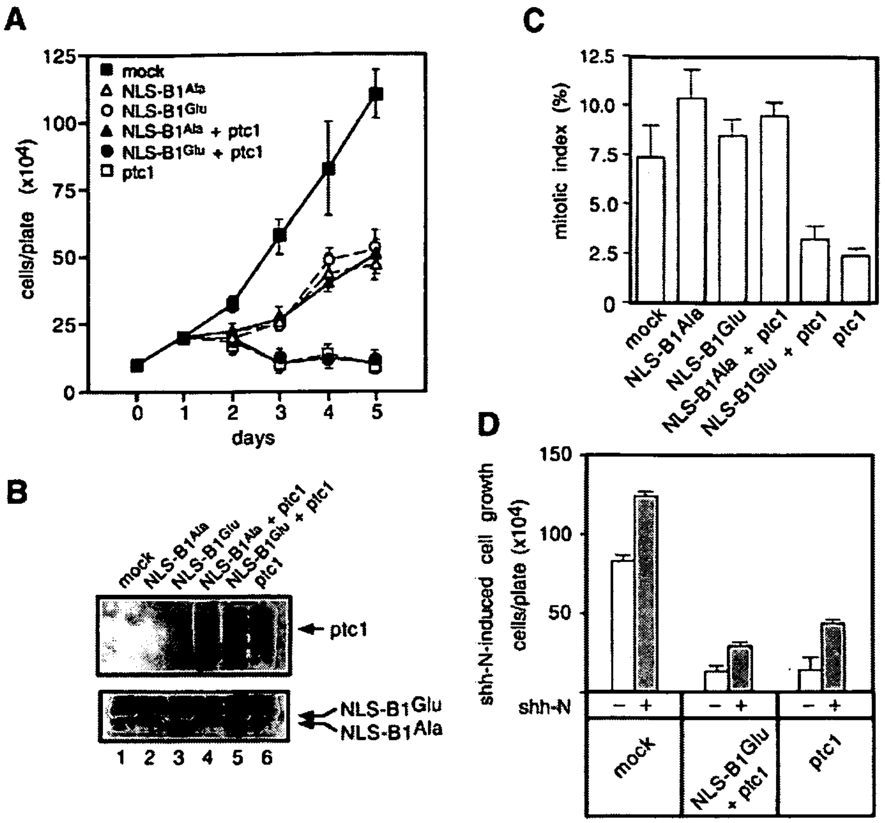

Fig. 6. Anti-proliferative function of the cyclin B1–ptc1 complex. (**A**) Growth curve of 293T cells transfected with the indicated constructs. There is a decrease in cell proliferation with cotransfection of ptc1 and NLS–B1^{Glu}. Error bars represent the standard error of the mean. (**B**) Upper panel, expression of Myc-tagged ptc1 in cell lysates obtained from the last day of the growth curve. Lower panel, expression of VSV-G-tagged cyclin B1 derivatives in cell lysates. (**C**) Decrease in mitotic index in cells cotransfected with ptc1 and NLS–B1^{Glu}. The percentage of cells showing a mitotic phenotype from three independent transfections with the standard deviation is shown. (**D**) Increase in cell proliferation with cellular exposure to shh-N. The average value of two experiments is shown.

(Stone *et al.*, 1996; Murone *et al.*, 1999). Previous findings have suggested that constitutive activation of smo, due to the aberrant inactivation of ptc1, can lead to the oncogenic effects of BCC (Stone *et al.*, 1996). Yet the mechanism of ptc1 as a tumor suppressor and the role of smo activation remain unclear. In this study we have identified a novel downstream component of the shh–ptc1 signaling pathway, which may represent a key factor in the mechanism by which shh and ptc1 control mitogenic effects.

Several known tumor suppressors (p53, pRb, p16) act in the nucleus as negative regulators of cell division by interaction with cyclin D–cdk4/cdk6 and/or cyclin E–cdk2 complexes (Weinberg, 1995; Dean, 1997). ptc1 was one of the first characterized tumor suppressors localized at the cell membrane. Two recent reports have characterized other areas of ptc1 localization. Denef *et al.* (2000) have demonstrated that ptc1 is internalized and degraded after shh has bound to the two large extracellular loops. Incardona *et al.* (2000) found ptc1 as populating endosomal vesicles, as well as the cell surface. In our hands, ptc1 shows a punctate distribution in the plasma membrane as seen by immunofluorescence studies, consistent with previous reports indicating atypical membrane staining for ptc1 (Stone *et al.*, 1996; Carpenter *et al.*, 1998).

Further investigation will be required to understand fully the significance of the interaction between cyclin B1 and ptc1 described here. Our results demonstrate that ptc1 binds cyclin B1 in a phosphorylation-dependent manner. Since cyclin B1 becomes phosphorylated only during late G_2 (Borgne *et al.*, 1999), ptc1 can presumably only bind cyclin B1 at the G_2 phase or G_2/M transition of the cell cycle. Our laboratory recently reported that when cyclin F interacts with cyclin B1, the complex localizes to the nucleus (Kong *et al.*, 2000). It is possible that in response to different cellular signals phosphorylated cyclin B1 is either sequestered by ptc1 or translocated to the nucleus by cyclin F, although this remains to be examined. However, none of these reports excludes the possibility of ptc1 interacting with cyclin B1.

Another issue for future investigation should include the effect of the interaction of active MPF with ptc1 with respect to the shh–ptc1 pathway or other signaling pathways. A recent report implies that smo may be phosphorylated indirectly by ptc1 and that this event would occur after shh has bound to ptc1 (Denef *et al.*, 2000). Since we have shown that ptc1 interacts directly with MPF, it is a distinct possibility that MPF represents the kinase responsible for phosphorylation and activation of smo. The association between ptc1 and cyclin B1 may fulfill at least two purposes: (i) ptc1 binding of MPF may mediate the anti-proliferative effects of ptc1; and (ii) cyclin B1 localization to the membrane may allow for the phosphorylation of ptc1 or smo.

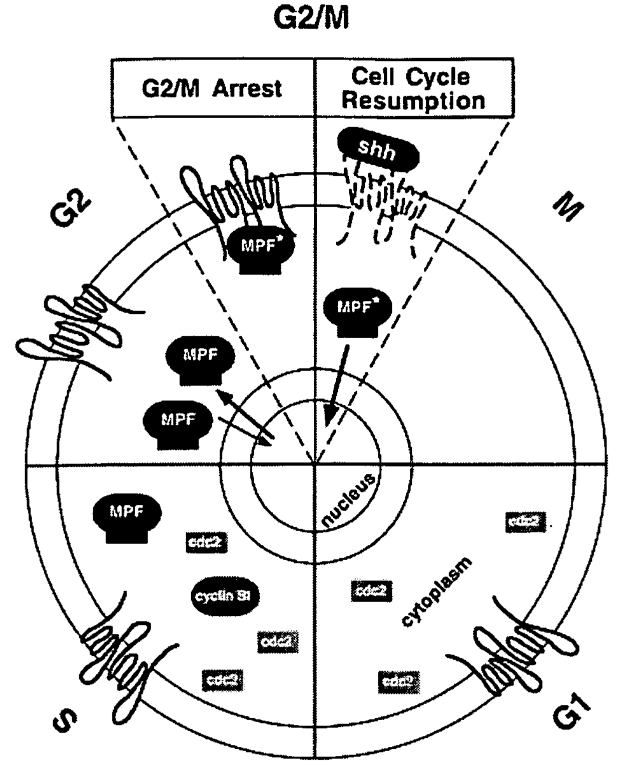

Fig. 7. Model of patched1 regulation of MPF. G_1 phase, cdc2 is present in abundance throughout the cell cycle. S phase, cyclin B1 is synthesized and begins to accumulate in the cytoplasm by late S phase. Cyclin B1 binds to cdc2 via a region termed the cyclin box. G_2 phase, before forming an active MPF complex, cyclin B1–cdc2 enters and rapidly exits the nucleus due to a NES located within the CRS domain. G_2/M transition, cyclin B1 becomes phosphorylated, which creates a fully active MPF complex (MPF*). ptc1 binds to phosphorylated cyclin B1 and sequesters an active MPF complex in pre-mitotic cells which inhibits the translocation of MPF to the nucleus. Cellular exposure to shh promotes the degradation of ptc1, which in turn facilitates the release of cyclin B1. MPF is now available for nuclear import.

In summary, the evidence presented here provides a link between ptc1 signaling and cell cycle progression. However, further work is warranted to assess the entire contribution of MPF activity in the shh–ptc1 pathway and to elucidate the biological conditions required for the regulation of MPF by ptc1.

Materials and methods

Construction of cyclin B1, ptc1 and shh derivatives

The lexA–CRS–CRS (*Xenopus*) fusion proteins for the yeast screen and the lexA–CRS–CRS (human) fusion proteins for the His^- minimal media assays were constructed as described previously (Kong *et al.*, 2000). To construct the fusion protein containing the intracellular loop of human patched1 for the yeast assays, oligonucleotides encoding residues 599–750 were synthesized and incorporated in-frame to the transactivation domain of pVP16.

To construct cyclin B1 derivatives for immunofluorescence studies, oligonucleotides encoding the human CRS domain consisting of residues 110–160 were synthesized and incorporated into the pcDNA3 vector.

To construct NLS–CRS derivatives, a DNA fragment encoding the human CRS domain, consisting of residues 110–160, was ligated in-frame to oligonucleotides encoding the NLS of *Xenopus* nucleoplasmin and then inserted into the pcDNA3 vector.

The full-length cyclin B1 derivatives, NLS–$B1^{Ala}$ and NLS–$B1^{Glu}$, were constructed as described previously (Li *et al.*, 1997). All cyclin B1 constructs used in this study were tagged at the C-terminus with an epitope (GLEVIVVPHSLPFML) derived from glycoprotein G of vesicular stomatitis virus (VSV-G), recognized by mAb P5D4 (Kreis and Lodish, 1986).

To construct the GST–ptc1 derivative (GST–$ptc1^{599-750}$), a DNA fragment encoding the large intracellular loop of human ptc1 consisting of residues 599–750 was ligated in-frame to the mammalian expression vector pEBG.

To construct an epitope-tagged and biologically active derivative of human shh protein (Marigo *et al.* 1996; Stone *et al.* 1996), oligonucleotides encoding residues 1–197 were synthesized and incorporated in-frame to DNA encoding the FLAG-epitope tag (DYKDDDDK) at the C-terminus and inserted into the pcDNA3 vector.

Yeast two-hybrid screen and assays

The *Saccharomyces cerevisiae* strain L40 generated by Dr Stan Hollenberg was transformed with derivatives of pBTM116 (constructed by Dr Paul Bartel and Dr Stan Fields). The derivatives constructed for this work encoded lexA–CRS^{Ala}–CRS^{Ala} (*Xenopus*) or lexA–CRS^{Glu}–CRS^{Glu} (*Xenopus*) fusion proteins; these were screened against a 9.5 d.p.c. mouse embryonic cDNA library encoding fusion proteins with the transactivation domain of pVP16, kindly provided by Dr Stan Hollenberg (Vojtek and Hollenberg, 1995). The two-hybrid screen and His^- minimal media assays were performed as described previously (Kong *et al.*, 2000). The ability to activate the lacZ reporter was also checked by filter assay as described (Vojtek *et al.*, 1993).

Immunoprecipitation assays

Two days after transfection (except for endogenous immunoprecipitations), cells were harvested and lysed with 1.0% NP-40 buffer (Kong *et al.*, 2000). Protein content was standardized as determined by the Bradford assay. Lysates were pre-cleared with protein A–Sepharose beads and then incubated with the indicated antibodies overnight at 4°C. Addition of protein A–Sepharose beads with incubation overnight at 4°C followed. Samples were washed with 0.5% NP-40 buffer and analyzed by SDS–PAGE, transferred to nitrocellulose membrane and detected by ECL. Antibody + blocker samples were treated as described by the manufacturer (Santa Cruz). In brief, antibody (2 μg) was incubated with blocking peptide (10 μg) in 1.0% NP-40 buffer for 2 h at room temperature, and then addition of lysate sample with further incubation overnight at 4°C. For the endogenous immunoprecipitation assay, ptc1 was immunoprecipitated from 1 mg of protein per sample. The lysate sample represents 60 μg of total cell lysate.

Histone H1 kinase assay

For detection of phosphorylation of histone H1 *in vitro* by MPF, 293T cells were transfected with plasmids encoding Myc-tagged ptc1 and proteins were immunoprecipitated with anti-Myc (9E10) antibody after lysis in 1.0% NP-40 buffer. Protein content was standardized as determined by the Bradford assay. Active MPF was obtained by immunoprecipitation with anti-cdc2 antibody (Santa Cruz). The immunoprecipitates were incubated at 30°C for 20 min in 50 μl of kinase reaction buffer as described previously (Li *et al.*, 1995). The reaction was terminated by addition of SDS sample buffer. Samples were analyzed by 10% SDS–PAGE.

Immunofluorescence

Two days after transfection using the calcium phosphate coprecipitation method, COS-1 cells were fixed with 3% paraformaldehyde and permeabilized with 0.1% Triton X-100, 0.2 M glycine and 2.5% fetal bovine serum in phosphate-buffered saline (PBS). Triple-label immunofluorescence was performed as follows: (i) VSV-G-tagged cyclin B1 derivatives were detected with mAb P5D4 and FITC-conjugated goat anti-mouse antiserum; (ii) patched1 expression was visualized using goat antibody pAb patched1 (Santa Cruz) and rhodamine-conjugated rabbit anti-goat antiserum; and (iii) nuclei were stained with Hoechst 33342. Using a modification of techniques described elsewhere (Stone *et al.*, 1996), COS-1 cells were exposed to shh-N-conditioned media from shh-N-expressing cells at 24 h after transfection and allowed to recover for 24 h.

Cellular fractionation

Fractionation samples prepared as described elsewhere (Greenwood and Johnson, 1995) were standardized for protein content by the Bradford assay and then analyzed by 10% SDS–PAGE and transferred to nitrocellulose membrane. VSV-G-tagged NLS–$B1^{Glu}$, Myc-tagged ptc1 and endogenous histone proteins were detected by ECL (Amersham) using mAb P5D4, mAb 9E10 (Santa Cruz) and mAb 052 (Chemicon), respectively. Quantitation of fractionation data is presented as a percentage of NLS-B1^{Glu} protein and was performed using NIH Image software. Using a modification of techniques described elsewhere (Stone *et al.*, 1996), 293T cells were exposed to shh-N-conditioned media from shh-N-expressing cells at 48 h after transfection and then allowed to recover for 24 h. All samples were harvested at the same time (72 h after transfection).

Cell proliferation assay

293T cells were seeded at a density of 1.0×10^5 cells/plate (60 mm) and transfected with 2.5 μg of cyclin B1 DNA and/or 5.0 μg of ptc1 DNA. Cells were trypsinized and counted every 24 h after transfection (day 1). The mean values of three plates are represented (±SEM). Cell lysate samples from the last day were analyzed by 10% SDS–PAGE for protein expression by ECL after transfer to nitrocellulose membrane. For shh-N-induced growth, 293T cells were seeded at a density of 1.0×10^5 cells/plate (60 mm) and transfected with 5.0 μg of cyclin B1 DNA and/or 5.0 μg of ptc1 DNA. Appropriate samples were exposed to shh-N-conditioned media at 24 and 48 h after transfection. At 72 h after transfection, samples were counted. The average of two plates per sample is represented.

Mitotic index assay

Transfected 293T cells were split onto collagen-coated coverslips and allowed to recover for 24 h. Cells were fixed and permeabilized as described previously. Nuclei were stained with Hoechst 33342. Five hundred cells of each sample from three independent transfections were counted (total cells counted per sample = 1500). Results shown represent the average percentage (±SD) of cells displaying a mitotic phenotype over the total number of cells counted.

Acknowledgements

We thank M.P.Scott and J.Ming for providing full-length ptc1 cDNA; S.Hollenberg for two-hybrid constructs; V.Malhotra for kindly providing mAb P5D4; J.-L.Lenormand for advice and encouragement; and members of the D.J.D. laboratory for critical review of the manuscript, particularly R.W.Dellinger for many helpful suggestions. Support from NIH/NCI CA34456 is gratefully acknowledged. E.A.B. is supported by NIH/NCI National Research Service Award #T32 CA09523 and M.K. is supported by NIH/GM07313.

References

Borgne,A. and Meijer,L. (1996) Sequential dephosphorylation of p34^{cdc2} on Thr-14 and Tyr-15 at the prophase/metaphase transition. *J. Biol. Chem.*, **271**, 27847–27854.

Borgne,A., Ostvold,A.C., Flament,S. and Meijer,L. (1999) Intra-M phase-promoting factor phosphorylation of cyclin B at the prophase/metaphase transition. *J. Biol. Chem.*, **274**, 11977–11986.

Carpenter,D., Stone,D.M., Brush,J., Ryan,A., Armanini,M., Frantz,G., Rosenthal,A. and de Sauvage,F.J. (1998) Characterization of two patched receptors for the vertebrate hedgehog protein family. *Proc. Natl Acad. Sci. USA*, **95**, 13630–13634.

Chen,Y. and Struhl,G. (1996) Dual roles for patched in sequestering and transducing hedgehog. *Cell*, **87**, 553–563.

Chidambaram,A., Goldstein,A.M., Gailani,M.R., Gerrard,B., Bale,S.J., DiGiovanna,J.J., Bale,A.E. and Dean,M. (1996) Mutations in the human homologue of the *drosophila/patched* gene in caucasian and African-American nevoid basal cell carcinoma syndrome patients. *Cancer Res.*, **56**, 4599–4601.

Dean,M. (1997) Towards a unified model of tumor suppression: lessons learned from the human *patched* gene. *Biochim. Biophys. Acta*, **1332**, M43–M52.

Denef,N., Neubuser,D., Perez,L. and Cohen,S.M. (2000) Hedgehog induces opposite changes in turnover and subcellular localization of patched and smoothened. *Cell*, **102**, 521–531.

Ducommun,B., Brambilla,P., Felix,M.-A., Franza,B.R.,Jr, Karsenti,E. and Draetta,G. (1991) Cdc2 phosphorylation is required for its interaction with cyclin. *EMBO J.*, **10**, 3311–3319.

Gailani,M.R. and Bale,A.E. (1997) Developmental genes and cancer: role of patched in basal cell carcinoma of the skin. *J. Natl Cancer Inst.*, **89**, 1103–1109.

Gailani,M.R. *et al.* (1996) The role of the human homologue of *drosophila/patched* in sporadic basal cell carcinomas. *Nature Genet.*, **14**, 78–81.

Goodrich,L.V. and Scott,M.P. (1998) Hedgehog and patched in neural development and disease. *Neuron*, **21**, 1243–1257.

Goodrich,L.V., Johnson,R.L., Milenkovic,L., McMahon,J.A. and Scott,M.P. (1996) Conservation of the *hedgehog/patched* signaling pathway from flies to mice: induction of a mouse *patched* gene by hedgehog. *Genes Dev.*, **10**, 301–312.

Gorlin,R.J. (1995) Nevoid basal cell carcinoma syndrome. *Dermatol. Clin.*, **13**, 113–125.

Greenwood,J.A. and Johnson,G.V.W. (1995) Localization and *in situ* phosphorylation state of nuclear tau. *Exp. Cell Res.*, **220**, 332–337.

Hagting,A., Karlsson,C., Clute,P., Jackman,M. and Pines,J. (1998) MPF localization is controlled by nuclear export. *EMBO J.*, **17**, 4127–4138.

Hagting,A., Jackman,M., Simpson,K. and Pines,J. (1999) Translocation of cyclin B1 to the nucleus at prophase requires a phosphorylation-dependent nuclear import signal. *Curr. Biol.*, **9**, 680–689.

Hahn,H. *et al.* (1996a) A mammalian *patched* homolog is expressed in target tissues of Sonic hedgehog and maps to a region associated with developmental abnormalities. *J. Biol. Chem.*, **271**, 12125–12128.

Hahn,H. *et al.* (1996b) Mutations of the human homolog of *drosophila/patched* in the nevoid basal cell carcinoma syndrome. *Cell*, **85**, 841–851.

Incardona,J.P., Lee,J.H., Robertson,C.P., Enga,K., Kapur,R.P. and Roelink,H. (2000) Receptor-mediated endocytosis of soluble and membrane-tethered sonic hedgehog by patched-1. *Proc. Natl Acad. Sci. USA*, **97**, 12044–12049.

Jin,P., Hardy,S. and Morgan,D.O. (1998) Nuclear localization of cyclin B1 controls mitotic entry after DNA damage. *J. Cell Biol.*, **141**, 875–885.

Johnson,R.L. *et al.* (1996) Human homolog of *patched*, a candidate gene for the basal cell nevus syndrome. *Science*, **272**, 1668–1671.

Kong,M., Barnes E.A., Ollendorff,V. and Donoghue,D.J. (2000) Cyclin F regulates the nuclear localization of cyclin B1 through a cyclin–cyclin interaction. *EMBO J.*, **19**, 1378–1388.

Kreis,T.E. and Lodish,H.F. (1986) Oligomerization is essential for transport of vesicular stomatitis viral glycoprotein to the cell surface. *Cell*, **46**, 929–937.

Krek,W. and Nigg,E.A. (1991) Differential phosphorylation of vertebrate p34^{cdc2} kinase at the G$_1$/S and G$_2$/M transitions of the cell cycle: identification of major phosphorylation sites. *EMBO J.*, **10**, 305–316.

Lee,J.J., Ekker,S.C., von Kessler,D.P., Porter,J.A., Sun,B.I. and Beachy,P.A. (1994) Autoproteolysis in *hedgehog* protein biogenesis. *Science*, **266**, 1528–1537.

Li,J., Meyer,A.N. and Donoghue,D.J. (1995) Requirement for phosphorylation of cyclin B1 for *Xenopus* oocyte maturation. *Mol. Biol. Cell*, **6**, 1111–1124.

Li,J., Meyer,A.N. and Donoghue,D.J. (1997) Nuclear localization of cyclin B1 mediates its biological activity and is regulated by phosphorylation. *Proc. Natl Acad. Sci. USA*, **94**, 502–507.

Marigo,V., Davey,R.A., Zuo,Y., Cunningham,J.M. and Tabin,C.J. (1996) Biochemical evidence that patched is the hedgehog receptor. *Nature*, **384**, 176–179.

Murone,M., Rosenthal,A. and de Sauvage,F.J. (1999) Sonic hedgehog signaling by the patched–smoothened receptor complex. *Curr. Biol.*, **9**, 76–84.

Murray,A.W., Solomon,M.J. and Kirschner,M.W. (1989) The role of cyclin synthesis and degradation in the control of maturation promoting factor activity. *Nature*, **339**, 280–286.

Norbury,C., Blow,J. and Nurse,P. (1991) Regulatory phosphorylation of the p34^{cdc2} protein kinase in vertebrates. *EMBO J.*, **10**, 3321–3329.

Peter,M., Nakagawa,J., Doree,M., Labbe,J.C. and Nigg,E.A. (1990) *In vitro* disassembly of the nuclear lamina and M phase-specific phosphorylation of lamins by cdc2 kinase. *Cell*, **61**, 591–602.

Pines,J. and Hunter,T. (1994) The differential localization of human cyclins A and B is due to a cytoplasmic retention signal in cyclin B. *EMBO J.*, **13**, 3772–3781.

Pondaven,P., Meijer,L. and Beach,D. (1989) Activation of M-phase-specific histone H1 kinase by modification of the phosphorylation of its p34^{cdc2} and cyclin components. *Genes Dev.*, **4**, 9–17.

Solomon,M.J., Glotzer,M., Lee,T.H., Philippe,M. and Kirschner,M.W. (1990) Cyclin activation of p34^{cdc2}. *Cell*, **63**, 1013–1024.

Stone,D.M. *et al.* (1996) The tumour-suppressor gene *patched* encodes a candidate receptor for Sonic hedgehog. *Nature*, **384**, 129–134.

Toyoshima,F., Moriguchi,T., Wada,A., Fukuda,M. and Nishida,E.

(1998) Nuclear export of cyclin B1 and its possible role in the DNA damage-induced G_2 checkpoint. *EMBO J.*, **17**, 2728–2735.

Unden,A.B., Holmberg,E., Lundh-Rozell,B., Stahle-Backdahl,M., Zaphiropoulos,P.G., Toftgard,R. and Vorechovsky,I. (1996) Mutations in the human homologue of *drosophila/patched* (*PTCH*) in basal cell carcinomas and the gorlin syndrome: different *in vivo* mechanisms of *PTCH* inactivation. *Cancer Res.*, **56**, 4562–4565.

Unden,A.B., Zaphiropoulos,P.G., Bruce,K., Toftgard,R. and Stahle-Backdahl,M. (1997) Human *patched* (*PTCH*) mRNA is overexpressed consistently in tumor cells of both familial and sporadic basal cell carcinoma. *Cancer Res.*, **57**, 2336–2340.

Verde,F., Dogterom,M., Stelzer,E., Karsenti,E. and Leibler,S. (1992) Control of microtubule dynamics and length by cyclin A- and cyclin B-dependent kinases in *Xenopus* egg extracts. *J. Cell Biol.*, **118**, 1097–1108.

Vojtek,A.B. and Hollenberg,S.M. (1995) Ras–raf interaction: two-hybrid analysis. *Methods Enzymol.*, **255**, 331–342.

Vojtek,A.B., Hollenberg,S.M. and Cooper,J.A. (1993) Mammalian ras interacts directly with the serine/threonine kinase raf. *Cell*, **74**, 205–214.

Weinberg,R.A. (1995) The retinoblastoma protein and cell cycle control. *Cell*, **81**, 323–330.

Yamashiro,S., Yamakita,Y., Hosoya,H. and Matsumura,F. (1991) Phosphorylation of non-muscle caldesmon by $p34^{cdc2}$ kinase during mitosis. *Nature*, **349**, 169–172.

Yang,J. and Kornbluth,S. (1999) All aboard the cyclin train: subcellular trafficking of cyclins and their CDK partners. *Trends Cell Biol.*, **9**, 207–210.

Yang,J., Bardes,E.S.G., Moore,J.D., Brennan,J., Powers,M.A. and Kornbluth,S. (1998) Control of cyclin B1 localization through regulated binding of the nuclear export factor CRM1. *Genes Dev.*, **12**, 2131–2143.

Received January 10, 2001; revised and accepted March 6, 2001

Cell, Vol. 75, 1431–1444, December 31, 1993, Copyright © 1993 by Cell Press

A Functionally Conserved Homolog of the Drosophila Segment Polarity Gene *hh* Is Expressed in Tissues with Polarizing Activity in Zebrafish Embryos

S. Krauss, J.-P. Concordet, and P. W. Ingham
Molecular Embryology Laboratory
Imperial Cancer Research Fund
Developmental Biology Unit
Department of Zoology
South Parks Road
Oxford OX1 3PS
England

Summary

The segment polarity gene *hedgehog* (*hh*) encodes a novel signaling protein that mediates local cell–cell interactions in the developing Drosophila embryo. Here we describe the existence of an *hh*-related gene family in the zebrafish, Brachydanio rerio. One of these genes, *sonic hedgehog* (*shh*), is expressed in the notochord, floor plate, and posterior fin mesoderm, tissues associated with polarizing activities in various vertebrate embryos. The pattern of *shh* expression in zebrafish mutants affecting axial structures, together with the consequences of its ectopic expression in normal embryos, is consistent with a role for *shh* in floor plate induction. By expressing *shh* in transgenic Drosophila embryos, we also demonstrate a strong functional conservation between the fish and fly *hh* genes.

Introduction

Inductive interactions are of fundamental importance to the development of all multicellular organisms, and understanding their molecular basis represents a major goal of contemporary developmental biology. Recent analyses have revealed a remarkable degree of conservation among the components of signal transduction pathways implicated in a number of such interactions, both within and between species (see Egan and Weinberg, 1993). Thus, it seems that relatively few pathways may have evolved to execute the variety of inductive interactions that characterize vertebrate and invertebrate development.

In the developing Drosophila embryo, positional specification along the anteroposterior axis of each body segment depends upon cellular interactions controlled by the segment polarity genes (Nüsslein-Volhard and Wieschaus, 1980), a molecularly heterogeneous group encoding proteins as diverse as transcription factors, such as the product of the *engrailed* gene (DiNardo et al., 1985; Jaynes and O'Farrell, 1991), or membrane-associated proteins, such as the β-catenin homolog encoded by *armadillo* (Peifer and Weischaus, 1990). Two members of the segment polarity class, *wingless* (*wg*) and *hedgehog* (*hh*), have been singled out as being key players in the cell patterning process; these genes are expressed in distinct groups of cells at each parasegment border that seem to organize the positional specification of cells within each segment (reviewed by Ingham and Martinez-Arias, 1992). Whereas *wg* belongs to the well-characterized *Wnt* gene family of growth factor–like molecules (reviewed by McMahon, 1992; Nusse and Varmus, 1992), the *hh* gene product has a primary structure unlike that of any previously described protein (Lee et al., 1992; Mohler and Vani, 1992; Tabata et al., 1992; Tashiro et al., 1993). Analysis of the *hh* sequence predicts a protein with a single hydrophobic region that may act either as a signal sequence or a membrane-spanning domain. This structure is consistent with the functional analysis of *hh*, which implicates it in cell–cell interactions that maintain the expression of *wg* at parasegment borders (Hidalgo and Ingham, 1990; Ingham and Hidalgo, 1993).

In vertebrate embryos, one of the best-characterized sources of signaling activity is the notochord, the derivative of the axial mesoderm. Several processes have been associated with the inductive properties of this tissue, including the induction of specialized ventral neural cells that form the floor plate (van Straaten et al., 1989; Placzek et al., 1990) and the specification of neuronal differentiation (Placzek et al., 1991; Yamada et al., 1991). Evidence for these interactions comes principally from experimental manipulations of developing embryos; in the chick, ablation of the notochord results in a failure of floor plate and motor neuron differentiation, whereas grafting of notochord to ectopic locations results in the induction of ectopic floor plate and motor neurons in close proximity to the graft. Since notochord is closely apposed to floor plate cells both in normal development and in the experimentally manipulated embryos, it has been suggested that the inductive signal must be contact dependent (Placzek et al., 1990), a conclusion supported by the results of in vitro studies (Placzek et al., 1993). Motor neuron differentiation, by contrast, depends upon diffusible factors that act in a contact-independent manner (Yamada et al., 1993).

Although a number of different genes have recently been shown to be specifically expressed in one or the other of these tissues, none presents itself as an outstanding candidate for either signaling activity (reviewed by Ruiz i Altaba and Jessell, 1993). In this paper we describe the cloning and characterization of a zebrafish homolog of the Drosophila segment polarity gene *hh*, which we show to be highly conserved both structurally and functionally. Several features of this gene makes its product a candidate for a floor plate–inducing factor; these features are discussed in the context of normal and mutant zebrafish development.

Results

Molecular Cloning of Zebrafish *hh* Homologs

In an initial attempt to isolate sequences homologous to Drosophila *hh*, a zebrafish genomic DNA library was screened at reduced stringency with a partial cDNA, *hhPCR4.1*, corresponding to the first and second exons of the Drosophila gene (Mohler and Vani, 1992). This screen proved unsuccessful; however, a similar screen of a

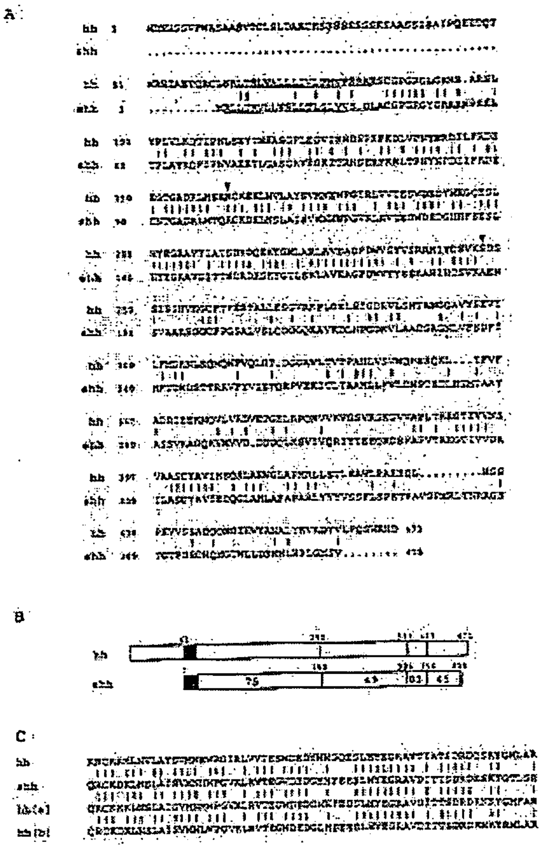

Figure 1. Comparison of Zebrafish Shh and Drosophila Hh Amino Acid Sequences

(A) Alignment of zebrafish shh and Drosophila hh amino acid sequences. Identical amino acids are linked by vertical bars; dots indicate gaps introduced for optimal alignment. Putative transmembrane/signal peptide sequences are underlined (Kyte and Doolittle, 1982). The position of exon boundaries in the Drosophila gene are indicated by arrowheads. The region of highest homology between *shh* and *hh* overlaps exon 2.

(B) Schematic comparison of zebrafish shh and Drosophila hh. Closed boxes indicate the position of the putative transmembrane/signal peptide sequences relative to the amino terminus. Sequence homologies were scored by taking into account the alignment of chemically similar amino acids, and percentage of homology in the boxed regions is indicated.

(C) A family of *hh* homologs in zebrafish. Using degenerate oligonucleotides corresponding to regions of high conservation between *hh* and the mouse homolog *Dhh*, three different fragments were amplified from zebrafish genomic DNA. One of these corresponded to *shh*, while the others define additional *hh* homologs in zebrafish, named *hh[a]* and *hh[b]*.

mouse genomic library performed by Echelard et al. (1993 [this issue of *Cell*]) yielded a single clone with significant homology to *hh*, subsequently designated *Desert hedgehog* (*Dhh*). A 264 bp BamHI–EcoRI fragment from this clone containing sequences homologous to the second exon of the Drosophila gene was subcloned and, together with the Drosophila partial cDNA fragment, was used to screen a λgt11 zebrafish cDNA library that was prepared from RNA extracted from 33-hr-old embryos (K. Zinn, personal communication). This screen yielded four clones with overlapping inserts, the longest of which is 1.6 kb in length; we refer to this gene as *sonic hedgehog* (*shh*).

A Family of Zebrafish Genes Homologous to the Drosophila Segment Polarity Gene *hh*

Alignment of the predicted amino acid sequences of the shh and hh proteins revealed an identity of 47%, confirming that *shh* is a true homolog of the Drosophila gene. A striking conservation occurs within exon 2: an 80 amino acid long domain shows 72% identity between shh and hh (Figures 1A and 1B). This domain is highly conserved in all the *hh*-related genes cloned so far (Figure 1C; Echelard et al., 1993; Riddle et al., 1993 [this issue of *Cell*]) and is therefore likely to be essential to the function of hh proteins. A second domain of approximately 30 amino acids close to the carboxy-terminal end, though it shows only 61% amino acid identity, possesses 83% similarity between shh and hh when allowing for conservative substitutions and could also, therefore, be of functional importance (Figure 1B). Although putative sites of posttranslational modification can be noted, their position is not conserved between shh and hh.

Lee et al. (1992) identified a hydrophobic stretch of 21 amino acids flanked downstream by a putative site of signal sequence cleavage (predicted by the algorithm of von Heijne, 1986) close to the amino-terminal end of hh. Both the hydrophobic stretch and the putative signal sequence

Figure 2. Localization of *shh* Transcripts in Wild-Type Zebrafish Embryos

Whole embryos were hybridized with digoxygenin-labeled *shh* riboprobe.

(A and B) Dorsal (A) and lateral (B) views of *shh* expression at 70% epiboly (the extent of spreading of the blastoderm over the yolk toward the vegetal pole is used as a staging index during epiboly) (Westerfield, 1989). Note the restriction of transcript to the inner cell layer (hypoblast).

(C) Lateral view of an embryo at the 100% epiboly bud stage; by this stage, *shh* expression extends to the animal pole.

(D) Embryo at 11.5 hr of development. The arrowhead denotes the row of floor plate cells in the neural keel and the underlying notochord cells that express *shh*.

(E) Embryo at 20 hr of development (22 somites). The arrowhead indicates the notochord that has now switched off *shh* expression; expression persists at high levels in the floor plate cells (shown in detail in [G]).

(F) Embryo at 26 hr of development (end of somitogenesis). The arrowhead marks *shh* expression in the telencephalon.

(G) Detail of the trunk region of a 20 hr embryo, similar to that shown in (E), showing *shh* expression exclusively in the floor plate.

(H and I) Lateral view (H) and top view (I) of an embryo at 33 hr of development, showing *shh* expression at the posterior end of the pectoral fin bud (arrowhead) and in the first gill (arrow).

(J) Pectoral fin bud of a 33 hr embryo; note that *shh* expression is confined to the mesoderm and that the superficial epithelial cell layer is devoid of *shh* expression.

Abbreviations: d, dorsal; eb, epiblast; fp, floor plate; hb, hypoblast; hp, head process; nc, notochord; nk, neural keel; and tb, tail bud.

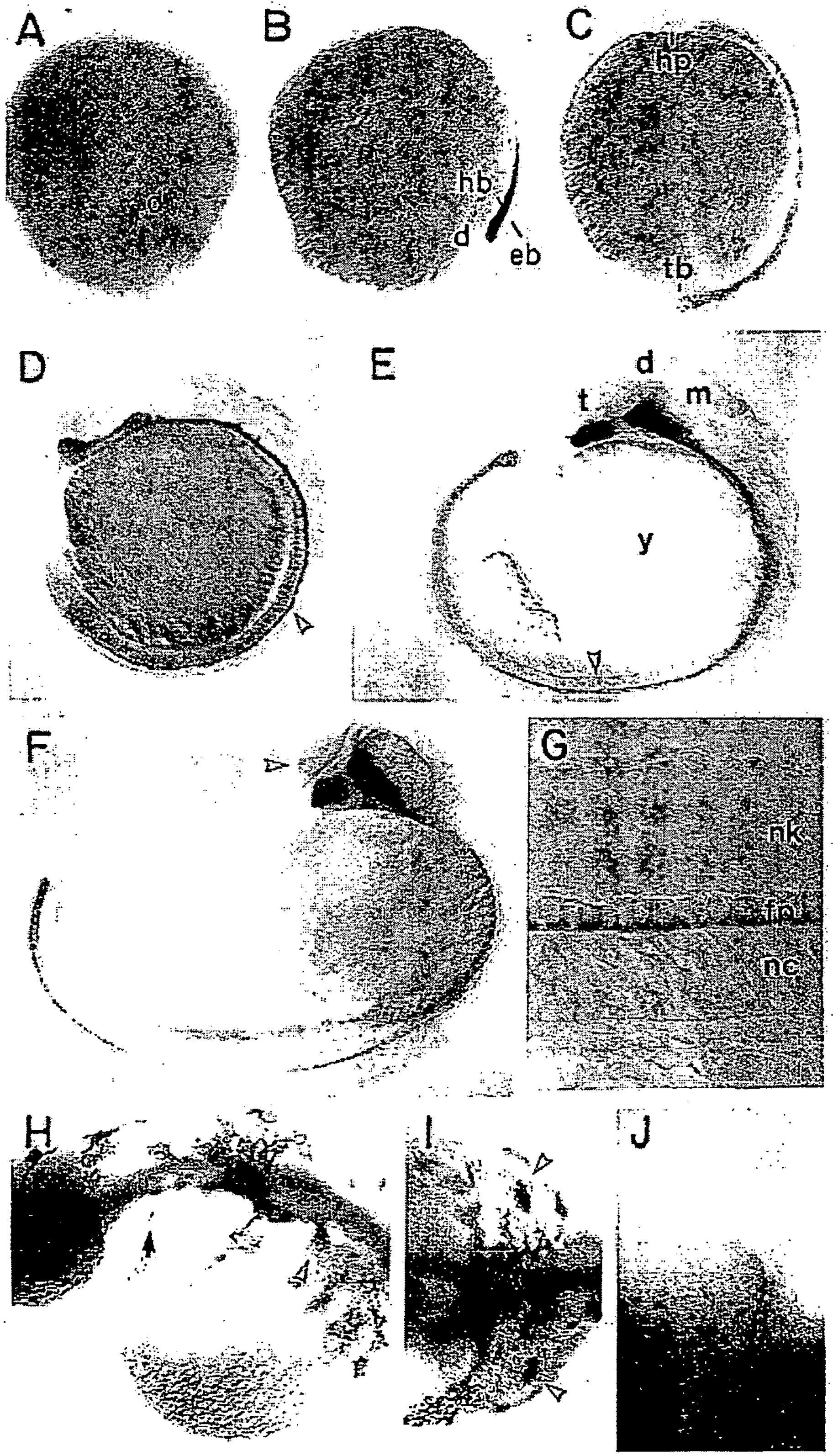
A
d
B
hb
d
eb
C
hp
tb
D
E
d
t
m
y
F
G
nk
fp
nc
H
I
J

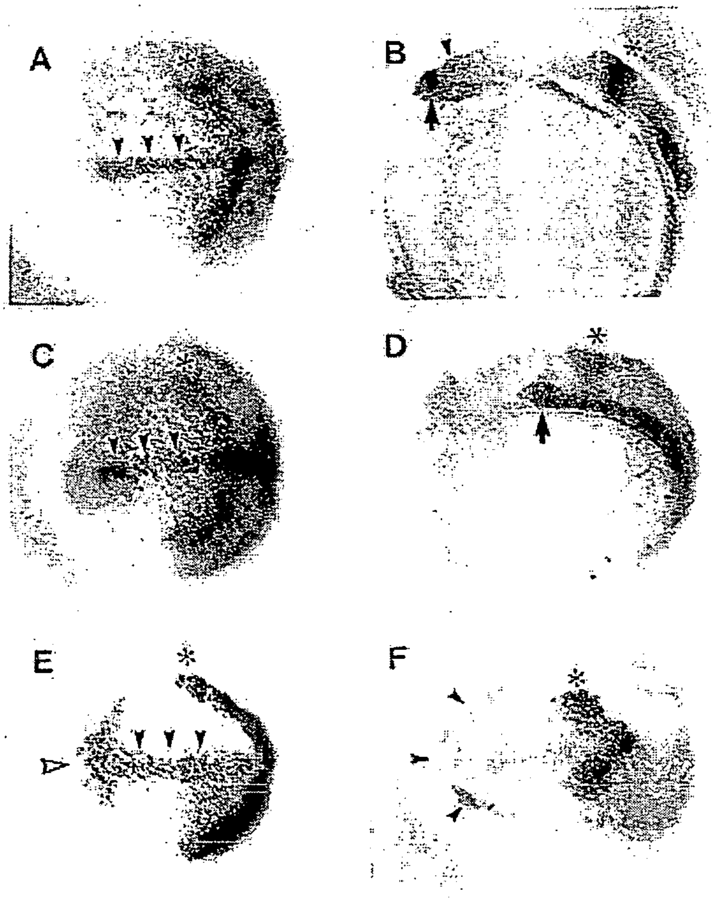

Figure 3. Comparison of *shh* Expression with Expression of *axial*, *gsc*, and *pax-2* in the Head Process of Wild-Type Embryos during Early Embryogenesis

(A, C, and E) At 10 hr of development (end of gastrulation). (B, D, and F) At the five somite stage. (A, C, E, and F) Viewed from the animal pole. (B and D) Lateral views.

(A) *shh* (horizontal line, marked by arrowheads) and *pax-2* (lateral stripes, marked by an asterisk) expression at the end of gastrulation.

(B) *shh* and *pax-2* at the 5 somite stage; *pax-2* expression in the posterior midbrain is marked by an asterisk; and the optic stalk is marked by a small arrowhead. *shh* expression in the tip of the neural keel is shown by an arrow.

(C) *axial* (arrowheads) and *pax-2* (asterisk) expression at the end of gastrulation. Note that the anterior *axial* expression at this developmental stage compares to the anterior boundary of the *shh* expression (see [A]).

(D) *axial* and *pax-2* (asterisk) expression at the 5 somite stage. Note that, in contrast with *shh*, *axial* expression in the forebrain has now been turned off and extends only to the ventral midbrain/hypothalamus boundary.

(E) *gsc* (arrowheads) and *pax-2* (asterisk) expression at the end of gastrulation. Note that *gsc* expression extends further rostral than *shh* (large arrowhead).

(F) *gsc* (arrowheads) and *pax-2* (asterisk) at the tail bud stage.

cleavage sites of hh, which suggest it to be a signaling molecule, are conserved in shh. In contrast to hh, shh does not extend amino-terminally to the hydrophobic stretch.

Using degenerate oligonucleotides corresponding to amino acids flanking the domain of high homology between Drosophila *hh* and mouse *Dhh* exons 2 described by Echelard et al. (1993), fragments of the expected size were amplified from zebrafish genomic DNA by polymerase chain reaction (PCR). Three different *hh*-related sequences were identified amongst 30 independent PCR products analyzed, all of which show high homology to one another and to Drosophila *hh* (Figure 1C). One of these corresponds to *shh*, while the other two represent additional zebrafish *hh* homologs. cDNAs corresponding to one of these additional homologs have recently been isolated (J.-P. C. and S. K., unpublished data), confirming that it is transcribed. Therefore, *shh* represents a member of a novel vertebrate gene family.

shh Expression in the Developing Zebrafish Embryo

Gastrula Stages

We first detect *shh* expression at around the 60% epiboly stage of embryogenesis in the dorsal mesoderm. Transcripts are restricted to the inner cell layer of the embryonic shield, the equivalent of the amphibian organizer (Figures 2A and 2B). During gastrulation, presumptive mesodermal

---

Figure 4. Tissue Sections of Hybridized Embryos Showing *shh* Expression at Different Developmental Stages

(A–D) Successive transverse sections through the hindbrain of an embryo at the 5 somite stage showing *shh* expression. (A) Anterior hindbrain. (B) Hindbrain at the anterior tip of the notochord. (C) Hindbrain at the position of the otic placode. (D) Posterior hindbrain.

(E) Transverse section through the tail of an embryo at the 5 somite stage.

(F) Horizontal section through the spinal cord of an embryo at 26 hr of development. Note the single row of floor plate cells that express *shh*.

(G and H) Transverse sections through a 48 hr zebrafish embryo. (G) Section through the diencephalon. *shh* expression is seen in the luminal cells of the foregut and in periventricular cells in the diencephalon (arrowheads). (H) Transverse section at the level of the pectoral fin buds.

(I–M) Serial transverse sections through the head of a 26 hr embryo.

Unless indicated, dorsal is to the top. Abbreviations: d, diencephalon; e, eye; fp, floor plate; ft, foregut; ht, hypothalamus; m, mesencephalon; nc, notochord; nt, neural tube; op, otic placode; pf, pectoral fin; s, somite; and t, telencephalon.

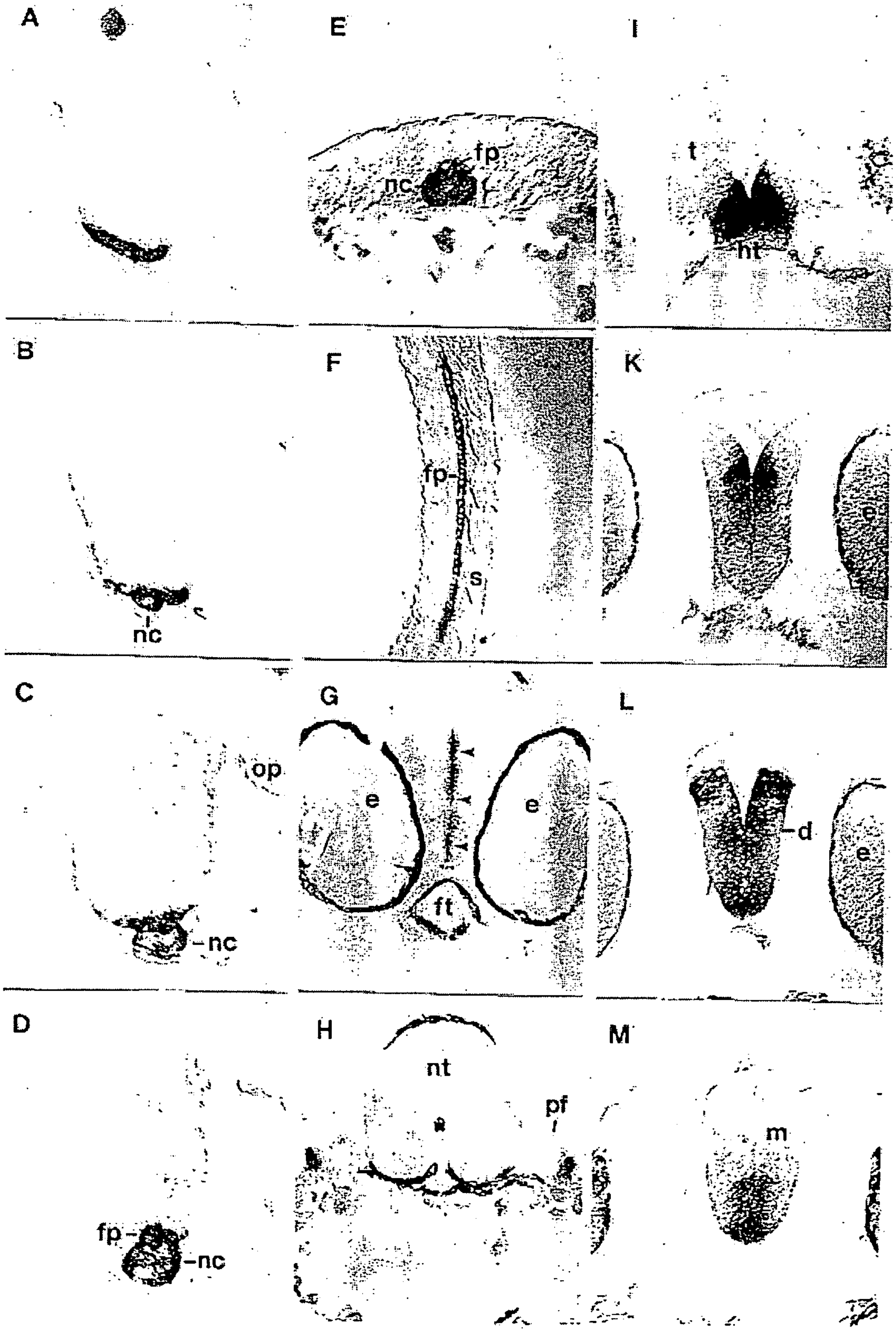
A
E
I
fp
nc
t
nt
B
F
K
fp
s
e
nc
C
G
L
op
e
e
d
e
ft
nc
D
H
M
nt
pf
m
fp
nc

cells involute to form the hypoblast and converge toward the future axis of the embryo, reaching the animal pole at approximately 70% epiboly. At this stage, *shh*-expressing cells extend over the posterior third of the axis; the signal intensity is not uniform, appearing stronger at the base than at the apex of the elongating triangle of cells. This early spatial distribution of *shh* transcript is reminiscent of that previously described for *axial*, a *forkhead/HNF3-B*-related gene; however, at 80% epiboly, *axial* expression extends further toward the animal pole of the embryo (compare Figure 2B with Figure 4D of Strähle et al., 1993).

By 100% epiboly, at 9.5 hr of development, the *shh* expression domain now constitutes a continuous band of cells that extends into the head (Figure 2C). To determine the precise anterior boundary of *shh* expression, embryos were simultaneously hybridized with probes for *shh* and the paired box–containing gene *pax-2* (previously *pax[b]*), the early expression domain of which marks the posterior midbrain (Krauss et al., 1991). By this stage, the anterior boundary of the *shh* expression domain is positioned in the center of the animal pole and coincides approximately with that of *axial* (compare Figures 3A and 3C). At the same stage, prechordal plate cells expressing the homeobox gene *goosecoid* (*gsc*) overlap and underly the presumptive forebrain (Schulte-Merker et al., 1994a; Stachel et al., 1993) (Figure 3E). Sections of stained embryos suggest that in the head, *shh* may by this stage be expressed exclusively in neuroectodermal tissue (data not shown).

Somitogenesis

By the onset of somitogenesis (approximately 10.5 hr of development), *shh* expression in the head is clearly restricted to the ventral floor of the brain, extending from the tip of the forebrain caudally through the hindbrain (Figure 3B). At this stage, expression of *axial* is similarly restricted to the floor of the brain; in contrast with *shh*, however, it extends only as far as the anterior boundary of the midbrain (Figure 3D). At this point, *gsc* expression has become very weak and is restricted to a ring of cells that appear to be migrating away from the dorsal midline (Figure 3F; see also Schulte-Merker et al., 1994a).

As somitogenesis continues, *shh* expression extends in a rostral to caudal progression throughout the ventral region of the central nervous system (CNS) (see Figure 2D). Along the spinal cord, the expression domain is restricted to a single row of cells, the floor plate (Figure 4E), but gradually broadens in the hindbrain and midbrain to become five to seven cells in diameter (Figures 4A–4D), with a triangular-shaped lateral extension in the ventral diencephalon and two strongly staining bulges at the tip of the forebrain, presumably in a region fated to become hypothalamus.

As *shh* transcription is activated in the floor plate, expression in the underlying mesoderm begins to fade away, in a manner similar to that in *axial* (Strähle et al., 1993). This down-regulation also proceeds in a rostral to caudal sequence, coinciding with the changes in cell shape that accompany notochord differentiation. By the 22 somite stage, *shh* expression is restricted to the caudal region of the notochord and to a bulge of undifferentiated cells in the expanding tail bud, but extends throughout the length of the floor plate (see Figures 2E and 2G; Figure 4F). Subsequently, expression in the ventral midbrain broadens into a rhomboid area, and a narrow stripe of expressing cells extends dorsally on either side of the third ventricle to the epiphysis (see Figure 2F; Figures 4K–4M). The most rostral *shh*-expressing cells are confined to the hypothalamus (Figure 4I). In the telencephalon, additional *shh* expression is initiated in two 1- to 2-cell wide stripes (see Figure 2F). By 36 hr of development, *shh* expression in the ventral CNS has undergone further changes. While expression persists in the floor plate of the tail bud, more rostrally located floor plate cells in the spinal cord cease to express the gene. In contrast, in the hindbrain and forebrain, *shh* expression persists and is further modified (data not shown).

At 26–28 hr, *shh* expression appears in the pectoral fin primordia, which are visible as placode-like accumulations of cells underneath the epithelium that covers the yolk. By 33 hr of development, high levels of transcript are present in the posterior margin of the pectoral buds (see Figures 2H–2J); at the same time, expression is initiated in a narrow stripe at the posterior margin of the first gill (see Figure 2H). Expression continues in the pectoral fin buds in lateral cells in the early larva (Figure 4H). At this stage, *shh* transcripts are also detectable in cells adjacent to the lumen of the foregut (Figure 4G).

Expression of *shh* in *no tail* and *cyclops* Mutants

Two mutations affecting axial tissues that express *shh* have been described in zebrafish. Homozygous *no tail* (*ntl*) embryos are characterized by a failure in notochord maturation and a disruption of normal development of tail

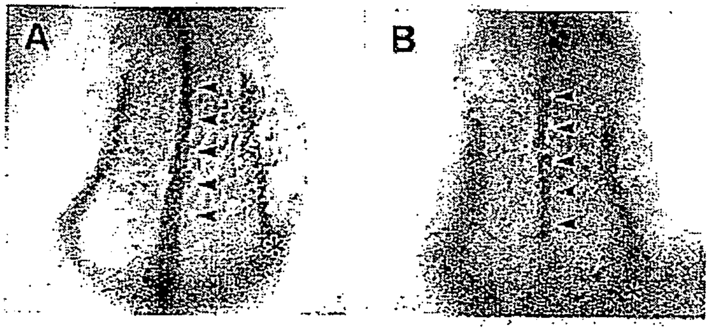

Figure 5. Comparison of *shh* Expression in *ntl* Mutant Embryos and Wild-Type Embryos at the Tail Bud Stage

Rostral is to the top. The expression of *pax-2* in the Wolffian duct (asterisk) serves as a positional marker. Note the slightly uneven distribution of *shh*-expressing cells in the notochord precursor cells (arrowheads) of the *ntl* embryo (see also Halpern et al., 1993) (B) compared with the even rod-like distribution in wild-type embryos (A).

structures (Halpern et al., 1993), whereas embryos homozygous for the *cyclops* (*cyc*) mutation have a normal notochord but lack a differentiated floor plate (Hatta et al., 1991).

No *shh* expression is seen in mesodermal tissue of *ntl* embryos at 24 hr of development, consistent with the lack of a notochord in these embryos; by contrast, *shh* expression throughout the ventral neural tube is unaffected (data not shown). At the tail bud stage, however, just prior to the onset of somitogenesis, *shh* expression is clearly detectable in notochord precursor cells (Figure 5B).

In homozygous *cyc* embryos, a change in *shh* expression is apparent as early as the end of gastrulation; at this stage, the anterior limit of expression coincides with the two *pax-2* stripes in the posterior midbrain (Figure 6A). Thus, in contrast with wild-type embryos, no *shh* expression is detected in midline structures of the midbrain and forebrain (compare Figures 6A and 6B). By the 5 somite stage, *shh* transcripts are present in the notochord, which at this stage extends up to rhombomere 4, beneath the otic placode. Furthermore, no *shh* expression is detected in the ventral neural keel, in particular in the ventral portions of the midbrain and forebrain (Figures 6C and 6D).

At 24 hr of development, the morphologically visible *cyc*

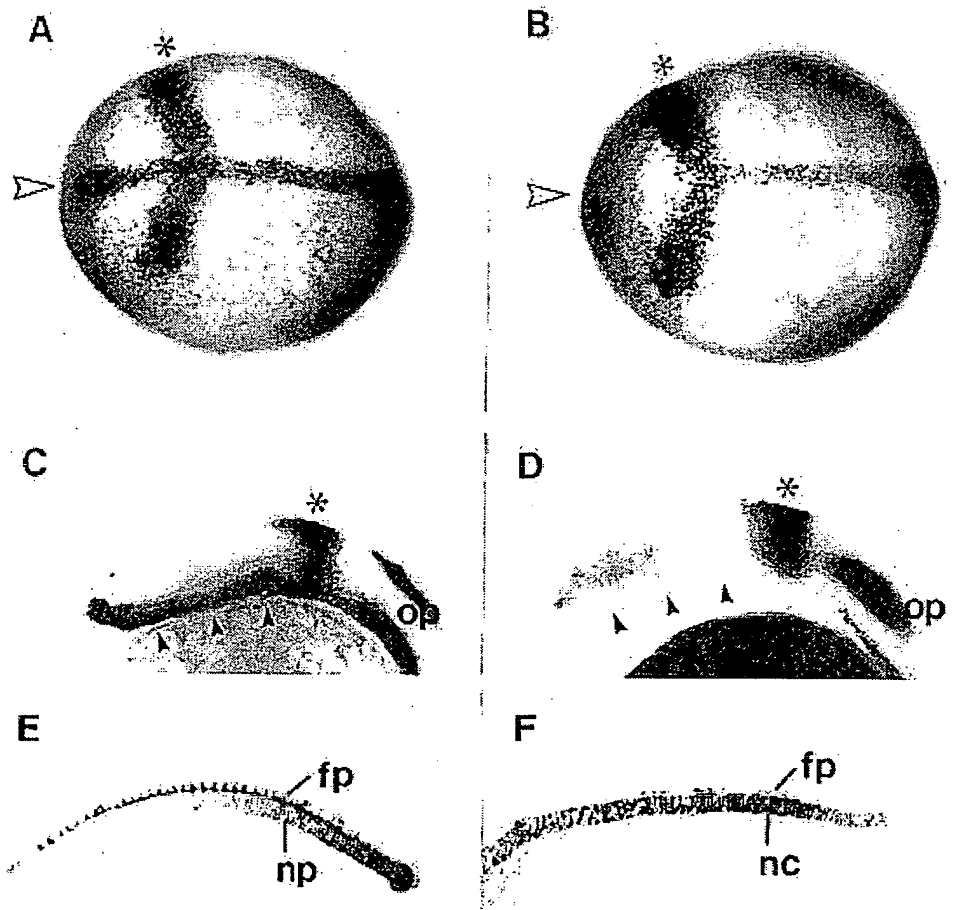

Figure 6. Comparison of *shh* Expression in *cyc* Mutant Embryos and Wild-Type Embryos

The right-hand panels show *cyc* mutant embryos; the left-hand ones show wild-type embryos. Animal pole and lateral views are shown; rostral is to the left. Embryos were simultaneously hybridized with a probe for *pax-2* that serves as a positional marker for the posterior midbrain (asterisk).

(A and B) Embryos at the end of gastrulation. Midline *shh* expression is marked by an arrowhead. Note the absence of the *shh* transcript in the head process rostral to the *pax-2* expression in the mutant embryo (B).

(C and D) Embryos at the 5 somite stage. *shh* expression in the ventral neural keel is indicated by arrowheads (C); its absence in *cyc* embryos (D) is indicated by arrowheads.

(E and F) *shh* expression in the tail bud at the end of somitogenesis. Note that *shh* is absent from the ventral CNS of *cyc* mutant embryos.

Abbreviations: fp, floor plate (in *cyc*, fp marks the region where the floor plate would normally form); and nc, notochord.

phenotype consists of a fusion of the eyes at the midline due to the complete absence of the ventral forebrain. As at earlier developmental stages, *shh* expression is absent from neural tissue. As shown in Figure 6E, *shh* expression in the extending tail bud of wild-type embryos is seen as a single row of floor plate cells throughout the spinal cord. In a *cyc* mutant, no such *shh* activation occurs in cells of the ventral spinal cord (Figure 6F), with the exception of some scattered cells that show transient expression near the tail. Similarly, no *shh* expression is seen rostrally in the ventral neural tube. However, a small group of *shh*-expressing cells is detected underneath the epiphysis that presumably correspond to the dorsal-most group of *shh*-expressing cells in the diencephalon of wild-type embryos (data not shown).

Injection of Synthetic *shh* Transcripts Into Zebrafish Embryos Induces Expression of a Floor Plate Marker

To investigate the activity of *shh* in the developing embryo, we adopted an overexpression strategy, similar to that employed in the analysis of gene function in Xenopus.

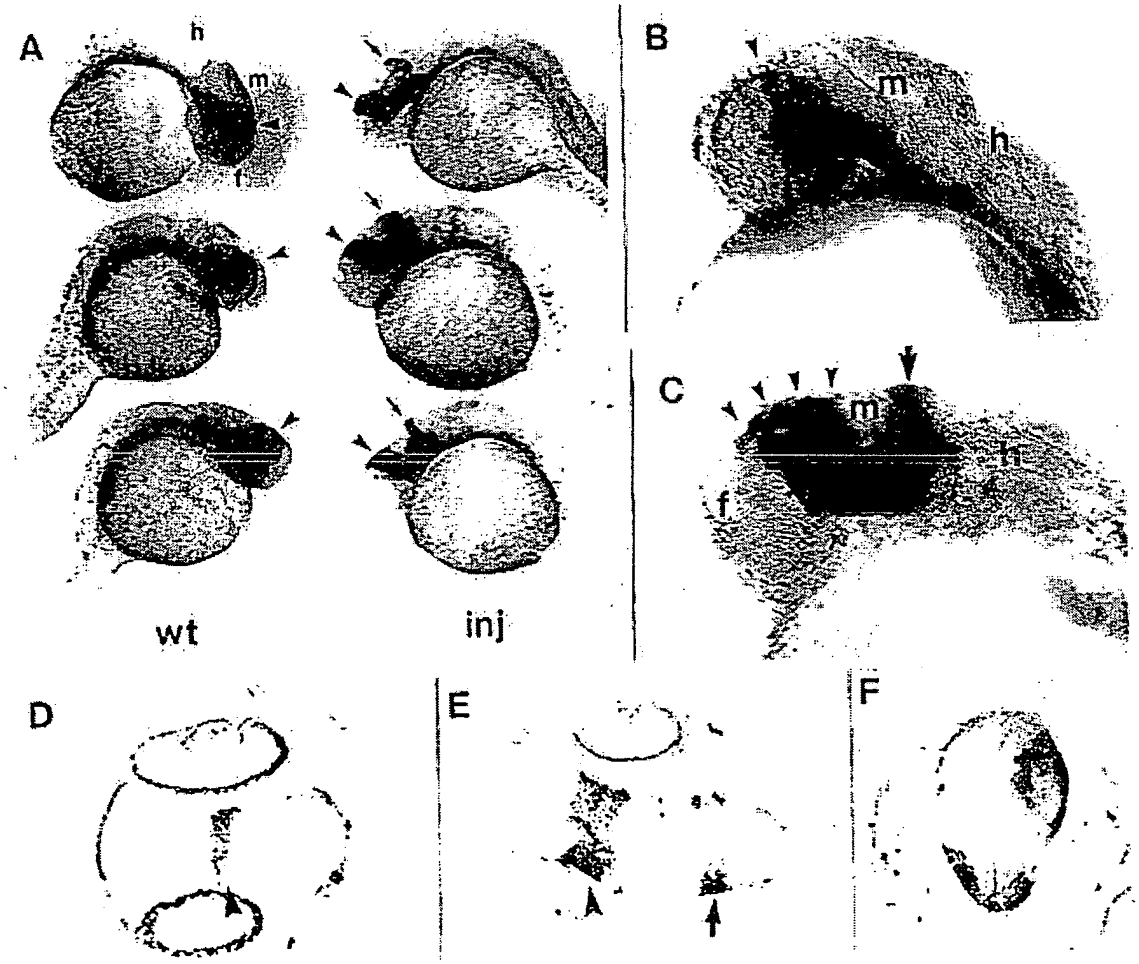

Figure 7. Ectopic Expression of *axial* after Injection of *shh* RNA into Fertilized Zebrafish Eggs

(A–C) Whole-mount uninjected and injected embryos hybridized with *axial* probe after 28 hr of development are shown. (A) *axial* expression in three wild-type (wt) embryos (left) and three embryos injected (inj) with *shh* mRNA at the 1- to 4-cell stage (right). Notice the different degree of ectopic *axial* expression in the head of different embryos, in particular in the ectopic posterior stripe (arrow). (B) *axial* expression in the head of a control embryo at 28 hr of development. The arrow shows the narrow *axial* stripe in the diencephalon. The dotted line shows the eye. (C) *axial* expression in the head of an embryo injected with *shh* synthetic RNA. Arrowheads mark the broadened *axial* expression in the diencephalon. The arrow shows the ectopic posterior stripe of *axial* expression in the midbrain/hindbrain region. The dotted line marks the rudimentary eye.

(D) Horizontal section through the head of a 28 hr wild-type embryo; note the narrow stripe of *axial* expression through the diencephalon (arrowhead).

(E) Horizontal section through the head of a 28 hr injected embryo; note the broadened stripe of *axial* expression in the diencephalon (arrowhead) and the ectopic expression in the midbrain (arrow).

(F) Transverse section through the midbrain of a 28 hr injected embryo showing asymmetric distribution of *axial*-expressing cells.

Abbreviations: d, diencephalon; f, forebrain; h, hindbrain; and m, midbrain.

Zebrafish embryos at the 1-cell to 4-cell stages were injected with synthetic *shh* RNA and were fixed 14 or 28 hr later. As an assay for possible changes in cell fate consequent upon the ectopic activity of *shh*, we decided to analyze *axial* expression, since this gene serves as a marker for cells in which *shh* is normally expressed. As seen in Figure 7, we observe a highly localized ectopic expression of *axial* in a significant proportion of the injected embryos (21 of 80) fixed after 28 hr of development. Affected embryos show a broadening of the *axial* expression domain in the diencephalon and ectopic *axial* expression in the midbrain; however, we did not observe ectopic expression in the telencephalon or spinal cord. Many of the injected embryos also showed disturbed forebrain structures, in particular, smaller ventricles and poorly developed eyes. Among embryos fixed after 14 hr, a similar proportion (8 of 42) exhibited the same broadening and dorsal extension of the *axial* stripe in the diencephalon as well as a dorsal extension of *axial* staining in the midbrain; again, no changes in *axial* expression were observed caudal to the hindbrain. Control embryos injected with similar concentrations of *lacZ* mRNA showed no such abnormalities (data not shown).

Overexpression of *shh* in Drosophila Embryos Activates the *hh*-Dependent Pathway

Because of the high degree of structural homology between the Drosophila and zebrafish *hh* genes, we wondered whether this conservation also extends to the functional level. In the Drosophila embryo, expression of *hh* is restricted to a stripe of cells at the anterior boundary of each parasegment, where it is required to maintain the transcription of *wg* and *patched* (*ptc*) in adjacent cells (Forbes et al., 1993; Ingham and Hidalgo, 1993). One way to investigate functional conservation between the fish and fly genes would be to replace endogenous *hh* with *shh*; however, such an approach requires extensive characterization of the cis-acting regulatory elements of Drosophila *hh*. To circumvent this requirement, we instead used an overexpression system to test the activity of *shh* in flies. Expression of Drosophila *hh* driven by the *hsp70* promoter results in the ectopic activation of both the normal targets of *hh* activity; the *wg* transcriptional domain expands to fill between one-third to one-half of each parasegment, whereas *ptc* is ectopically activated in all cells except those expressing *engrailed* (Ingham, 1993). To compare the activities of the fly and fish genes, flies transgenic for a *HS–shh* construct were generated (see Experimental Procedures) and subjected to the same heat shock regime as *HS–hh* transgenic flies. *HS–shh* embryos fixed immediately after the second of two 30 min heat shocks exhibit ubiquitous transcription of the *shh* cDNA. Similarly treated embryos were fixed 30 or 90 min after the second heat shock and assayed for *wg* or *ptc* transcription. Both genes were found to be ectopically activated in a similar manner to that seen in heat-shocked *HS–hh* embryos (Figure 8; data not shown); thus, the zebrafish *shh* gene can activate the same pathway as the endogenous *hh* gene.

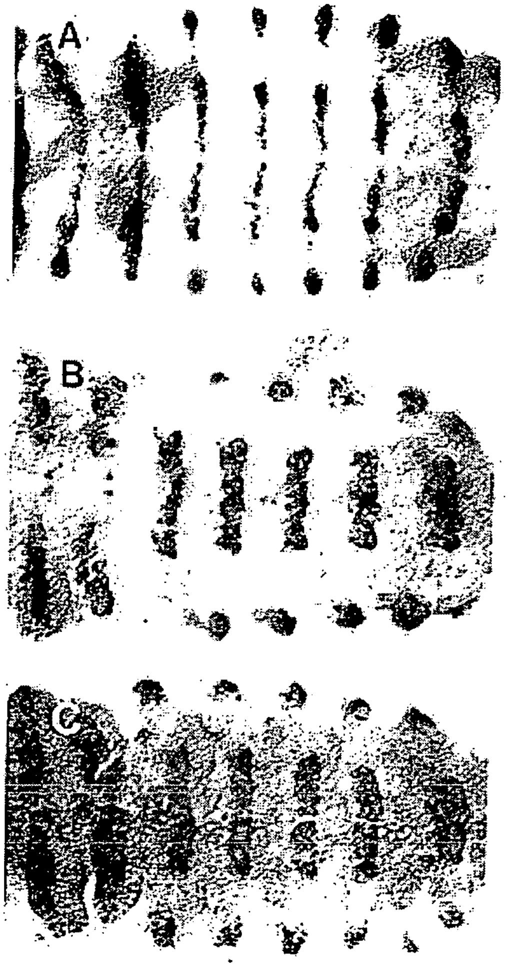

Figure 8. Consequences of Ubiquitous *shh* Expression in the Drosophila Embryo

Ventral aspects of stage 11 Drosophila embryos hybridized with *wg* probe.

(A) Wild-type embryo. Expression in each parasegment is restricted to narrow stripes of cells at the posterior boundaries, interrupted by lateral repression.

(B) *HS–hh* embryo, heat shocked for 30 min at 5 ± 1 and 7 ± 1 hr after fertilization and fixed 40 min later. Each stripe of cells expressing *wg* at the parasegment boundary is considerably broader than in wild type owing to the ectopic activation of transcription in cells anterior to the normal domain of *wg* transcription.

(C) *HS–shh* embryo treated identically to that shown in (B). As in Drosophila *hh*, overexpression of the zebrafish *shh* gene leads to ectopic activation of *wg* transcription.

Discussion

The results presented in this and the accompanying papers (Echelard et al., 1993; Riddle et al., 1993) provide evidence for the conservation of the *hh* gene during evolution; *hh* thus joins a growing list of Drosophila segment polarity genes (*armadillo, cubitus interruptus, engrailed, gooseberry, wg, zeste-white3*) that have their counterparts in vertebrates (reviewed by Ingham, 1991). In addition to *shh*, described in detail here, we have identified two other genes exhibiting a high degree of sequence homology, indicating the existence of a family of genes related to *hh* in the zebrafish genome.

Various lines of evidence have implicated *hh* in cell–cell signaling during Drosophila development. Although transcription of *hh* is spatially restricted, being limited in the embryo to narrow stripes of cells that coincide with parasegmental boundaries (Lee et al., 1992; Mohler and Vani, 1992; Tabata et al., 1992; Tashiro et al., 1993), the absence of *hh* activity during embryogenesis has drastic consequences for the polarity and patterning of cells throughout every parasegment (Nüsslein-Volhard and Wieschaus, 1980). Similarly, in the imaginal discs, the fates of cells several cell diameters away from those in which the gene is normally expressed appear to be affected by its inactivation (Mohler, 1988; Ma et al., 1993). Taken together, these mutant phenotypes are consistent with a role for hh as a long-range signaling molecule or morphogen; in line with this, in vitro studies have shown that hh protein can be processed to yield a secreted form when translated in the presence of microsomes (Lee et al., 1992).

Detailed studies of the regulation of two targets of *hh* activity in the embryo, however, present a different picture of *hh* function, implicating it instead in short-range, possibly contact-dependent, interactions. The maintenance of expression of *ptc* and *wg* by *hh* activity is extremely suggestive of such a mechanism, since transcription of both genes is restricted to only those cells that contact *hh*-expressing cells (Forbes et al., 1993). Moreover, hh protein, though apparently secreted, shows a restricted distribution around the *hh* transcriptional domain (Taylor et al., 1993). When this distribution is changed by overexpressing *hh* using a heat shock promoter, both *ptc* and *wg* are ectopically induced, demonstrating that the restricted expression of both genes is due to the limited influence of the *hh* signal rather than the limited competence of cells that respond to that signal (Ingham, 1993). Based on these data, the long-range influence of *hh* in each parasegment can be interpreted as an indirect consequence of its role in regulating the expression of other genes, such as *wg*. In a similar manner, *hh* may exert a long-range influence in the developing eye via its short-range activation of the transforming growth factor β family member, *decapentaplegic*, in neighboring cells (see Ma et al., 1993). Thus, in both developmental contexts, *hh* may be seen as an organizer of sources of signaling molecules, rather than as a long-range signal per se.

In vertebrate embryos, a combination of contact-dependent and diffusible signals is known to organize the pattern of differentiation in the ventral spinal cord. These signals have been shown to emanate from the notochord, the axial mesoderm derivative, and the floor plate of the neural tube, initiating in the former but persisting for longer in the latter (Placzek et al., 1990, 1993; Yamada et al., 1991, 1993). Our finding that a homolog of *hh* is similarly expressed first in the axial mesoderm and subsequently in the floor plate is thus highly suggestive of a role for this gene in CNS patterning.

Two distinct signaling activities have been distinguished in both tissues: one of these is responsible for inducing cells to differentiate as floor plate (Placzek et al., 1990, 1993), whereas the other controls neuronal differentiation (Yamada et al., 1991, 1993). Although our data cannot rule out a role for *shh* as the latter activity, we consider this to be unlikely for two reasons. First, while the functional analysis of *hh* in Drosophila points to its encoding a short-range, possibly contact-dependent signal, neuronal-inducing activity has been shown to be mediated by a diffusible factor (Yamada et al., 1993). Second, subject to the limitations inherent in comparisons between embryonic stages of different species, the timing of *shh* transcription appears to be inconsistent with the temporal profile of this activity. Thus, in the chick embryo, neuron-inducing activity is first detectable after the onset of somitogenesis and persists in the notochord until close to the end of this process (Yamada et al., 1993); this contrasts with the early onset of expression of *shh* in both axial mesoderm and floor plate and with the rapid elimination of *shh* expression from the notochord once somitogenesis begins.

Floor plate–inducing activity, on the other hand, is at maximal levels in the notochord of stage 6 chick embryos, just prior to the onset of somitogenesis, but dissipates by stage 10, when 10 somites have formed (Placzek et al., 1991, 1993); this temporal profile corresponds more closely to the expression of *shh* in the axial mesoderm of the zebrafish embryo. Moreover, the inducing activity of the floor plate cells themselves persists until well after the completion of somitogenesis in the chick embryo (Placzek et al., 1993), and in line with this we find that floor plate expression of *shh* persists after transcription ceases in the notochord. Given the contact-dependent nature of floor plate induction (Placzek et al., 1991, 1993), the *shh* gene product would thus seem an attractive candidate for such an activity.

To investigate this possibility, we injected synthetic *shh* mRNA into fertilized zebrafish embryos. Following such injections, we observe a consistent phenotypic effect, the ectopic activation of the *axial* gene in the midbrain/hindbrain region. Since *axial* expression is normally restricted to the floor plate in this region of the brain (Strähle et al., 1993), it is tempting to interpret this result as being indicative of a change in fate of more dorsally located cells. A definitive demonstration that these cells have been induced to differentiate as floor plate must await the availability of other floor plate–specific markers. We note, however, that ectopic *axial* activation is never observed in other regions of the neural keel; a simple explanation for this could be that, posterior to the midbrain, more than one factor is required for floor plate induction. Interestingly, ectopic expression of a mouse homolog of *axial*, *HNF3β*, in response to ectopic *shh* activity is similarly restricted to the midbrain/hindbrain region of mouse embryos (Echelard et al., 1993). Another possibility is that the restricted response to ectopic *shh* is indicative of a difference in the susceptibility of differing regions of the CNS to fate changes under these particular experimental circumstances. In this regard, it is interesting that ectopic induction of floor plate markers was similarly found to be restricted to the midbrain following injection of transcript for the *axial*-related gene *pintallavis* into Xenopus embryos (Ruiz i Altaba et al., 1993).

Recent studies of the *ntl* mutation unexpectedly revealed that floor plate differentiation can proceed in the absence of a notochord (Halpern et al., 1993). The *ntl* gene encodes the zebrafish ortholog of the mouse *Brachyury* (Schulte-Merker et al., 1994b), a transcription factor required for notochord differentiation (Kispert and Herrmann, 1993). Careful analysis of *ntl* mutant embryos shows that undifferentiated mesenchymal cells persist beneath the neural keel of mutant embryos, and it has been suggested that these cells correspond to the notochord precursors (Halpern et al., 1993). Since floor plate induction occurs prior to the differentiation of the notochord, these precursor cells are thought to produce floor plate–inducing activity independent of the function of the *ntl* gene; accordingly, any gene encoding such an activity should still be expressed in *ntl* embryos. Our finding that *shh* expression in the axial mesodermal of *ntl* mutants is unaltered just prior to the onset of somitogenesis is thus consistent with a role for *shh* in floor plate induction.

The failure of floor plate differentiation in cyc mutations results from a cell-autonomous defect in the ability of midline neural plate cells to respond to the inducing signal (Hatta et al., 1991). Expression of the signal itself by axial mesoderm cells appears unimpaired by the mutation as revealed by the ability of genetically wild-type cells to differentiate as floor plate when transplanted into cyc mutant embryos (Hatta et al., 1991). In line with this, *shh* expression is unaffected in axial mesoderm but is not activated in the ventral neural keel in *cyc* mutants. That wild-type floor plate cells are capable of inducing surrounding *cyc* mutant cells in mosaic animals has led to the suggestion that the planar signal mediating this homeogenetic induction differs from the notochord signal (Hatta et al., 1991); in this case, despite its floor plate expression, *shh* could not fulfill both functions. Yet it may be that the persistent high level of expression of *shh* in the floor plate compared with the notochord in wild-type embryos provides the basis for this rescuing behavior: thus, floor plate cells may produce more of the same signal and for longer, enough to overcome the attenuated receptor activity caused by the *cyc* mutation. In this context, it is interesting that floor plate differentiation is rescued in *cyc; ntl* double mutants (K. Hatta, C. Kimmel, and M. Halpern, personal communication), quite possibly as a result of the prolonged presence of undifferentiated and potentially signal-producing notochord precursors.

A notable feature of the *shh* expression pattern is its extension and expansion rostral to the notochord, which in the fish terminates at the level of the fourth rhombomere (Hatta et al., 1991). From the hindbrain to the forebrain, there is a continuous domain of *shh* expression that broadens from the 1-cell wide stripe characteristic of the floor plate to a band of several cell diameters in the ventral diencephalon. Based upon morphological criteria and on the expression patterns of molecular markers, such as the zn5 antigen in zebrafish (Hatta et al., 1991) or the FP3 and FP4 antigens in rat (Placzek et al., 1993), the floor plate is generally considered to terminate at the midbrain/forebrain boundary in all vertebrate species; however, Hatta et al. (1993) have recently suggested that cells with similar signaling properties as floor plate cells populate the ventral diencephalon, where they direct the specification of surrounding cells. This proposal stems from the observation that the most extreme aspect of the *cyc* phenotype is manifested anterior to the midbrain, cyclopia ensuing as a consequence of the elimination of a substantial part of the ventral forebrain (Hatta et al., 1991), and is supported by our finding that *shh* expression is completely absent from the forebrain of *cyc* embryos. Surprisingly, we find that *shh* expression disappears anterior to the midbrain as early as the 100% epiboly stage. Assuming that *cyc* specifically blocks the induction of ventral midline cells throughout the CNS, this finding supports our view that even at this early stage, *shh* expression in the head is already restricted to the neurectoderm. Exactly when this precocious induction of floor plate–equivalent cells occurs is unclear; it seems likely, however, that they are induced by the underlying mesoderm as both cell layers migrate toward the animal pole.

In addition to its expression in midline structures of the mesoderm and ectoderm, we have found that *shh* is expressed in the posterior mesodermal cells of the pectoral fin buds. Such expression is notable given the homology between pectoral fins and tetrapod limbs. Experimental manipulations of chick limb buds have shown that cells in a similar position possess a polarizing activity capable of inducing mirror image digit duplications when transplanted to the anterior side of the limb bud. Strikingly, two other tissues that express *shh*, the notochord and floor plate, exhibit similar properties when transplanted into the anterior side of limb buds (Wagner et al., 1990) and in the accompanying paper (Riddle et al., 1993) provide compelling evidence that the polarizing activity in all of these tissues is the *shh* gene product. That *shh* is expressed in a similar region of both fin and limb rudiments implies a remarkable evolutionary conservation of the mechanism that patterns these structures.

The early expression of *shh* in the embryonic shield of zebrafish embryos is reminiscent of and overlaps the early expression domains of other genes, such as *axial* (Strähle et al., 1993), *ntl* (Schulte-Merker et al., 1994a, 1994b), and *gsc* (Schulte-Merker et al., 1994a; Stachel et al., 1993); whether such early *shh* transcription has any functional significance remains to be seen. As the convergence and extension movements of gastrulation proceed, the *shh* expression domain remains substantially coextensive with those of *axial* and *ntl*. Both of these latter genes encode putative transcription factors, raising the possibility that one or the other of them might regulate *shh* expression. While our finding that expression of *shh* is unaffected in the absence of *ntl* activity eliminates it from having such a role, the case for such a regulatory relationship between *axial* and *shh* remains attractive. Not only are both genes coexpressed within the axial mesoderm, *axial* is also expressed in midline neural plate cells, where it could also activate *shh* transcription. If, as suggested by our ectopic *shh* expression analysis, *axial* is itself a target for *shh* activity, this would imply a cascade of mutual activation between the two genes. We note, however, that while the *shh* and *axial* expression domains appear to overlap caudal to the midbrain, expression of *shh* within the diencephalon is significantly more widespread. Thus, some factor other than *axial* must be required for *shh* expression, at least in the forebrain.

Despite the structural differences between the two proteins, the consequences of overexpressing *shh* in developing Drosophila embryos are remarkably similar to those that ensue when the endogenous gene is similarly overexpressed. This implies that the zebrafish *shh*-encoded protein can recognize the receptor for Drosophila hh; by extension, this receptor may be similarly conserved through evolution. Although the *hh* signaling pathway has been extensively analyzed in Drosophila (Forbes et al., 1993; Ingham, 1993; Ingham and Hidalgo, 1993), the identity of any putative hh receptor still remains uncertain. The strongest candidate to date is the product of the segment polarity gene *ptc* (Ingham et al., 1991); however, the implication of *ptc* in such a role is based entirely on genetic data, and it remains possible that this gene acts in a parallel pathway to *hh* (Forbes et al., 1993). Whether counterparts of this and other genetically identified components of *hh* signaling in Drosophila are involved in *shh* function in vertebrates remains to be seen.

Experimental Procedures

Cloning and Sequencing

Approximately 1.5 × 10^6 plaques of a 33 hr zebrafish embryonic λgt11 cDNA library were screened by plaque hybridization at low stringency (McGinnis et al., 1984) using a mix of two *hh* sequences as a probe: a Drosophila *hh* 400 bp EcoRI fragment (provided by J. Mohler) and a murine *Dhh* 264 bp BamHI–EcoRI exon 2 fragment (provided by A. McMahon). Four clones were isolated and subcloned into the EcoRI sites of pUC18 T3T7 (Pharmacia). Both strands of clone *hh[c]8.3* were sequenced using nested deletions (Pharmacia) and internal oligonucleotide primers. DNA sequences and derived amino acid sequences were analyzed using Geneworks (Intelligenetics) and the Genetics Computer Group software packages.

PCR Amplification

Degenerate oligonucleotides *hh5.1* and *hh3.3* were used to amplify genomic zebrafish DNA: *hh5.1*, AG(C/A)GITG(C/T)AA(A/G)GA(A/G)I(C/A)(A/G)I(G/C/T)IAA, and *hh3.3*, CTCIACIGCIA(G/A)IC(G/T)IGCIA. PCR was performed with an initial denaturation at 94°C, followed by 35 cycles of 47°C for 1 min, 72°C for 2 min, and 94°C for 1 min with a final extension at 72°C. Products were subcloned in pUC18.

In Situ Hybridization

In situ hybridizations of zebrafish embryos were performed as described by Oxtoby and Jowett (1993) with the following modifications. Embryos were rehydrated through ethanol rather than methanol series; the proteinase K digestion was reduced to 5 min, and subsequent washes were done in PBTw without glycine; the antibody was preadsorbed in PBTw, 2 mg/ml bovine serum albumin without sheep serum, and antibody incubation was performed in PBTw, 2 mg/ml bovine serum albumin. Drosophila embryos were processed and hybridized as previously described (Ingham et al., 1991).

Histology

Stained embryos were dehydrated through ethanol:butanol series, as previously described (Godsave et al., 1988) and embedded in Fibrowax. Sections (8 μm) were cut on an Anglian rotary microtome.

RNA Probe Synthesis

For analysis of *shh* expression, two different templates were used with consistent results: *phh[c]8.3* linearized with BglII to transcribe an antisense RNA probe that excludes sequences coding for amino acids upstream of amino acid 281 and therefore excludes the region conserved between different *hh* genes; and *phh[c]8.3* linearized with HindIII to transcribe an antisense RNA that covers the complete cDNA. All in situ hybridizations shown were performed with the latter probe, which gives a better signal. Other probes were as follows: *axial* DraI-linearized pBT1N (Strähle et al., 1993) using T3 RNA polymerase; *gsc* linearized with EcoRI (Schulte-Merker et al., 1994a) and transcribed with T7 RNA polymerase; and *pax-2* BamHI-linearized pcF16 (Krauss et al., 1991) using T7 RNA polymerase. In situ hybridizations were performed using labeled antisense RNA at a final concentration of 1 ng/ml. Antisense RNA probes were synthesized according to the protocol of the manufacturer (digoxygenin RNA labeling kit, Boehringer Mannheim).

Zebrafish Strains

Wild-type fish were bred from a founder population obtained from the Goldfish Bowl, Oxford, England. The mutant *cyc* strain b16 and the mutant *ntl* strains b160 and b195 were obtained from Eugene, Oregon. Fish were reared at 28°C in a continuous flow system (three changes of water per hour) on a 14 hr light–10 hr dark cycle.

RNA Injections

The open reading frame of *shh* was amplified by PCR, using oligonucleotides 5'-CTGCAGGGATCCACCATGCGGCTTTTGACGAG-3' (which contains a consensus Kozak sequence for translation initiation) and 5'-CTGCAGGGATCCTTATTCCACACGAGGGATT-3', and was subcloned into the BglII site of pSP64T (Kreig and Melton, 1984). This vector includes 5' and 3' untranslated Xenopus β-globin sequences for RNA stabilization and is commonly used for RNA injections experiments in Xenopus. In vitro transcribed *shh* RNA at a concentration of approximately 100 μg/ml was injected into a single cell of naturally spawned zebrafish embryos at 1-cell to 4-cell stages using a pressure-pulsed Narishige microinjector. The injected volume was within the picoliter range. Embryos were fixed at 14 or 28 hr after injection in BT-Fix (Westerfield, 1989) and processed as described above for whole-mount in situ hybridizations with the *axial* probe.

Transgenic Drosophila

An EcoRI fragment, containing the entire *shh* open reading frame, was purified from the plasmid phh[c]8.3 and ligated with phosphatased EcoRI-digested transformation vector pCaSpeRhs (Thummel et al., 1988). The recombinant plasmid pHSshh, containing the *shh* open reading frame in the correct orientation relative to the heat shock promoter, was used to transform Drosophila embryos using standard microinjection procedures (Ingham and Forbes, 1993).

Ectopic Expression in Drosophila Embryos

Embryos carrying the appropriate transgenes were collected over 2 hr intervals, transferred to thin layers of 1% agarose on glass microscope slides, and incubated in a plastic petri dish floating in a water bath at 37°C for 30 min intervals. Following heat treatment, embryos were returned to 25°C prior to being fixed for in situ hybridization with digoxygenin-labeled single-stranded *shh*, *wg*, or *ptc* RNA probes as previously described (Ingham et al., 1991).

Acknowledgments

We are grateful to many people for their cooperation in the course of this study. In particular, we thank the members of the McMahon and Tabin labs for the continual and rapid exchange of data, information, and ideas that has characterized this collaboration; J. Mohler for providing the Drosophila *hh* clone ahead of publication; C. Kimmel for supplying mutant fish strains; L. Lettice, T. Jowett, and S. Schulte-Merker for procuring mutant embryos; U. Strähle and P. Blader for providing various fish materials; M. Fietz and A. Taylor for help in producing and analyzing the *HS–shh* transgenics; K. Zinn for the cDNA library; I. Goldsmith for oligonucleotide synthesis; M. Fietz for computer wizardry; K. Hatta for illuminating discussions about floor plate specification; and J. Adam for introducing us to the mysteries of color printing. S. K. was a European Science Foundation fellow; J.-P. C. is a European Community Human Capital and Mobility Program fellow. This research was supported by the Imperial Cancer Research Fund and by a Human Frontiers Science Program grant to P. W. I., C. Tabin, and A. McMahon.

Received November 17, 1993; revised November 30, 1993.

References

DiNardo, S., Kuner, J. M., Theis, J., and O'Farrell, P. H. (1985). Development of embryonic pattern in D. melanogaster as revealed by accumulation of the nuclear *engrailed* protein. Cell *43*, 59–69.

Echelard, Y., Epstein, D. J., St-Jacques, B., Shen, L., Mohler, J., McMahon, J. A., and McMahon, A. P. (1993). Sonic hedgehog, a member of a family of putative signaling molecules, is implicated in the regulation of CNS polarity. Cell *75*, this issue.

Egan, S. E., and Weinberg, R. A. (1993). The pathway to signal achievement. Nature *365*, 781–783.

Forbes, A. J., Nakano, Y., Taylor, A. M., and Ingham, P. W. (1993). Genetic analysis of *hedgehog* signalling in the *Drosophila* embryo. Development *119* (Suppl.), in press.

Godsave, S. F., Isaacs, H. V., and Slack, J. M. W. (1988). Mesoderm-inducing factors: a small class of molecules. Development *102*, 555–566.

Halpern, M. E., Ho, R. K., Walker, C., and Kimmel, C. B. (1993). Induction of muscle pioneers and floor plate is distinguished by the zebrafish *no tail* mutation. Cell *75*, 99–111.

Hatta, K., Kimmel, C. B., Ho, R. K., and Walker, C. (1991). The *cyclops* mutation blocks specification of the floor plate of the zebrafish central nervous system. Nature *350*, 339–341.

Hatta, K., Püschel, A. W., and Kimmel, C. (1993). Midline signaling in the primordium of the zebrafish anterior central nervous system. Proc. Natl. Acad. Sci. USA, in press.

Hidalgo, A., and Ingham, P. (1990). Cell patterning in the *Drosophila* segment: spatial regulation of the segment polarity gene *patched*. Development *110*, 291–301.

Ingham, P. W. (1991). Segment polarity genes and cell patterning within the *Drosophila* body segment. Curr. Opin. Genet. Dev. *1*, 261–267.

Ingham, P. W. (1993). Localized *hedgehog* activity controls spatial limits of *wingless* transcription in the *Drosophila* embryo. Nature *366*, 560–562.

Ingham, P. W., and Forbes, Z. (1993). Microinjection into *Drosophila* embryos. In Essential Developmental Biology: A Practical Approach. C. D. Stern and P. W. H. Holland, eds. (Oxford: IRL Press), pp. 97–102.

Ingham, P. W., and Hidalgo, A. (1993). Regulation of *wingless* transcription in the *Drosophila* embryo. Development *117*, 283–291.

Ingham, P. W., and Martinez-Arias, A. (1992). Boundaries and fields in early embryos. Cell *68*, 221–235.

Ingham, P. W., Taylor, A. M., and Nakano, Y. (1991). Role of the *Drosophila patched* gene in positional signaling. Nature *353*, 184–187.

Jaynes, J. B., and O'Farrell, P. H. (1991). Active repression of transcription by the engrailed homeodomain protein. EMBO J. *10*, 1427–1433.

Kispert, A., and Herrmann, B. G. (1993). The *brachyury* gene encodes a novel DNA-binding protein. EMBO J. *12*, 3211–3220.

Krauss, S., Johansen, T., Korzh, V., and Fjose, A. (1991). Expression of the zebrafish paired box gene *pax[zf-b]* during early neurogenesis. Development *113*, 1193–1206.

Krieg, P. A., and Melton, D. A. (1984). Functional messenger RNAs are produced by SP6 *in vitro* transcription of cloned cDNAs. Nucl. Acids Res. *12*, 7057–7070.

Kyte, J., and Doolittle, R. F. (1982). A simple method for displaying the hydropathic character of a protein. J. Mol. Biol. *157*, 105–132.

Lee, J. J., von Kessler, D. P., Parks, S., and Beachy, P. A. (1992). Secretion and localized transcription suggest a role in positional signaling for products of the segmentation gene *hedgehog*. Cell *71*, 33–50.

Ma, C., Zhou, Y., Beachy, P. A., and Moses, K. (1993). The segment polarity gene *hedgehog* is required for progression of the morphogenetic furrow in the developing Drosophila eye. Cell *75*, 927–938.

McGinnis, W., Levine, M. S., Hafen, E., Kuroiwa, A., and Gehring, W. J. (1984). A conserved DNA sequence found in homeotic genes of the *Drosophila Antennapedia* and *bithorax* complexes. Nature *308*, 428–433.

McMahon, A. (1992). The *wnt* family of developmental regulators. Trends Genet. *8*, 236–242.

Mohler, J. (1988). Requirements for *hedgehog*, a segment polarity gene, in patterning larval and adult cuticle of *Drosophila*. Genetics *120*, 1061–1072.

Mohler, J., and Vani, K. (1992). Molecular organisation and embryonic expression of the *hedgehog* gene involved in cell–cell communication in segmental patterning of *Drosophila*. Development *115*, 957–971.

Nusse, R., and Varmus, H. E. (1992). *Wnt* genes. Cell *69*, 1073–1087.

Nüsslein-Volhard, C., and Wieschaus, E. (1980). Mutations affecting segment number and polarity in Drosophila. Nature *287*, 795–801.

Oxtoby, E., and Jowett, T. (1993). Cloning of the zebrafish *krox-20* gene (*krx-20*) and its expression during hindbrain development. Nucl. Acids Res. *21*, 1087–1095.

Peifer, M., and Wieschaus, E. (1990). The segment polarity gene *armadillo* encodes a functionally modular protein that is the Drosophila homolog of human plakoglobin. Cell *63*, 1167–1178.

Placzek, M., Jessell, T. M., and Dodd, J. (1993). Induction of floor plate differentiation by contact dependent, homeogenetic signals. Development *117*, 205–218.

Placzek, M., Tessier-Lavigne, M., Yamada, T., Jessell, T., and Dodd, J. (1990). Mesodermal control of neural cell identity: floor plate induction by the notochord. Science *250*, 985–988.

Placzek, M., Yamada, T., Tessier-Lavigne, M., Jessell, T., and Dodd, J. (1991). Control of dorsoventral pattern in vertebrate neural development: induction and polarising properties of the floor plate. Development *113* (Suppl.), 105–122.

Riddle, R., Johnson, R. L., Laufer, E., and Tabin, C. (1993). *Sonic hedgehog* mediates the zone of polarizing activity. Cell *75*, this issue.

Ruiz i Altaba, A., and Jessell, T. M. (1993). Midline cells and the organization of the vertebrate neuraxis. Curr. Opin. Genet. Dev. *3*, 633–640.

Ruiz i Altaba, A., Cox, C., Jessell, T. M., and Klar, A. (1993). Ectopic neural expression of a floor plate marker in frog embryos injected with the midline transcription factor *pintallavis*. Proc. Natl. Acad. Sci. USA *90*, 8268–8272.

Schulte-Merker, S., Hammerschmidt, M., Beuchle, D., Cho, K. W., De Robertis, E. M., and Nüsslein-Volhard, C. (1994a). Expression of zebrafish *goosecoid* and *no tail* products in wild-type and mutant *no tail* embryos. Development, in press.

Schulte-Merker, S., van Eeden, F., Halpern, M., Kimmel, C., and Nüsslein-Volhard, C. (1994b). The zebrafish gene *no tail* (*ntl*) is the homologue of the mouse T (*Brachyury*) gene. Development, in press.

Stachel, S. E., Grunwald, D. J., and Myers, P. (1993). Lithium perturbation and *goosecoid* expression identify a dorsal specification pathway in the pregastrula zebrafish. Development *117*, 1261–1274.

Strähle, U., Blader, P., Henrique, D., and Ingham, P. W. (1993). *Axial*, a zebrafish gene expressed along the developing body axis, shows altered expression in *cyclops* mutant embryos. Genes Dev. *7*, 1436–1446.

Tabata, T., Eaton, S., and Kornberg, T. B. (1992). The *Drosophila hedgehog* gene is expressed specifically in posterior compartment cells and is a target of *engrailed* regulation. Genes Dev. *6*, 2635–2645.

Tashiro, S., Michiue, T., Higashijima, S., Zenno, S., Ishimaru, S., Takahashi, F., Orihara, M., Kojima, T., and Saigo, K. (1993). Structure and expression of *hedgehog*, a *Drosophila* segment–polarity gene required for cell–cell communication. Gene *124*, 183–189.

Taylor, A. M., Nakano, Y., Mohler, J., and Ingham, P. W. (1993). Contrasting distributions of patched and hedgehog proteins in the *Drosophila* embryo. Mech. Dev. *43*, 89–95.

Thummel, C. S., Boulet, A. M., and Lipshitz, H. D. (1988). Vectors for *Drosophila* P-element-mediated transformation and tissue culture transfection. Gene *74*, 445–456.

van Straaten, H. W. M., Hekking, J. W. M., Beursgens, J. P. W. M., Terwindt-Rouwenhorst, E., and Drukker, J. (1989). Effect of the notochord on proliferation and differentiation in the neural tube of the chick embryo. Development *107*, 793–803.

von Heijne, G. (1986). A new method for predicting signal sequence cleavage sites. Nucl. Acids Res. *14*, 4683–4690.

Wagner, M., Thaller, C., Jessell, T., and Eichele, G. (1990). Polarizing activity and retinoid synthesis in the floorplate of the neural tube. Nature *345*, 819–821.

Westerfield, M. (1989). The Zebrafish Book (Eugene, Oregon: University of Oregon Press).

Yamada, T., Pfaff, S. L., Edlund, T., and Jessell, T. M. (1993). Control of cell pattern in the neural tube: motor neuron induction by diffusible factors from notochord and floor plate. Cell *73*, 673–686.

Yamada, T., Placzek, M., Tanaka, H., Dodd, J., and Jessell, T. M. (1991). Control of cell pattern in the developing nervous system: polarizing activity of the floor plate and notochord. Cell *64*, 635–647.

© 1996 Nature Publishing Group http://www.nature.com/naturegenetics

Mutations in the human *Sonic Hedgehog* gene cause holoprosencephaly

Erich Roessler[1], Elena Belloni[2], Karin Gaudenz[1], Philippe Jay[3], Philippe Berta[3], Stephen W. Scherer[2], Lap-Chee Tsui[2] & Maximilian Muenke[1]

[1]The Children's Hospital of Philadelphia, Division of Human Genetics and Molecular Biology and Departments of Pediatrics and Genetics, University of Pennsylvania School of Medicine, Philadelphia, 34th & Civic Center Boulevard, Pennsylvania 19104-4399, USA
[2]The Hospital for Sick Children, Department of Genetics, 555 University Avenue, Toronto, Ontario M5G1X8, Canada
[3]Centre de Recherches de Biochimie Macromoléculaire, CNRS ERS 155-INSERM U249, 34033 Montpellier cedex, France

Correspondance should be addressed to M.M. e-mail: muenke@mail.med.upenn.edu

Holoprosencephaly (HPE) is a common developmental defect of the forebrain and frequently the midface in humans, with both genetic and environmental causes. HPE has a prevalence of 1:250 during embryogenesis and 1:16,000 newborn infants, and involves incomplete development and septation of midline structures in the central nervous system (CNS) with a broad spectrum of clinical severity[1–3]. Alobar HPE, the most severe form which is usually incompatible with postnatal life, involves complete failure of division of the forebrain into right and left hemispheres and is characteristically associated with facial anomalies including cyclopia, a primitive nasal structure (proboscis) and/or midfacial clefting. At the mild end of the spectrum, findings may include microcephaly, mild hypotelorism, single maxillary central incisor and other defects (Fig. 1). This phenotypic variability also occurs between affected members of the same family. The molecular basis underlying HPE is not known, although teratogens, non-random chromosomal anomalies, and familial forms with autosomal dominant and recessive inheritance have been described[4]. *HPE3* on chromosome 7q36 is one of at least four different loci implicated in HPE[5–9]. Here, we report the identification of human *Sonic Hedgehog* (*SHH*) as *HPE3* — the first known gene to cause HPE. Analyzing 30 autosomal dominant HPE (ADHPE) families, we found five families that segregate different heterozygous *SHH* mutations. Two of these mutations predict premature termination of the SHH protein, whereas the others alter highly conserved residues in the vicinity of the alpha-helix-1 motif or signal cleavage site.

As shown in the accompanying report, the human *SHH* gene maps in the *HPE3* critical region, making it an excellent candidate for the *HPE3* locus[10]. *SHH* is one of three human genes (the others being *Indian Hedgehog* and *Desert Hedgehog*)[11] homologous to the *Drosophila* segment polarity gene *hedgehog*[12,13]. Additional members of this gene family have been described in vertebrates such as *Xenopus*[14], chicken[15], mouse[16], rat[17] and zebrafish[18]. These genes encode secreted proteins that undergo post-translational trafficking to microsomes, cleavage of a signal peptide and autoproteolytic cleavage into a 19-kD amino terminus and a 25-kD carboxy terminus. The N-terminal fragment, Shh-N, has all of the known biological activity and is loosely associated with the plasma membrane near its site of synthesis[19–21]; the C-terminal polypeptide is readily diffusible from the site of secretion[22,23]. The hedgehog genes have inductive effects in the developing embryo, including patterning effects on the midline ventral CNS along the entire rostrocaudal axis[24], ventral specifica-

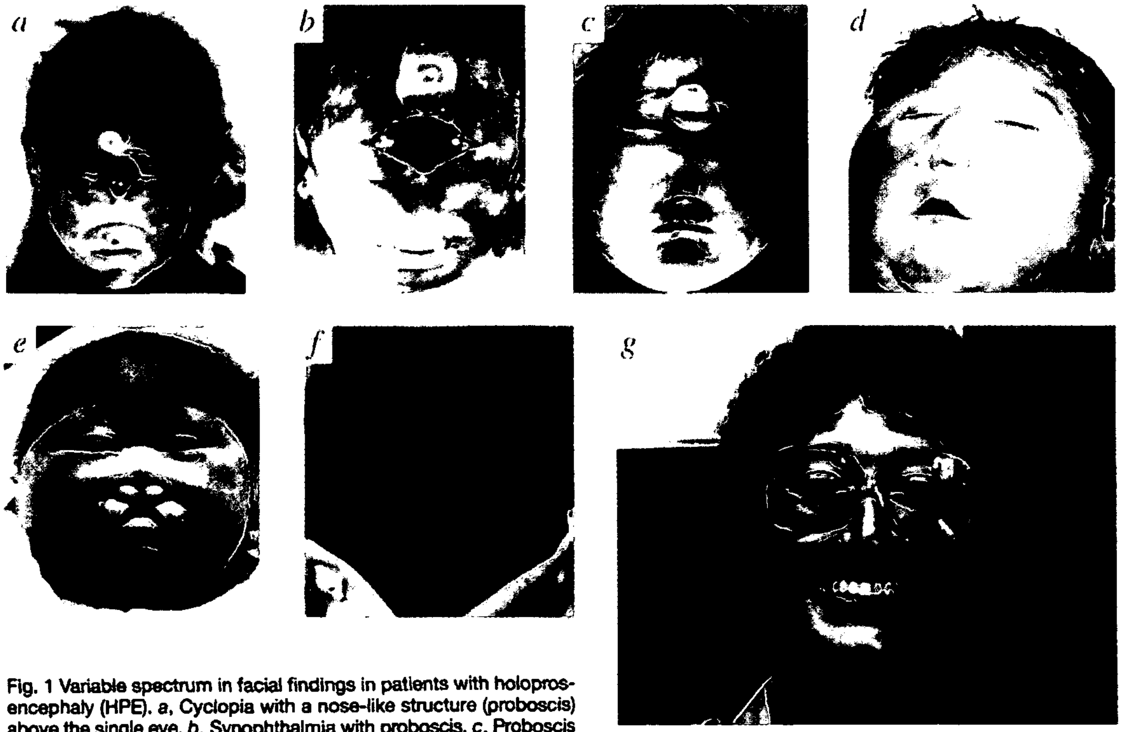

Fig. 1 Variable spectrum in facial findings in patients with holoprosencephaly (HPE). *a*, Cyclopia with a nose-like structure (proboscis) above the single eye. *b*, Synophthalmia with proboscis. *c*, Proboscis between separated eyes. *d,e*, Autosomal dominant (AD) HPE family 14 (see Fig. 2) with two HPE patients[36]: closely spaced eyes (hypotelorism) and single-nostril nose (*d*) and ocular hypotelorism, midfacial hypoplasia with midline cleft lip (*e*). *f*, *g*, AD HPE family 2 (see Fig. 2)[37]: oldest affected daughter with microcephaly, severe hypotelorism, absence of the nasal bones and midline cleft lip (*f*), and her mother with a single central upper incisor (*g*).

© 1996 Nature Publishing Group http://www.nature.com/naturegenetics

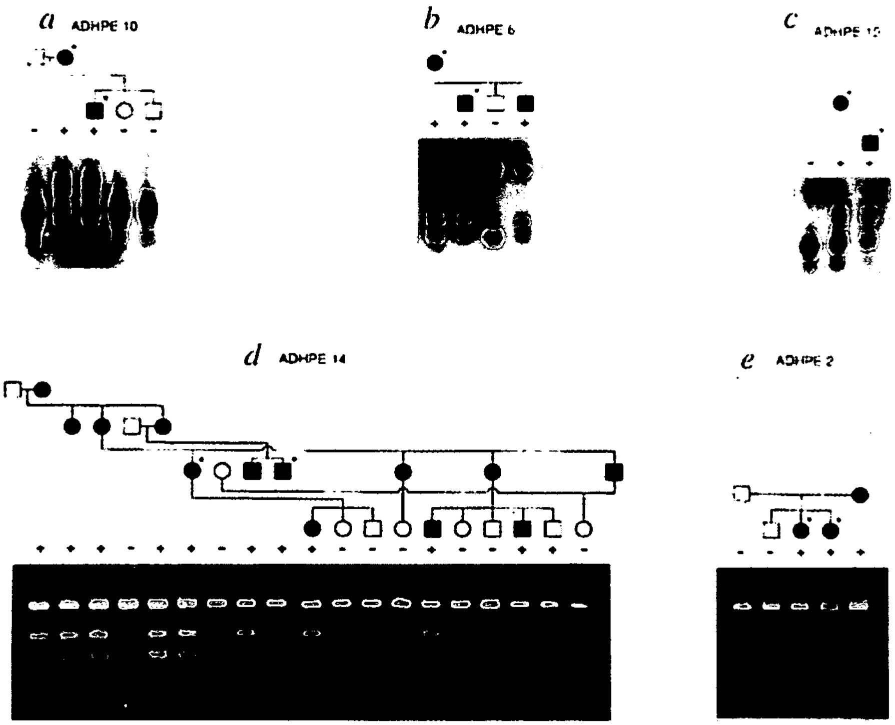

Fig. 2 The pedigree structure of the five autosomal dominant (AD) HPE families and mutations in *hSHH* (+) are shown with unaffected individuals (open symbols) and affected patients or HPE carriers (closed symbols). Four families have been previously reported to be linked to chromosome 7q36 (ADHPE 2, 6, 10 and 14)[5]; a mutation was also uncovered in a new fifth family, ADHPE 15, identified from a total of 30 ADHPE families by SSCP analysis. DNA from at least two HPE patients (indicated by an asterisk (*)) in each family, was sequenced. *a*, ADHPE 10 segregates a Gly31Arg mutation demonstrated by SSCP and sequencing. *b*, ADHPE 6 segregates a Gln100stop mutation at the last codon of exon 1. The mother and two of her two sons (+) have band shifts in exon 1 and a CAG to TAG mutation, that can also be detected by the creation of a novel *Dde*I restriction site (data not shown). c, ADHPE 15 segregates a Trp117Gly mutation demonstrated by sequencing DNA from the mother (*) and son (*). The maternal grandmother is clinically unaffected and lacks a band shift by SSCP (–). *d*, ADHPE 14 carries a Lys105stop mutation in exon 2 as demonstrated by SSCP analysis (data not shown). This creates a novel *Spe*I restriction site within the amplicon of the mutated chromosome in all affected individuals (+) that is absent in unaffected members (–). One male in the fourth generation who appears to be clinically unaffected is positive for the Lys105stop mutation, consistent with the notion of phenotypically unaffected carriers in AD HPE families. *e*, ADHPE 2 segregates a Trp117Arg mutation which can be demonstrated by SSCP analysis (data not shown) and the creation of a novel *Fnu4*H1 restriction site in the mother (+) and her two affected daughters (+).

tion of somites[22,25], and patterning of the developing limb buds[15,18]. During the formation of the vertebrate CNS, *Shh* is expressed within Hensen's node, the notochord and the ventral midline neural tube. *Shh* triggers differentiation of the floor plate and subsequently differentiation of ventral neurons throughout the neural tube including dopaminergic neurons in the forebrain[24], motor neurons in the spinal chord. It also alters *Pax2* and *Pax6* expression in the developing eye[26,27]. The crystal structure of murine Shh has been solved allowing structure/function analysis of mutations within the *hedgehog* genes[28]. Finally, the recent analysis of the phenotype of $Shh^{-/-}$ mice, including cyclopia[29], recapitulates the developmental role of *Shh* in the developing midline of the CNS established in other vertebrates. All of these patterning effects are consistent with a role for *SHH* in causing HPE.

Human *SHH* has a simple genomic architecture including three exons[10], like other members of this gene family. Having defined the intron–exon boundaries of *SHH* by direct DNA sequencing[10], we designed primer pairs for exon amplification and single-strand conformation polymorphism (SSCP) analysis in 30 ADHPE families. Patients who revealed SSCP band shifts were further analyzed by DNA sequencing of two affected members of each family. We analysed exons 1 and 2 for mutations, representing 96% of the SHH-N fragment.

Two of the 30 ADHPE families, both previously linked to chromosome 7q36 (ref.5), demonstrated different band shifts on SSCP for exon 1, which encodes the first 100 amino acids of the pre-protein (Fig. 2*a*,*b*). The mutation in ADHPE 10 is Gly31Arg (GGG to AGG) at a conserved residue among the *hedgehog* genes adjacent to the putative signal cleavage site (Figs 2*a*, 3*a*, 4). A stop codon (CAG to TAG) is present in ADHPE 6 at Gln 100, the last codon within exon 1, creating a predicted truncation in the protein (Figs 2*b*, 3*b*, 4).

Exon 2 encodes 87 amino acids of the mature SHH-N protein and was amplified in two segments. Analysing the first 248-bp subfragment of exon 2, we found three additional mutations within the 50 amino acids encoded by this amplicon. ADHPE 14 is a large multi-generational family containing a nonsense mutation at position Lys 105 resulting in a stop codon (AAG to TAG) (Figs 2*d*, 3*d*, 4). We also detected two different missense mutations at Trp117: Trp117Gly (TGG to GGG) in ADHPE 15 and Trp117Arg (TGG to CGG) in ADHPE 2 (Figs. 2*c*,*e*; 3*c*,*e*). This residue is invariant in all of the available hedgehog protein sequences (Fig. 4) and occurs immediately following the first alpha helix of the murine Shh-N fragment[28].

The two nonsense mutations predict premature termination of the SHH protein and are consistent with loss of function of one of the *SHH* genes. The Gly31Asp substitution immediately follows a six-amino acid consensus signal cleavage site (Fig. 4)[16], and might cause incorrect signal sequence processing resulting in loss of function, as secretion of the Shh protein is critical for biological responses[21]. This implies that haploinsufficiency is the genetic mechanism in ADHPE involving *SHH*. These findings are consistent with our experience that cytogenetic deletions of 7q36 which include *SHH* are strongly correlated with HPE (E.R. *et al.*, submitted). The remaining two missense mutations in exon 2 occur at an invariant amino acid, Trp 117, immediately following a crucial alpha helix-1 motif[28]. We speculate that this mutation may destabilize the SHH-N fragment, which can now be tested by functional studies.

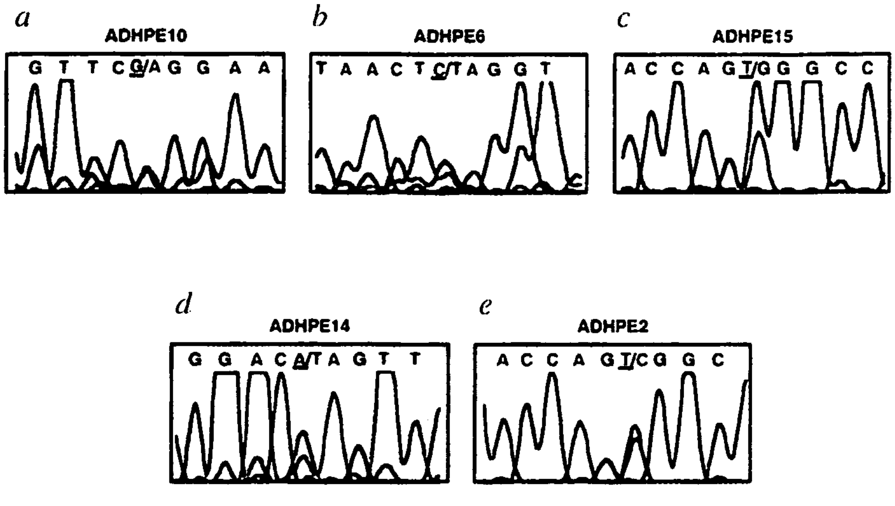

Fig. 3 Represenatative chromatograms of DNA sequence mutations of the *SHH* gene from affected individuals in ADHPE families 10 (*a*), 6 (*b*), 15 (*c*), 14 (*d*), and 2 (*e*). The sequence of the wild-type DNA is underlined.

In humans, loss of one *SHH* allele is sufficient to cause HPE, whereas both alleles need to be lost in the *Shh*$^{-/-}$ mouse to produce a similar CNS phenotype[29]. We observe that haploinsufficiency for *SHH* in humans is sufficient to disturb ventral midline neurogenesis, but insufficient to cause ventralization defects of sclerotome or limb abnormalities. These species differences might be explained, in part, by the requirement for different concentrations of *Shh* to produce various biological responses. For example, floor plate induction in the chick requires five times the concentration of Shh-N than does motor neuron induction[30]. Therefore, haploinsufficiency for *SHH* appears to be more critical in humans, for short-range effects (such as floor plate induction) than for long-range effects (for example, limb patterning or formation of vertebrae and ribs).

HPE is a genetically heterogeneous malformation with significant morbidity and mortality in humans. The identification of *SHH* as the *HPE3* gene is a step toward better understanding of normal and abnormal brain development in humans, based on studies of *SHH* and related genes in other vertebrates. The striking evolutionary conservation of *sonic hedgehog* genes suggests that the molecular pathogenesis of deficiencies of *Shh* expression will provide important and useful models for HPE. For example, the zebrafish mutation *cyclops*[31] alters the forebrain expression of *Shh*[18] that may set up a chain of developmental events mimicking the human HPE malformation. Similarly, the zebrafish *no tail* mutation[32], and the homologous mouse gene *brachyury*, have been shown to disturb the expression of *Shh* in caudal structures accompanied by degeneration of the notochord[18]. This phenotype suggests a mechanism for caudal regression (a human disorder that also maps to the same

```
dhh        MDNSSVPWASAASVTCLSLGCQMPQFQFQFQLQIRSELHLRKPARRTQTMRH
          IASTQRCLSRLTSLVA

            exon 1                       R  (ADHPE 10)
                                                         50
hSHH       MLLLARCLLLVLVSSLLVCSGLACGPGRGFGKRRHPKKLTPLAYKQFIPNVA
mSHH      MLLLLARCFLVILASSLLVSPGLACGPGRGFGKRRHPKKLTPLAYKQFIPNVA
zSHH       MRLLTRVLLVSLLTLSLVVSGLACGPGRGYGRRRHPKKLTPLAYKQFIPNVA
dhh              LLLIVLPMVFSPAHSCGPGRGLGRHRARN  LYPLVLKQTIPNLS

                                   exon 1    (ADHPE 6)   stop
                                                            100
hSHH       EKTLGASGRYEGKISRNSERFKELTPNYNPDIIFKDEENTGAKRLMTQ  RCKD
hIHH                                                RRLMTQ  RCKD
hDHH                                   IIFKDEENSGADRLMTE  RCKE
mShh       EKTLGASGRYEGKITRNSERFKELTPNYNPDIIFKDEENTGADRLMTQ  RCKD
zShh       EKTLGASGRYEGKITRNSERFKELTPNYNPDIIFKDEENTGADRLMTQ  RCKD
dhh        EYTNSASGPLEGVIRRDSPKFKDLVPNYNRDILFRDEEGTGADGLMSK  RCKE

          stop  (ADHPE 14)              exon 2                exon
                          R  (ADHPE 2)
                          G  (ADHPE 15)
                                                            150
hSHH       KLNALAISVMNQWPGVKLRVTEGWDEDGHHSEESLHYEGRAVDITT  SDRDRS
hIHH       RLNSLAISVMNQWPGVKLRVTEGWDEDGHHSEESLHYEGRAVDITT  SDRDRN
hDHH       RVNALAIAVMNMWPGVRLRVTEGWDEDGHHAQDSLHYEGRALDITT  SDRDRN
mShh       KLNALAISVMNQWPGVRLRVTEGWDEDGHHSEESLHYEGRAVDITT  SDRDRS
zShh       KLNSLAISVMNHWPGVKLRVTEGWDEDGHHGEESLHYEGRAVKITT  SDRDKS
dhh        KLNVLAYSVMN WPGIRLLVTESWDEDYHHGQESLHYEGRAVTIAT   DRDQS

                                                            200
hSHH       KYGMLARLAVEAGFDWVYYESKAHIHCSVKAENSVAAKSGGCFPGSATVHLE
hIHH       KYGLLARLAVEAGFDWVYYESKAHVHCSVKSEHSAAAKTGGCFPAGAQVRLE
hDHH       KYGLLARLAVEAGFDWVYYGS
mShh       KYGMLARLAVEAGFDWVYYESKAHIHCSVKAENSVAAKSGGCFPGSATVHLE
zShh       KYGTLSRLAVEAGFDWVYYESKAHIHCSVKAENSVAAKSGGCFPGSALVSLQ
dhh        KYGMLARLAVEAGFDWNSYVSRRHIYCSVKSDSSISSHVHGCFTPESTALLE

                                                            250
hSHH       QGGTKLVKDLSPGDRVLAADDQGRLLYSDFLTFLDRDDGAKKVFYVIETREP
hIHH       SGARVALSAVRPGDRVLAMGEDGSPTFSDVLIFLDREPHRLRAFQVIETQDP
mShh       QGGTKLVKDLRPGDRVLAADDQGRLLYSDFLTFLDRDEGAKKVFYVIETLEP
zShh       DGGQKAVKDLNPGDKVLAADSAGNLVFSDFIMFTDRDSTTRRVFYVIETQEP
dhh        SGVRKPLGELSIGDRVLSMTANGQAVYSEVILFMDRNLE  QMQNFVQLETDG

                                                            300
hSHH       RERLLLTAAHLLFVAPHNDSATGEPEASSGSGPPSGGALGPRALFASRVRPG
hIHH        PRLLALTPAHLLF TADNET    EPAARF             RATFASHVQPG
mShh       RERLLLTAAHLLFVAPHNDSGP                  TPGPSALFASRVRPG
zShh       VEKITLTAAHLLFVL   DNSTEDLHTMT                  AAYASSVRAG
dhh         AVLTVTPAHLVSV          WQPES              QKLTFVFADRIEE

                                                            350
hSHH       QRVYVVAERDGDRRLLPAAVHSVTLSEEAAGAYAPLTAQGRILINRVLASCYA
hIHH       QYVLVA    GVPGLQPARVAAVS  THVALGAYAPLTKHGTLVVEDVVASCFA
mShh       QRVYVVAERGGDRRLLPAAVHSVTLREEEAGAYAPLTAHGTILINRVLASCYA
zShh       QKVMVVD     DSGQLKSVIVQRIYTEEQRGSFAPVTAHGTIVVDRILASCYA
dhh        K   NQVLVRDVETGELRPQRVVKLGSVRSKGVVAPLRE  GRIVVNSVAASCYA

                                                            400
hSHH       VIEEHSWAHRAFAPFRLAHALLAALAPARTDRGGDSGGGDRGGGGGRVALTAP
hIHH        AVADHHLAQLAFWPLRLFHSL                AWGSW             TP
mShh       VIEEHSWAHRAGAPFRLAHALLAALAPARTD              GGGGGSIP  AAQ
zShh       VIEDQGLAHLAFAPARLYYYVSSFLPP                            QHSS
dhh        VINSQSLAHWGLAPMRL  LSTLEAWLPAK               EQLHSSPKVVSSAQ

hSHH       GAADAPGAGATAGIHWYSQLLYQIGTWLLDSEALHPLGMAVKSS
hIHH       GE           GVHWYPQLLYRLGRLLLEEGSFHPLGMSGAGS
mShh        SATEARGAEPTAGIHWYSQLLYHIGTWLLDSETMHPLGMAVKSS
zShh        SRSHATLQQ   EGVHWYSRLLYQMGTWLLDSNMLHPLGMSVNSS
dhh        GGN            GIHWYANALYKVK      DYV    LPQSWRHD
```

Fig. 4 Comparison of protein sequences for human Sonic (hSHH)[11], human Indian (hIHH)[11], human Desert (hDHH)[11], mouse Sonic (mShh)[16], zebrafish Sonic (zShh)[18] and *Drosophila* hedgehog (dhh)[13] were compared by the program ALIGN; a similar analysis[16] and crystal structure of the murine Shh-N fragment has been published[27]. The functional N-terminal fragment of murine Shh-N begins with cleavage of the first 24 amino acids of the signal sequence and ends by autocatalytic cleavage between Lys195 and Ser196, resulting in a 19-kD domain that shows extensive homology among the *hedgehog* genes (*SHH*: exon 1: amino acids 1–100, exon 2: 101–187, exon 3: 188–462). Identical amino acids are shown in red, and the sites of mutations in green. A gap is introduced in the protein sequence to mark the exon boundaries. The Gly31Arg mutation in ADHPE 10 occurs at an invariant residue in the six sequences shown, as well as mosquito[28], rat[17] and *Xenopus*[14]. The presumptive signal cleavage site precedes a consensus sequence CGPGRG[16]. The mutations in ADHPE 6 and 14 are stop codons at the positions indicated. Mutations in ADHPE 2 and 15 involve the invariant Trp117 codon and cause the substitution of Arg or Gly, respectively. This amino acid immediately follows the first alpha helix of the murine Shh-N structure[28].

© 1996 Nature Publishing Group http://www.nature.com/naturegenetics

region of 7q36 as *SHH*[33]) if we propose that low level *SHH* expression in the caudal region mimics absence of the caudal notochord. Further studies of the regulation of *Shh* gene expression and signaling mechanisms[19,34] may ultimately suggest candidate genes for additional *HPE* loci.

Methods

Patients. Thirty unrelated families with ADHPE, including 8 families previously shown to be linked to 7q36 (ref. 5), were studied for SSCP changes in the first two exons of *SHH*. None of the five detected SSCP alterations were found in over 100 normal chromosomes.

Mutation analysis. DNA was extracted from lymphocytes or established lymphoblastoid cell lines from affected and unaffected members of each family by routine methods and SSCP analysis was performed essentially as described[35]. Amplicons demonstrating SSCP band shifts were analyzed by the Nucleic Acid/Protein Core facility of the Children's Hospital of Philadelphia using an ABI 373A automated sequencer. The primers used for exon amplification are described below. For exon 1, the *SHH*/1F1 primer 5'–CAGCCAGCGAGGGAGAGAGCGAGCGGGCGA–3' and *SHH*/1R1 primer 5'–TAAGTCTGGAAGTGTTCGGCTTCTC–3' were used with the cycle parameters: 94 °C for 1 min, 60 °C for 45 sec, 72 °C for 1 min, 35 cycles. After amplification the reaction was digested with *Bgl*II into subfragments (170 bp and 350 bp) and resolved on a 6% glycerol polyacrylamide gel. Exon 2 was amplified as two subfragments. For the first portion of exon 2 we used *SHH*/2F2 5'–GGCAGGCTGATGGAGGGGCCGGGA–3' and *SHH*/2R3 5'–GACGTGGTGATGTCCACTGCGCGGC–3' which gives a 248-bp product. The second portion of exon 2 was amplified with primers *SHH*/2F3 5'–CCACTCAGAGGAGTCTCTGCACTA–3' and *SHH*/2R1 5'–AAAGCAGTCATGCCCAGCGACCCTGC–3' which gives a 293-bp product. The cycle parameters for both portions of exon 2 were the same (94 °C for 1 min, 70 °C for 45 sec, 72 °C for 1 min, 35 cycles). Standard PCR reaction conditions were (50 μl) 50 ng genomic DNA, 200 μM dNTP, 25 pmol of each primer, 1% formamide, 10 mM Tris-HCl pH 8.3, 50 mM KCl, 1.5 mM $MgCl_2$, 0.0001% w/v gelatin and 1 U AmpliTaq polymerase (Perkin Elmer). Attempts to amplify all or part of exon 3 were unsuccessful, possibly due to the high GC content.

Acknowledgements

We are grateful to H. H. Ardinger for providing panels d and e and V.P. Johnson for panels f and g in Fig. 1. We thank D. Telem for technical assistance, and M.M. Cohen, Jr., H.H. Kazazian, Jr., C.L. Bevins, M. Tessier-Lavigne and C. Tabin for comments and suggestions. E.R. was supported by a postdoctoral training grant from the NIH (5T32HD07107). E.B. is a recipient of a fellowship from Telethon, Italia. This work was supported by grants from the Canadian Genetic Disease Network, the Canadian Genome Analysis and Technology Program, a Howard Hughes International fellowship, and the Medical Research Council of Canada to L.-C. T., and NIH grants (R29HD28732 and RO1HD29862) to M.M.

Received 4 October; accepted 11 October 1996.

1. Cohen, M.M., Jr. Perspectives on holoprosencephaly, Part I. Epidemiology, genetics, and syndromology. *Teratology* **40**, 211–235 (1989).
2. Cohen, M.M., Jr. Perspectives on holoprosencephaly, Part III. Spectra, distinctions, continuities, and discontinuities. *Am. J. Med. Genet.* **34**, 271–288 (1989).
3. Cohen, M.M., Jr. & Sulik, K.K. Perspectives on holoprosencephaly. Part II. Central nervous system, craniofacial anatomy, syndrome commentary, diagnostic approach, and experimental studies. *J. Craniofac. Genet. Dev. Biol.* **12**, 196–244 (1992).
4. Muenke, M. Holoprosencephaly as a genetic model for normal craniofacial development. *Sem. Dev. Biol.* **5**, 293–301 (1994).
5. Muenke, M. *et al.* Linkage of a human malformation, familial holoprosencephaly, to chromosome 7 and evidence for genetic heterogeneity. *Proc. Nat. Acad. Sci. U.S.A.* **91**, 8102–8106 (1994).
6. Muenke, M. *et al.* Physical mapping of the holoprosencephaly critical region in 21q22.3, exclusion of *SIM2* as a candidate gene for holoprosencephaly, and mapping of *SIM2* to a region of chromosome 21 important for Down syndrome. *Am. J. Hum. Genet.* **57**, 1074–1079 (1995).
7. Schell, U. *et al.* Molecular characterization of breakpoints in patients with holoprosencephaly and definition of the *HPE2* critical region 2p21. *Hum. Mol. Genet.* **5**, 223–229 (1995).
8. Gurrieri, F. *et al.* Physical mapping of the holoprosencephaly critical region of 7q36. *Nature Genet.* **3**, 247–251 (1993).
9. Overhauser, J. *et al.* Physical mapping of the holoprosencephaly critical region in 18p11.3. *Am. J. Hum. Genet.* **57**, 1080–1085 (1995).
10. Belloni, E. *et al.* Identification of *Sonic Hedgehog* as a canddiate gene for holoprosencephaly. *Nature Genet.* **14**, 353–356 (1996).
11. Marigo, V. *et al.* Cloning, expression, and chromosomal location of *SHH* and *IHH*: two human homologues of the *Drosophila* segment polarity gene *Hedgehog*. *Genomics* **28**, 44–51 (1995).
12. Nüsslein-Volhard, C. & Wieschaus, E. Mutations affecting segment number and polarity in *Drosophila*. *Nature* **287**, 795–801 (1980).
13. Lee, J.J., von Kessler, D.P., Parks, S. & Beachy, P.A. Secretion and localized transcription suggest a role in positional signaling for products of the segmentation Gene *hedgehog*. *Cell* **71**, 33–50 (1992).
14. Ekker, S.C. *et al.* Distinct expression and shared activities of members of the *hedgehog* gene of *Xenopus laevis*. *Development* **121**, 2337–2347 (1995).
15. Riddle, R.D., Johnson, R.L., Laufer, E. & Tabin C. *Sonic hedgehog* mediates the polarizing activity of the ZPA. *Cell* **75**, 1401–1416 (1993).
16. Echelard, Y. *et al.* *Sonic hedgehog*, a member of a family of putative signaling molecules, is implicated in the regulation of CNS polarity. *Cell* **75**, 1417–1430 (1993).
17. Roelink, H. *et al.* Floor plate and motor neuron induction by *vhh-1*, a vertebrate homolog of *hedgehog* expressed by the notochord. *Cell* **76**, 761–775 (1995).
18. Krauss, S., Concordet, J.P. & Ingham, P.W. A functionally conserved homolog of the *Drosophila* segment polarity gene *hh* is expressed in tissues with polarizing activity in zebrafish embryos. *Cell* **75**, 1431–1444 (1993).
19. Fan, C.-M., Porter, J. A., Chiang, C., Chang, D. T., Beachy, P.A. & Tessier-Lavigne, M. Long-range sclerotome induction by sonic hedgehog: direct role of the amino-terminal cleavage product and modulation by the cyclic AMP signalling pathway. *Cell* **81**, 457–465 (1995).
20. Tanabe, Y., Roelink, H. & Jessell, T. M. Induction of motor neurons by *Sonic hedgehog* independent of floor plate differentiation. *Curr. Biol.* **5**, 651–658 (1995).
21. Fietz, M.J., Jacinto, A., Taylor, A.M., Alexandre, C. & Ingham, P.W. Secretion of the amino-terminal fragment of the Hedgehog protein is necessary and sufficient for hedgehog signalling in *Drosophila*. *Curr. Biol.* **5**, 643–649 (1995).
22. Porter, J.A. *et al.* The product of hedgehog autoproteolytic cleavage is active in local and long-range signalling. *Nature* **374**, 363–366 (1995).
23. Marti, E, Bumcrot, D.A., Takada, R. & McMahon, A.P. Requirement of the 19K form of Sonic hedgehog for induction of distinct ventral cell types in CNS explants. *Nature* **375**, 322–325 (1995).
24. Ericson, J., Muhr, J., Piaczek, M., Lints, T., Jessell, T. M. & Edlund T. Sonic hedgehog induces the differentiation of ventral forebrain neurons: a common signal for ventral patterning within the neural tube. *Cell* **81**, 747–756 (1995).
25. Johnson, R.L., Laufer, E., Riddle, R.D. & Tabin, C. Ectopic expression of Sonic hedgehog alters dorsal-ventral patterning of somites. *Cell* **79**, 1165–1173 (1994)
26. Huang, Z. & Krauss, S. Hedgehog, transmitted along retinal axons, triggers neurogenesis in the developing visual centers of the *Drosophila* brain. *Cell* **86**, 411–422 (1996).
27. Macdonald, R., Barth, K.A., Xu, Q., Holder, N., Mikkola, I. & Wilson, S.W. Midline signalling is required for Pax gene regulation and patterning of the eyes. *Development* **121**, 3267–3278 (1995).
28. Hall, T.M.T., Porter, J.A., Beachy, P.A. & Leahy, D.J. A potential catalytic site revealed by the 1.7-A crystal structure of the amino-terminal signalling domain of Sonic hedgehog. *Nature* **378**, 212–216 (1995).
29. Chiang, C. *et al.* Cyclopia and defective axial patterning in mice lacking *Sonic hedgehog* gene function. *Nature* **383**, 407–413 (1996).
30. Roelink, H. *et al.* Floor plate and motor neuron induction by different concentrations of the amino-terminal cleavage product of Sonic hedgehog autoproteolysis. *Cell* **81**, 445–455 (1995).
31. Hatta, K., Kimmel, C.B., Ho, R.K. & Walker, C. The *cyclops* mutation blocks specification of the floor plate of the zebrafish central nervous system. *Nature* **350**, 339–341 (1991).
32. Schulte-Merker, S., van Eeden, F.J.M., Halpern, M.E., Kimmel, C.B. & Nüsslein-Volhard, C. *No tail* (nt) is the zebrafish homologue of the mouse *T (Brachyury)* gene. *Development* **120**, 1009–1015 (1994).
33. Lynch, S.A. *et al.* A gene for autosomal dominant sacral agenesis maps to the holoprosencephaly region at 7q36. *Nature Genet.* **11**, 93–95 (1995).
34. Hammerschmidt, M., Bitgood, M.J. & McMahon, A.P. Protein kinase A is a common negative regulator of Hedgehog signaling in the vertebrate embryo. *Genes & Devel.* **10**, 647–658 (1996).
35. Muenke, M. *et al.* A common mutation in the fibroblast growth factor receptor 1 gene in Pfeiffer syndrome. *Nature Genet.* **8**, 269–274 (1994).
36. Ardinger, H.H. & Bartley, J.A. Microcephaly in familial holoprosencephaly. *J. Craniofac. Genet. Dev. Biol.* **8**, 53–61 (1988).
37. Johnson, V.P. Holoprosencephaly: a developmental field defect. *Am J. Med. Genet.* **34**, 258–264 (1989).

Cyclopia and defective axial patterning in mice lacking *Sonic hedgehog* gene function

Chin Chiang*†, Ying Litingtung*†, Eric Lee*, Keith E. Young†, Jeffrey L. Corden†, Heiner Westphal* & Philip A. Beachy†

* Laboratory of Mammalian Genes and Development, National Institute of Health, Bethesda, Maryland 20892, USA
† Howard Hughes Medical Institute, Department of Molecular Biology and Genetics, Johns Hopkins University School of Medicine, Baltimore, Maryland 21205, USA

Targeted gene disruption in the mouse shows that the *Sonic hedgehog* (*Shh*) gene plays a critical role in patterning of vertebrate embryonic tissues, including the brain and spinal cord, the axial skeleton and the limbs. Early defects are observed in the establishment or maintenance of midline structures, such as the notochord and the floorplate, and later defects include absence of distal limb structures, cyclopia, absence of ventral cell types within the neural tube, and absence of the spinal column and most of the ribs. Defects in all tissues extend beyond the normal sites of *Shh* transcription, confirming the proposed role of Shh proteins as an extracellular signal required for the tissue-organizing properties of several vertebrate patterning centres.

EXPERIMENTAL vertebrate embryology has demonstrated the capacity of certain tissues to influence the pattern of cell types within adjacent embryonic tissues, presumably through the action of secreted signalling molecules. Vertebrate gene products related to that of *hedgehog* (*hh*), first characterized as encoding a secreted protein signal in *Drosophila*[1,2], have emerged as the molecules likely to be responsible for several such patterning activities. The most-studied member of this multi-gene family in vertebrates is *Sonic hedgehog* (*Shh*), which has been isolated from many species, including mouse, chicken, rat, frog, fish and human[3-9]. These initial studies of *Shh* gene expression demonstrated an association with embryonic structures such as the notochord, the floorplate of the neural tube, and the posterior margin of tetrapod limb buds, all of which are known to have organizing properties in transplantation and grafting experiments.

The expression of *Shh* at these locations and the secretion of the Shh protein suggest that it is involved in patterning. Support for this suggestion comes from experimental expression or placement of the Shh protein at ectopic locations in embryos, and from treatment of explanted embryonic target tissues with purified protein. Thus, for example, cells infected with a retrovirus carrying the chicken *Shh* gene or transfected with a mouse *Shh* expression construct are capable of inducing mirror-image limb-digit duplications when grated to the anterior margin of the embryonic chick limb bud[6,7]; similar duplications resulted from grafting of beads impregnated with purified protein to the anterior limb bud margin[10]. In the neural tube, ectopic expression of *Shh* promotes the expression of genes normally expressed at or near the ventral midline, analogous to the effects of ectopic notochord grafts[3,5,6,11]. These ventral patterning effects extend to the brain and eyes[9,12-14] and to the somites, where *Shh* seems to promote formation of sclerotome ventrally and to repress more dorsal somite fates[15,16]. Treatment of neural plate and presomitic mesoderm explants with purified protein also induced cell type-specific genes, with floorplate markers induced at high concentrations and motor neuron and sclerotome markers at lower concentrations[16-18].

These experimental approaches demonstrated a potential role for *hh* activity in several aspects of embryonic patterning. However, because multiple vertebrate *hh* genes display similar signalling activities[8,9,14], these studies did not establish a unique requirement for *Shh*. To examine more directly the role of *Shh* in normal embryonic patterning and to search for other as-yet unidentified patterning activities, we undertook the targeted mutagenesis of the *Shh* gene in the mouse.

Targeted disruption of *Shh*

Mice homozygous for a disrupted *Shh* gene were generated by using homologous recombination in embryonic stem (ES) cells (Fig. 1*a*). In the targeting vector, a PGK-*neo* cassette replaced exon 2 and portions of the flanking introns, leaving coding sequences that would result in a truncated protein (Fig. 1*a*). This deletion causes a loss of 97 of the 198 residues within the N-terminal product of *Shh* autocatalytic processing, including most of the $\alpha + \beta$ sandwich (both of the α-helices and the central four of six β-strands) that forms the core of the N-terminal domain structure[19]. This domain is responsible for all Shh signalling activity, including the induction of a variety of ventral neural and somite cell types, and also the induction and patterning of distal limb structures[9,10,12,17,18,20,21]. The targeting vector also contains two thymidine kinase genes at positions flanking the *Shh* genomic region for counter-selection of ES cells.

Southern analysis of 200 ES clones selected for thymidine kinase and neo resistance revealed 19 with a 5.5-kb *Eco*RI fragment, indicative of the deletion of exon 2 (data not shown). Chimaeric mice were generated by blastocyst injections from six independent ES cell lines containing the disrupted *Shh* allele. Two *Shh* mutant lines were then established through germline transmission of ES clones 199 and 184. Genotypes of the progeny were determined using Southern and polymerase chain reaction (PCR) analyses (Fig. 1*b*, *c*). Heterozygous mice seem normal, but only two homozygous mutant stillborn pups from more than a thousand progeny were recovered from crosses of $Shh^{+/-}$ individuals. Genotypic analysis of embryos from 7.5 to 18.5 days post-coitum (d.p.c.) showed no obvious deviation from the expected Mendelian ratio (data not shown), indicating that most *Shh* mutant embryos die at or just before birth, with probable rapid cannibalization of stillborn pups.

Abnormal anatomy and histology

The earliest detectable morphological defects occur in the future forebrain region of homozygous mutant embryos at embryonic day 9.5 (E8.5). The cephalic neural tube at this stage has not yet closed, and the neural folds are quite extensive with well-defined lips that extend to a clearly defined ventral midline. In *Shh* mutant

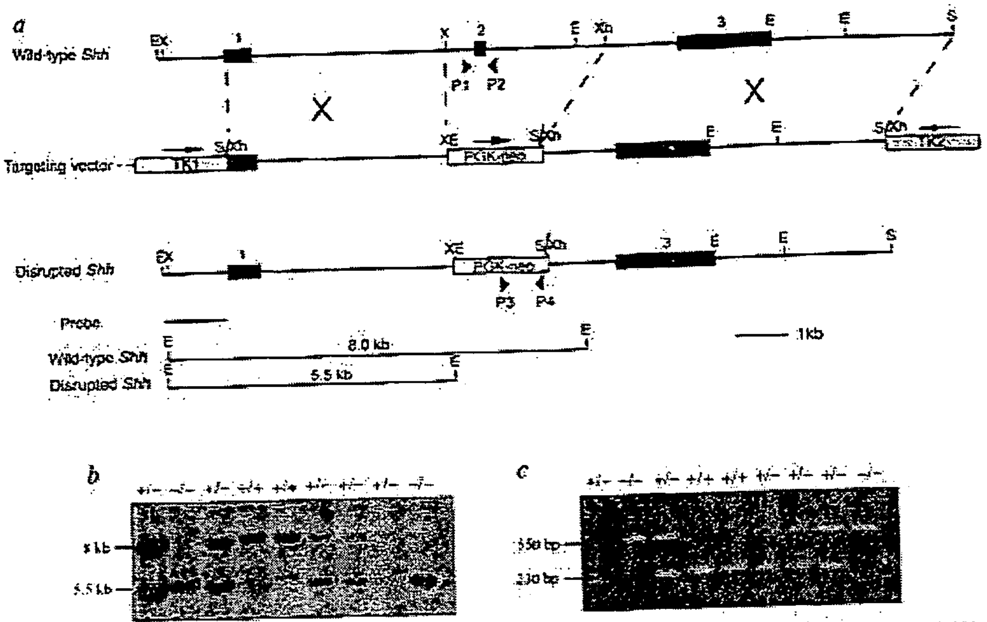

FIG. 1 Disruption of the *Shh* gene by targeted recombination. *a*, Maps of the wild-type *Shh* locus, the targeting vector, and the disrupted *Shh* allele. Relative positions of the three *Shh* exons are indicated by black boxes. The map of the targeting vector shows the replacement of exon 2 and flanking genomic sequences by the Neomycin gene (*neo*), and the locations of two flanking HSV thymidine kinase genes (TK). Arrowheads denote the sites within the wild-type and the disrupted *Shh* alleles from which PCR primers are derived; lines at the bottom indicate expected sizes for *Eco*RI-generated fragments detected with a 5′ flanking genomic probe from wild-type and disrupted *Shh* alleles. *b*, Southern analysis of DNA from individual embryos, the progeny of a heterozygous mating. Sizes of the wild-type and the targeted alleles are indicated by 8-kb and 5.5-kb hybridizing bands, respectively. *c*, PCR analysis of the same DNA samples as in *b*. The 230-bp (primers P1 and P2) and 550-bp (primers P3 and P4) amplification products are specific to exon 2 of the wild-type *Shh* and to the *neo* gene within the disrupted *Shh* locus, respectively.

embryos, however, the midline is indistinct (compare Fig. 2*a* with Fig. 2*b*; arrow), the ventral lips of the cephalic folds are fused, and the normally separate optic vesicles appear instead as a continuous single vesicle protruding at the ventral midline. The cephalic defects in *Shh* mutant embryos become even more apparent when the neural tube closes, with an overall reduction in size of the brain and spinal cord. This is especially apparent at the mesencephalic/diencephalic junction of E9.5 embryos, where floor and roof of the neural tube are almost in contact with each other (arrowhead in Fig. 2*c*). By E11.5, as normal brain structures become more prominent, the small size and defects in the presumptive midbrain and forebrain of *Shh* mutant embryos can be clearly observed (Fig. 2*d*); the most obvious specific defect is the absence of externally visible lateral eye structures. By E15.5 (Fig. 2*e*), *Shh* mutant embryos exhibit severe growth retardation throughout most of the embryo and lack the distinct forelimb and hindlimb structures found in their normal littermates. In addition, relative growth deficits in the forebrain and in craniofacial structures are so extreme that normal facial features such as the eyes, nose and oral structures are not identifiable, and the sole remaining external feature of the mutant head is a proboscis-like extension that protrudes from the rostral midline. Gross inspection and preliminary histological analysis of the internal organs of E18.5 mutant embryos revealed abnormalities of heart, lung, kidney and foregut development (C.C. *et al.*, unpublished data), although asymmetry of early heart looping and internal organ situs appeared normal in all mutant embryos examined.

As noted above, bilateral eye structures are not observed in *Shh* mutant embryos at any stage of development, and the optic vesicle is single and continuous from its earliest appearance at ~E8.5. At E9.5, expression of the gene *microphthalmia* can be detected throughout this vesicle (Fig. 2*f*, *g*), suggesting that these cells are precursors of pigmented retinal epithelium[22]. Indeed, by E15.5 an accumulation of pigmented tissue is found consistently at the base of and just under the proboscis of these mutant embryos (Fig. 2*c*, arrowhead). In addition, expression of *Fgf-8* at E10.5 revealed a single nasal pit at the midline instead of the bilateral pits normally observed (compare Fig. 2*h* with Fig. 2*i*). Cross-sections of the neural tube at the level of the spinal cord and at other axial levels also revealed the absence of a morphologically distinct floorplate in E9.5 *Shh* mutants, with the ventral region of the neural tube consisting instead of a thick epithelium (compare Fig. 2*j* with Fig. 2*k*; arrow). Notochord tissue is evident in cross-sections from caudal and some rostral axial levels in mutant embryos at this stage (see also Fig. 3).

Staining of bone and cartilage also revealed defects in the cranio-facial, axial and appendicular skeleton of *Shh* mutant embryos. Cranio-facial bones are severely affected and are almost entirely absent (Fig. 2*m*, *n*) despite the presence and nearly normal appearance of the branchial arches at E9.5 (Fig. 2*c*). Defects of the cranio-facial skeleton are commonly observed in association with neural tube defects, and in the case of *Shh* mutants these may be a secondary consequence of the extreme midbrain and forebrain defects. In the axial skeleton of *Shh* mutant embryos, most sclerotomal derivatives including the entire vertebral column are absent, with only five or six rib cartilages remaining. Other rib structures are difficult to assign in the absence of a vertebral column, but their cartilaginous composition suggests an anterior and ventral nature. In the appendages, distal structures are most affected, with a complete absence of digits and absence or fusion of the paired distal limb bones. Thus, in the hindlimb, which is more severely affected, the tibia and fibula are completely absent, although the femur is formed (Fig. 2*m*, *n*). In the forelimb, a bony extension of the humerus may represent either a fused ulna/radius or simply a long, bent humerus; these possibilities are difficult to distinguish given the absence of cartilage, which normally separates these bones at the elbow joint (Fig. 2*m*, *n*; arrow).

Defective axial structures

Because notochord tissue seems to be present in caudal but not rostral cross-sections of E9.5 *Shh* mutant embryos, we sought to determine whether the notochord is established normally or displays defects at earlier stages. Fate mapping and transplant studies have shown that the regressing node is the primary source of notochord tissue during early embryonic development[23,24]. The *Brachyury* gene, which encodes a DNA-binding protein and is required for differentiation of the notochord, is normally expressed in the primitive steak and in the node and developing notochord of E7.5 and E8.5 embryos[25]. In E7.75 *Shh* mutant embryos, *Brachyury* gene expression appears normal, consistent with the presence of the node at this early stage of development

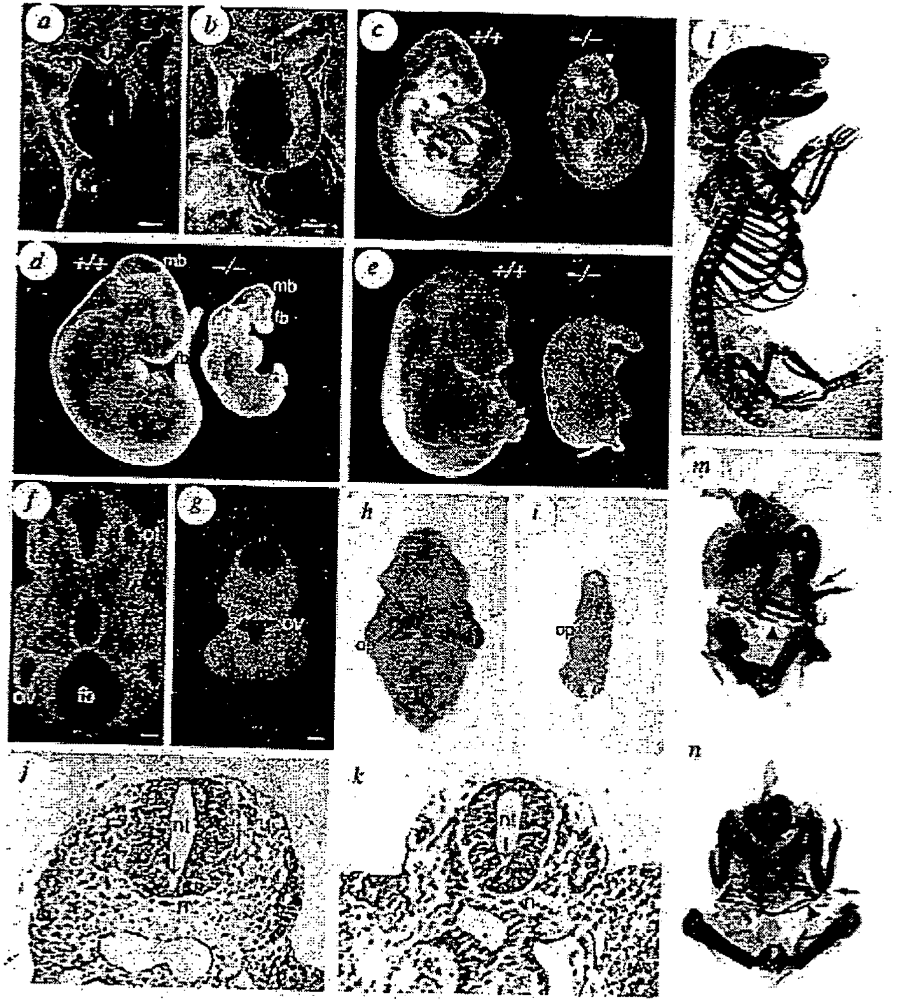

FIG. 2 Abnormal anatomy and histology of *Shh* mutant embryos. *a*–*e*, External morphology of wild-type (+/+) and mutant (−/−) embryos. *a*, *b*, Scanning electron micrographs of the rostral ends of E8.5 wild-type (*a*) and mutant (*b*) embryos; note the lack of a distinct midline (arrow) and the single continuous optic vesicle at the ventral midline of the mutant embryo. *c*, Lateral view of E9.5 embryos. An abnormal cephalic flexure and the apposition of ventral and dorsal neural tube surfaces is indicated by the arrowhead. *d*, Lateral view of E11.5 embryos. Note the reduction in overall size, the abnormal forebrain morphology, and the lack of bilateral eye structures in the mutant embryo. *e*, Lateral view of E15.5 embryos. At this stage the craniofacial region of the mutant embryo consists of a long proboscis, at the base of which is an accumulation of pigmented cells (arrowhead). Note the stunted limbs of the mutant. *f*, *g*, Cross-sections of E9.5 wild-type (*f*) and $Shh^{-/-}$ (*g*) embryos at the level of the optic vesicles hybridized with *microphthalmia* (*mi*) antisense RNA. Note the presence of a single *mi*-expressing optic vesicle in $Shh^{-/-}$ embryos. *h*, *i*, Facial view of whole-mount *in situ* hybridization with *Fgf8* antisense RNA to E10.5 wild-type (*h*) and $Shh^{-/-}$ (*i*) embryos. *Fgf8* expression highlights a single nasal pit forming within a single olfactory placode in the mutant embryo. *j*, *k*, Cross-sections at the level of the hind limb of wild-type (*j*) and $Shh^{-/-}$ (*k*) stained with haematoxylin and eosin. Note the lack of a floorplate in the ventral midline of the mutant neural tube (arrow), despite the apparent presence of notochord tissue. *l*–*n*, Bone (brown) and cartilage (blue) stains of E18.5 wild-type (*l*) and $Shh^{-/-}$ embryos (*m*, *n*). In $Shh^{-/-}$ embryos, most of the sclerotomal derivatives such as spinal column (*l*, arrow) are missing with the exception of some rib cartilages (*m*, *n*, arrowhead). The distal limb structures are also missing; note the absence of cartilage at the elbow joint in the mutant (*m*, *n*, arrow). Abbreviations: fb, forebrain; mb, midbrain; n, notochord; nt, neural tube; op, olfactory placode; ov, optic vesicle; ot, otic vesicle. Scale bar, 100 μm. For comparison, mutant embryos in *m* and *n* are shown at 2.5-fold magnification relative to the wild-type in *l*.

(data not shown). By E8.5, however, *Brachyury* gene expression becomes discontinuous in the rostral portion of mutant embryos (Fig. 3*a*). By E9.5, the rostral-most expression of the *Brachyury* gene is completely lost (Fig. 3*b*); this loss progresses in a rostral-to-caudal direction, as indicated by patchy *Brachyury* gene expression more caudally. The progressive, rostral-to-caudal loss of notochord tissue concomitant with loss of *Brachyury* gene expression suggests that *Shh* is required for the maintenance, but not the formation, of the notochord.

The *HNF-3β* gene, which encodes a winged-helix transcription factor required for development of the axial structures[26,27], is expressed in the node, developing notochord, head process, floorplate and gut endoderm, in a spatial pattern that is similar to but slightly precedes that of *Shh*[3]. At E7.75, although the localization of *HNF-3β* expression seems normal in *Shh* mutant embryos, the level of expression is consistently reduced in the notochord and in the head process (Fig. 3c). By E8.5, *HNF-3β* expression in axial mesoderm is completely absent (Fig. 3*d*), although gut expression persists for at least one more day of embryonic development (data not shown); expression of *HNF-3β* in the ventral neural tube of mutant embryos is never initiated. Initiation of *HNF-3β* expression in the ventral neural tube in normal embryos occurs before the stage at which the notochord degenerates in *Shh* mutant embryos; the failure to initiate *HNF-3β* expression in mutant neural tube thus suggests that Shh protein is the notochord-derived signal required for *HNF-3β* induction in the normal neural tube.

The notochord is also known to induce differentiation of other ventral cell types within the neural tube, including motor neurons[28]. The *Islet-1* gene (*Isl-1*) encodes a LIM homeodomain protein that is expressed in motor neurons, and mice lacking function of this gene fail to form motor neurons[29]. We therefore examined mutant embryos for the expression of Isl-1 protein as a marker for the presence of motor neurons. Normal expression of Isl-1 in the neural tube is first detected at E9.5 in a punctate pattern of nuclear staining lateral to the floorplate (Fig. 3*e*). In *Shh* mutant embryos, Isl-1 expression is absent in the neural tube at all axial levels (Fig. 3*f*), including caudal levels where the notochord persists. Failure to induce the Isl-1 marker even in the presence of the notochord suggests that Shh protein from the notochord may be required for differentiation of motor neurons. Alternatively, differentiation of motor neurons may require signalling from the floorplate, or from both the notochord and the floorplate.

Dorsoventral pattern defects in the neural tube

Given the degeneration of the notochord and failure of the floorplate to develop in *Shh* mutant embryos, we examined dorsoventral (D–V) patterning of the neural tube at E11.5 by assaying the expression patterns of various *Pax* gene family members (reviewed in ref. 30). In the neural tube at the level of the prospective spinal cord, *Pax-3* is normally expressed in the alar palte, corresponding to the dorsal half of the neural tube (Fig. 4*a*).

Pax-6, in contrast, is expressed only weakly in the alar plate and more strongly throughout the basal plate except at the ventral midline (Fig. 4*c*). In *Shh* mutant embryos, high levels of *Pax-3* expression extend ventrally and across the midline where floorplate would normally be present (Fig. 4*b*). Similarly, expression of *Pax-6* also extends across the ventral midline in mutant embryos and is reduced to a level more characteristic of normal alar plate expression (Fig. 4*d*). In *Shh* mutant embryos, gene expression patterns in the ventral neural tube thus appear to lose the characteristics of normal basal plate (exclusion of *Pax-3*) and floorplate (exclusion of *Pax-6* from the midline) and acquire alar plate characteristics such as a high level of *Pax-3* expression and a reduced but uniform overall level of *Pax-6* expression. *Pax-2* expression, normally restricted to interneuronal regions of the alar and basal plates that lie adjacent to the sulcus limitans, also expands across the ventral midline in mutant embryos (Fig. 4*e*, *f*). The normal exclusion of *Pax-2* from dorsal parts of the neural tube is preserved, however, suggesting that dorsal pattern is maintained within *Shh* mutant embryos.

Because the notochord degenerates in *Shh* mutant embryos, the abnormal patterning of the ventral neural tube may be an indirect consequence of this loss rather than a direct consequence of loss of *Shh* function. To assess this possibility, expression of *Pax-3* within the E9.5 neural tube was examined in the caudal portion of mutant embryos where some notochord tissue is still present (compare Fig. 5*a* with Fig. 5*b*). The inability of notochord lacking *Shh* function to exclude *Pax-3* expression from the ventral portion of the neural tube, in conjunction with the results of ectopic expression[3,5,6,9,11–13] and explant studies[6,17,18,21], suggests a direct role for *Shh* in neural tube patterning.

Patterning of paraxial mesoderm

Differentiation of the somite into dorsal dermatome, medial myotome and ventral sclerotome is mediated by inductive signals derived from surrounding tissues[31]. Previous studies have shown that *Shh* is capable of inducing expression of the ventral sclerotomal marker *Pax-1* and of suppressing the dorsal dermomyotomal marker *Pax-3*, either when expressed ectopically in the chick or when applied to presomitic mesoderm explants[15,16,20]. The expression of *Pax-3* normally is confined to the dermomyotome of the differentiating somite (Fig. 5*a*). In E9.5 mutant embryos *Pax-3* expression is ventrally expanded (Fig. 5*b*), suggesting that the sclerotome may also be affected. Surprisingly, we observed weak but reproducible *Pax-1* expression in E9.5 mutant somites (compare Fig. 5*c* with Fig. 5*d*), with a region of higher expression in a block of five or six somites (compare Fig. 5*e* with Fig. 5*f*). By E11.5 all somite expression of *Pax-1* is lost (Fig. 5*g*, *h*), indicating that *Shh* is essential for the maintenance, but not the initiation, of sclerotomal *Pax-1* expression.

The presence of skeletal muscle in later-stage *Shh* mutant embryos (data not shown) indicates that differentiation of myotomal derivatives does not require *Shh* function. However, at least two myotomal components have been resolved within the somite, the medial *myf-5*-expressing component and the lateral MyoD-expressing component (reviewed in ref. 32). We observed significantly reduced accumulation of *myf-5* transcripts at E9.5 (Fig. 5*i*, *j*) and normal levels of MyoD protein at E10.5 (Fig. 5*k*, *l*) throughout the axis of mutant embryos. These results are consistent with reports that medial but not lateral myotomal components are dependent on axial structures[33,34], and further suggests the possibility that *Shh* function contributes to this signal. As also observed for the *Pax-1* sclerotomal marker, however, *Shh* function appears not to initiate but to enhance or maintain expression of the *myf-5* lateral myotomal markers.

Patterning of brain and eye

In comparison with their normal littermates, the brains of *Shh*$^{-/-}$ embryos are reduced in size, with progressively more severe morphological defects observed in the hindbrain, midbrain and forebrain. To characterize these abnormalities further we examined the expression in *Shh* mutant embryos of several homeobox genes that are expressed in restricted regions of normal E11.5 brain. In the normal forebrain, *Emx-1* expression[35] is restricted to the dorsal telecephalon corresponding to the neocortex (Fig. 6*a*). In *Shh* mutant embryos, *Emx-1* expression can be detected throughout a single vesicle present in the midline (Fig. 6*d*), suggesting that the normally bilateral lobes of the telencephalon are fused to form a single midline structure and that ventral forebrain structures are lost. Consistent with this interpretation, expression of the *Otx-2* gene[36] is also lost in ventral domains of the telencephalon and in the diencephalon (compare Fig. 6*b* with Fig. 6*e*); indeed, most of the diencephalon as an identifiable structure is absent in *Shh* mutant embryos. Reduced expression of *Otx-2* in the mesencephalon is also consistent with the reduction in size and the abnormal morphology of the midbrain in the *Shh* mutant (Fig. 6*e*). The deficit in the midbrain would appear to be in the anterior, as most of the remaining midbrain cells express the *En-2* gene[37], normally restricted to the posterior midbrain (compare Fig. 6*c* with Fig. 6*f*). Expression of the *En-2* gene at the isthmus is essentially normal, consistent with the presence of the midbrain/hindbrain constriction and also with the normal appearance of *Pax-2* expression at this constriction (data not shown). The expression in normal anterior/posterior sequence of *Emx-1*, *Otx-2* and *En-2* in prospective forebrain, midbrain and hindbrain domains suggests that the major requirement for *Shh* gene function is for ventral cell fate specification rather than anteroposterior patterning.

The vertebrate eye originates from evagination of the optic vesicles from the lateral walls of the forebrain (reviewed in ref. 38). After the optic vesicles have formed they undergo an additional invagination to form double-layered cups that differentiate into a neural retina and a pigmented epithelium; these cups remain connected to the diencephalon by the optic stalks. In *Shh* mutant embryos the optic vesicles are fused at the midline and the optic stalks are deficient or absent. There is no invagination to form the characteristic double-layered optic cups, and the fused eye tissue at the midline forms a pigmented epithelium with no apparent differentiation of retinal tissue (Fig. 2*f*, *g*). To analyse eye patterning defects in mutant embryos further we examined the expression patterns of *Pax-6*, *Otx-2* and *Pax-2* genes in the E11.5 mutant eye. *Pax-2* and *Pax-6* have been shown to play important roles during eye development (reviewed in ref. 38) and serve as early markers for proximal cells that contribute to the future optic stalk, and for distal cells that contribute to both layers of the optic cup[2,13], respectively. The expression of *Pax-6* throughout most of the normal optic cup, including the pigmented epithelium and the neural retina, is shown in Fig. 6*g*. *Pax-6* expression occurs throughout the cyclopic mutant eye structure (Fig. 6*j*), which is constituted solely of pigmented epithelium. *Otx-2* expression similarly persists in the cyclopic *Shh* mutant eye (Fig. 6*h*, *k*). The expression of *Pax-2*, normally restricted to the optic stalks connecting the eye primordia to the brain (Fig. 6*i*), is absent in *Shh* mutant embryos (Fig. 6*l*), consistent with the histologically apparent absence of the optic stalk and the loss of ventral forebrain structures.

Discussion

Roles of *Shh* expression in neural patterning and notochord maintenance. One of the early functions of the notochord is to induce differentiation of ventral cell types such as floorplate cells and motor neurons in the overlying neural ectoderm. Our studies demonstrate, however, that, despite the presence of a differentiated notochord during early stages of development, floorplate cells and motor neurons are not induced in *Shh* mutants. Conversely, in other vertebrate mutants, such as the zebrafish *floating head* (*flh*) mutant[39], or the murine *Brachyury* (T) mutant[25] and its zebrafish homologue *no tail* (*ntl*)[40], floorplate cells develop in rostral portions of the embryo despite the absence of a differentiated notochord. These notochord mutants, however, express *Shh* in presumptive notochord precursor cells in the midline. Expression of *Shh* in the absence of definitive notochord differentiation may therefore be sufficient for ventral neural patterning, whereas notochord differentiation in the absence of *Shh* function is not. Together with the results of neural plate explant studies[6,17,18,21], these results suggest that ventral patterning by the *Shh* signal can operate independently of notochord development.

Our finding that *Shh* is not essential for node formation or for notochord differentiation is not surprising, as expression of *Shh* in the node is first detectable at the late streak to early head-fold stages, by which time a morphologically recognizable node and notochord are already present. The requirement for *Shh* in maintenance of the notochord, however, represents a previously

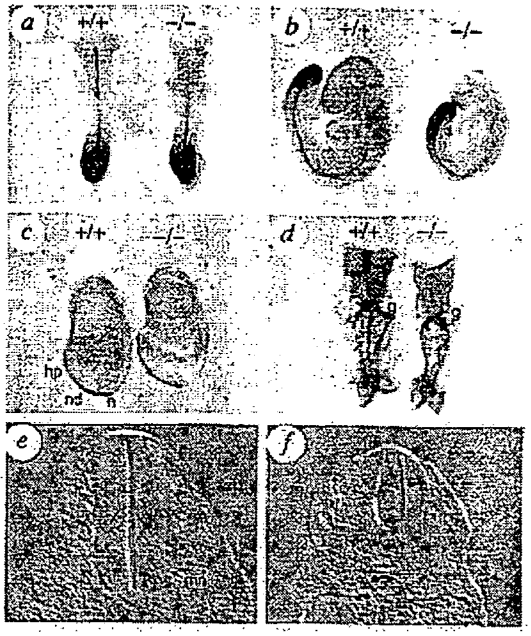

FIG. 3 Defective axial structures in *Shh* mutant embryos. *a*, *b*, Expression of *Brachyury* in E8.5 (*a*) and 9.5 (*b*) embryos. Note the discontinuity and loss of *Brachyury* expression in the rostral part of *Shh* mutant (−/−) embryos. *c*, *d*, Expression of HNF-3β expression in the node (*n*); notochord (nd) and head process (hp) of $Shh^{-/-}$ embryos is similar to the normal pattern, although the level of expression is reduced. At E8.5 (*d*, ventral view), HNF-3β expression in the floorplate and the notochord (arrow) is completely absent, although expression persists in the gut (g). *e*, *f*, Cross-sections through E9.5 wild-type (*e*) and $Shh^{-/-}$ (*f*) embryos at the level of the forelimbs labelled with Islet-1 antibody. Accumulation of Islet-1 protein in the motor neurons (mn, arrow) can be detected as bilateral punctate staining within the ventrolateral portion of the normal neural tube (*e*). This staining is completely absent in $Shh^{-/-}$ embryos (*f*).

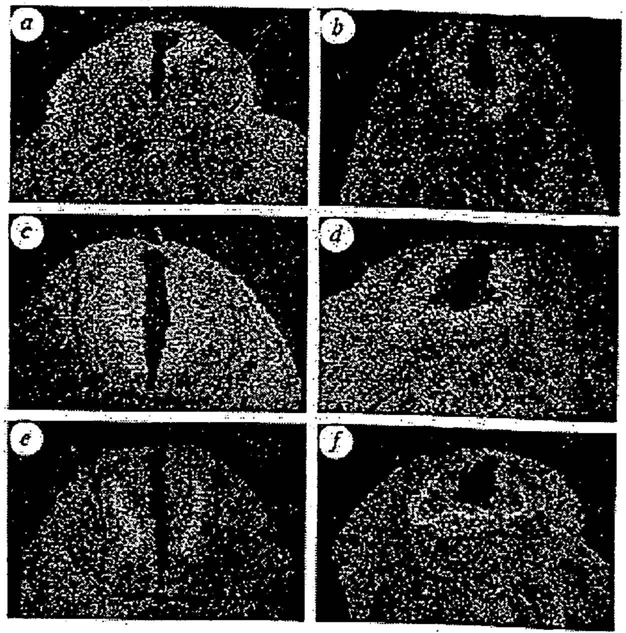

FIG. 4 Dorsoventral patterning defects in the neural tube of *Shh* mutant embryos. *a*–*f*, Cross-sections through E11.5 wild-type (*a*, *c*, *e*) and $Shh^{-/-}$ (*b*, *d*, *f*) embryos hybridized with ^{33}P-labelled antisense RNAs. *a*, *b* *Pax-3* is normally expressed in the alar plate of the neural tube (*a*) but in $Shh^{-/-}$ (*b*) expression expands across the ventral midline of the neural tube. *c*, *d*, *Pax-6* expression, normally high in the basal plate and weak in the alar plate (*c*), is distributed uniformly throughout the neural tube including the ventral midline at a reduced level characteristic of normal alar plate expression (*d*). *e*, *f*, Normal *Pax-2* expression is restricted to the interneuron region flanking the sulcus limitans (*e*) but in $Shh^{-/-}$ mutants it expands across the ventral midline of the neural tube (*f*). Note the exclusion of *Pax-2* expression from the dorsal midline in both wild-type and mutant embryos. Scale bar, 100 μm.

FIG. 5 Somite development in $Shh^{-/-}$ embryos. *a*–*d*, Cross-sections of wild-type (*a*, *c*) and $Shh^{-/-}$ (*b*, *d*) E9.5 embryos showing somite expression of *Pax-3* (*a*, *b*) and *Pax-1* (*c*, *d*). Normal expression of *Pax-3* in the dermomyotome (dm) is ventrally expanded in $Shh^{-/-}$ embryos and *Pax-1* expression is reduced. *e*–*h*, Whole-mount E9.5 (*e*, *f*) and E11.5 (*g*, *h*) embryos showing *Pax-1* expression in wild-type (*e*, *g*) and $Shh^{-/-}$ (*f*, *h*) mutant embryos. Relative to wild type, the reduced level of *Pax-1* sclerotome expression in the E9.5 mutant (*f*) is completely lost by E11.5 (*h*), whereas forelimb expression is largely normal (asterisks). *i*, *j*, Whole-mount E9.5 wild-type (*i*) and $Shh^{-/-}$ (*j*) embryos showing expression of *myf-5* RNA. *k*, *l*, E10.5 wild-type (*k*) and $Shh^{-/-}$ (*l*) embryos showing MyoD protein accumulation in the myotome (arrows). MyoD protein expression in $Shh^{-/-}$ mutant embryos is similar to that in wild type, but expression of *myf-5* RNA in mutant embryos is significantly reduced. Abbreviations: br, branchial arches; dm, dermomyotome; sc, sclerotome.

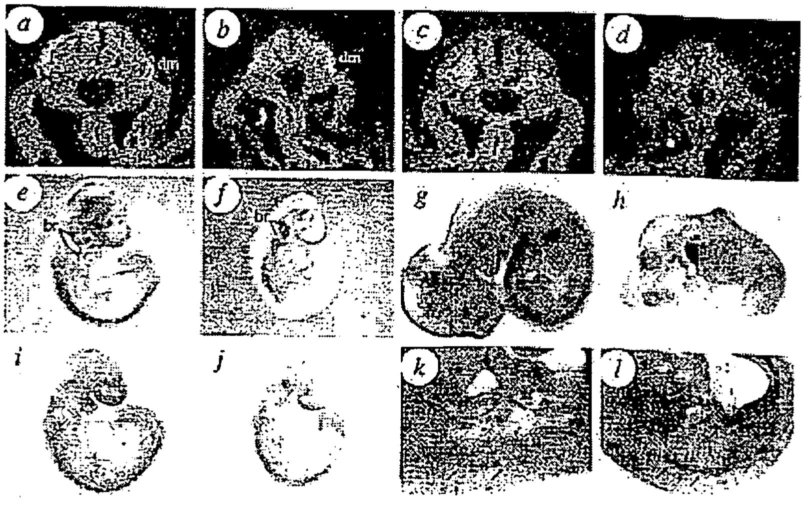

unforeseen role. This maintenance function may represent an autocrine action of the *Shh* signal produced within the notochord. Alternatively, notochord maintenance may require signals derived from other tissues, such as the floorplate, whose formation is dependent on earlier *Shh* function; this possibility seems unlikely, however, given the persistence of notochord in *cyclops* mutants of the zebrafish, which lack floorplate cells[41], and in chick embryos from which the neural tube has been extirpated before floorplate formation[33].

Regulatory interactions in axial tissues. Analysis of the *Shh* mutant phenotype revealed several features of the regulatory interactions between genes expressed in axial tissues. Previous studies had suggested the existence of a positive feedback between the *Shh* signal and the transcription factor *HNF-3β* for mutual maintenance of expression in the neural tube. We have found here that *Shh* is indeed required for the later *HNF-3β* expression, but our analysis also shows that early expression of *HNF-3β* in the axial mesoderm of late streak to early head-fold stages is initiated independently of *Shh* function. Regulation of *HNF-3β* expression thus changes from early independence to a later requirement for *Shh* function.

Another example of changing regulatory relationships in axial structures is the shift of *Brachyury* gene expression from early dependence on *HNF-3β* function[26,27] to later independence, as indicated by our observation in the *Shh* mutant that *Brachyury* gene expression persists considerably longer than expression of *HNF-3β*. Previous studies have suggested that the maintenance of *Brachyury* expression in the notochord is mediated through autoregulation[42]. Alternatively, maintenance of *Brachyury* expression could involve mouse homologues of genes such as *flh*, whose function is required for *ntl* expression in zebrafish[39].

The developmental logic underlying these dynamically changing regulatory relationship seems to be an early marshalling of axial gene expression under the regulatory control of the HNF-3β transcription factor (or perhaps other transcription factors acting upstream). Once expression of axial genes is established, *Shh* and *HNF-3β* expression become mutually interdependent and expression of both genes is established in the ventral midline of the neural tube through the signalling action of the Shh protein. Restriction of other early axial genes such as *Brachyury* to expression in the notochord is accomplished by uncoupling expression from *HNF-3β* regulatory input, and possibly by an increasing reliance on auto-regulation or regulation by other notochord-specific genes such as *flh*.

The role of *Shh* in development of the axial skeleton. Shh protein has been implicated as the notochord-derived signal responsible for induction of the sclerotome[15,38,39], and the reduced level of *Pax-1* expression and the absence of most sclerotomal derivatives in *Shh*$^{-/-}$ embryos suggest a role for *Shh*. Furthermore, the observed skeletal defects in *Shh*$^{-/-}$ embryos overlap with those of *Pax-1* null embryos, in which ventral portions of the vertebrae, such as vertebral bodies, intervertebral discs and a few medial portions of the ribs, are missing[43]. Nevertheless, some expression of *Pax-1* occurs in the absence of *Shh* function, indicating that *Shh* is not absolutely required *in vivo* for specification of sclerotomal cell fates. The role of *Shh* thus might be to maintain or expand the population of committed sclerotome cells. Consistent with this view is the observation that *Shh* protein is a potent mitogen for presomitic explants[39], and that low levels of *Pax-1* are expressed in these explants even in the absence of induction by notochord or Shh protein[16]. The absence of the entire vertebral column in *Shh*$^{-/-}$ embryos, as opposed to a partial loss in *Pax-1* mutant embryos, suggests that sclerotome-promoting effects of *Shh* may involve modulation of other genes in addition to *Pax-1*; one such gene could be *Pax-9*, which is expressed in the sclerotome and has an expression pattern similar to that of *Pax-1* (ref. 44).

The role of *Shh* in limb development. Based on the initial view of *Shh* and the zone of polarizing activity in anteroposterior limb patterning, an early prediction might have been that loss of *Shh* function would lead simply to anterior/posterior mispatterning of

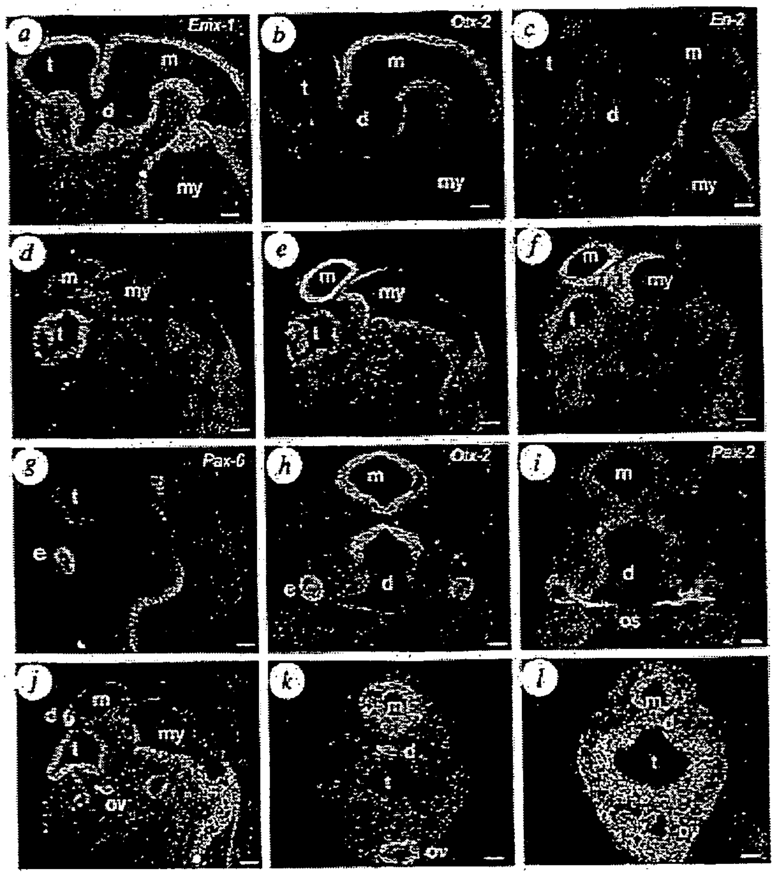

FIG. 6 Brain and eye patterning defects in *Shh* mutant embryos. *a–f*, Parasagittal sections of E11.5 wild-type (*a–c*) and *Shh*$^{-/-}$ (*d–f*) embryos. *a*, *d*, Expression of *Emx-1* is normally restricted to the dorsal telencephalon (*a*). In the *Shh*$^{-/-}$ embryo, *Emx-1* expression can be detected throughout a single telencephalic vesicle located at the midline (*d*). *b*, *e*, Normal expression of Otx-2 in the ventral telencephalon (*b*) is absent in *Shh*$^{-/-}$ embryos (*e*). *c*, *f*, *En-2* expression marks the midbrain/hindbrain boundary, which is present in *Shh*$^{-/-}$ embryos. *g–l*, Parasagittal (*g*); midsagittal (*j*) and coronal (*h*, *i*, *k*, *l*) sections through the eye of E11.5 wild-type (*g–i*) and *Shh*$^{-/-}$ (*j–l*) embryos. *g*, *j*, *Pax-6* expression is retained in the single optic vesicle present in *Shh*$^{-/-}$ embryos. *Pax-6* is also expressed in the remnant of the dorsal diencephalon of *Shh*$^{-/-}$ embryos. *h*, *k*, Otx-2 is expressed in the midbrain, the remnant of the dorsal diencephalon, and the single optic vesicle of *Shh*$^{-/-}$ embryos. Arrow indicates the floorplate in the normal mesencephalon, which is absent in *Shh*$^{-/-}$ embryos. *i*, *l*, The optic stalks and *Pax-2* expression are absent in *Shh*$^{-/-}$ embryos. Abbreviations: d, diencephalon; e, eye; m, mesencephalon; my, myelencephalon; ov, optic vesicle; os, optic stalk; t, telencephalon. Scale bar in *a–j*, 100 μm; in *k*, *l*, 35 μm.

the limbs[4]. The dramatic loss of distal structures observed here, however, indicates that *Shh* plays an important role in promoting distal limb fates. Consistent with such a role for *Shh*, experimental amputations of posterior portions of chick limb buds produced dramatic losses of distal structures[45]. These distal truncations resemble those observed in *Shh* mutant mice, and are far more severe than defects caused by anterior amputations of comparable extent. One possible link between the distal truncations caused by posterior limb-bud amputation and loss of *Shh* function is the apparent role for fibroblast growth factor (FGF) signals in limb outgrowth and the requirement for *Shh* in maintenance of FGF-4 expression in the posterior apical ectodermal ridge[46] (C.C. *et al.*, manuscript in preparation). Normal expression of *Shh* at the posterior margin of the limb bud is thus implicated in dynamically shaping limb pattern during outgrowth, presumably through a fairly local induction of cell proliferation, with distal structures deriving largely from the postaxial region of the limb bud[47].

The role of *Shh* in establishing the ventral midline of the brain and spinal cord. Throughout the neural tube, loss of *Shh* function results in failure to establish cell fates and gene expression patterns characteristic of the ventral midline. Perhaps the most striking defects in *Shh* mutant embryos occur in the forebrain and its derivatives, which at E11.5 consist of a single fused telencephalic vesicle that overlies a single fused optic vesicle situated at the base of an externally apparent proboscis. This phenotype is reminiscent of a spectrum of human congenital malformations referred to collectively as holoprosencephaly, which in its most severe form is accompanied by cyclopia, a single nasal chamber, a single telencephalic vesicle, and other forebrain and facial midline defects[48]. An extensive review of cyclopia and associated developmental malformations raised the key question of whether the eye anlage in the early rostral neural plate is normally single and continuous or instead is bilaterally divided[49,50], and concluded that the early eye field is continuous across the midline and that later subdivision of this single eye field at the midline depends on influences from prechordal plate mesoderm. These conclusions were based on elegant experiments involving *in vivo* culture of median or lateral strips form rostral neural plate, either alone or recombined with underlying prechordal mesoderm or prechordal plate mesoderm. Also consistent with these conclusions is the induction of cyclopia by the removal of prechordal plate mesoderm from beneath the early neural plate of amphibian embryos (reviewed in refs 49, 50).

Our study is consistent with the idea that *Shh* expression in prechordal plate mesoderm contributes to the signal that establishes the ventral midline of the brain and subdivides the eye field. The expression of *Shh* is normally first detected in the prechordal mesoderm underlying the rostral neural plate of mouse embryos at the midstreak stage[17]. In the early head-fold stage of *Shh*$^{-/-}$ embryos, *HNF-3β* and *Brachyury* expression appear normal, indicating that the prechordal plate mesoderm is present during early embryogenesis. Rostral neural plate defects are morphologically apparent shortly thereafter, suggesting that, as observed for spinal cord regionalization and morphogenesis, it is the absence of the *Shh* signal rather than absence of axial mesoderm that is responsible for patterning defects. With regard to eye patterning, we have demonstrated that *Shh* is required for *Pax-2* expression and for optic stalk formation in the forebrain. These results are consistent with previous evidence from zebrafish studies suggesting that *hh* activity from the ventral midline normally stimulates expression of *Pax-2* in the adjacent optic stalk precursors and represses expression of *Pax-6*, thus restricting *Pax-6* expression and its associated retinal and epithelial fates to distal portions of the optic vesicle[5,15]. These effects of *Shh* signalling identify a molecular pathway by which bilateral subdivision of the eye field at the midline might be accomplished while simultaneously imposing a proximo-distal patterning influence on the developing optic vesicle. □

Methods

Targeted recombination of the *Shh* gene. The targeting vector was constructed by inserting a 14-kb *Sal*I (*Sal* sites were vector-derived) fragment of *Shh* genomic DNA into the *Xho*I site of a thymidine kinase-containing vector. To delete the *Shh* exon 2 region, the 3.0-kb *Xba*I/*Xho*I fragment was replaced with the *Xba*I/*Sal*I fragment containing the Pgk-neo cassette. The final targeting vector was linearized at a unique *Xho*I site before use in the transfection of ES cells. R1 ES cells were grown, transfected and subjected to double selection[36,51]. Homologous recombinant ES clones were identified by Southern analysis and further analysed using PCR primers specific to *Shh* exon 2 and to the neo gene to confirm the absence of exon 2 sequences in the disrupted gene. Frozen cells were expanded and used for injection into C57Bl/6J blastocysts. The primers were: P1, 5′-GACCATGTCTGCACACTTAGGTTCC-3′; P2, 5′-GAAGGCCAGGAGGAGAAGGCTCAC-3′; P3, 5′-CTGTGCTCGACGTTGTCACTG-3′; P4, 5′-GATCCCCTCAGAAGAACTCGT-3′.

Histology and *in situ* detection of RNA and protein expression. Embryos were fixed in 4% paraformaldehyde overnight at 4 °C, dehydrated, embedded in paraplast, and sectioned at 5 μm. Sections were stained with haematoxylin and eosin for histological analysis. Cartilage and bones were stained with alcian blue and alizarin red[3]. *In situ* hybridization to tissue sections[7] and *in situ* hybridization to whole embryos were performed[28]. Whole-mount immunohistochemistry using Islet-1 antibody was performed essentially as described[29]. After immunostaining, embryos were sectioned at 5 μm.

Received 9 May; accepted 22 August 1996.

1. Nüsslein-Volhard, C. & Wieschaus, E. Nature 287, 795–801 (1980).
2. Lee, J. J., von Kessler, D. P., Parks, S. & Beachy, P. A. Cell 71, 33–50 (1992).
3. Echelard, Y. et al. Cell 75, 1417–1430 (1993).
4. Riddle, R. D., Johnson, R. L., Laufer, E. & Tabin, C. Cell 75, 1401–1416 (1993).
5. Krauss, S., Concordet, J.-P. & Ingham, P. W. Cell 75, 1431–1444 (1993).
6. Roelink, H. et al. Cell 76, 761–775 (1994).
7. Chang, D. T. et al. Development 120, 3339–3353 (1994).
8. Ekker, S. C. et al. Development 121, 2337–2347 (1995).
9. Ekker, S. C. et al. Curr. Biol. 5, 944–955 (1995).
10. Lopez-Martinez, A. et al. Curr. Biol. 5, 791–796 (1995).
11. Ruiz i Altaba, A., Jessell, T. M. & Roelink, H. Mol. Cell. Neurosci. 6, 106–121 (1995).
12. Lai, C.-J., Ekker, S. C., Beachy, P. A. & Moon, R. T. Development 121, 2349–2360 (1995).
13. Macdonald, R. et al. Development 121, 3267–3278 (1995).
14. Hammerschmidt, M., Bitgood, M. J. & McMahon, A. P. Genes Dev. 10, 647–658 (1996).
15. Johnson, R. L., Laufer, E., Riddle, R. D. & Tabin, C. Cell 79, 1165–1173 (1994).
16. Fan, C.-M. & Tessier-Lavigne, M. Cell 79, 1175–1186 (1994).
17. Roelink, H. et al. Cell 81, 445–455 (1995).
18. Marti, E., Bumcrot, D. A., Takada, R. & McMahon, A. P. Nature 375, 322–325 (1995).
19. Hall, T. M. T., Porter, J. A., Beachy, P. A. & Leahy, D. J. Nature 378, 212–216 (1995).
20. Fan, C.-M. et al. Cell 81, 457–465 (1995).
21. Hynes, M. et al. Neuron 15, 35–44 (1995).
22. Hodgkinson, C. A. et al. Cell 74, 395–404 (1993).
23. Lawson, K. A., Meneses, J. J. & Pedersen, R. A. Development 113, 891–911 (1991).
24. Beddington, R. S. Development 120, 613–620 (1994).
25. Herrmann, B. G. et al. Trends Genet. 10, 280–286 (1994).
26. Ang, S.-L. & Rossant, J. Cell 78, 561–574 (1994).
27. Weinstein, D. C. et al. Cell 78, 575–588 (1994).
28. Yamada, T., Pfaff, S. L., Edlund, T. & Jessell, T. M. Cell 73, 673–686 (1993).
29. Pfaff, S. L., Mendelsohn, M., Stewart, C. L., Edlund, T. & Jessell, T. M. Cell 84, 309–320 (1996).
30. Mansouri, A., Stoykova, A. & Gruss, P. J. Cell Sci. (suppl.) 18, 35–42 (1994).
31. Christ, B. & Ordahl, C. P. Anat. Embryol. 191, 381–396 (1995).
32. Cossu, G., Tajbakhsh, S. & Buckingham, M. Trends Genet. 12, 218–223 (1996).
33. Rong, P. M., Teillet, M.-A., Ziller, C. & Le Douarin, N. M. Development 115, 657–672 (1992).
34. Christ, B., Brand-Saberi, B., Grim, M. & Wilting, J. Anat. Embryol. 186, 505–510 (1992).
35. Boncinelli, E., Gulisano, M. & Broccoli, V. J. Neurobiol. 24, 1356–1366 (1993).
36. Simeone, A. et al. EMBO J. 12, 2735–2747 (1993).
37. Joyner, A. L. & Martin, G. R. Genes Dev. 1, 29–38 (1987).
38. Macdonald, R. & Wilson, S. W. Curr. Opin. Neurobiol. 6, 49–56 (1996).
39. Talbot, W. S. et al. Nature 378, 150–157 (1995).
40. Halpern, M. E., Ho, R. K., Walker, C. & Kimmel, C. B. Cell 75, 99–111 (1993).
41. Hatta, K., Kimmel, C. B., Ho, R. K. & Walker, C. Nature 350, 339–341 (1991).
42. Herrmann, B. G. Development 113, 913–917 (1991).
43. Wallin, J. et al. Development 120, 1109–1121 (1994).
44. Neubüser, A., Koseki, H. & Balling, R. Dev. Biol. 170, 701–716 (1995).
45. Hinchliffe, J. R. & Gumpel-Pinot, M. J. Embryol. Exp. Morphol. 62, 63–82 (1981).
46. Cohn, M. J. & Tickle, C. Trends Genet. 12, 253–257 (1996).
47. Sordino, P. & Duboule, D. Trends Ecol. Evol. 11, 114–119 (1996).
48. Fitz, C. R. Neuroimag. Clin. N. Am. 4, 263–281 (1994).
49. Adelmann, H. B. Q. Rev. Biol. 11, 116–182 (1936).
50. Adelmann, H. B. Q. Rev. Biol. 11, 284–304 (1936).
51. Nagy, A., Rossant, J., Nagy, R., Abramow-Newerly, W. & Roder, J. C. Proc. Natl Acad. Sci. USA 90, 8424–8428 (1993).

ACKNOWLEDGEMENTS. H.W. and P.A.B. are senior co-authors. We thank J. Gearhart and D. Bell for a 129 ES cell genomic library; A. Nagy and J. Rossant for R1 ES cells; M. Capecchi for the thymidine kinase-containing vector; P. Soriano for Pgk-neo; and Syntex Discovery Research for gancyclovir; E. Boncinelli, H. Sasaki, B. Hogan, B. G. Herrmann, H. Arnheiter, P. Gruss, T. Jessell, A. Joyner, G. Dressler and G. Martin for probes; K. Ceplova for help in tail DNA preparation; V. Tanner for help with scanning electron microscopy; and C.-M. Fan, M. Halpern and D. Sunnia for criticism of this manuscript. P.A.B. is an investigator of the Howard Hughes Medical Institute.

CORRESPONDENCE should be addressed to C.C. (e-mail: chiangc@dr6.nichd.nih.gov) or P.A.B. (e-mail: phil.beachy@qmail.bs.jhu.edu), and requests for materials to H.W. (e-mail: hw@nichd.nih.gov) or P.A.B.

J Mol Med (1999) 77:459–468
Digital Object Identifier (DOI) 10.1007/s001099900018

© Springer-Verlag 1999

REVIEW

**Heidi Hahn · Leszek Wojnowski · Georgina Miller
Andreas Zimmer**

The patched signaling pathway in tumorigenesis and development: lessons from animal models

Received: 22 February 1999 / Accepted: 6 April 1999 / Published online: 1 July 1999

HEIDI HAHN
received her M.D. at the University of Würzburg, Germany. After 5 years of research training at the National Institutes of Health, Bethesda, MD., USA, she is presently head of the Pathogenetics Section at the Institute of Pathology, GSF Research Center of Environment and Health, Neuherberg, Germany, sponsored by the Biofuture Research Program. Her research interests are developmental and tumor biology.

ANDREAS ZIMMER
worked on the development of gene targeting technology for his doctoral thesis at the Max Planck Institute for Biophysical Chemistry in Göttingen, Germany. After moving to the National Institute of Mental Health in 1989, he became interested in the genetics of neuronal development and animal behavior. He is currently an investigator at the Laboratory of Genetics, NIMH.

H. Hahn (✉)
Institute of Pathology,
GSF Research Center of Environment and Health,
Ingolstädter Landstrasse 1, D-85758 Neuherberg, Germany
e-mail: heidi.hahn@gsf.de
Tel.: +49-89-31872313; Fax: +49-89-31873360

H. Hahn · L. Wojnowski · A. Zimmer
Laboratory of Genetics, NIMH, National Institutes of Health,
Building 36, Room 3D06, Bethesda, MD 20892, USA

L. Wojnowski
Epidauros Biotechnologie AG, Am Neuland 1,
D-82347 Bernried, Germany

G. Miller
Veterinary Resources Program, Office of the Director,
National Institutes of Health, Building 28a, Room 117,
Bethesda, MD 20892-5230, USA

Abstract The identification of mutations in the human homolog of the *Drosophila* segment polarity gene *Patched* in basal cell carcinoma has sparked intense interest in the role of this gene in human disorders. The transmembrane protein Patched is a receptor for the morphogene Sonic Hedgehog. Sonic Hedgehog/Patched signaling involves another transmembrane protein, Smoothened, and its intracellular effectors, including the proto-oncogene *GLI1*. During the past 2 years it has become evident that mutations in *Patched* or in one of the components of its signaling pathway contribute to the formation of several common human tumors. It is now well established that *Patched* is a tumor suppressor gene. The *Sonic Hedgehog/Patched/Smoothened* signaling pathway is thus rapidly emerging as one of the most important regulators of oncogenic transformation. This pathway also plays an important role during mammalian embryonic development. This dual role is especially visible in humans with inherited *Patched* mutations. Such patients suffer from Gorlin, or nevoid basal cell carcinoma, syndrome and exhibit a variety of developmental defects accompanied by a predisposition to tumor formation. Activating mutations in *Sonic Hedgehog* and *Smoothened* lead to similar phenotypes as do loss-of function mutations in *Patched.* By means of transgenic and gene targeting technologies the respective mutations have been expressed in the mouse. Such mutant mouse strains exhibit many symptoms observed in humans. These strains are useful models to study the pathogenesis of several common human tumors and developmental defects. Furthermore they provide important tools to study the Sonic Hedgehog/Patched/Smoothened signaling at the molecular and biochemical level.

Key words Tumorigenesis · Embryogenesis · Basal cell carcinoma · Medulloblastoma

Abbreviations *BCC* Basal cell carcinoma of the skin · *Ci* Cubitus interruptus · *HH* Hedgehog · *HPE* Holoprosencephaly · *IR* Ionizing radiation · *LOH* Loss of heterozygosity · *NBCCS*/GS Nevoid basal cell carcinoma syndrome/Gorlin syndrome · *PNET* Primitive neuroectodermal tumor · *PTC* Patched · *RMS* Rhabdomyosarcoma · *SHH* Sonic hedgehog · *SMO* Smoothened

The *Sonic Hedgehog/Patched/Smoothened* signaling pathway

The *Patched (PTC)* mutation was originally described in 1980 in the Nobel Prize winning work of Nuesslein-Volhard and Wieschaus as an embryonic lethal mutant of *Drosophila* [1]. In the fly *PTC* functions as a segment polarity gene. Segment polarity genes control cell-cell interactions in the formation of patterns within the segments of the embryonic epidermis. *PTC* fly mutants display a mirror image duplication of the segment borders within each segment. Genetic analysis reveals that *PTC* acts in a signaling pathway with *Hedgehog (HH)* and *Smoothened (SMO)*. HH is a secreted ligand of PTC, which itself is a transmembrane protein. Within the plasma membrane, PTC interacts with the seven transmembrane domain protein SMO [2]. In the absence of HH, PTC inhibits SMO, thereby blocking the expression of target genes. Binding of HH to PTC suspends this inhibition. The subsequent cytoplasmic events are poorly understood, but they ultimately result in the activation of the transcription factor *Cubitus interruptus* (*Ci*). The possible cytoplasmic regulators of *Ci* include the serine/threonine kinase Fused, the kinesin-related protein Costal2, and protein kinase A. Furthermore, the transcriptional activity of Ci protein is regulated by proteolysis. Together with dCBP, the *Drosophila* homolog of cAMP-response element binding protein, Ci regulates transcription of downstream genes such as *Decapentaplegic*, *Wingless*, and *PTC* itself [3]. A more detailed discussion of *Drosophila PTC* signaling can be found in several recent reviews [4, 5, 6].

Although some genes involved in this pathway have not yet been identified in higher animals, the HH/PTC/SMO signaling pathway exhibits a remarkable degree of conservation between *Drosophila* and vertebrates [5, 6]. In vertebrates this pathway has been implicated in tissue patterning during development and in the regulation of cell proliferation. Sonic hedgehog (SHH) is the best characterized of at least three mammalian HH homologs [7]. SHH plays a central role in the patterning of the limbs, axial skeleton, and central nervous system [7]. Binding of SHH to PTC suspends the inhibitory effect of PTC on its signaling partner SMO [8]. Since vertebrate PTC and SMO can be coimmunoprecipitated, they are believed to form a receptor complex within the plasma membrane [8]. The suspension of the inhibitory effect of PTC on SMO upon SHH binding is most likely caused by a conformational change in the PTC/SMO complex without its dissociation [8, 9]. This conformational change is thought to activate SMO and, via an unknown downstream mechanism, to trigger the expression of targets of the pathway. Downstream targets of the pathway in vertebrates include *GLI1* (the vertebrate homolog of *Drosophila Ci*) [10, 11] and *PTC* [12, 13]. Other possible targets are the members of the *TGF-beta* family of genes, which are the vertebrate homologs of the *Drosophila Decapentaplegic* gene [14, 15].

PTC without HH or SMO in *Caenorhabditis elegans*

The recent completion of the genome sequence of the nematode *C. elegans*, another major model organism in developmental biology, has provided interesting insights into the evolutionary history of signal transduction pathways. Surprisingly, the genome of *C. elegans* contains a *PTC* ortholog as well as a second *PTC*-like gene, but neither *HH* nor *SMO* [16], indicating that *PTC* signaling in *C. elegans* may involve other ligands and signaling partners. The function of *PTC* in *C. elegans* is at present unknown. The *GLI1* ortholog in *C. elegans*, *Tra-1*, has been implicated in sex determination [17, 18], but it remains to be determined whether *PTC* also regulates *Tra-1*. The functional characterization of the *C. elegans PTC* may help to reveal potential *PTC* functions that are independent of *SHH* and *SMO*.

SHH/PTC/SMO signaling pathway in human disease

Nevoid basal cell carcinoma syndrome/Gorlin syndrome

Inherited mutations of the human homolog of *PTC* lead to a rare autosomal dominant disorder known as Gorlin, or nevoid basal cell carcinoma, syndrome (NBCCS/GS; Table 1) [19, 20]. NBCCS/GS has an incidence of 1:56000 and is characterized by a combination of developmental defects with a predisposition to tumor formation [21]. Consistent with its name, the most frequent type of tumor in patients with the syndrome are basal cell carcinomas of the skin (BCCs). The incidence of BCCs increases with age, and these tumors are observed in up to 97% of individuals with NBCCS/GS [22]. The number of BCCs ranges from 1 to more than 1000, and they can develop in any area of the skin. However, they are encountered more frequently on the face, neck, and upper part of the trunk, i.e., areas of the skin exposed to UV light [21, 22]. Consequently UV light is thought to exacerbate the development of BCCs in these patients, although it is probably not an essential etiological factor [23]. Patients with NBCCS/GS are also predisposed to medulloblastoma, a very malignant tumor of the cerebellum which is observed in 4% of children with the syndrome [22, 24, 25]. Menigioma [21, 22, 26] and fibroma [22, 25, 27, 28, 29, 30] occur in 5% and 18% of NBCCS/GS cases, respectively. Other tumors associated with NBCCS/GS are rhabdomyoma [21, 31, 32] and rhabdomyosarcoma (RMS) [33].

Other characteristics of the syndrome are developmental abnormalities [21]. They typically include malformations of the skeleton such as syn- and polydactyly,

Table 1 Orthologs of the SHH/PTC/SMO signaling pathway and the associated disorders in mammals

C. elegans	*Drosophila*	Mammals	Disorders reported in humans	Phenotype in mutant mice
–	Hedgehog	Sonic hedgehog	Holoprosencephaly [41, 42] Basal cell carcinoma [75] Medulloblastoma [75] Breast carcinoma [75]	Holoprosencephaly-like [79] Basal cell carcinoma-like [75]
		Indian Hedgehog	?	?
		Desert Hedgehog	?	?
Patched	Patched	Patched	Gorlin Syndrome [19, 20] Basal cell carcinoma [52] Medulloblastoma [56, 59, 61] Trichoepithelioma [58] Menigioma [53] Breast carcinoma [53] Esophageal carcinoma [57] Cerebral PNET [69]	Gorlin syndrome-like [70, 71] Medulloblastoma [70] Rhabdomyosarcoma [71] Intest. Adenocarcinoma (Fig. 2) Uterine sarcoma (Fig. 2) PNET-like (Fig. 2)
		Patched2	Basal cell carcinoma? [66]	?
		TRC8	Renal cell carcinoma [67]	?
–	Smoothened	Smoothened	Basal cell carcinoma [54, 78] Medulloblastoma [54]	Basal cell carcinoma-like [78]
Tra-1	Cubitus interruptus	Gli1	Glioma [73]	?
		Gli2	?	
		Gli3	Greig syndrome [100] Pallister-Hall syndrome [101]	Malformation of lung and esophagus (Gli 2 and Gli3) [102]

closure defects of the spinal cord, skoliosis, rib defects, palate abnormalities, coarse face, hypertelorism, and macrocephaly. The location of these defects is correlated with sites of *PTC* expression during mammalian embryogenesis [12, 34]. Furthermore, patients with NBCCS/GS may exhibit pits of palms and soles, cysts of the jaw, and ectopic calcifications As well as a generalized overgrowth [21, 35, 36]. The skeletal defects are usually the only symptoms present at birth, and other stigmata of the syndrome appear later in life.

Developmental defects and tumors arise through different genetic mechanisms. Individuals with NBCCS/GS are haploinsufficient in *PTC*, due to the inheritance of one mutated copy of the gene. Haploinsufficiency might be responsible for developmental abnormalities such as closure defects of the neural tube, skeletal defects, as well as the generalized overgrowth. In contrast, tumor formation is thought to involve loss of heterozygosity (LOH), i.e., loss of the intact second copy of *PTC* later in life. The same mechanism is most likely responsible for the formation of jaw cysts in patients with NBCCS/GS, since epithelium of these cysts exhibits LOH at the *PTC* locus [37]. It remains to be seen whether other abnormalities such as calcifications and pits of the palms and soles arise through a similar mechanism.

Screening of NBCCS/GS patients has revealed that *PTC* mutations are dispersed throughout the entire coding sequence of the gene without any apparent hot spots. Likewise, no correlation has been found between the symptoms of the syndrome and the location of mutations within the *PTC* gene. Although most mutations result in truncations of the PTC protein, NBCCS/GS patients show extensive inter- as well as intrafamilial variability of the phenotype [38, 39]. Specifically, patients with the same molecular lesion in the PTC gene can exhibit very different symptoms of the syndrome [39], thus suggesting that the NBCCS/GS phenotype is modified by factors different from *PTC*. Possible candidates include alleles of other genes as well as epigentic and environmental factors [38, 39, 40].

Holoprosencephaly

Loss of function mutations of *SHH* have been found in a fraction of familial cases of holoprosencephaly (HPE) [41, 42]. HPE is a frequent human developmental defect of the anterior neural tube with a prevalence of 1:250 during embryogenesis and 1:16000 in newborn infants [43]. HPE is caused by the incomplete development and septation of midline structures. The phenotypic manifestations range from mild hypotelorism through alobar HPE to cyclopia. These developmental defects can be considered "inverse" of midline abnormalities observed in patients with NBCCS/GS. This is consistent with the interpretation that PTC is a negative regulator of SHH signaling.

Sporadic tumors with mutations in PTC

Mutations of *PTC* have been identified in sporadic cases of tumors associated with NBCCS/GS. Thus *PTC* is in line with Knudson's [44] hypothesis that tumors in inherited cancer predisposition syndromes have mutations of the same genes as sporadic cases of these tumors [45].

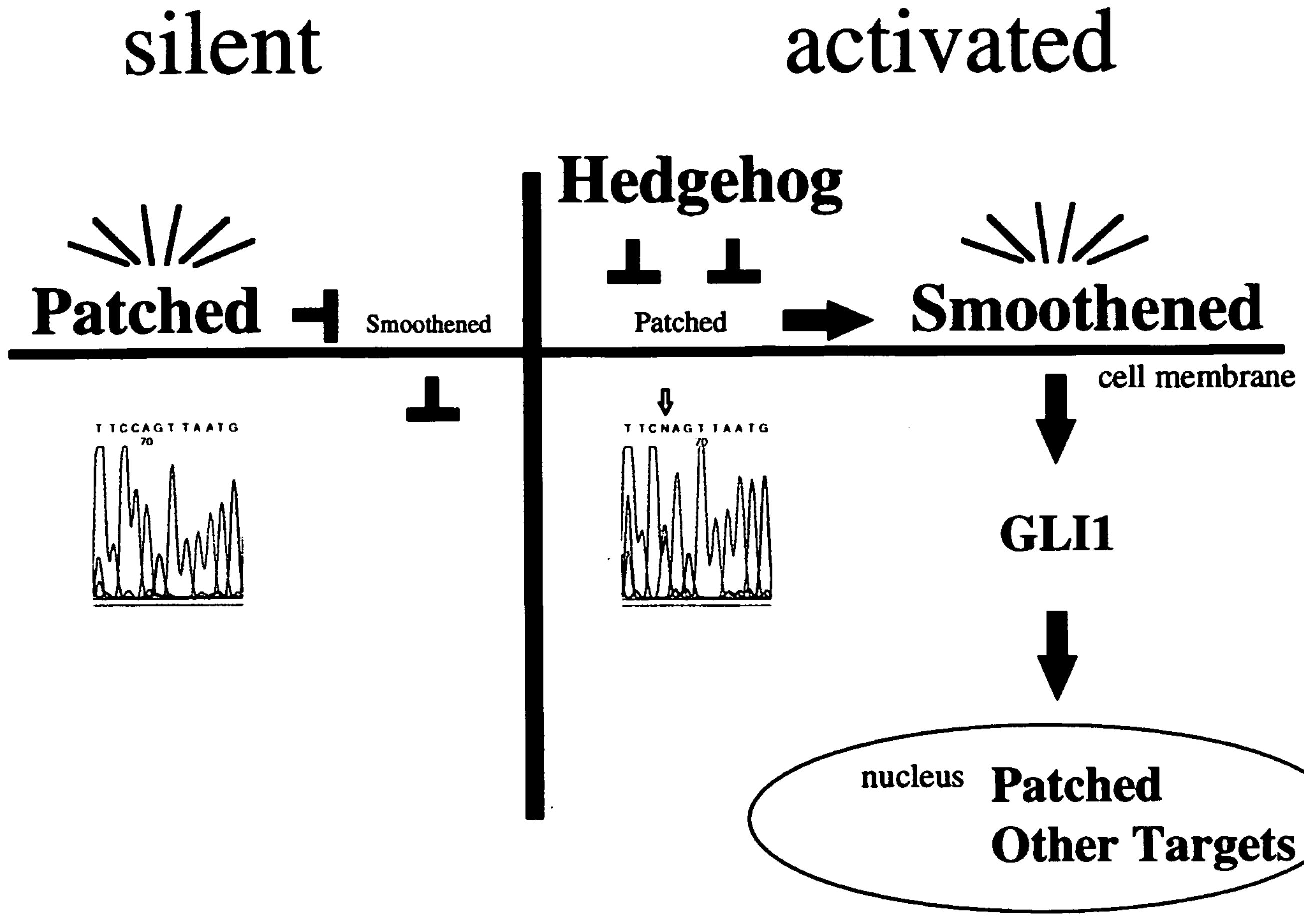

Fig. 1 Composition and activation of the SHH/PTC/SMO signaling pathway. *Left* In the absence of the ligand SHH, PTC blocks the activity of SMO; *right* activation of the pathway can be triggered by binding of SHH to PTC, by activating SHH or SMO mutations or by loss of function PTC mutations. Among the three proteins, mutations of PTC (*empty arrow*) are the most frequent cause of tumorigenesis

BCCs are the most common sporadic tumors in humans, with more than 750,000 cases per year alone in the United States [46]. BCCs are semimalignant, and they rarely metastasize, but they can lead to extensive morbidity due to local tissue destruction [47]. LOH at the *PTC* locus has been found in more than 50% of BCCs [48, 49, 50, 51] whereas inactivating mutations of the remaining allele (or both alleles) have been detected in 30% of these tumors [52]. Considering the technical limitations of the detection techniques used in these studies, loss of both functional alleles of *PTC* could be responsible for at least 30% of sporadic BCCs [53, 54].

The list of sporadic tumors with mutations in *PTC* has grown during the past 2 years beyond BCCs and presently includes primitive neuroectodermal tumors (PNETs) of the central nervous system such as medulloblastoma [55, 56], meningioma [53], esophageal squamous cell carcinoma [57], and trichoepithelioma [58]. Inactivating mutations of one *PTC* allele have been found in more than 10% of sporadic medulloblastoma [53, 59]. Medulloblastoma is a very malignant primitive neuroectodermal tumor of the cerebellum and accounts for one-quarter of all intracranial tumors in children [60]. Since the presence of point mutations is strongly correlated with the LOH at the *PTC* locus in medulloblastoma biopsies [53, 56, 59, 61], loss of both copies of the gene appears to be necessary for the development of this type of tumor. Interestingly, a recent first report describes mutations of *PTC* in two of seven breast cancers examined [53]. Should the involvement of *PTC* in the development of breast cancer be confirmed in a more representative study, this gene would acquire yet another level of sociomedical importance. It is important to note that at present the true extent and the spectrum of tumors with mutations in *PTC* is far from established, due to the small number of tumors examined in most studies and to the limitations of methods used for mutation detection. Furthermore, a fraction of these tumors could be caused by mutations in one of the two recently discovered *PTC* homologs. Mammalian genomes harbor a second *PTC* gene, *PTC2* [62, 63], and the encoded protein is capable of both SHH binding and formation of a complex with SMO [63]. This suggests functional similarities between the human PTC proteins on the cellular level, although their expression patterns suggest that they have partly different target tissues [64]. *PTC2* is upregulated in both familial and sporadic BCCs with mutations in *PTC*, suggesting a negative regulation of *PTC2* by *PTC* [65]. A first report suggests that *PTC2* mutations play no major role in the etiology of BCCs and medulloblastoma [66]. Another candidate for mutation screen is *TRC8* which exhibits significant similarity to *PTC* and has been implicated in renal cell carcinoma [67].

Since PTC acts as a negative regulator of the SHH/PTC/SMO signaling pathway, loss of function mutations in *PTC* would be expected to result in a constitutive activation of its downstream genes (Fig. 1). Indeed, *PTC* transcription is upregulated in tumors associated with inactivating mutations of this gene [52, 68, 69, 70, 71]. Overexpression of *GLI1* has been demonstrated in all sporadic human BCCs examined [72] as well as in medulloblastoma and RMS in *PTC* mutant mice [70, 71]. *GLI1* was originally cloned from a glioma cell line [73] and has subsequently been shown to have oncogenic potential [72, 74]. Altogether, these results suggest that overexpression of *GLI1* is a common denominator for tumors with mutations in the *SHH/PTC/SMO* signaling pathway. If this hypothesis is correct, *GLI1* would become an attractive target for therapeutic interventions of several common tumors such as BCCs, medulloblastoma, and RMS.

Sporadic tumors with mutations in SHH and SMO

Within the *SHH/PTC/SMO* pathway, tumor formation can be also caused by mutations in *SHH* or *SMO*. A missense mutation His133 Tyr of *SHH* has been found in sporadic cases of BCC, medulloblastoma, and breast carcinoma [75]. The authors of the study predicted that *SHH* may be a dominant oncogene in several common tumors. Experimental constitutive overexpression of *SHH* in human skin leads to the abnormal histological features characteristic of BCCs [76]. Interestingly, a recent work describes the expression of *SHH* in the squamous carcinoma of the lung but not in the normal lung tissue of the same patient [77].

Single-strand conformation polymorphism and sequencing analysis of *SMO* in DNA samples from 47 BCCs has identified one Arg562Gln and two Trp535Leu missense mutations [78]. Overexpression of either of these mutations together with the adenovirus *E1A* results in the transformation of rat embryonic fibroblasts, whereas overexpression of wild-type *SMO* with *E1A* does not. The transformed cells overexpress *GLI1*. In the murine skin these mutations result in the formation of BCCs [78]. These findings, together with a recent report of a missense *SMO* mutation in a human medulloblastoma [54], support the hypothesis that, similarly to *SHH*, *SMO* is a proto-oncogene.

Altogether, the *SHH/PTC/SMO* signaling pathway consists of a tumor suppressor (*PTC*) and of at least two proto-oncogenes (*SHH, SMO*). A tumorigenic activation of the pathway appears to be possible for any of its known signaling components.

Animal models with genetic alterations in the SHH/PTC/SMO signaling pathway

Recently, mouse strains with mutations in the components of the *SHH/PTC/SMO* pathway have been established to investigate the molecular function of these genes. Loss of function mutations of *PTC* or *SHH* recapitulate in the mouse many symptoms of the respective human phenotypes.

Heterozygous *PTC* knockout mice display the typical symptoms of the NBCCS/GS including skeletal abnormalities, neural tube closure defects, a generalized overgrowth, and a predisposition to tumor formation [70, 71]. A fraction of heterozygous animals die before weaning, some of them due to the closure defect of the anterior neural tube known as exencephaly [71]. Interestingly, the phenotype of *PTC* heterozygous mice is dependent on the genetic background. For example, PTC heterozygous embryos are more likely to die prenatally on an inbred background than on an outbred background [71]. Thus *PTC* signaling probably undergoes modification by mouse strain-specific alleles of other genes. In addition, the marked lethality of *PTC* heterozygotes during embryogenesis indicates that, by analogy, the surviving human *PTC* heterozygotes may represent only milder cases of NBCCS/GS whereas the more severely affected individuals may die in utero.

Homozygous *PTC* mutants die in utero during early organogenesis. At E9.0, most of the homozygous mutants are dead. The intermediate cause of the lethality could be a defect in heart development [70]. Other abnormalities in these embryos include an overgrowth of the neural folds, and a failure of the neural tube to close. These observations indicate that abnormal *PTC* signaling could be responsible for a fraction of neural tube closure defects which are a frequent developmental defect in humans.

The developmental defects of the midline in *PTC* homozygotes are "inverse" of those caused by loss of function mutations of *SHH*. Mice deficient in *SHH* display an overall reduction in size of the brain and spinal cord [79]. The abnormalities of midline structures such as fused cephalic folds and a single fused optic vesicle (cyclopia) resemble the spectrum of human congenital malformations observed in HPE. Whereas all cells of the neural tube in *PTC* homozygous mutant embryos adopt characteristics of the floorplate, which is the most ventral part of the neural tube, [70], ventral cell types in *SHH* mutants are absent [79]. These findings are consistent with the hypothesis that PTC acts as a negative regulator of SHH.

Similarly to what is observed in humans, mutations in the genes constituting the *SHH/PTC/SMO* pathway in the mouse result in increased tumorigenesis. Up to 30% heterozygous *PTC* mice develop medulloblastoma [70, 71]. This is consistent with studies in humans, in which *PTC* mutations predispose to medulloblastoma in NBCCS/GS patients and are found in 10% of sporadic medulloblastoma [53, 59].

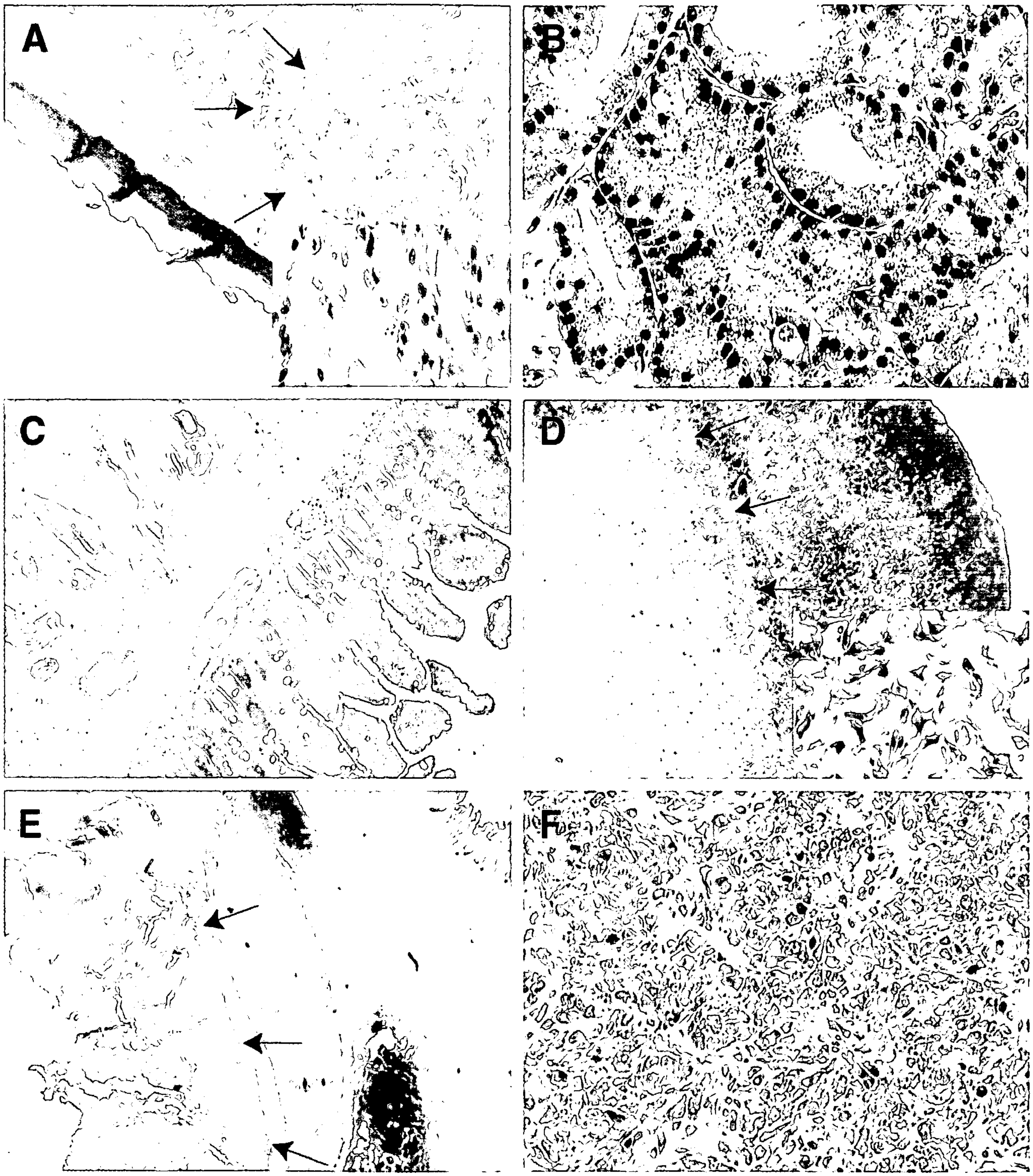

Fig. 2 Low-frequency tumors in *PTC* heterozygous mice. **A** RMS of the tongue. ×10 **B** Cystadenoma of the Harderian gland. ×40 **C** Invasive adenocarcinoma of the jejunum. ×10 **D** Endometrial stromal sarcoma of the uterus. ×5 **E,F** Leg tumor resembling human PNETs. **E** ×2,5. **F** ×40. *Arrows* tumor masses. *Insets* ×40

RMS is the other major tumor type in the heterozygous *PTC* mice [71]. Sporadic RMS is considered one of the rarest tumors in laboratory rodents, with the frequency for the BALB/cJ strain estimated to be 2.4/100,000 mice [80]. In contrast, RMSs are observed in 10% of *PTC* heterozygotes maintained on a CD1 background. The frequency of RMSs is modified by genetic background-specific alleles of other genes, since on a C57BL/6 background these tumors arise only in 2% of *PTC* heterozygotes. RMSs develop in young animals, usually during the first 4 months of life. Previously, a high incidence of RMSs was reported in mice transgenic for the β-globin locus control region fused with simian virus 40 large T antigen gene [81]. At present it is unknown whether *PTC* is mutated in human RMSs. However, the high frequency of RMSs in murine *PTC* mutants makes a screen of human RMSs for mutations in this and in other components of the pathway worth undertaking.

We have now analyzed more than 1000 heterozygous *PTC* mice. We found that *PTC* heterozygotes not only develop RMSs and medulloblastoma but also appear to be predisposed to microphthalmia, hemangioma, glomerulonephropathy, RMS of the tongue, cystadenoma of the Harderian gland, intestinal carcinoma, endometrial stromal sarcoma of the uterus, and primitive malignant neoplasms which resemble human PNETs. Examples of these novel pathological features and tumors in heterozygous *PTC* knockout mice are shown in Fig. 2. These pathological features are never observed in their wild-type littermates. The possible involvement of the *PTC* signaling pathway in the pathogenesis of these disorders in humans awaits further studies.

Thus far no BCCs have been reported in murine *PTC* heterozygotes. On the other hand, skin abnormalities similar to human BCCs have been described following the overexpression of *SHH* and mutant *SMO* in the murine skin [75, 78]. Altogether, *PTC* and *SHH* mutant mice are useful tools to investigate the role of SHH/PTC/SMO signaling in the pathogenesis of human developmental defects and tumors.

What is the physiological function of PTC pathway?

Many aspects of PTC signaling remain unknown. We understand very little about the physical interaction of PTC with SHH or SMO, and the absence of HH and SMO orthologs in *C. elegans* suggests that PTC has additional roles that are independent of these signaling partners. We also know very little about downstream signaling events or cellular responses to PTC activation.

Below we discuss two aspects PTC function that are currently under investigation: (a) Is PTC function regulated by cholesterol homeostasis, or is PTC involved in regulating cholesterol homeostasis? (b) Is PTC involved in the regulation of genomic stability and regulation of imprinting?

Cholesterol

With the exception of binding of SHH and inhibition of SMO, the biochemical functions of the PTC protein are unknown. PTC is most likely a plasma membrane protein with 12 putative transmembrane domains. Thus the topology of PTC resembles that of the ABC transporters, although it lacks the ATP-binding cassette that is characteristic of this protein family [82, 83]. Furthermore, PTC protein sequence suggests a relationship to a suprafamily of genes involved in cholesterol homeostasis [84]. In addition to PTC, this family includes the 3-hydroxy-3-methylglutaryl coenzyme A reductase and the gene mutated in patients with Niemann-Pick type C disease [84, 85]. A common feature of these proteins is the presence of a sterol-sensing domain. In the PTC protein this domain possibly mediates the binding of the PTC ligand, SHH. Indeed, the active, truncated form of SHH, designated N-SHH, is covalently coupled to cholesterol. The presence of a cholesterol moiety is indispensable for the spatially restricted tissue localization of the N-SHH signal [86]. Fetal exposure to inhibitors of cholesterol biosynthesis causes developmental defects [87] identical to those described in murine *SHH* mutants [79] and in HPE [43]. All these observations led to a model in which cholesterol inhibitors interfere with the addition of the cholesterol moiety to SHH [86]. However, a recent work shows that inhibitors of cholesterol biosynthesis have no effect on the cholesterol modification of SHH but rather perturb the responsiveness of the PTC-expressing tissues to SHH [88]. These new observations have led to the hypothesis that abnormal signaling of the pathway result in perturbations of cholesterol in SHH target tissues, and that PTC is a regulator of cholesterol homeostasis [88]. If this is true, SHH-responsive tissues in *PTC* mutants would be expected to contain abnormal levels of cholesterol or of its precursors or metabolites. The experimental verification of this hypothesis will be facilitated by the availability of murine *SHH* and *PTC* mutants.

Imprinting and genomic stability

Several lines of evidence suggest that *PTC* is involved in the regulation of genomic stability and imprinting. For example, there is an interaction between *PTC* signaling and activity of the imprinted, tumor growth-promoting *insulin-like growth factor 2* (*IGF2*). *IGF2* is consistently overexpressed in RMS in *PTC* mutant mice [71]. It is not known how loss of *PTC* function activates *IGF2*, but there are striking similarities in phenotypes.

Overexpression of *IGF2,* due to loss of imprinting of the *IGF2* gene, has been implicated in the Beckwith-Wiedemann syndrome which is characterized by a generalized overgrowth and by a predisposition to childhood tumors such as Wilms tumor and RMS [89]. Overexpression of *IGF2* in the mouse leads to a variety of skeletal abnormalities [89]. Significantly, similar symptoms are caused by the demethylating agent 5-aza-deoxycytidine when administrated during embryogenesis [90], which is consistent with the postulated role of methylation in the maintenance of imprinting. Abnormal DNA methylation also leads to elevated mutation rates, suggesting that defects in DNA methylation contribute to genomic instability [91]. The phenotypical similarities of NBCCS/GS, due to the loss of PTC function, with Beckwith-Wiedemann syndrome and the teratogenic effects of demethylating agents suggest the interesting possibility that loss of *PTC* leads to abnormal methylation, which in turn results in loss of imprinting of *IGF2*, genomic instability, and tumorigenesis. This hypothesis is consistent with the recent finding that cell lines isolated from patients with NBCCS/GS display increased genomic instability [92].

Further evidence of a potential role of *PTC* in the regulation of genomic stability has been provided by analysis of the effects of ionizing radiation (IR). Indeed, the developmental defects in human and murine *PTC* heterozygotes exhibit striking similarities to those described in mouse embryos exposed to IR. Embryos irradiated during organogenesis develop defects of the neural tube (exen-, micro-, or anencephaly, spina bifida), of the derived structures (eye defects), and of the limbs and of the skeleton [93, 94]. The location of those defects is strongly correlated with the expression pattern of *PTC* during organogenesis [12, 34]. The sensitivity to IR has been investigated for some time in cells isolated from humans with NBCCS/GS, but the results are still inconclusive [95, 96, 97, 98], perhaps due to the fact that cell lines do not always recapitulate the in vivo sensitivity to DNA-damaging agents [99]. Recently the effects of IR were investigated in murine *PTC* heterozygotes. The frequency of IR-induced developmental defects was 4.1 times higher in *PTC* heterozygotes than in wild-type littermates at the lowest defect-inducing dose [71]. These data suggest that *PTC* heterozygotes are more sensitive to IR, and that, in addition to its role in patterning, *PTC* is involved in cellular responses to IR. An involvement of *PTC* signaling in radiation response would explain the characteristic distribution of developmental defects induced by IR. Indeed, many effects of IR on murine embryos are too general (growth retardation) or complex (neural tube closure defects, polydactyly) to comply with the stochastic model of IR action [93, 94]. In addition to developmental defects, hypersensitivity to IR should also manifest in increased tumorigenesis. Consistent with this notion, human *PTC* heterozygotes are hypersensitive to IR-induced tumorigenesis. Children with NBCCS/GS develop multiple BCCs in the irradiated area of the skin following radiation therapy for medulloblastoma [21].

Conclusions

The 2 years of research since the discovery of *PTC* mutations in patients with NBCCS/GS have produced a remarkable progress in the understanding of the role of the gene in a growing list of human disorders. The rapid elucidation of *PTC* signaling pathway has relied upon the work of developmental biologists on animal models ranging from *Drosophila* mutants to genetically manipulated mice. The development of therapies for disorders with abnormal function of the *PTC* signaling pathway is likely to further benefit from the remarkable convergence of developmental biology and human genetics.

References

1. Nusslein-Volhard C, Wieschaus E (1980) Mutations affecting segment number and polarity in Drosophila. Nature 287: 795–801
2. Chen Y, Struhl G (1996) Dual roles for patched in sequestering and transducing Hedgehog. Cell 87:553–563
3. Akimaru H, Chen Y, Dai P, Hou DX, Nonaka M, Smolik SM, Armstrong S, Goodman RH, Ishii S (1997) Drosophila CBP is a co-activator of cubitus interruptus in hedgehog signalling. Nature 386:735–738
4. Goodrich LV, Scott MP (1998) Hedgehog and patched in neural development and disease. Neuron 21:1243–1257
5. Ingham PW (1998) Transducing Hedgehog: the story so far. EMBO J 17:3505–3511
6. Johnson RL, Scott MP (1998) New players and puzzles in the Hedgehog signaling pathway. Curr Opin Genet Dev 8:450–456
7. Hammerschmidt M, Brook A, McMahon AP (1997) The world according to hedgehog. Trends Genet 13:14–21
8. Stone DM, Hynes M, Armanini M, Swanson TA, Gu Q, Johnson RL, Scott MP, Pennica D, Goddard A, Phillips H, Noll M, Hooper JE, de Sauvage F, Rosenthal A (1996) The tumour-suppressor gene patched encodes a candidate receptor for Sonic hedgehog. Nature 384:129–134
9. Marigo V, Davey RA, Zuo Y, Cunningham JM, Tabin CJ (1996) Biochemical evidence that patched is the Hedgehog receptor. Nature 384:176–179
10. Ruiz i Altaba A (1998) Combinatorial Gli gene function in floor plate and neuronal inductions by Sonic hedgehog. Development 125:2203–2212
11. Lee J, Platt KA, Censullo P, Ruiz i Altaba A (1997) Gli1 is a target of Sonic hedgehog that induces ventral neural tube development. Development 124:2537–2552
12. Goodrich LV, Johnson RL, Milenkovic L, McMahon JA, Scott MP (1996) Conservation of the hedgehog/patched signaling pathway from flies to mice: induction of a mouse patched gene by Hedgehog. Genes Dev 10:301–312
13. Marigo V, Scott MP, Johnson RL, Goodrich LV, Tabin CJ (1996) Conservation in hedgehog signaling: induction of a chicken patched homolog by Sonic hedgehog in the developing limb. Development 122:1225–1233
14. Bitgood MJ, McMahon AP (1995) Hedgehog and Bmp genes are coexpressed at many diverse sites of cell- cell interaction in the mouse embryo. Dev Biol 172:126–138
15. Urase K, Mukasa T, Igarashi H, Ishii Y, Yasugi S, Momoi MY, Momoi T (1996) Spatial expression of Sonic hedgehog in the lung epithelium during branching morphogenesis. Biochem Biophys Res Commun 225:161–166
16. Ruvkun G, Hobert O (1998) The taxonomy of developmental control in Caenorhabditis elegans. Science 282:2033–2041
17. Zarkower D, Hodgkin J (1992) Molecular analysis of the C. elegans sex-determining gene tra-1: a gene encoding two zinc finger proteins. Cell 70:237–249
18. Hodgkin JA, Brenner S (1977) Mutations causing transformation of sexual phenotype in the nematode Caenorhabditis elegans. Genetics 86:275–287
19. Johnson RL, Rothman AL, Xie J, Goodrich LV, Bare JW, Bonifas JM, Quinn AG, Myers RM, Cox DR, Epstein EH Jr, Scott MP (1996) Human homolog of patched, a candidate gene for the basal cell nevus syndrome. Science 272:1668–1671
20. Hahn H, Wicking C, Zaphiropoulous PG, Gailani MR, Shanley S, Chidambaram A, Vorechovsky I, Holmberg E, Unden AB, Gillies S, Negus K, Smyth I, Pressman C, Leffell DJ, Gerrard B, Goldstein AM, Dean M, Toftgard R, Chenevix-Trench G, Wainwright B, Bale AE (1996) Mutations of the human homolog of Drosophila patched in the nevoid basal cell carcinoma syndrome. Cell 85:841–851
21. Gorlin RJ (1987) Nevoid basal-cell carcinoma syndrome. Medicine (Baltimore) 66:98–113
22. Kimonis VE, Goldstein AM, Pastakia B, Yang ML, Kase R, DiGiovanna JJ, Bale AE, Bale SJ (1997) Clinical manifestations in 105 persons with nevoid basal cell carcinoma syndrome. Am J Med Genet 69:299–308

23. Goldstein AM, Bale SJ, Peck GL, DiGiovanna JJ (1993) Sun exposure and basal cell carcinomas in the nevoid basal cell carcinoma syndrome. J Am Acad Dermatol 29:34–41
24. Evans DG, Farndon PA, Burnell LD, Gattamaneni HR, Birch JM (1991) The incidence of Gorlin syndrome in 173 consecutive cases of medulloblastoma. Br J Cancer 64:959–961
25. Evans DG, Ladusans EJ, Rimmer S, Burnell LD, Thakker N, Farndon PA (1993) Complications of the naevoid basal cell carcinoma syndrome: results of a population based study. J Med Genet 30:460–464
26. Alegre M, Puig L, de Moragas JM (1995) The Gorlin syndrome. A review of 11 cases. Rev Clin Esp 195:684–687
27. Burke AP, Rosado-de-Christenson M, Templeton PA, Virmani R (1994) Cardiac fibroma: clinicopathologic correlates and surgical treatment. J Thorac Cardiovasc Surg 108:862–870
28. Coffin CM (1992) Congenital cardiac fibroma associated with Gorlin syndrome. Pediatr Pathol 12:255–262
29. Herman TE, Siegel MJ, McAlister WH (1991) Cardiac tumor in Gorlin syndrome. Nevoid basal cell carcinoma syndrome. Pediatr Radiol 21:234–235
30. Shanley S, Ratcliffe J, Hockey A, Haan E, Oley C, Ravine D, Martin N, Wicking C, Chenevix-Trench G (1994) Nevoid basal cell carcinoma syndrome: review of 118 affected individuals. Am J Med Genet 50:282–290
31. DiSanto S, Abt AB, Boal DK, Krummel TM (1992) Fetal rhabdomyoma and nevoid basal cell carcinoma syndrome. Pediatr Pathol Lab Med 12:441–447
32. Klijanienko J, Caillaud JM, Micheau C, Flamant F, Schwaab G, Avril MF, Ponzio-Prion A (1988) Basal-cell nevomatosis associated with multifocal fetal rhabdomyoma. A case. Presse Med 17:2247–2250
33. Beddis IR, Mott MG, Bullimore J (1983) Case report: nasopharyngeal rhabdomyosarcoma and Gorlin's naevoid basal cell carcinoma syndrome. Med Pediatr Oncol 11:178–179
34. Hahn H, Christiansen J, Wicking C, Zaphiropoulos PG, Chidambaram A, Gerrard B, Vorechovsky I, Bale AE, Toftgard R, Dean M, Wainwright B (1996) A mammalian patched homolog is expressed in target tissues of sonic hedgehog and maps to a region associated with developmental abnormalities. J Biol Chem 271:12125–12128
35. Bale SJ, Amos CI, Parry DM, Bale AE (1991) Relationship between head circumference and height in normal adults and in the nevoid basal cell carcinoma syndrome and neurofibromatosis type I. Am J Hum Genet 40:206–210
36. Gorlin RJ (1995) Nevoid basal cell carcinoma syndrome. Dermatol Clin 13:113–125
37. Levanat S, Gorlin R, Fallet S, Johnson D, Fantasia J, Bale A (1996) A two-hit model for developmental defects in Gorlin syndrome. Nat Genet 12:85–87
38. Shimkets R, Gailani MR, Siu VM, Yang-Feng T, Pressman CL, Levanat S, Goldstein A, Dean M, Bale AE (1996) Molecular analysis of chromosome 9q deletions in two Gorlin syndrome patients. Am J Hum Genet 59:417–422
39. Wicking C, Shanley S, Smyth I, Gillies S, Negus K, Graham S, Suthers G, Haites N, Edwards M, Wainwright B, Chenevix-Trench G (1997) Most germ-line mutations in the nevoid basal cell carcinoma syndrome lead to a premature termination of the Patched protein, and no genotype-phenotype correlations are evident. Am J Hum Genet 60:21–26
40. Bale AE (1997) Variable expressivity of patched mutations in flies and humans. Am J Hum Genet 60:10–12
41. Belloni E, Muenke M, Roessler E, Traverso G, Siegel-Bartelt J, Frumkin A, Mitchell HF, Donis-Keller H, Helms C, Hing AV, Heng HH, Koop B, Martindale D, Rommens JM, Tsui LC, Scherer SW (1996) Identification of Sonic hedgehog as a candidate gene responsible for holoprosencephaly. Nat Genet 14:353–356
42. Roessler E, Belloni E, Gaudenz K, Jay P, Berta P, Scherer SW, Tsui LC, Muenke M (1996) Mutations in the human Sonic Hedgehog gene cause holoprosencephaly. Nat Genet 14: 357–360
43. Cohen MM Jr (1989) Perspectives on holoprosencephaly. III. Spectra, distinctions, continuities, and discontinuities. Am J Med Genet 34:271–288
44. Knudson AG Jr (1971) Mutation and cancer: statistical study of retinoblastoma. Proc Natl Acad Sci USA 68:820–823
45. Sidransky D (1996) Is human patched the gatekeeper of common skin cancers? Nat Genet 14:7–8
46. Miller SJ (1991) Biology of basal cell carcinoma. I. J Am Acad Dermatol 24:1–13
47. Canterbury TD, Wheeler WE, Madan E (1990) Giant basal cell carcinoma of the back. W V Med J 86:291–292
48. Gailani MR, Leffell DJ, Ziegler A, Gross EG, Brash DE, Bale AE (1996) Relationship between sunlight exposure and a key genetic alteration in basal cell carcinoma. J Natl Cancer Inst 88:349–354
49. Shanley SM, Dawkins H, Wainwright BJ, Wicking C, Heenan P, Eldon M, Searle J, Chenevix-Trench G (1995) Fine deletion mapping on the long arm of chromosome 9 in sporadic and familial basal cell carcinomas. Hum Mol Genet 4:129–133
50. Quinn AG, Sikkink S, Rees JL (1994) Basal cell carcinomas and squamous cell carcinomas of human skin show distinct patterns of chromosome loss. Cancer Res 54:4756–4759
51. van der Riet P, Karp D, Farmer E, Wei Q, Grossman L, Tokino K, Ruppert JM, Sidransky D (1994) Progression of basal cell carcinoma through loss of chromosome 9q and inactivation of a single p53 allele. Cancer Res 54:25–27
52. Gailani MR, Stahle-Backdahl M, Leffell DJ, Glynn M, Zaphiropoulos PG, Pressman C, Unden AB, Dean M, Brash DE, Bale AE, Toftgard R (1996) The role of the human homologue of Drosophila patched in sporadic basal cell carcinomas. Nat Genet 14:78–81
53. Xie J, Johnson RL, Zhang X, Bare JW, Waldman FM, Cogen PH, Menon AG, Warren RS, Chen LC, Scott MP, Epstein EH Jr (1997) Mutations of the PATCHED gene in several types of sporadic extracutaneous tumors. Cancer Res 57:2369–2372
54. Reifenberger J, Wolter M, Weber RG, Megahed M, Ruzicka T, Lichter P, Reifenberger G (1998) Missense mutations in SMOH in sporadic basal cell carcinomas of the skin and primitive neuroectodermal tumors of the central nervous system. Cancer Res 58:1798–17803
55. Cowan R, Hoban P, Kelsey A, Birch JM, Gattamaneni R, Evans DG (1997) The gene for the naevoid basal cell carcinoma syndrome acts as a tumour-suppressor gene in medulloblastoma. Br J Cancer 76:141–145
56. Vorechovsky I, Tingby O, Hartman M, Stromberg B, Nister M, Collins VP, Toftgard R (1997) Somatic mutations in the human homologue of Drosophila patched in primitive neuroectodermal tumours. Oncogene 15:361–366
57. Maesawa C, Tamura G, Iwaya T, Ogasawara S, Ishida K, Sato N, Nishizuka S, Suzuki Y, Ikeda K, Aoki K, Saito K, Satodate R (1998) Mutations in the human homologue of the Drosophila patched gene in esophageal squamous cell carcinoma. Genes Chromosomes Cancer 21:276–279
58. Vorechovsky I, Unden AB, Sandstedt B, Toftgard R, Stahle-Backdahl M (1997) Trichoepitheliomas contain somatic mutations in the overexpressed PTCH gene: support for a gatekeeper mechanism in skin tumorigenesis. Cancer Res 57:4677–4681
59. Raffel C, Jenkins RB, Frederick L, Hebrink D, Alderete B, Fults DW, James CD (1997) Sporadic medulloblastomas contain PTCH mutations. Cancer Res 57:842–845
60. Fletcher CDM (1995) Diagnostic histopathology of tumors, vol 2. Churchill Livingstone
61. Pietsch T, Waha A, Koch A, Kraus J, Albrecht S, Tonn J, Sorensen N, Berthold F, Henk B, Schmandt N, Wolf HK, von Deimling A, Wainwright B, Chenevix-Trench G, Wiestler OD, Wicking C (1997) Medulloblastomas of the desmoplastic variant carry mutations of the human homologue of Drosophila patched. Cancer Res 57:2085–2088
62. Motoyama J, Takabatake T, Takeshima K, Hui C (1998) Ptch2, a second mouse Patched gene is co-expressed with Sonic hedgehog. Nat Genet 18:104–106
63. Carpenter D, Stone DM, Brush J, Ryan A, Armanini M, Frantz G, Rosenthal A, de Sauvage FJ (1998) Characterization of two patched receptors for the vertebrate hedgehog protein family. Proc Natl Acad Sci USA 95:13630–13634
64. Motoyama J, Heng H, Crackower MA, Takabatake T, Takeshima K, Tsui LC, Hui C (1998) Overlapping and non-overlap-

ping ptch2 expression with shh during mouse embryogenesis. Mech Dev 78:81–84

65. Zaphiropoulos PG, Unden AB, Rahnama F, Hollingsworth RE, Toftgard R (1999) PTCH2, a novel human patched gene, undergoing alternative splicing and up-regulated in basal cell carcinomas. Cancer Res 59:787–792
66. Smyth I, Narang MA, Evans T, Heimann C, Nakamura Y, Chenevix-Trench G, Pietsch T, Wicking C, Wainwright BJ (1999) Isolation and characterization of human Patched 2 (PTCH2), a putative tumor suppressor gene in basal cell carcinoma and medulloblastoma on chromosome 1p32. Hum Mol Genet 6:291–297
67. Gemmill RM, West JD, Boldog F, Tanaka N, Robinson LJ, Smith DI, Li F, Drabkin HA (1998) The hereditary renal cell carcinoma 3;8 translocation fuses FHIT to a patched-related gene, TRC8. Proc Natl Acad Sci USA 95:9572–9577
68. Unden AB, Zaphiropoulos PG, Bruce K, Toftg~ard R, St~ahle-Backdahl M (1997) Human patched (PTCH) mRNA is overexpressed consistently in tumor cells of both familial and sporadic basal cell carcinoma. Cancer Res 57:2336–2340
69. Wolter M, Reifenberger J, Sommer C, Ruzicka T, Reifenberger G (1997) Mutations in the human homologue of the Drosophila segment polarity gene patched (PTCH) in sporadic basal cell carcinomas of the skin and primitive neuroectodermal tumors of the central nervous system. Cancer Res 57: 2581–2585
70. Goodrich LV, Milenkovic L, Higgins KM, Scott MP (1997) Altered neural cell fates and medulloblastoma in mouse patched mutants. Science 277:1109–1113
71. Hahn H, Wojnowski L, Zimmer AM, Hall J, Miller G, Zimmer A (1998) Rhabdomyosarcomas and radiation hypersensitivity in a mouse model of Gorlin syndrome. Nat Med 4:619–622
72. Dahmane N, Lee J, Robins P, Heller P, Ruiz i Altaba A (1997) Activation of the transcription factor Gli1 and the Sonic hedgehog signalling pathway in skin tumours. Nature 389: 876–881
73. Kinzler KW, Bigner SH, Bigner DD, Trent JM, Law ML, O'Brien SJ, Wong AJ, Vogelstein B (1987) Identification of an amplified, highly expressed gene in a human glioma. Science 236:70–73
74. Ruppert JM, Vogelstein B, Kinzler KW (1991) The zinc finger protein GLI transforms primary cells in cooperation with adenovirus El a. Mol Cell Biol 11:1724–1728
75. Oro AE, Higgins KM, Hu Z, Bonifas JM, Epstein EH Jr, Scott MP (1997) Basal cell carcinomas in mice overexpressing sonic hedgehog. Science 276:817–821
76. Fan H, Oro AE, Scott MP, Khavari PA (1997) Induction of basal cell carcinoma features in transgenic human skin expressing Sonic Hedgehog. Nat Med 3:788–792
77. Fujita E, Khoroku Y, Urase K, Tsukahara T, Momoi MY, Kumagai H, Takemura T, Kuroki T, Momoi T (1997) Involvement of Sonic hedgehog in the cell growth of LK-2 cells, human lung squamous carcinoma cells. Biochem Biophys Res Commun 238:658–664
78. Xie J, Murone M, Luoh SM, Ryan A, Gu Q, Zhang C, Bonifas JM, Lam CW, Hynes M, Goddard A, Rosenthal A, Epstein EH Jr, de Sauvage FJ (1998) Activating Smoothened mutations in sporadic basal-cell carcinoma. Nature 391:90–92
79. Chiang C, Litingtung Y, Lee E, Young KE, Corden JL, Westphal H, Beachy PA (1996) Cyclopia and defective axial patterning in mice lacking Sonic hedgehog gene function. Nature 383:407–413
80. Sundberg JP, Adkison DL, Bedigian HG (1991) Skeletal muscle rhabdomyosarcomas in inbred laboratory mice. Vet Pathol 28:200–206
81. Teitz T, Chang JC, Kitamura M, Yen TS, Kan YW (1993) Rhabdomyosarcoma arising in transgenic mice harboring the beta-globin locus control region fused with simian virus 40 large T antigen gene. Proc Natl Acad Sci USA 90:2910–2914
82. Doige CA, Ames GF (1993) ATP-dependent transport systems in bacteria and humans: relevance to cystic fibrosis and multidrug resistance. Annu Rev Microbiol 47:291–319
83. Saier MH Jr (1994) Convergence and divergence in the evolution of transport proteins. Bioessays 16:23–29
84. Loftus SK, Morris JA, Carstea ED, Gu JZ, Cummings C, Brown A, Ellison J, Ohno K, Rosenfeld MA, Tagle DA, Pentchev PG, Pavan WJ (1997) Murine model of Niemann-Pick C disease: mutation in a cholesterol homeostasis gene. Science 277:232–235
85. Carstea ED, Morris JA, Coleman KG, Loftus SK, Zhang D, Cummings C, Gu J, Rosenfeld MA, Pavan WJ, Krizman DB, Nagle J, Polymeropoulos MH, Sturley SL, Ioannou YA, Higgins ME, Comly M, Cooney A, Brown A, Kaneski CR, Blanchette-Mackie EJ, Dwyer NK, Neufeld EB, Chang TY, Liscum L, Tagle DA, and, et al (1997) Niemann-Pick C1 disease gene: homology to mediators of cholesterol homeostasis. Science 277:228–231
86. Porter JA, Young KE, Beachy PA (1996) Cholesterol modification of hedgehog signaling proteins in animal development. Science 274:255–2559 [published erratum appears in 274: 1597]
87. Xu G, Salen G, Shefer S, Ness GC, Chen TS, Zhao Z, Salen L, Tint GS (1995) Treatment of the cholesterol biosynthetic defect in Smith-Lemli-Opitz syndrome reproduced in rats by BM 15.766. Gastroenterology 109:1301–1307
88. Cooper MK, Porter JA, Young KE, Beachy PA (1998) Teratogen-mediated inhibition of target tissue response to Shh signaling. Science 280:1603–1607
89. Sun FL, Dean WL, Kelsey G, Allen ND, Reik W (1997) Transactivation of Igf2 in a mouse model of Beckwith-Wiedemann syndrome. Nature 389:809–815
90. Branch S, Francis BM, Brownie CF, Chernoff N (1996) Teratogenic effects of the demethylating agent 5-aza-2'-deoxycytidine in the Swiss Webster mouse. Toxicology 112:37–43
91. Chen RZ, Pettersson U, Beard C, Jackson-Grusby L, Jaenisch R (1998) DNA hypomethylation leads to elevated mutation rates. Nature 395:89–93
92. Shafei-Benaissa E, Savage JR, Papworth D, Babin P, Larregue M, Tanzer J, Bonnetblanc JM, Vaillant L, Huret JL (1995) Evidence of chromosomal instability in the lymphocytes of Gorlin basal-cell carcinoma patients. Mutat Res 332:27–32
93. Hall EJ (1994) Effects of radiation on the embryo and fetus. In: Radiobiology for the radiologist. Lippincott, Philadelphia
94. Rugh R (1990) The mouse: its reproduction and development. Oxford University Press, New York
95. Arlett CF, Harcourt SA (1980) Survey of radiosensitivity in a variety of human cell strains. Cancer Res 40:926–932
96. Chan GL, Little JB (1983) Cultured diploid fibroblasts from patients with the nevoid basal cell carcinoma syndrome are hypersensitive to killing by ionizing radiation. Am J Pathol 111:50–55
97. Weichselbaum RR, Nove J, Little JB (1980) X-ray sensitivity of fifty-three human diploid fibroblast cell strains from patients with characterized genetic disorders. Cancer Res 40:920–925
98. Featherstone T, Taylor AM, Harnden DG (1983) Studies on the radiosensitivity of cells from patients with basal cell naevus syndrome. Am J Hum Genet 35:58–66
99. Waldman T, Zhang Y, Dillehay L, Yu J, Kinzler K, Vogelstein B, Williams J (1997) Cell-cycle arrest versus cell death in cancer therapy. Nat Med 3:1034–1036
100. Wild A, Kalff-Suske M, Vortkamp A, Bornholdt D, Konig R, Grzeschik KH (1997) Point mutations in human GLI3 cause Greig syndrome. Hum Mol Genet 6:1979–1984
101. Kang S, Graham JM Jr, Olney AH, Biesecker LG (1997) GLI3 frameshift mutations cause autosomal dominant Pallister-Hall syndrome. Nat Genet 15:266–268
102. Motoyama J, Liu J, Mo R, Ding Q, Post M, Hui CC (1998) Essential function of Gli2 and Gli3 in the formation of lung, trachea and oesophagus. Nat Genet 20:54–57

Oncogene (1999) 18, 7844-7851
© 1999 Stockton Press All rights reserved 0950-9232/99 $15.00
http://www.stockton-press.co.uk/onc

The hedgehog signalling pathway in tumorigenesis and development

Carol Wicking*,[1], Ian Smyth[1] and Allen Bale[2]

[1]*Centre for Molecular and Cellular Biology, University of Queensland, St Lucia 4072, Queensland, Australia;* [2]*Department of Genetics, Yale University School of Medicine, New Haven, Connecticut, CT 06520, USA*

The hedgehog signalling pathway is responsible for the embryonic patterning of a range of tissues, and it is now known that dysregulation of this pathway can result in the formation of several tumour types. This cascade is regulated at the cell surface by the opposing actions of the patched and smoothened molecules which together form a receptor complex for hedgehog. The discovery that inactivation of the human *patched* gene is responsible for familial and sporadic forms of basal cell carcinoma firmly established a role for dysregulation of hedgehog signalling in tumorigenesis. Other key members of this pathway have also been shown to be involved in tumour formation, as have more distal downstream targets of hedgehog signalling. Since it appears that tumorigenesis results from constitutive activation of hedgehog responsive genes, the identification of novel downstream targets of hedgehog signalling in given cell types is likely to increase our understanding of the molecular processes underlying tumour formation.

Keywords: patched; hedgehog; basal cell carcinoma

The hedgehog signalling pathway is one of the most fundamental signal transduction pathways in embryonic development, being responsible for patterning the developing neural tube, axial skeleton, limbs, lungs, skin, hair and teeth (Bellusci *et al*., 1997; Hardcastle *et al*., 1998; Marigo and Tabin, 1996; Riddle *et al*., 1993; St-Jacques *et al*., 1998). Much of what is known of the function of this pathway has been derived from studies in *Drosophila*, and many of the key elements have been conserved from flies through to humans (Goodrich *et al*., 1996; Hahn *et al*., 1996a). Several of the putative downstream targets of hedgehog signalling have been implicated in tumorigenesis, and some of these are the subject of other review articles in this edition. However, it was the discovery that mutation of the gene encoding the receptor molecule patched is responsible for familial and sporadic forms of basal cell carcinoma (BCC) which provided direct evidence for involvement of the key regulatory members of this signalling pathway in tumour formation (Hahn *et al*., 1996b; Johnson *et al*., 1996). Dysregulation of the hedgehog signalling pathway is the major determinant of BCC formation, as well as being involved in the development of several other tumour types. It appears that tumour formation results when mutation of regulatory genes leads to constitutive activation of downstream hedgehog responsive genes. This article will review the role of hedgehog signalling in tumorigenesis, concentrating on the proteins responsible for receiving and transmitting the hedgehog signal at the cell membrane. In addition, progress towards producing mouse models of NBCCS and associated tumours will be discussed.

Hedgehog signalling pathway

The hedgehog (hh) pathway was originally delineated in *Drosophila*, and its members are encoded by segment polarity genes which are responsible for determining the anterior-posterior orientation of developing structures in the *Drosophila* embryo and larva (Nusslein-Volhard and Wieschaus, 1980; Basler and Struhl, 1994; Rodriguez and Basler, 1997). Epistatic relationships suggested that, in addition to hedgehog, other members of this pathway included patched, the serpentine membrane protein smoothened (smo; Alcedo *et al*., 1996; van den Heuvel and Ingham, 1996), the kinesin-like protein costal-2 (cos-2; Sisson *et al*., 1997), the serine/threonine kinase fused (fu; Preat *et al*., 1990), the novel protein suppressor of fused (Monnier *et al*., 1998), and the zinc finger transcription factor cubitus interruptus (ci; Orenic *et al*., 1990). Initial studies of this signalling pathway focused on the hedgehog molecule whose expression defines the development of many embryonic and adult structures in both the fly and vertebrates.

Hedgehog and its receptor complex Hedgehog is a secreted molecule which undergoes autocatalytic cleavage to give an active N-terminal fragment (Lee *et al*., 1992, 1994; Porter *et al*., 1995) which is modified by addition of a cholesterol moiety at its C-terminus (Porter *et al*., 1996). While there is only a single *Drosophila* hedgehog gene, three vertebrate homologues have been identified, *Sonic (Shh)*, *Desert (Dhh)*, and *Indian hedgehog (Ihh)* (Echelard *et al*., 1993). *In vitro* studies suggest that each of these proteins can act through the same signal transduction pathway, and that the different hedgehog genes regulate patterning of different organ systems by virtue of their unique expression pattern (Echelard *et al*., 1993; Marigo *et al*., 1996; Stone *et al*., 1996). The most extensively studied of the vertebrate hedgehog genes is *Shh* which is expressed widely throughout the developing CNS, limb, lung, gut, teeth and hair-follicle (Bellusci *et al*., 1997; Goodrich *et al*., 1996; Hardcastle *et al*., 1998; Litingtung *et al*., 1998; Marigo and Tabin, 1996; Riddle *et al*., 1993; St-Jacques *et al*., 1998). *Dhh* and *Ihh* are primarily involved in development of the germline and skeletal system respectively (Bitgood *et al*., 1996; Vortkamp *et al*., 1996).

The molecule responsible for acting as a receptor for hedgehog at the cell surface was the subject of debate for some time. Epistatic studies in *Drosophila* identified smoothened and patched as acting upstream of fused, suppressor of fused, costal-2 and cubitus interruptus in the signalling pathway. Both smoothened and patched are putative transmembrane proteins, either of which could potentially act as the hedgehog receptor. It was not until *in vitro* studies were undertaken using vertebrate patched and smoothened proteins that patched was shown to bind hedgehog directly and hence act as the hedgehog receptor (Stone *et al.*, 1996; Marigo *et al.*, 1996).

---

*Correspondence: C Wicking

Patched encodes a 12-pass transmembrane glycoprotein with two large extracellular domains and a smaller intracellular domain. While the protein is similar in structure to a channel protein, no transport function has been attributed to it despite studies of the possible trafficking of Ca+, K+, Na+ and Cl− (Marigo *et al.*, 1996). Interestingly however, five of the membrane spanning domains of patched show homology with sterol sensing domains in several proteins involved in cholesterol homeostasis (Carstea *et al.*, 1997; Loftus *et al.*, 1997). These include the protein responsible for the neurovisceral lipid storage disorder Niemann-Pick C disease, HMG-CoA reductase and SREBP cleavage-activating protein (SCAP). The role of the sterol sensing domain of patched is yet to be determined, but it does not appear to be simply involved in targeting hedgehog to the appropriate part of the adjacent membrane, since a *Sonic hedgehog* construct encoding the N-terminal fragment which is not modified by cholesterol is capable of inducing both floor plate cells and motor neurons in neural explants (Roelink *et al.*, 1995). It has been proposed that the response of target tissues to hedgehog is dependent on the detection of intracellular sterol levels by the sterol sensing domain (Cooper *et al.*, 1998). Recently a second patched gene was identified in vertebrates, and while it appears to act in a similar manner to patched *in vitro*, its role in hedgehog signalling remains to be elucidated (Carpenter *et al.*, 1998; Motoyama *et al.*, 1998; Smyth *et al.*, 1999; Takabatake *et al.*, 1997).

While patched has been shown to directly bind the hedgehog ligand, smoothened also has a role in reception and transduction of the hedgehog signal. This was determined following the finding that patched also interacts with smoothened, and that hedgehog, smoothened and patched can be immunoprecipitated in a single complex (Stone *et al.*, 1996). Smoothened, which is structurally similar to the family of serpentine G-protein coupled receptors, is responsible for triggering intracellular signalling and the subsequent activation of target genes. The current model for hedgehog signalling suggests that, in the absence of hedgehog, patched interacts at the membrane with smoothened, rendering it inactive. However when hedgehog binds to patched, the inhibition of smoothened signalling is released and downstream genes are transcriptionally upregulated (Figure 1). While it is known that the two large extracellular loops of the patched molecule are required for binding of hedgehog (Marigo *et al.*, 1996), the domains of patched which are responsible for binding smoothened have yet to be elucidated, although these interactions do appear to be modulated by the extracellular N-terminus of smoothened (Murone *et al.*, 1999).

While we now have a plausible model for how the hedgehog signal is received at the cell surface, we are just beginning to identify the complex and diverse mechanisms which regulate intracellular components of hedgehog signalling.

From the membrane to the nucleus In *Drosophila* the *cubitus interruptus (ci)* gene encodes the transcription factor primarily responsible for the activation and repression of hedgehog target genes (Von Ohlen *et al.*,

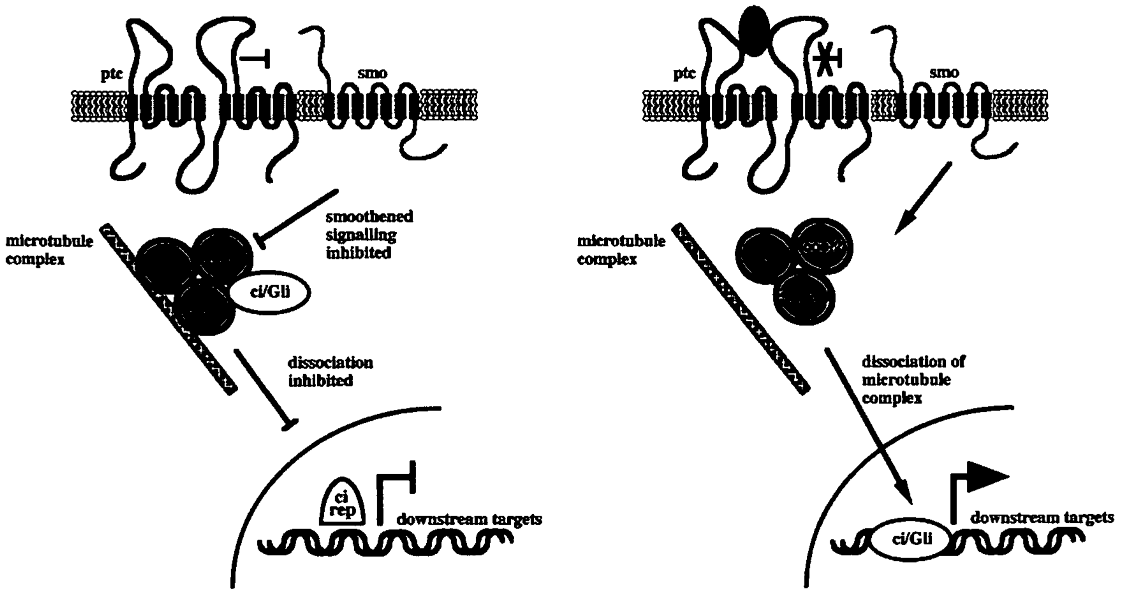

Figure 1 The hedgehog signalling pathway based on what is known in *Drosophila*. In the absence of hedgehog (hh), the patched protein (ptc) inhibits signalling by smoothened (smo). Upon binding of hedgehog this repression is released leading to dissociation of a complex of segment polarity proteins normally associated with the microtubules (Fu-fused, Su(Fu)- suppressor of fused, cos-2-costa-2, ci-cubitus interruptus). In vertebrates the role of ci is achieved by complex interactions involving three Gli genes

1997). Mediation of the hedgehog signal by Ci is controlled at the post-translational level (Aza-Blanc *et al.*, 1997). In cells not exposed to hedgehog signal full-length Ci, which forms a complex with costal-2, fused and suppressor of fused at the microtubules, is cleaved to give a 75 kDa N-terminal fragment which is localized in the nucleus and appears to act as a transcriptional repressor. This processing of Ci is thought to be mediated by the phosphorylation of the full-length form of the protein (Chen *et al.*, 1999). In the presence of hedgehog, cleavage of Ci is inhibited, the microtubule complex is dissociated and activation of target genes results (Figure 1). This activation is thought to result from a combination of lifting of repression by Ci75 (Aza-Blanc *et al.*, 1997), nuclear import of full-length Ci (Chen *et al.*, 1999) and maturation of full-length Ci into a labile transcriptional activator (Ohlmeyer and Kalderon, 1998). Suppressor of fused opposes the conversion of Ci into a transcriptional activator and hence acts as a negative regulator of signalling (Ohlmeyer and Kalderon, 1998).

While not all components of the *Drosophila* microtubule complex have yet been shown to have vertebrate homologues, it is likely that a similar mechanism is responsible for regulating vertebrate signalling. The role of Ci is achieved in vertebrates by the three Gli genes (Gli1, 2 and 3), with the precise role of each of these being the subject of much debate. Recent evidence suggests that like ci, Gli genes, in particular Gli2 and Gli3, act as bipotential transcription factors possessing both activation and repression domains (Altaba *et al.*, 1999; Dai *et al.*, 1999; Sasaki *et al.*, 1999). It is proposed that Gli2 and Gli3 act as the major mediators of hedgehog signalling (Sasaki *et al.*, 1999), and when converted to their active forms they activate Gli1 at the transcriptional level (Dai *et al.*, 1999; Sasaki *et al.*, 1999). Activation of hedgehog target genes is thought to result from the synergistic action of Gli1, 2 and 3. In an analogous situation to that seen in *Drosophila*, human suppressor of fused has been shown to inhibit transcriptional activation by Gli1, at least in part by sequestering it in the cytoplasm (Kogerman *et al.*, 1999).

Downstream targets of hedgehog signalling In *Drosophila*, known downstream targets of hedgehog signalling include *wingless* (homologous to the vertebrate Wnt genes), *decapentaplegic* (a member of the TGFβ superfamily most homologous to the vertebrate bone morphogenetic proteins (Bmps)), as well as *patched* itself (reviewed in Ingham, 1998). While it is likely that members of these gene families will be activated by hedgehog signaling in the vertebrate system, other as yet unidentified genes will undoubtedly be regulated by this pathway. In addition, the identity of target genes is known to be cell type and organ specific. For example, the closest vertebrate homologues of decapentaplegic, the *Bmp2* and *Bmp4* genes, while activated by hedgehog signalling in the developing limb (Bitgood and McMahon, 1995) appear to be unaffected by loss of hedgehog in the hair follicle (St-Jacques *et al.*, 1998). Other examples include the hepatocyte nuclear factor 3β (HNF3β) which is regulated by hedgehog signalling exclusively in the neural tube where its expression in the floor plate is induced by Sonic hedgehog from the notochord (Roelink *et al.*, 1995).

Recently several other genes have been shown to be responsive to hedgehog signalling, and while they are likely to be involved in the regulation of the pathway, their precise role is yet to be determined. The first of these, which has been termed *hip* (for *hedgehog interacting protein*), encodes a membrane glycoprotein which binds all three hedgehog proteins with similar affinity to patched (Chuang and McMahon, 1999). Like *patched, Hip* is transcriptionally activated by hedgehog signalling, and it has also been proposed to be a negative regulator of signalling (Chuang and McMahon, 1999). Another gene shown to be responsive to hedgehog signalling in both the somites and limb buds is a member of a novel family of SOCS (suppressor of cytokine signalling) box-containing WD-proteins and has been termed both *WSB1* and *SWIP-1* (Hilton *et al.*, 1998; Vasiliauskas *et al.*, 1999). This gene is one of the earliest markers to respond to sonic hedgehog in the limb, but its role in the signalling pathway remains unclear (Vasiliauskas *et al.*, 1999).

It is the regulation and identity of the downstream target genes which is likely to determine the role of hedgehog signalling in tumorigenesis. In general tumorigenesis results from constitutive activation of these genes, and it will be essential to determine novel hedgehog target genes in specific tissues to more fully understand the molecular pathogenesis of the tumours associated with dysregulation of hedgehog signalling.

Hedgehog signalling in disease and tumorigenesis

Several components of the hedgehog pathway have been implicated in tumorigenesis and in dysmorphology syndromes. Heterozygous mutation of sonic hedgehog is responsible for a subset of familial holoprosencephaly, a defect of the forebrain and midface (Roessler *et al.*, 1996). Similarly, Gli3 has been implicated in three distinct developmental syndromes all of which are characterized by limb abnormalities (Kang *et al.*, 1997; Radhakrishna *et al.*, 1997; Vortkamp *et al.*, 1991). In terms of tumour phenotypes, *Gli1* was first identified by and named for its involvement in glioma formation (Kinzler *et al.*, 1988), and *Wnt1* is known to be involved in murine mammary tumorigenesis (Nusse *et al.*, 1990). These genes, along with the *Smad* genes which mediate TGFβ signalling and are involved in the formation of a range of tumour types, are the subject of other reviews in this edition. However, it was the discovery that *patched* is mutated in both familial and sporadic forms of basal cell carcinoma which firmly established this pathway as a major determinant of human cancer and disease.

Patched and nevoid basal cell carcinoma syndrome The human patched gene (*PTCH*) was first implicated in tumorigenesis when it was shown to be mutated in the autosomal dominant cancer predisposition syndrome nevoid basal cell carcinoma syndrome or Gorlin's syndrome (Hahn *et al.*, 1996b; Johnson *et al.*, 1996). NBCCS is characterized by a predisposition to a range of tumour types, most notably basal cell carcinoma, but also medulloblastoma, ovarian fibroma, meningioma, fibrosarcoma, rhabdomyosarcoma and cardiac fibroma (Gorlin, 1995; Shanley *et al.*, 1994). In addition to cancer predisposition, NBCCS is also associated with a range of developmental abnormalities including skeletal defects, dyskeratotic pitting of the hands and feet, progressive intracranial calcification, craniofacial anomalies and limb deformities including poly and syndactyly (Gorlin, 1995). Many of these anomalies can now be correlated with the role of hedgehog signalling in patterning diverse structures during embryonic development, and it is thought that most of these developmental defects are due to haploinsufficiency of the patched protein (Hahn *et al.*, 1996b). This is supported by the finding that by far the majority of *PTCH* mutations (>80%) in the germline of NBCCS individuals result in truncation of the protein and are therefore likely to represent null mutations (Wicking *et al.*, 1997). The tumours in NBCCS individuals are likely to arise with inactivation of the remaining *PTCH* allele in a given cell type, consistent with *PTCH* acting as a tumour suppressor gene. The finding of *PTCH* mutations in a proportion of sporadic BCCs, in many cases with both alleles inactivated by either mutation or loss of heterozygosity (Gailani *et al.*, 1996), supports this putative function. Since the initial discovery of *PTCH* mutations in NBCCS and BCCs, the role of members of the patched/hedgehog signalling pathway in the pathogenesis of a range of tumour types has been the subject of intensive study.

Patched and BCCs BCCs are common non-melanocytic skin tumours resulting from loss of growth control in keratinocytes. While BCCs rarely metastasise they are locally invasive and can infiltrate underlying dermis and bone if left untreated (Weedon, 1991). The site of origin of these tumours remains a matter of some contention, although their keratin expression profiles and occasional pilosebaceous differentiation suggest that they may arise from the hair follicle (Markey *et al.*, 1992), consistent with the expression of *patched* in this structure (Figure 2).

Over-expression of both *PTCH* (Gailani *et al.*, 1996; Unden *et al.*, 1997; Wolter *et al.*, 1997) and *GLI1* (Dahmane *et al.*, 1997) has been reported in BCCs, indicating dysregulation of hedgehog signalling in a high proportion of these tumours. The estimated frequency of *PTCH* mutations in sporadic BCCs ranges from 12–38%, although in all cases this may represent an underestimate based on the mutation detection procedures employed (Aszterbaum *et al.*, 1998b; Gailani *et al.*, 1996; Unden *et al.*, 1997; Wolter *et al.*, 1997). In addition to mutations in the *PTCH* gene, loss of heterozygosity of markers on the region of chromosome 9q encompassing *PTCH* is observed in upwards of 50% of BCCs (Gailani *et al.*, 1992). Like NBCCS germline mutations, the majority of *PTCH* mutations in BCCs result in premature protein termination (Gailani *et al.*, 1996). In addition, many of the mutations detected in sporadic BCCs are C→T substitutions at dipyrimidine sites, indicating a role for ultraviolet-B irradiation in their genesis (Gailani *et al.*, 1996). In the most extensive analysis of *PTCH* mutations in sporadic BCCs to date, it was found that seven out of 16 mutations detected were of this type, and all tumours with such mutations had been removed from sun-exposed sites of the body (Gailani *et al.*, 1996). However, there is evidence from epidemiological data that factors other than sun exposure may be involved in BCC induction (Scotto *et al.*, 1996), with one such factor being the trivalent form of inorganic arsenic (Nakjang and Kullavanijaya, 1994; Tay and Seah, 1975; Wong *et al.*, 1998; Yeh, 1973). It

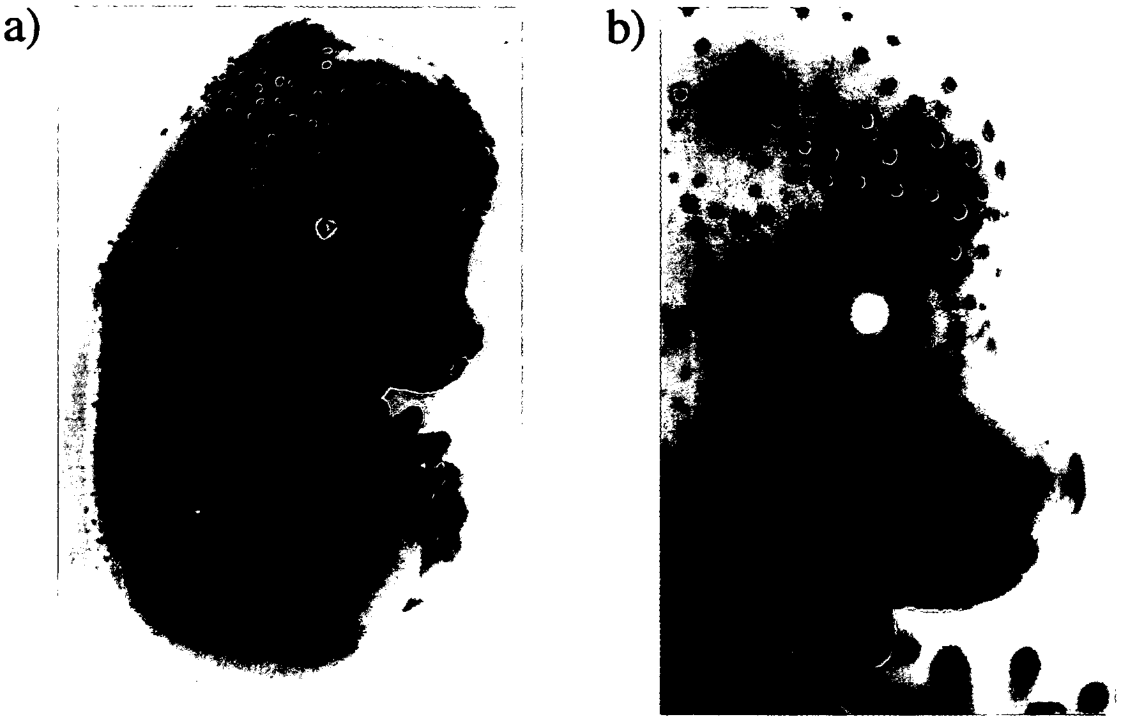

Figure 2 Patched is expressed in the developing hair follicle. Whole amount *in situ* analysis of *patched* expression in a 15.0 dpc mouse embryo (**a** and **b**). The probe used has been described previously (Hahn *et al.*, 1996a)

has yet to be shown definitively if these other agents contribute to BCC formation through mutation of the *PTCH* gene. In addition to sporadic BCCs and those associated with NBCCS, *PTCH* mutations have recently been identified in BCCs associated with xeroderma pigmentosum (XP), a rare autosomal recessive disorder characterized by hyperphotosensitivity and predisposition to skin cancer (Bodak *et al.*, 1999). Individuals with XP are deficient in the repair of UV-induced DNA lesions, and the proportion of BCCs with UV-specific mutations was found to be higher in those tumours derived from XP patients than in sporadic BCCs.

Smoothened and BCCs Given that constitutive activation of smoothened is likely to upregulate transcription of hedgehog target genes in the same way as patched inactivation, it is not surprising that activating mutations in the *smoothened* gene have been detected in 10–20% of sporadic BCCs (Lam *et al.*, 1999; Reifenberger *et al.*, 1998; Xie *et al.*, 1998). In particular one common mutation (Trp535Leu) in the seventh transmembrane domain of smoothened has been detected in several independent studies in up to 20% of BCCs (Lam *et al.*, 1999; Xie *et al.*, 1998). In contrast to wild-type smoothened, the mutant form has been shown to result in constitutive smoothened signalling in an *in vitro* focus forming assay and in transgenic mice (Xie *et al.*, 1998). *In vitro* studies assessing activation of a Gli1 reporter construct have subsequently been used to identify which regions of the smoothened protein interact with patched and which are involved in signalling (Murone *et al.*, 1999). Consistent with some of the mutations observed in BCCs, the third intracellular loop and the seventh transmembrane domain were shown to be important in activation of signalling. Modelling of the Trp535Leu smoothened mutation, as well as a second mutation (Arg562Gln) in the C-terminus, leads to constitutive signalling of the protein in a manner which is not repressed by patched. The interactions of patched and smoothened were found to be mediated primarily through the cysteine rich N-terminus of smoothened, but to date no mutations in this region have been found in BCCs (Murone *et al.*, 1999).

Since hedgehog itself is primarily responsible for activation of this pathway, it is feasible that it also may be mutated in associated tumours, a premise supported by the finding that transgenic mice overexpressing *Sonic hedgehog* develop BCC-like skin lesions (Oro *et al.*, 1997). Accordingly, a single recurrent mutation in *Sonic hedgehog* was initially reported in a range of tumour types including BCC (Oro *et al.*, 1997), but failure of other workers to detect this mutation suggests that it is extremely rare (Reifenberger *et al.*, 1998; Wicking *et al.*, 1998).

Taken together, inactivation of *PTCH* or oncogenic activation of *smoothened* occurs in a large proportion of BCCs, suggesting that dysregulation of hedgehog signalling is a requirement for BCC formation. Although it has previously been suggested that *patched* is the gatekeeper gene for BCC formation (Sidransky, 1996), it may be more accurate to regard the entire hedgehog signalling pathway as the BCC gatekeeper. The term gatekeeper was coined by Kinzler and Vogelstein (Kinzler and Vogelstein, 1996) to describe genes which must be inactivated or activated to give rise to a particular type of tumour. While mutations in the *p53* tumour suppressor gene have been described in 50% of BCCs (Zeigler *et al.*, 1993), these would be considered insufficient to cause neoplasia without dysregulation of hedgehog signalling.

Dysregulation of hedgehog signalling in other tumour types Mutations in genes of the hedgehog signalling pathway have also been described in a range of tumours other than BCCs. In keeping with the predisposition of NBCCS patients to developing the childhood brain tumour medulloblastoma, mutations of both *PTCH* and *smoothened* have been detected in sporadic medulloblastomas and other primitive neuroectodermal tumours (Pietsch *et al.*, 1997; Raffel *et al.*, 1997; Reifenberger *et al.*, 1998; Vorechovsky *et al.*, 1997a; Wolter *et al.*, 1997). NBCCS patients develop the desmoplastic histological subtype of medulloblastoma, and while one study reported *PTCH* mutations exclusively in this subtype (Pietsch *et al.*, 1997), mutations in classic medulloblastomas have also been described (Wolter *et al.*, 1997). In all cases, the incidence of mutations in these tumours was significantly less than that observed in BCCs, indicating it is likely that only a subset of these neoplasias are caused by mutations in *PTCH* or other members of the hedgehog signalling pathway. This notion is also supported by the frequency of loss of heterozygosity of the *PTCH* locus in medulloblastomas which is reduced when compared to BCCs (Pietsch *et al.*, 1997). It is also possible that *PTCH2* may play a minor role in the pathogenesis of medulloblastoma since a screen for mutations in a large collection of medulloblastomas revealed a single protein truncating mutation (Smyth *et al.*, 1999).

Other tumours which carry *PTCH* mutations include the benign skin lesions tricoepitheliomas (TEs), esophageal squamous cell carcinomas and transitional cell carcinomas of the bladder (Vorechovsky *et al.*, 1997b; Maesawa *et al.*, 1998; McGarvey *et al.*, 1998). In addition, although mutations in *PTCH* are yet to be demonstrated in rhabdomyosarcomas, mice heterozygous for a null allele of *patched* develop this soft tissue tumour of the muscle at a high frequency (Hahn *et al.*, 1998). Since this tumour is also found at an increased incidence in NBCCS individuals, it is likely that this pathway plays a role in its pathogenesis.

Mouse models of NBCCS and associated tumours

The creation of mouse models of human disease by gene targeting or transgenic technology provides a powerful tool for the functional dissection of the disease phenotype. To date a range of mouse models have been produced by manipulation of members of the hedgehog signalling pathway. This section will focus on those animals which represent models for NBCCS and tumours associated with dysregulation of hedgehog signalling.

Patched null mutants To date two independent groups have generated *patched* null mice by targeted disruption of the *patched* gene (Goodrich *et al.*, 1997; Hahn *et al.*, 1998). As would be expected from inactivation of such a developmentally important gene, homozygous null animals died during embryogenesis. However, in both cases the heterozygous mice showed a subset of both the developmental and neoplastic features associated with NBCCS.

The first *patched* null mutant to be produced involved inactivation of *patched* by replacement of part of exon one and the entire exon two by a lacZ/neo cassette, an insertion which results in removal of the primary start codon and deletion of transmembrane domain 1 (Goodrich *et al.*, 1997). The second was generated by the replacement of exons six and seven of *patched* with a neomycin cassette (Hahn *et al.*, 1998). In both cases homozygous mice die around 9.0 dpc by which stage failure of neural tube closure was evident. The heterozgous mice varied in phenotype between the two null alleles, though in both cases they displayed the generalized overgrowth and limb deformities characteristic of NBCCS.

Heterozygous animals displayed a tumour phenotype at a stage and frequency which would suggest that, unlike a classical tumour suppressor gene, somatic inactivation of the remaining allele was not occurring in all tumours. Heterozygotes for both null alleles developed medulloblastoma like lesions, this being seen at a particularly high frequency and young age in the $Ptc^{+/neolacZ12}$ mice (Goodrich *et al.*, 1997). These mice also developed BCC-like skin tumours as adults, a feature which was enhanced by exposure to UV or cesium irradiation (Aszterbaum *et al.*, 1998a). The $Ptc^{+/neo67}$ animals also developed rhabdomyosarcomas (RMS), a soft tissue tumour of the muscle which is seen in a small proportion of NBCCS patients (Hahn *et al.*, 1998). The difference in phenotype between these null mice is likely to result from genetic background differences, since even within the same null allele the percentage of mice that developed rhabdomyosarcomas varied on different mouse backgrounds (Hahn *et al.*, 1998). Genetic background effects are also likely to contribute to the wide variation in neural defects seen in transgenic mice overexpressing *patched* in the neural tube (Goodrich *et al.*, 1999). The contribution of genetic background to phenotype closely parallels the situation in humans where the phenotype of NBCCS individuals varies widely despite a predominance of truncating mutations which in most cases are presumed to be null alleles (Wicking *et al.*, 1997).

Overexpression of Sonic hedgehog and smoothened: Given the opposing actions of patched compared to hedgehog and smoothened at the cell membrane, overexpression of *hedgehog* or *smoothened* would be predicted to result in a similar phenotype to inactivation of *patched.* In an attempt to produce a transgenic mouse model of BCC formation, Oro and co-workers ectopically expressed full-length *Sonic hedgehog* under the control of the Keratin 14 (K14) promoter (Oro *et al.*, 1997). K14 is expressed as early as 9.5 dpc in many epithelial tissues and in skin in both follicular and interfollicular cells (Byrne *et al.*, 1994). Although these animals died either peri- or postnatally, BCC-like epidermal proliferations were evident, as were a number of NBCCS-like features including limb anomalies reminiscent of polydactyly. In a similar fashion, a transgenic human tissue model of BCC was developed by regeneration of human skin on immune deficient mice following retroviral transduction of human keratinocytes with *Sonic hedgehog* (Fan *et al.*, 1997).

It is assumed that the *Sonic hedgehog* models of BCC described above result from constitutive activation of smoothened signalling. While overexpression of wild type *smoothened* did not result in a tumour phenotype, ectopic expression of an activated *smoothened* gene under the control of the Keratin-5 promoter resulted in a microscopic skin phenotype consistent with BCCs, although no developmental anomalies were noted (Xie *et al.*, 1998). The *smoothened* gene in this case carried the Trp535Leu missense mutation observed in up to 20% of BCCs (Lam *et al.*, 1999; Xie *et al.*, 1998). The absence of developmental anomalies in these mice fits with restricted expression in the skin of a membrane bound protein, while these anomalies in the K14-*Shh* mice may result from diffusion of ectopically expressed *Sonic hedgehog.*

The mouse models outlined above provide a framework within which to dissect the contribution of hedgehog signalling to tumorigenesis at the molecular level. Combined with analyses of human tumours and *in vitro* approaches, a model for the role of this pathway in tumorigenesis is emerging. However, it is the discovery of novel hedgehog responsive target genes in given cell types which is likely to provide the final link to how dysregulation of hedgehog signalling results in the neoplastic phenotype.

References

Alcedo J, Ayzenzon M, Von Ohlen T, Noll M and Hooper JE. (1996). *Cell*, **86**, 221–232.

Altaba AR. (1999). *Development*, **126**, 3205–3216.

Aszterbaum M, Epstein JH, Oro AE, Goodrich LV, Scott MP and Epstein Jr EH. (1998a). *Am. J. Hum. Genet.*, **63**, A39.

Aszterbaum M, Rothman A, Johnson RL, Fisher M, Xie J, Bonifas JM, Zhang X, Scott MP and Epstein Jr EH. (1998b). *J. Invest. Dermatol.*, **110**, 885–888.

Aza-Blanc P, Ramirez-Weber FA, Laget MP, Schwartz C and Kornberg TB. (1997). *Cell*, **89**, 1043–1053.

Basler K and Struhl G. (1994). *Nature*, **368**, 208–214.

Bellusci S, Furuta Y, Rush MG, Henderson R, Winnier G and Hogan BL. (1997). *Development*, **124**, 53–63.

Bitgood MJ and McMahon AP. (1995). *Dev. Biol.*, **172**, 126–138.

Bitgood MJ, Shen L and McMahon AP. (1996). *Curr. Biol.*, **6**, 298–304.

Bodak N, Queille S, Avril MF, Bouadjar B, Drougard C, Sarasin A and Daya-Grosjean L. (1999). *Proc. Natl. Acad. Sci. USA*, **96**, 5117–5122.

Byrne C, Tainsky M and Fuchs E. (1994). *Development*, **120**, 2369–2383.

Carpenter D, Stone DM, Brush J, Ryan A, Armanini M, Frantz G, Rosenthal A and de Sauvage FJ. (1998). *Proc. Natl. Acad. Sci. USA*, **95**, 13630–13634.

Carstea ED, Morris JA, Coleman KG, Loftus SK, Zhang D, Cummings C, Gu J, Pavan WJ, Krizman DB, Nagle J, Polymeropoulos MH, Sturley SL, Ioannou YA, Higgins ME, Comly M, Cooney A, Brown A, Kaneski CR, Blanchettemackie EJ, Dwyer NK, Neufeld EB, Chang TY, Liscum L, Strauss JF and Pentchev PG. (1997). *Science*, **277**, 228–231.

Chen C-H, von Kessler DP, Park W, Wang B, Ma Y and Beachy PA. (1999). *Cell*, **98**, 305–316.

Chaung PT and McMahon AP. (1999). *Nature*, **397**, 617–621.

Cooper MK, Porter JA, Young KE and Beachy PA. (1998). *Science*, **280**, 1603–1607.

Dahmane N, Lee J, Robins P, Heller P and Altaba AR. (1997). *Nature*, **389**, 876–881.

Dai P, Akimaru H, Tanaka Y, Maekawa T, Nakafuku M and Ishii S. (1999). *J. Biol. Chem.*, **274**, 8143–8152.

Echelard Y, Epstein DJ, St-Jacques B, Shen L, Mohler J, McMahon JA and McMahon AP. (1993). *Cell*, **75**, 1417–1430.

Fah H, Oro AE, Scott MP and Khavari PA. (1997). *Nat. Med.*, **3**, 788–792.

Gailani M, Stahle-Backdahl M, Leffell D, Glynn M, Zaphiropolous P, Pressman C, Unden AB, Dean M, Brach DE, Bale AE and Toftgard R. (1996). *Nat. Genet.*, **14**, 78–81.

Gailani MR, Bale SJ, Leffell DJ, DiGiovanna JJ, Peck GL, Poliak S, Drum MA, Passtakia B, McBride OW, Kase R, Greene M, Mulvihill JJ and Bale AE. (1992). *Cell*, **69**, 111–117.

Goodrich LV, Johnson RJ, Milenkovic L, McMahon JA and Scott MP. (1996). *Genes Dev.*, **10**, 301–312.

Goodrich LV, Milenkovic L, Higgins KM and Scott MP. (1997). *Science*, **277**, 1109–1113.

Goodrich LV, Jung D, Higgins KM, Scott MP. (1999). *Dev. Biol.*, **211**, 323–334.

Gorlin RJ. (1995). *Dermatol. Clin.*, **13**, 113–125.

Hahn H, Christiansen J, Wicking C, Zaphiropoulos PG, Chidambaram A, Gerrard B, Vorechovsky I, Bale AE, Toftgard R, Dean M and Wainwright B. (1996a). *J. Biol. Chem.*, **271**, 12125–12128.

Hahn H, Wicking C, Zaphiropoulos PG, Gailani MR, Shanley S, Chidambaram A, Vorechovsky I, Holmberg E, Unden AB, Gillies S, Negus K, Smyth I, Pressman C, Leffell DJ, Gerrard B, Goldstein AM, Dean M, Toftgard R, Chenevix-Trench G, Wainwright B and Bale AE. (1996b). *Cell*, **85**, 841–851.

Hahn H, Wojnowski L, Zimmer AM, Hall J, Miller G and Zimmer A. (1998). *Nat. Med.*, **4**, 619–622.

Hardcastle Z, Mo R, Hui C-C and Sharpe PT. (1998). *Development*, **125**, 2803–2811.

Hilton DJ, Richardson RT, Alexander WS, Viney EM, Willson TA, Sprigg NS, Starr R, Nicholson SE, Metcalf D and Nicola NA. (1998). *Proc. Natl. Acad. Sci. USA*, **95**, 114–119.

Ingham PW. (1998). *EMBO J.*, **17**, 3505–11.

Johnson RL, Rothman AI, Xie J, Goodrich LV, Bare JW, Bonifas JM, Quinn AG, Myers RM, Cox DR, Epstein Jr EH and Scott MP. (1996). *Science*, **272**, 1668–1671.

Kang S, Graham JM, Olney AH and Biesecker LG. (1997). *Nature Genet.*, **15**, 266–268.

Kinzler KW, Ruppert JM, Bigner SH and Vogelstein B. (1988). *Nature*, **332**, 371–374.

Kinzler KW and Vogelstein B. (1996). *Cell*, **87**, 159–170.

Kogerman P, Grimm T, Kogerman L, Krause D, Unden AB, Sandstedt B, Toftgard R and Zaphiropoulos P. (1999). *Nat. Cell Biol.* **1**, 312–319.

Lam CW, Xie J, To KF, Ng HK, Lee KC, Yuen NW, Lim PL, Chan LY, Tong SF and McCormick F. (1999). *Oncogene*, **18**, 833–836.

Lee JJ, Ekker SC, von Kessler DP, Porter JA, Sub BI and Beachy PA. (1994). *Science*, **266**, 1528–1537.

Lee JJ, von Kessler DP, Parks S and Beachy PA. (1992). *Cell*, **71**, 33–50.

Litingung Y, Lei L, Westphal H and Chiang C. (1998). *Nature Genet.*, **20**, 58–61.

Loftus SK, Morris JA, Carstea ED, Gu JZ, Cummings C, Brown A, Ellison J, Ohno K, Rosenfeld MA, Tagle DA, Pentchev PG and Pavan WJ. (1997). *Science*, **277**, 232–235.

Maesawa C, Tamura G, Iwaya T, Ogasawara S, Ishida K, Sato N, Nishizuka S, Suzuki Y, Ikeda K, Aoki K, Saito K and Satodate R. (1998). *Genes Chrom. Cancer*, **21**, 276–279.

Marigo V, Davey RA, Zuo Y, Cunningham JM and Tabin CJ. (1996). *Nature*, **384**, 176–179.

Marigo V and Tabin CJ. (1996). *Proc. Natl. Acad. Sci. USA*, **93**, 9346–9351.

Markey AC, Lane EB, Macdonald DM and Leigh IM. (1992). *Br. J. Dermatol.*, **126**, 154–160.

McGarvey TW, Maruta Y, Tomaszewski JE, Linnenbach AJ and Malkowicz SB. (1998). *Oncogene*, **17**, 1167–1172.

Monnier V, Dussillol F, Alves G, Lamour-Isnard C and Plessis A. (1998). *Curr. Biol.*, **8**, 583–586.

Motoyama J, Heng H, Crackower MA, Takabatake T, Takeshima K, Tsui LC and Hui C-C. (1998). *Mech. Dev.*, **78**, 81–84.

Murone M, Rosenthal A and de Sauvage FJ. (1999). *Curr. Biol.*, **9**, 76–84.

Nakjang Y and Kullavanijaya P. (1994). *J. Dermatol.*, **21**, 660–663.

Nusse R, Theunissen H, Wagenaar E, Rijsewijk F, Gennissen A, Otte A, Schuuring E and van Ooyen A. (1990). *Mol. Cell. Biol.*, **10**, 4170–4179.

Nusslein-Volhard C and Wieschaus E. (1980). *Nature*, **287**, 795–801.

Ohlmeyer JT and Kalderon D. (1998). *Nature*, **396**, 749–753.

Orenic TV, Slusarski DC, Kroll KL and Holmgren RA. (1990). *Genes Dev.*, **4**, 1053–1067.

Oro AE, Higgins KM, Hu Z, Bonifas JM, Epstein Jr EH and Scott MP. (1997). *Science*, **276**, 817–821.

Pietsch T, Waha A, Koch A, Kraus J, Albrecht S, Tonn J, Sorenson N, Berthold F, Henk B, Wolk HK, von Deimling A, Wainwright B, Chenevix-Trench G, Weistler OD and Wicking CA. (1997). *Cancer Res.*, **57**, 2085–2088.

Porter JA, von Kessler DP, Ekker SC, Young KE, Lee JJ, Moses K and Beachy PA. (1995). *Nature*, **374**, 363–366.

Porter JA, Young KE and Beachy PA. (1996). *Science*, **274**, 255–259.

Preat T, Therond P, Lamour-Isnard C, Limbourg-Bouchon B, Tricoire H, Erk I, Mariol MC and Busson D. (1990). *Nature*, **347**, 87–89.

Radhakrishna U, Wild A, Grzeschik K-H and Antonarakis SE. (1997). *Nature Genet.*, **17**, 269–271.

Raffel C, Jenkins RB, Frederick L, Hebrink D, Alderete B, Fults DW and James CD. (1997). *Cancer Res.*, **67**, 842–845.

Reifenberger J, Wolter M, Weber RG, Megahed M, Ruzicka T, Lichter P and Reifenberger G. (1998). *Cancer Res.*, **58**, 1798–1803.

Riddle RD, Johnson RL, Laufer E and Tabin C. (1993). *Cell*, **75**, 1401–1416.

Rodriguez I and Basler K. (1997). *Nature*, **389**, 614–618.

Roelink H, Porter JA, Chiang C, Tanabe Y, Chang DT, Beachy PA and Jessell TM. (1995). *Cell*, **81**, 445–455.

Roessler E, Belloni E, Gaudenz K, Jay P, Berta P, Scherer SW, Tsui L-C and Muenke M. (1996). *Nature Genet.*, **14**, 357–360.

Sasaki H, Nishizaki Y, Hui C-C, Nakafuku M and Kondoh H. (1999). *Development*, **126**, 3915–3924.

Scotto J, Fears T, Kraemer KH and Fraumeni JJ. (1996). *Cancer Epidemiology and Prevention*. Schottenfeld D and Fraumeni, JF (eds). Oxford University Press: Oxford, pp. 1313–1330.

Shanley S, Ratcliffe J, Hockey A, Haan E, Oley C, Ravine D, Martin N, Wicking C and Chenevix-Trench G. (1994). *Am. J. Med. Genet.*, **50**, 282–290.

Sidransky D. (1996). *Nat. Genet.*, **14**, 7–8.

Sisson JC, Ho KS, Suyama K and Scott MP. (1997). *Cell*, **90**, 235–245.

Smyth I, Narang MA, Evans T, Heimann C, Nakamura Y, Chenevix-Trench G, Pietsch T, Wicking C and Wainwright BJ. (1999). *Hum. Mol. Genet.*, **8**, 291–297.

St-Jacques B, Dassule HR, Karavanova I, Botchkarev VA, Li J, Danielian PS, McMahon JA, Lewis PM, Paus R and McMahon AP. (1998). *Curr. Biol.*, **8**, 1058–1068.

Stone DM, Hynes M, Armanini M, Swanson TA, Gu Q, Johnson RL, Scott MP, Pennica D, Goddard A, Philips H, Noll M, Hooper JE, de Sauvage D and Rosenthal A. (1996). *Nature*, **384**, 129–134.

Takabatake T, Ogawa M, Takahashi TC, Mizuno M, Okamoto M and Takeshima K. (1997). *FEBS Lett.*, **410**, 485–489.

Tay CH and Seah CS. (1975). *Med. J. Aust.*, **2**, 424–428.

Unden AB, Zaphiropoulos PG, Bruce K, Toftgard R and Stahle-Backdahl M. (1997). *Cancer Res.*, **57**, 2336–2340.

van den Heuvel M and Ingham PW. (1996). *Nature*, **382**, 547–551.

Vasiliauskas D, Hancock S and Stern CD. (1999). *Mech. Dev.*, **82**, 79–94.

Van Ohlen T, Lessing D, Nusse R and Hooper JE. (1997). *Proc. Natl. Acad. Sci. USA*, **94**, 2404–2409.

Vorechovsky I, Tingby O, Hartman M, Stromberg B, Nister M, Collins VP and Toftgard R. (1997a). *Oncogene*, **15**, 361–366.

Vorechovsky I, Unden AB, Sandstedt B, Toftgard R and Stahl-Backdahl M. (1997b). *Cancer Res.*, **57**, 4677–4681.

Vortkamp A, Gessler M and Grzeschik K-H. (1991). *Nature*, **352**, 539–540.

Vortkamp A, Lee K, Lanske B, Segre GV, Kronenberg HM and Tabin CJ. (1996). *Science*, **273**, 613–622.

Weedon D. (1991). *Malignant Skin Tumours*. Emmett J and O'Rourke M (eds). Churchill Livingstone: New York, pp. 109–127.

Wicking C, Evans T, Henk B, Hayward N, Simms LA, Chenevix-Trench G, Pietsch T and Wainwright B. (1998). *Oncogene*, **16**, 1091–1093.

Wicking C, Shanley S, Smyth I, Gillies S, Negus K, Graham S, Suthers G, Haites N, Edwards M, Wainwright B and Chenevix-Trench G. (1997). *Am. J. Hum Genet.*, **60**, 21–26.

Wolter M, Reifenberger J, Sommer C, Ruzicka T and Reifenberger G. (1997). *Cancer Res.*, **57**, 2581–2585.

Wong SS, Tan KC and Goh CL. (1998). *J. Am. Acad. Dermatol.*, **38**, 179–185.

Xie J, Murone M, Luoh S-M, Ryan A, Gu Q, Zhang C, Bonifas JM, Lam C-W, Hynes M, Goddard A, Rosenthal A, Epstein Jr EH and de Sauvage FJ. (1998). *Nature*, **391**, 90–92.

Yeh S. (1973). *Hum. Pathol.*, **4**, 469–485.

Zeigler A, Leffell DJ, Kunala S, Sharma HW, Gailani M, Halperin AJ, Baden HP, Shapiro PE, Bale AE and Brash DE. (1993). *Proc. Natl. Acad. Sci. USA*, **90**, 4216–4220.

30% sucrose/PBS, and 15-μm sections hybridized at 52 °C in 50% formamide containing 0.3 M NaCl, 20 mM Tris, pH 7.4, 5 mM EDTA, 10 mM NaH_2PO_4, 1× Denhardt's solution, 10% dextran sulphate, and 0.5 mg ml^{-1} yeast RNA to ^{35}S-labelled RNA probes transcribed from linearized plasmid templates and hydrolysed in alkali to ~300 nucleotide fragments[29]. After washes in 50% formamide and digestion with RNase A, the slides were autoradiographed.

Immunofluorescence. Primary hippocampal cultures were grown on poly-D-lysine-coated glass coverslips for two weeks, fixed in 4% paraformaldehyde/PBS for 20 min, rinsed in PBS, blocked in 0.02% saponin, 2% BSA, 1% fish skin gelatin/PBS (blocking buffer) for 1 h and incubated for 90 min with anti-rVGAT polyclonal rabbit and anti-synaptophysin monoclonal mouse antibodies diluted 1 : 100 in blocking buffer, all at room temperature. The cells were then washed, incubated in secondary anti-rabbit antibody conjugated to fluorescein and anti-mouse antibody conjugated to rhodamine (both Cappel) both diluted 1 : 100, washed, the coverslips mounted on class slides, and viewed under epifluorescence.

Membrane preparation. The rat *unc-47* homologue cDNA subcloned into the plasmid expression vector pcDNA3-Amp (Invitrogen) was introduced into PC12 cells by electroporation[30]. The cells were then selected in 800 μg ml^{-1} G418 (effective) and the resulting clones examined by immunofluorescence[18] using a rabbit polyclonal antibody (R.R., S.M. & R.H.E., manuscript in preparation). Using the two cell clones with the highest level of immunoreactivity, membranes were prepared by first resuspending the washed cells in 0.3 M sucrose, 10 mM HEPES-KOH, pH 7.4 (SH buffer) containing 0.2 mM diisopropylfluorophosphate (DFP), 1 μg ml^{-1} pepstatin, 2 μg ml^{-1} aprotinin, 2 μg ml^{-1} leupeptin, 1 μg ml^{-1} E64 and 1.25 mM MgEGTA. The cells were then disrupted by homogenization at 4 °C through a ball-bearing device at a clearance of 10 μm. The nuclear debris was sedimented at 1,000*g* for 5 min and heavier membranes were eliminated by centrifugation at 27,000*g* for 1 h. The remaining light membrane vesicles were sedimented at 65,000*g* for 1 h and resuspended in SH containing the same protease inhibitors at a final concentration of ~10 μg protein per μl.

Transport assay. To initiate the reaction, 10 μl of membranes was added to 200 μl SH buffer containing 4 mM $MgCl_2$, 4 mM KCl, 4 mM ATP, 40 μM unlabelled GABA and 2 μCi ^3H-GABA (NEN). Incubation was performed at 29 °C for varying intervals and the reaction was terminated by rapid filtration (Supor 200, Gelman), followed by immediate washing with 6 ml cold 0.15 M KCl. Background uptake was determined by incubation at 4 °C for 0 min. The bound radioactivity was measured by scintillation counting in 2.5 ml Cytoscint (ICN). To determine K_m, unlabelled GABA was added at a range of concentrations and uptake were measured at 30 s. Nigericin and valinomycin dissolved in ethanol added to final concentrations of 5 μM and 20 μM, respectively. Transport measurements were performed in duplicate and repeated three or more times using at least two different membrane preparations.

Received 18 July; accepted 29 September 1997.

1. Schuldiner, S., Shirvan, A. & Linial, M. Vesicular neurotransmitter transporters: from bacteria to humans. *Physiol. Rev.* 75, 369–392 (1995).
2. Liu, Y. & Edwards, R. H. The role of vesicular transport proteins in synaptic transmission and neural degeneration. *Annu. Rev. Neurosci.* 20, 125–156 (1997).
3. McIntire, S., Jorgensen, E. & Horvitz, H. R. Genes required for GABA function in *Caenorhabditis elegans*. *Nature* 364, 337–341 (1993).
4. Liu, Y. *et al.* A cDNA that supresses MPP+ toxicity encodes a vesicular amine transporter. *Cell* 70, 539–551 (1992).
5. Erickson, J. D., Eiden, L. E. & Hoffman, B. J. Expression cloning of a reserpine-sensitive vesicular monoamine transporter. *Proc. Natl Acad. Sci. USA* 89, 10993–10997 (1992).
6. Alfonso, A., Grundahl, K., Duerr, J. S., Han, H.-P. & Rand, J. B. The *Caenorhabditis elegans unc-17* gene: a putative vesicular acetylcholine transporter. *Science* 261, 617–619 (1993).
7. McIntire, S., Jorgensen, E., Kaplan, J. & Horvitz, H. R. The GABAergic nervous system of *Caenorhabditis elegans*. *Nature* 364, 334–337 (1993).
8. Wilson, R. *et al.* 2.2 Mb of contiguous nucleotide sequence from chromosome III of *C. elegans*. *Nature* 368, 32–38 (1994).
9. Brenner, S. The genetics of *Caenorhabditis elegans*. *Genetics* 77, 71–94 (1974).
10. Chalfie, M., Tu, Y., Euskirchen, G., Ward, W. W. & Prasher, D. C. Green fluorescent protein as a marker for gene expression. *Science* 263, 802–805 (1994).
11. Clark, S. G., Lu, X. & Horvitz, H. R. The *Caenorhabiditis elegans* locus *lin-15*, a negative regulator of a tyrosine kinase signaling pathway, encodes two different proteins. *Genetics* 137, 987–997 (1994).
12. Ferguson, E. L. & Horvitz, H. R. Identification and characterization of 22 genes that affect the vulval cell lineages of the nematode *Caenorhabidits elegans*. *Genetics* 110, 17–72 (1985).
13. Jorgensen, E. M. *et al.* Defective recycling of synaptic vesicles in synaptotagmin mutants of *Caenorhabditis elegans*. *Nature* 378, 196–199 (1995).
14. Nonet, M. L., Grundahl, K., Meyer, B. J. & Rand, J. B. Synaptic function is impaired but not eliminated in *C. elegans* mutants lacking synaptotagmin. *Cell* 73, 1291–1306 (1993).
15. Nonet, M. L. *et al.* Functional synapses are partially depleted of vesicles in *C. elegans rab-3* mutants. *J. Neurosci.* (in the press).
16. Hall, D. H. & Hedgecock, E. M. Kinesin-related gene *unc-104* is required for axonal transport of synaptic vesicles in *C. elegans*. *Cell* 65, 837–847 (1991).
17. Thomas-Reetz, A. *et al.* γ-aminobutyric acid transporter driven by a proton pump is present in synaptic-like microvesicles of pancreatic B cells. *Proc. Natl Acad. Sci. USA* 90, 5317–5321 (1993).
18. Liu, Y. *et al.* Preferential localization of a vesicular monoamine transporter to dense core vesicle in PC12 cells. *J. Cell Biol.* 127, 1419–1433 (1994).
19. Varoqui, H. & Erickson, J. D. Active transport of acetylcholine by the human vesicular acetylcholine transporter. *J. Biol. Chem.* 271, 27229–27232 (1996).
20. Fykse, E. M. & Fonnum, F. Uptake of γ-aminobutyric acid by a synaptic vesicle fraction isolated from rat brain. *J. Neurochem.* 50, 1237–1242 (1988).
21. Hell, J. W., Maycox, P. R., Stadler, H. & Jahn, R. Uptake of GABA by rat brain synaptic vesicles isolated by a new procedure. *EMBO J.* 7, 3023–3029 (1988).
22. Kish, P. E., Fischer-Bovenkerk, C. & Ueda, T. Active transport of γ-aminobutyric acid and glycine into synaptic vesicles. *Proc. Natl Acad. Sci. USA* 86, 3877–3881 (1989).
23. Burger, P. M. *et al.* GABA and glycine in synaptic vesicles: storage and transport characteristics. *Neuron* 7, 287–293 (1991).
24. Naito, S. & Ueda, T. Adenosine triphosphate-dependent uptake of glutamate into protein I-associated synaptic vesicles. *J. Biol. Chem.* 258, 696–699 (1983).
25. Maycox, P. R., Deckwerth, T., Hell, J. W. & John, R. Glutamate uptake by brain synaptic vesicles. Energy dependence of transport and functional reconstitution in proteoliposomes. *J. Biol. Chem.* 263, 15423–15428 (1988).
26. Carlson, M. D., Kish, P. E. & Ueda, T. Glutamate uptake into synaptic vesicles: competitive inhibition by bromocriptine. *J. Neurochem.* 53, 1889–1894 (1989).
27. Christensen, H., Fykse, E. M. & Fonnum, F. Inhibition of γ-aminobutyrate and glycine uptake into synaptic vesicles. *Eur. J. Pharmacol.* 207, 73–79 (1991).
28. Fischer, W. N., Kwart, M., Hummel, S. & Frommer, W. B. Substrate specificity and expression of profile of amino acid transporters (AAPs) in *Arabidopsis*. *J. Biol. Chem.* 270, 16315–16320 (1995).
29. Sassoon, D. & Rosenthal, N. in *Guide to Techniques in Mouse Development* (eds Wassarman, P. M. & DePamphilis, M. L.) 384–404 (Academic, San Diego, 1993).
30. Grote, E., Hao, J. C., Bennett, M. K. & Kelly, R. B. A targeting signal in VAMP regulating transport ot synaptic vesicles. *Cell* 81, 581–589 (1995).

Acknowledgements. We thank B. Westlund for unpublished *unc-47* map data; E. King for help with the confocal microscope; H. Rausch and K. Knobel for integrating the *unc-47*::GFP transcriptional fusion construct; Y. Jin for the *n2476* allele; D. P. Morse and B. Bamber for the gift of RNA and cDNA; R. Barstead and P. Okkema for the *C. elegans* cDNA libraries; J. Boulter and D. Julius for the mammalian cDNA libraries; D. Rice and D. Eisenberg for the analysis of hydrophobic moment; A. Tobin and S. Baekkeskov for the GAD-67 cDNA; Y. Liu and P. Tan for assistance in the isolation of PC12 cell clones and the preparation of membranes; J. Hell and P. Finn for suggestions about the measurement of transport activity; S. Craven and D. Bredt for assistance with the primary hippocampal cultures; and M. Horner, E. Kofoid, C. Bargmann and members of the Edwards and Jorgensen laboratories for discussions. This work was supported by the Gallo Center (S.L.M.), the Giannini Foundation (R.J.R.), an NIH Developmental Biology training grant (K.S.), the Klingenstein Foundation (E.M.J.), NINDS (S.L.M., R.H.E., E.M.J.) and NIMH (R.H.E.).

Correspondence and requests for materials should be addressed to R.H.E. (e-mail: edwards@itsa.ucsf.edu) or E.M.J. (e-mail: jorgensen@bioscience.biology.utah.edu).

Activation of the transcription factor Gli1 and the Sonic hedgehog signalling pathway in skin tumours

N. Dahmane*, J. Lee*, P. Robins†, P. Heller† & A. Ruiz i Altaba*

* *The Skirball Institute, Developmental Genetics Program and Department of Cell Biology, and † Department of Dermatology, New York University Medical Center, 540 First Avenue, New York, New York 10016, USA*

Sporadic basal cell carcinoma (BCC) is the most common type of malignant cancer in fair-skinned adults. Familial BCCs and a fraction of sporadic BCCs have lost the function of Patched (Ptc), a Sonic hedgehog (Shh) receptor[1–3] that acts negatively on this signalling pathway. Overexpression of Shh can induce BCCs in mice[4]. Here we show that ectopic expression of the zinc-finger transcription factor Gli1 in the embryonic frog epidermis results in the development of tumours that express endogenous *Gli1*. We also show that *Shh* and the *Gli* genes are normally expressed in hair follicles, and that human sporadic BCCs consistently express *Gli1* but not *Shh* or *Gli3*. Because Gli1, but not Gli3, acts as a target and mediator of Shh signalling[5], our results suggest that expression of Gli1 in basal cells induces BCC formation. Moreover, loss of Ptc or overexpression of Shh cannot be the sole causes of Gli1 induction and sporadic BCC formation, as they do not occur consistently. Thus any mutations leading to the expression of Gli1 in basal cells are predicted to induce BCC formation.

Gli1, which was originally isolated as an amplified gene in a glioma[6], is a member of a multigene family[7–9] and can transform fibroblasts in cooperation with adenovirus E1A[10]. Ectopic expression of Gli1 in frog embryos activates Shh target genes, including that encoding HNF-3β, both in neural and epidermal non-neural ectoderm[5,11], showing that epidermal cells can respond to Shh signalling. Frog embryos injected with plasmids driving the expression of frog *Gli1* developed abnormal growths, or tumours, in the otherwise normal, smooth tadpole epidermis (78%, $n = 25$; Fig. 1a). The tumours were independent of HNF-3β expression, as only a fraction contained cells expressing HNF-3β (30%, $n = 27$). Because the plasmid DNA was targeted to the animal-most region of the two-cell embryo, only ectodermal derivatives inherit plasmids, indicating that the growths of focal epidermal hyperplasia (the tumours) observed are caused by expression of Gli1 in the epidermis. Indeed, detection of epitope-tagged Gli1 in injected embryos showed exclusive expression in the ectoderm[5] (not shown). Histological sections of 1-week-old (stage ~45) injected tadpoles revealed tumours in the epidermis, sometimes consisting of densely packed cells (Fig. 1f). These cells were clearly distinct from all normal tissues (Fig. 1e) and did not express the cement-gland marker *XAG-1* (ref. 12) ($n = 10$; not shown). Taken together, these results show that transient epidermal expression of Gli1 leads to tumour formation *in vivo*.

To determine whether tumours formed from cells inheriting injected *Gli1*, embryos were co-injected with frog *Gli1* RNA and *lacZ* RNA as tracer. Injected tadpoles showed prominent tumours of the skin (80%, $n = 12$) formed from the superposition of epidermal cells that inherited *Gli1*, as these invariably expressed β-galactosidase (Fig. 1b–d). Labelled epidermal cells located inside the tumours were distinct from the underlying lateral-plate mesoderm, which was always unlabelled. The uninjected side displayed typical smooth embryonic epidermis (Fig. 1c, right) and injection of *lacZ* alone had no effect. Because not all epidermal cells inheriting *Gli1* RNA become tumorigenic, there could be a requirement for a certain level of Gli1 to initiate tumour formation. The effects of Gli1 are specific, as injection of plasmids driving the expression of human *Gli3* (ref. 7) had no effect[5] ($n = 45$; not shown). Inappropriate expression of Gli1 therefore leads to tumour formation, although it is not clear if this represents epidermal neoplastic transformation.

The finding of mutated *Ptc* alleles in familial and some sporadic BCCs[1–3] together with the development of skin tumours in tadpoles overexpressing Gli1 raised the possibility that Gli1 could be expressed in and underlie the development of sporadic adult basal cell cancer. Sections of freshly excised human BCCs were analysed by *in situ* hybridization. All but one of the samples examined showed unambiguous expression of *Gli1*, although the level of expression varied (46 of 47; Table 1, Fig. 2). The variability observed in *Gli1* RNA expression could be due to inherent differences in the tumours or to differences in the preservation of the excised material. No correlation was detected between the level of *Gli1* expression and the site or the aggressiveness of the tumour. In contrast to the consistent expression of *Gli1*, only 76% (23 of 30; Table 1) of the cases displayed unequivocal expression of *Gli3* (Fig. 2k), which is often coexpressed with *Gli1* (refs 5, 9, 13, 14). Analysis of ten cases of squamous cell carcinoma (SCC) *in situ* showed *Gli* gene expression to be absent (Table 1, Fig. 2s, t). Control hybridizations with sense RNA probes showed no signal (Table 1, Fig. 2l).

Tumour nodules infiltrating the dermis showed the highest levels of *Gli1* expression (Fig. 2a–f, i, j, n), and here it was often concentrated in the periphery (Fig. 2f, j), where most proliferating cells appear to be located[15]. In tumorigenic regions, the basal layer of the epidermis also displayed high levels of *Gli1* expression (Fig. 2c–e). The pattern of expression of *Gli3* was distinct from that of *Gli1* but was also detected primarily in the periphery of tumour nodules (Fig. 2k). *Gli* gene expression was not detected in the interfollicular epidermis or the dermis in normal regions distal from the tumour (Fig. 2q, r), although *Gli1* mRNA was detected in histologically normal basal cells immediately surrounding the tumour site (Fig. 2a, b, right). Cells of the sebaceous glands, dermis and blood vessels were negative. Single cells surrounding the main BCC tumour masses were rarely positive for *Gli1* (3 of 47) or *Gli3* expression (1 of 30; Fig. 2j, k), and could represent early invading tumour cells that are histologically unrecognizable. Alternatively, these single cells may be non-BCC cells that express *Gli1* in response to a secreted tumour-derived factor.

Expression of Gli1 was also analysed by immunocytochemistry with an affinity-purified anti-human Gli1 polyclonal antibody[5]. All samples showed specific Gli1 expression (6 of 6; Table 1; Fig. 2u–w). Control antibody labelling with an anti-HNF-3β polyclonal antibody[11,16] showed no specific labelling (Table 1 and data not shown). In BCCs, Gli1 protein was detected in the cytoplasm (Fig. 2u, w), consistent with the prevalent cytoplasmic localization of frog Gli1 (ref. 5). This is also consistent with an association of Gli proteins with the cytoskeleton[17], but contrasts with the nuclear localization of Gli1 in COS cells transfected with the glioma-derived cDNA[5] (Fig. 2x) and in a glioma line showing a 75-fold over-expression of *Gli1* (D259MG[6,18]). The glioma cDNA[6] thus appears to encode a mutated protein that escapes cytoplasmic retention.

The possibility that Gli1 could activate components of the Shh signal-transduction pathway in sporadic BCCs, including endogenous human *Shh* itself[19,20], was suggested by the regulatory loop

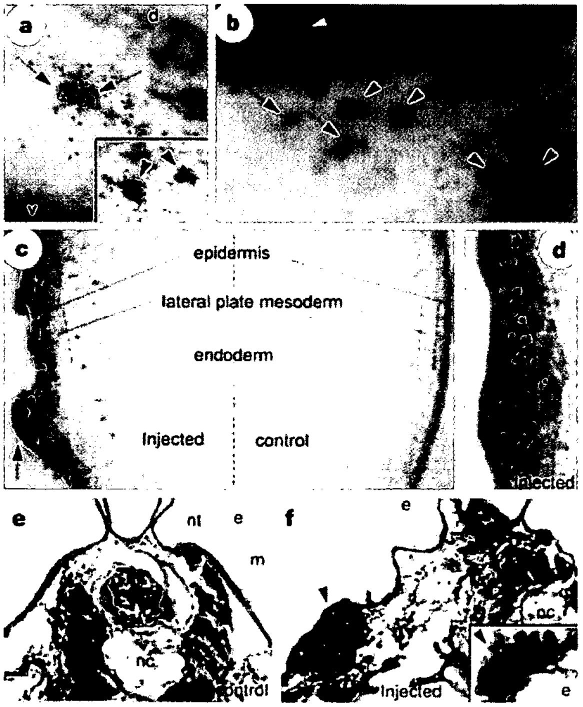

Figure 1 Ectopic expression of Gli1 in frog embryos leads to the formation of epidermal tumours. **a**, **b**, Whole-mount view of the flank of injected tadpoles (stages ~32-34) showing epidermal tumours (arrows) and cells expressing HNF-3β (brown). The embryo in **b** was co-injected with *Gli* synthetic RNA and *lacZ* RNA as tracer. β-Gal activity is shown in blue; d, dorsal; v, ventral. **c**, **d**, Histological cross-sections through the trunk of embryos unilaterally injected with Gli1. The affected side is blue (arrow, left in **c**). **d**, Detail of a tumour similar to that shown in **c** in which β-gal activity is detected as small cytoplasmic inclusions. The boundaries between the epidermis and the underlying lateral plate mesoderm and between this and the endoderm are denoted by broken lines. **e**, **f**, Histological sections stained with haematoxylin and eosin through the trunk of control (**e**) and Gli1-injected (**f**) stage ~45 tadpoles. An epidermal tumour is detected in the flank (arrow in **f**). The inset in **f** shows an outwardly growing epidermal tumour (arrow); e, epidermis; m, muscle; nc, notochord; nt, neural tube. Dorsal side is up in all cases. In **a** and **b**, anterior is to the left.

Nature © Macmillan Publishers Ltd 1997

defined in the Shh signalling pathway in which Shh signalling triggers a cascade of events leading to the activation of *Gli1*, which in turn may activate the transcription of Shh target genes including *Shh* and *Ptc*. By *in situ* hybridization, 44% (15 of 34) of BCCs were positive for *Shh*, with expression localized to the tumour masses that also expressed *Gli1* (Fig. 2o, Table 1). Analysis of nine SCCs *in situ* showed no *Shh* expression (Table 1). Sense *Shh* RNA probes showed no specific signal (Table 1). Reverse transcription–polymerase chain reaction (RT–PCR) analyses revealed *Shh* expression in two cases of BCC, whereas this was below the level of detection in three BCCs and one SCC *in situ*. All these samples showed low levels of *Gli3* expression, and all five BCCs, but not the SCC, showed elevated levels of *Gli1* and *Ptc* mRNAs. Expression of the ribosomal gene *S17* was monitored as a control (not shown). The lower frequency of *Shh* (17 or 37 cases overall) compared with *Gli1* expression (49 of 50 cases overall) in BCCs, together with the inability of injected Shh to initiate epidermal tumour formation in frog embryos[11], suggests that Shh is unlikely to be the only cause of *Gli1* expression in BCCs, and that *Shh* may not be regulated solely by Gli1. In contrast, Ptc was expressed in all BCCs examined[3] (16 of 16; Fig. 2p, Table 1 and not shown), and was coincident with *Gli1* and *Shh* (Fig. 2m–o), consistent with *Ptc* being a target of Gli1.

Tadpole tumours induced by Gli1 could be the equivalent of human BCCs. However, morphological analyses, the main criteria of dermatopathologists, cannot be applied to the tadpole tumours as early tadpoles do not have dermis. Our molecular analysis of BCCs provides an alternative test for the BCC-like nature of tadpole tumours, as endogenous *Gli1* is expressed consistently in the human tumours (Table 1, Fig. 2). Injection of human Gli1, which we have previously shown has a similar activity to frog Gli1 (ref. 5), resulted in the formation of epidermal tumours (79%, $n = 24$), and all tumours displayed expression of the endogenous frog *Gli1* gene (Fig. 3a–c). Endogenous *Gli1* expression was not detected in non-tumorigenic regions of the epidermis in injected embryos or control siblings (Fig. 3a). In contrast, only a small fraction (12–23%) of embryos injected with *Gli1* mRNA or pDNA showed ectopic *Shh* expression, mostly in the non-tumorigenic epidermis of injected tadpoles (3 of 25 for RNA, Fig. 3e; and 7 of 30 for pDNA) and early neurulae[11], not observed in controls (Fig. 3d). The low incidence of *Shh* expression and the consistent expression of *Gli1* in tadpole epidermal tumours parallels that found in BCCs and points to their having a BCC-like nature.

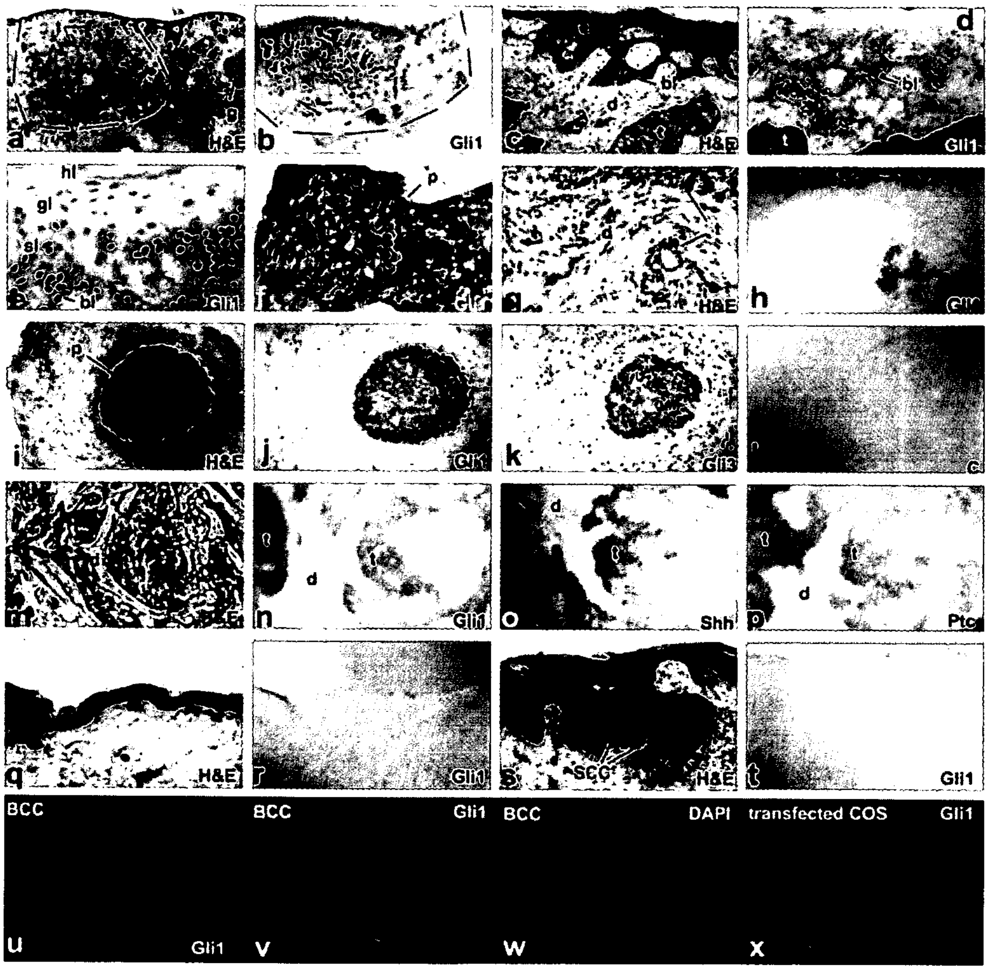

Figure 2 Gene expression in basal cell carcinomas and cell lines. **a**-**p**, Sections of BCC excisions showing the distribution of tumour masses as seen by histological staining (**a**, **c**, **g**, **i**, **m**), *Gli1* mRNA (**b**,**d**,**e**,**f**,**h**,**j**,**n**), *Gli3* mRNA (**k**), *Shh* mRNA (**o**) or *Ptc* mRNA (**p**). As a control, absence of label is seen after hybridization with a *Gli1* sense probe (**l**). Matched samples from the same specimens are shown in **a** and **b**, **c** and **d**, **g** and **h**, **i** to **l**, and **m** to **p**. **e**, **f**, Details of the specimen shown in **a**-**d**, respectively. **q**, **r**, Sections of normal skin distal from tumorigenic regions in a BCC excision showing the absence of *Gli1* expression. **s**, **t**, Sections of an excised sample of squamous cell carcinoma (SCC) *in situ* showing the absence of *Gli1* expression. **u**-**x**, Labelling of excised BCC sections with affinity-purified anti-human Gli1 antibodies (**u**, **v**, **x**) or with the DNA-binding dye DAPI showing the position of nuclei (blue in **w**). **x**, Expression of nuclear Gli1 protein in COS-7 cells transfected with plasmids driving the expression of the human glioma *Gli1* cDNA. H&E, haematoxylin and eosin stain; bl, basal layer; d, dermis; e, epidermis; gl, granular layer; hl, horny layer; p, pallisade in the periphery of the tumour nodule; sl, spiny layer; t, tumour. In all cases the skin surface is up except in **i**-**l** in which it is to the left. **a**-**f**, case no. 5; **g**, **h**, case no. 7; **i**-**l**, case no. 12; **m**-**p**, case no. 61; **q**, **r**, a normal skin region of case no. 18; **s**, **t**, case no. 15; all as listed in Table 1.

Table 1 Gene expression in human skin tumours

Case	type	location	Gli1 ab	HNF-3β Ab	Gli1-as	Gil1-s	Gli3-as	Gli3-s	Shh-as	Shh-s	Ptc-as	H&E
1	BCC	auricular	+									+
2	BCC	nasolabial fold	+	–								+
3	BCC	temple	+	–								+
4	BCC	forehead	+									+
5	BCC	post-auricular			++							+
6	BCC	inner canthus	+	–	++							+
7	BCC	post-auricular	+	–	++	–						+
8	BCC	nasolabial fold			++							+
9	BCC	post-auricular			++							+
10	BCC	canthus			+/–	–	+/–					+
11	BCC	canthus			+	–	+					+
12	BCC	back			++	–	++	–				+
13	BCC	nasal rim			++	–		–				+
14	BCC	nasal rim			++	–	–	–				+
17	BCC	nasal rim			+/–	–	–	–				+
18	BCC	nasal rim			++	–	–	–				+
24	BCC	nose			+		–		+			+
26	BCC	periareolar			++		+		++	–		+
27	BCC	eyelid			+		–		–	–		+
28	BCC	nose			+		+/–	–	–			+
29	BCC	temple			+		+		+	–		+
30	BCC	midback			++		+		+	–		+
32	BCC	lat. forehead			+		–		–			+
33	BCC	eyebrow			+		+		+			+
34	BCC	nosetip			+		+		–			+
37	BCC	lat. upper cheek			+/–		+/–		+/–			+
39	BCC	upper lip			+		+		+/–			+
41	BCC	malar ocular			++		++		+/–			+
42	BCC	malar ocular			++		+		–			+
43	BCC	temple			++		+		–			+
44	BCC	nose			+		+		–			+
45	BCC	cheek			++		+		+			+
46	BCC	nostril			++		++		–			+
47	BCC	zygoma			++		+		–			+
48	BCC	upper eyelid			+		++		+			+
51	BCC	glabella			++		+		+			+
52	BCC	nose			+		++		–			+
53	BCC	nose			+		+/–		–			+
54	BCC	ear			++		+/–		+/–			+
57	BCC	clavicle			+		–		–			+
59	BCC	nose			++				+	–	++	+
61	BCC	nose			++				++	–	+	+
63	BCC	nose			+						++	+
64	BCC	forehead			+/–				–	–	++	+
66	BCC	temple			+				–	–	+	+
67	BCC	forehead			+				+	–	++	+
69	BCC	forehead			++				–	–	++	+
70	BCC	scalp			++				–	–	++	+
71	BCC	eye			+				–	–	+	+
72	BCC	nose			++				–	–	++	+
74	BCC	temple			+				–	–	+	+
15	SCC	upper back			–	–	–	–				+
23	SCC	preauricular			–		–		–	–		+
25	SCC	eyelid			–		–		–	–		+
31	SCC	elbow			–		–		–			+
35	SCC	cheek			–		–		–			+
40	SCC	cheek			–		–		–			+
49	SCC	cheek			–		–		–	–		+
55	SCC	hand			–		+/–		–	–		+
56	SCC	neck			–		–		–	–		+
58	SCC	bridge nose			–		–		–	–		+

The case number, type of tumour (BCC or SCC *in situ*) and location of the tumour is given on the left. The presence (+) or absence (–) of gene expression is indicated, with strong expression indicated by ++. A section of each excision was also stained with haematoxylin and eosin (H&E) for histological examination and confirmation of the presence of tumour. Case no. 10 was ambiguous and was counted as negative for *Gli1* expression. Abbreviations: as, antisense RNA probe; s, sense RNA probe; Ab, antibody; lat., lateral.

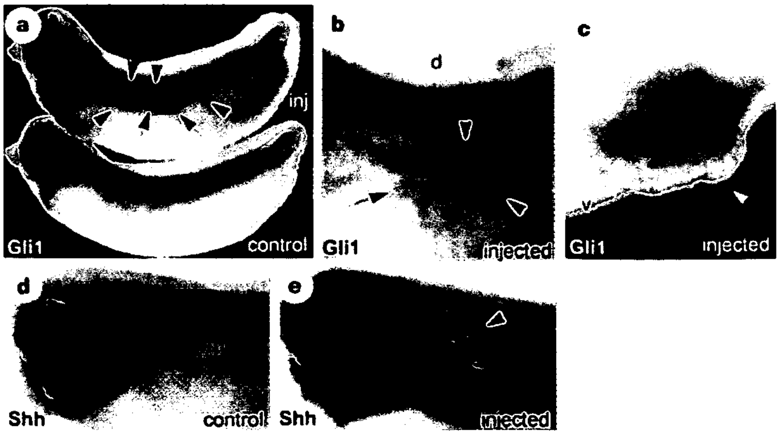

Figure 3 Expression of endogenous *Gli1* and *Shh* in Gli1-induced tadpole tumours. Frog tadpoles (stages 34–36) injected with human *Gli1* plasmids (**a**–**c**) or synthetic frog *Gli1* RNA (**e**), but not control embryos (**a** bottom **d**), show ectopic expression of endogenous *Gli1* (arrows in **a** top, **b**, **c**) or *Shh* (arrow in **e**). Human and frog *Gli1* do not cross-hybridize *in situ* hybridization. Gli1 is normally expressed in several tissues including the neural tube but not the early epidermis[11]. *Shh* is normally expressed in the nervous system and head structures including the branchial arches[6]. Anterior is to the left and dorsal side is up. Embryos were not cleared.

Nature © Macmillan Publishers Ltd 1997

Interfollicular human basal cells and the early tadpole epidermis do not normally express *Gli1* genes, and the reason why the epidermis is responsive to Shh and Gli1 is not clear. However, we detected expression of *Gli1* and *Shh* in human hair follicles, and *Shh*, *Gli1*, *Gli2* and *Gli3* were also expressed in mouse hair follicles[14,21,22] during the growing phases with highest expression of *Shh* and *Gli1* in matrix keratinocytes of the bulb (not shown). This indicates that normal epidermal development involves the selective activation of the Shh signalling pathway during follicular formation and provides a context for the ability of embryonic and non-follicular-basal epidermal cells to respond to overexpression of Gli1.

Gli1 has been found to be amplified only in a small number of gliomas and other tumours[6,24,25]. The high incidence of *Gli1* expression in BCCs contrasts with the relatively infrequent occurrence of other oncogenes, such as mutated *ras* alleles[23]. Because hair follicles normally activate the Shh signalling pathway during growth, BCCs could derive from the neoplastic transformation of these cells. Indeed, BCCs show traits of follicular differentiation[26], including the expression of *Gli3*. It is possible, however, that BCCs derive from non-follicular basal cells which express Gli1 ectopically. In this case, the normal interaction taking place between the dermal papilla and the hair bulb could be activated inappropriately in non-follicular basal cells, resulting in the activation of the Shh signalling pathway and formation of BCCs. We propose that any mutations that activate the Shh signalling pathway will lead to ectopic Gli1 expression and BCC formation. In familial BCCs showing loss of Ptc function[1,2], we predict that Gli1 will be ectopically expressed. However, mutations in Ptc cannot account entirely for Gli1 activation. We found that *Gli1* and *Ptc* are consistently expressed in sporadic BCCs, whereas in other studies only a fraction of sporadic BCCs showed an altered *Ptc* allele[2,3]. Because there may be a regulatory loop in the Shh signalling pathway, Gli1 expression would appear to be both a cause and an effect of BCC development.

Ectopic expression of Shh in basal cells of transgenic mice has recently been shown to result in the development of BCC-like tumours[4]. However, the inability of Shh to induce tumour formation in the tadpole epidermis and its inconsistent expression in BCCs and tadpole tumours raise the possibility that normally there may be restrictions to the induction and action of Shh in epidermis similar to those present in the neural plate[11]. Such restrictions could prevent BCC formation adjacent to follicle cells expressing Shh during normal hair growth and after plucking, and the uncontrolled spread of BCCs throughout the surrounding tissue when the tumours induce Shh. Independent of whether Shh can initiate BCC formation, its expression in BCCs suggests a mode of autocrine tumour maintenance as secreted Shh from the tumour cells could activate its signalling pathway, leading to new expression of *Gli1*. Activation of autocrine Shh signalling could underlie the formation of persistent epidermal tumours in embryos that transiently expressed Gli1 through microinjection. However, transcription of endogenous *Gli1* but not *Shh* was always detected in Gli1-induced tumours and BCCs, suggesting that a Gli1 regulatory loop operating downstream of Shh is functional.

The recurrence of BCCs at sites adjacent to previous tumours could result from the observed ectopic expression of Gli1 in basal cells in a wide region extending beyond the neoplastic sites. This raises the possibility that Gli1 expression in basal cells is an early event and could be used as a diagnostic tool. Finally, therapeutic agents for BCCs are likely to include inhibitors of the Shh signalling pathway and Gli1 function. ☐

Methods

Embryos and microinjection. *Xenopus laevis* embryos were obtained and manipulated by standard procedures[27]. Microinjections were performed into the animal-most region of one cell at the two-cell stage to bias the distribution of the injected plasmids or RNAs to the ectoderm and to have half of the embryo as an undisturbed internal control. Plasmid DNA (200 pg) or synthetic RNAs (2 ng) made by *in vitro* transcription were delivered by microinjection. Frog *Gli1*, human *Gli1* and *Gli3* plasmids were as described[5].

***In situ* hybridization, immunocytochemistry, histology and cell lines.** Frog embryos were processed for *in situ* hybridization with digoxigenin-labelled RNA probes[28]. Frog *Gli1* and *Shh* plasmids to make sense or antisense RNA probes were as described[5]. Frozen cryostat sections of tumour specimens excised by the Mohs technique (by P.R.) were processed by *in situ* hybridization with digoxigenin-labelled RNA probes[29]. Plasmids with human *Gli1* and *Gli3* cDNAs[6,7] and mouse *Shh* and *Gli1–3* cDNAs used to make sense and anti-sense RNA probes were as described[5]. The human *Shh* probes were made from a plasmid subclone of a 409-base pair RT–PCR product or from a human cDNA[19]. Immunocytochemistry with anti-human Gli1 affinity-purified polyclonal antibodies[5], anti-frog HNF-3β or anti-rat HNF-3β polyclonal antibodies[11,16] were performed in whole-mount labelling or in 5–15 μm cryostat sections. Nuclei were visualized by staining with the DNA-binding dye DAPI after antibody incubations. Histological sections of injected tadpoles were obtained by cutting paraplast-embedded samples in a microtome[5]. These sections and one section of each tumour sample were also stained with haematoxylin and eosin for histological and pathological examination (by P.H.). β-Galactosidase activity was revealed by the X-gal reaction. COS-7 cells were obtained from ATCC and cultured under the specified conditions. Transfections were performed with lipofectamine (Gibco-BRL) as specified by the manufacturer. Cells were assayed 24–48 h after transfection.

RNA isolation and RT-PCR. RNA from frozen excisions was extracted by the guanidinium isothiocyanate, acid phenol method. cDNA was made with random hexamers and BRL Superscript reverse transcriptase. PCR was performed at 57 °C for 40 cycles with the following primers to human *Gli1*: Gli1-U, CAGAGAATGGAGCATCCTCC; and Gli1-D, TTCTGGCTCTTCCTGTAGCC, yielding a 412-bp product. Human *Gli3*: Gli3-U, GCAGCCACAGAATGTCC; and Gli3-D, AGGGATATCCAATCGAGGAATCG, yielding a 293-bp product. Human *Shh*: Shh-U2, GAAGATCTCCAGAAACTCC; and Shh-D, TCGTAGTGCAGAGACTCC, yielding a 233-bp product. Mouse *S17*, which works well with human cDNA: S17-U, GCTATGTCACGCATCTGATG; and S17-D, CCTCAATGATCTCCTGATC, yielding a 137-bp product. Human *Ptc*: Ptc-U, GAATCCAGGCATCACCCACC; and Ptc-D, CCACGTCCTGCAGCTCAATG, yielding a 490-bp product. The RT–PCR *shh* clone used to make RNA probes derived from a reaction using Shh-U1, AGATGTCTGCTGCTAGTCC, and Shh-D. *Shh* RNA probes were also made from a large human cDNA[19].

Received 26 June; accepted 5 August 1997.

1. Hahn, H. *et al.* Mutations of the human homolog of *Drosophila patched* in the nevoid basal cell carcinoma syndrome. *Cell* **85**, 841–851 (1996).
2. Johnson, R. L. *et al.* Human homolog of patched, a candidate gene for the basal cell nevus syndrome. *Science* **272**, 1668–1671 (1996).
3. Gailani, M. R. *et al.* The role of the human homologue of the *Drosophila* patched in sporadic basal cell carcinomas. *Nature Genet.* **14**, 78–81 (1996).
4. Oro, A. E. *et al.* Basal cell carcinomas in mice overexpressing Sonic hedgehog. *Science* **276**, 817–821 (1997).
5. Lee, J., Platt, K. A., Censullo, P. & Ruiz i Altaba, A. *Gli1* is a target of Sonic hedgehog that induces ventral neural tube development. *Development* **124**, 2537–2552 (1997).
6. Kinzler, K. W. *et al.* Identification of an amplified, highly expressed gene in a human glioma. *Science* **236**, 70–73 (1987).
7. Ruppert, J. M., Vogelstein, B., Arheden, K. & Kinzler, K. W. GLI3 encodes a 190 kilodalton protein with multiple regions of GLI similarity. *Mol. Cell. Biol.* **10**, 5048–5415 (1990).
8. Walterhouse, D. *et al.* Gli, a zinc finger transcription factor and oncogene, is expressed during normal mouse development. *Dev. Dyn.* **196**, 91–102 (1993).
9. Hui, C.-C., Slusarski, D., Platt, K. A., Holmgren, R. & Joyner, A. L. Expression of three mouse homologs of the *Drosophila* segment polarity gene cubitus interruptus, Gli, Gli2 and Gli3 in ectoderm and mesoderm-derived tissues suggests multiple roles during postimplantation development. *Dev. Biol.* **162**, 402–413 (1994).
10. Ruppert, J. M., Vogelstein, B. & Kinzler, K. W. The zinc finger protein GLI transforms primary cells in cooperation with adenovirus E1A. *Mol. Cell. Biol.* **11**, 1724–1728 (1991).
11. Ruiz i Altaba, A., Jessell, T. M. & Roelink, H. Restrictions to floor plate induction by *hedgehog* and winged helix genes in the neural tube of frog embryos. *Mol. Cell. Neurosci.* **6**, 106–121 (1995).
12. Sive, H. L., Hattori, K. & Weintraub, H. Progressive determination during formation of the anteroposterior axis in *Xenopus laevis*. *Cell* **58**, 171–180 (1989).
13. Marigo, V., Johnson, R. L., Vortkamp, A. & Tabin, C. J. Sonic hedgehog differentially regulates expression of Gli and Gli3 during limb development. *Dev. Biol.* **180**, 273–283 (1996).
14. Platt, K. A., Michaud, J. & Joyner, A. L. Expression of the mouse Gli and Ptc genes is adjacent to embryonic sources of hedgehog signals suggesting a conservation of pathways between flies and mice. *Mech. Dev.* **62**, 121–135 (1997).
15. Grimwood, R. E., Ferris, C. F., Mercill, D. B. & Hugg, J. C. Proliferating cells of human basal cell carcinoma are located on the periphery of tumor nodules. *J. Invest. Dermatol.* **86**, 191–194 (1986).
16. Ruiz i Altaba, A., Placzek, M., Baldassare, M., Dodd, J. & Jessell, T. M. Early stages of notochord and floor plate development in the chick embryo defined by normal and induced expression of HNF-3β. *Dev. Biol.* **1270**, 299–313 (1995).
17. Ruiz i Altaba, A. Catching a Gli-mpse of hedgehog. *Cell* **90**, 193–196 (1997).

Nature © Macmillan Publishers Ltd 1997

18. Kinzler, K. W. & Vogelstein, B. The *GLI* gene encodes a nuclear protein which binds specific sequences in the human genome. *Mol. Cell. Biol.* 10, 634–642 (1990).
19. Belloni, E. *et al.* Identification of Sonic hedgehog as a candidate gene responsible for holoprosencephaly. *Nature Genet.* 14, 353–356 (1996).
20. Roessler, E. *et al.* Mutations in the human Sonic hedgehog gene cause holoprosencephaly. *Nature Genet.* 14, 357–360 (1996).
21. Iseki, S. *et al.* Sonic hedgehog is expressed in epithelial cells during development of whisker, hair, and tooth. *Biochem. Biophys. Res. Commun.* 218, 688–693 (1996).
22. Bitgood, M. J. & McMahon, A. P. Hedgehog and Bmp genes are coexpressed at many diverse sites of cell-cell interaction in the mouse embryo. *Dev. Biol.* 172, 126–138 (1996).
23. van der Schroeff, J. G., Evers, L. M., Boot, A. J. M. & Box, J. L. Ras oncogene mutations in basal cell carcinomas and squamous cell carcinomas of human skin. *J. Invest. Dermatol.* 94, 423–425 (1990).
24. Roberts, W. M., Douglass, E. C., Peiper, S. C., Houghton, P. J. & Look, A. T. Amplification of the *gli* gene in childhood sarcomas. *Cancer Res.* 49, 5407–5413 (1989).
25. Xiao, H., Goldthwait, D. A. & Mapstone, T. A search for Gli expression in tumors of the central nervous system. *Pediatr. Neurosurg.* 20, 178–182 (1994).
26. Ackerman, A. B., DeViragh, P. A. & Chongchitnant, N. *Neoplasms with Follicular Differentiation* (Lea and Febinger, Philadelphia, 1993).
27. Ruiz i Altaba, A. in *Essential Developmental Biology—A Practical Approach* (eds Stern, C. & Holland, P. W. H.) (IRL, Oxford, 1993).
28. Harland, R. M. In situ hybridization: an improved whole mount method for *Xenopus* embryos. *Methods Enzymol.* 36, 675–685 (1991).
29. Scharen-Wiemers, N. & Gerlin-Moser, A. A single protocol to detect transcripts of various types and expression levels in neural tissue and cultures cells: in situ hybridization using digoxygenin-labeled cRNA probes. *Histochemistry* 100, 431–440 (1993).

Acknowledgements. We thank E. Ziff, G. Fishell, R. Brewster and C. Loomis for comments on the manuscript; K. Schulman for advice on selected tumour samples; L. Bernardo for cryostat sectioning; P. Censullo for help with tissue culture; E. Belloni and L. C. Tsui for a human *Shh* cDNA; E. Cordero for secretarial assistance; and J. Weider for help and advice with imaging. P.H. was a recipient of an Anne and Irving Holtzman fellowship in dermatopathology. This work was supported by a start-up grant from the Skirball Institute, a Basil O'Connor Award from the March of Dimes, and a fellowship from The Pew Scholars program in the biomedical sciences to A.R.A.

Correspondence and requests for materials should be addressed to A.R.A. (e-mail: ria@saturn.med.nyu.edu).

A SNARE involved in protein transport through the Golgi apparatus

Stephen Loucian Lowe, Frank Peter,
V. Nathan Subramaniam, Siew Heng Wong & Wanjin Hong

Membrane Biology Laboratory, Institute of Molecular and Cell Biology,
15 Lower Kent Ridge Road, Singapore 119076, Singapore

In eukaryotic cells, the Golgi apparatus receives newly synthesized proteins from the endoplasmic reticulum (ER) and delivers them after covalent modification to their destination in the cell. These proteins move from the inside (*cis*) face to the plasma-membrane side (*trans*) of the Golgi, through a stack of cisternae, towards the *trans*-Golgi network (TGN), but very little is known about how proteins are moved through the Golgi compartments. In a model known as the maturation model[1-3], no special transport process was considered necessary, with protein movement along the Golgi being achieved by maturation of the cisternae. Alternatively, proteins could be transported by vesicles[4-6] or membrane tubules[7,8]. Although little is known about membrane-tubule-mediated transport[7,8], the molecular mechanism for vesicle-mediated transport is quite well understood, occurring through docking of SNAREs on the vesicle with those on the target membrane[4-6,9-13]. We have now identified a protein of relative molecular mass 27K which is associated with the Golgi apparatus. The cytoplasmic domain of this protein or antibodies raised against it quantitatively inhibit transport *in vitro* from the ER to the *trans*-Golgi/TGN, acting at a stage between the *cis*/medial- and the *trans*-Golgi/TGN. This protein, which behaves like a SNARE and has been named GS27 (for Golgi SNARE of 27K), is identical to membrin, a protein implicated earlier in ER-to-Golgi transport[14]. Our results suggest that protein movement from medial- to the *trans*-Golgi/TGN depends on SNARE-mediated vesicular transport.

Database searches using a *Caenorhabditis elegans* protein sequence (accession number P41941) that is weakly related to that of the yeast protein Bos1p, a v-SNARE involved in ER–Golgi transport[15-17], led to the identification of expressed-sequence tags (ESTs) encoding the potential human (accession number T88746) and mouse (accession numbers AA165867, W75416 and W30385) counterparts. Rat complementary DNAs were isolated by screening

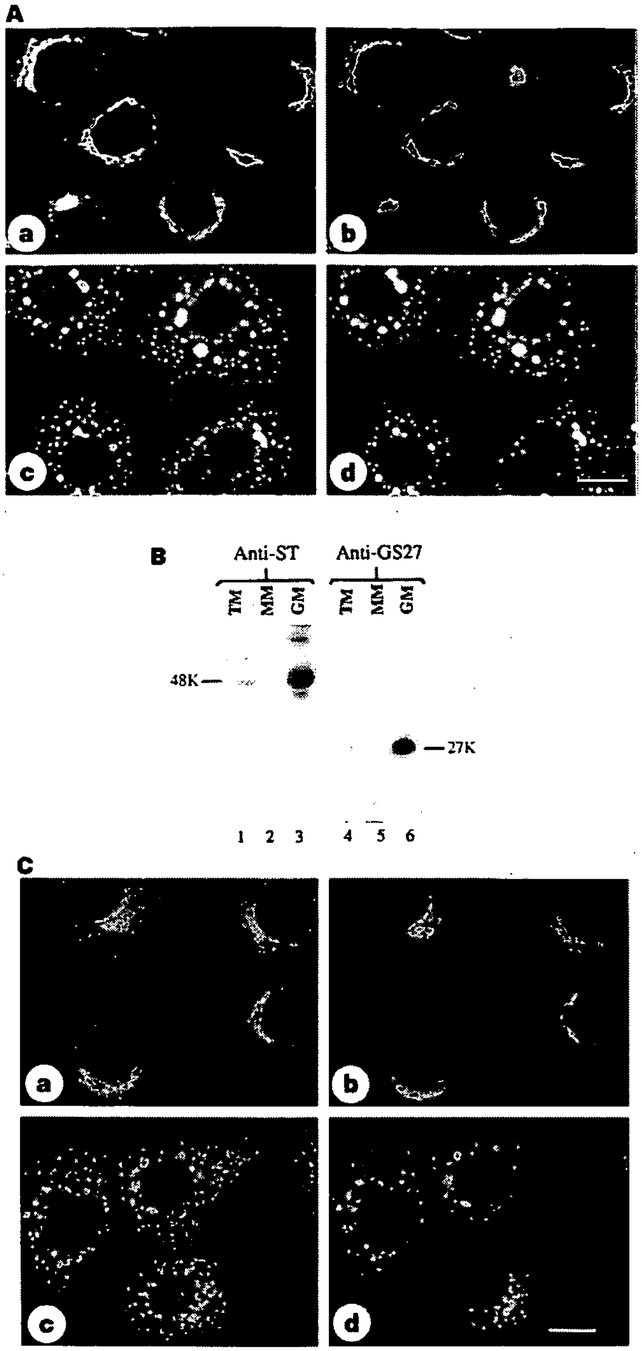

Figure 1 **A**, HA-epitope-tagged GS27/membrin is associated with the Golgi apparatus and vesicular structures. HA-GS27 (**a** and **c**) and Golgi mannosidase II (**b** and **d**) were double-labelled in control (**a**, **b**) and nocodazole-treated (**c**, **d**) cells. HA-GS27 was co-localized with mannosidase II in the control and in fragmented Golgi. The vesicular structures marked by GS27/membrin were devoid of mannosidase II labelling. **B**, Enrichment of GS27/membrin in the Golgi membrane. Proteins of total membranes (TM), microsomal membranes (MM) and Golgi-enriched membranes (GM) were analysed by immunoblot analysis using antibodies against α2, 6-sialyltransferase (ST) (lanes 1-3) or antibodies against GS27/membrin (lanes 4-6). **C**, Endogenous GS27/membrin is associated with the Golgi apparatus and its vesicular structures. Control (**a**, **b**) or nocodazole-treated (**c**, **d**) cells were double-labelled with antibodies against GS27/membrin (**a** and **c**) or Golgi mannosidase II (**b** and **d**).

Nature © Macmillan Publishers Ltd 1997

Basal cell carcinomas in mice overexpressing *Gli2* in skin

© 2000 Nature America Inc. • http://genetics.nature.com

Approximately 1,000,000 epithelial skin cancers are diagnosed in the United States each year and most are basal cell carcinomas (BCCs). The pathogenesis of these tumours involves constitutive activation of the Sonic hedgehog (Shh) signalling pathway (for review, see ref. 1). In many BCCs this can be attributed to loss-of-function mutations of *PTCH* (refs 2,3), which encodes a SHH receptor and antagonist. The specific downstream effector in the Shh pathway leading to cancer development is unknown. Here we show that transgenic mice overexpressing the transcription factor Gli2 in cutaneous keratinocytes develop multiple BCCs. These results establish Gli2 as a potent oncogene in skin and suggest a pivotal role for this transcription factor in the development of human BCC.

Given the central function of the transcription factor Cubitus interruptus in the *Drosophila melanogaster* Hedgehog pathway, the homologous vertebrate Gli proteins (Gli1, Gli2 and Gli3) are likely to mediate cellular responses to Shh signalling[4]. *Gli1* expression is tightly correlated with Shh pathway activity under normal and pathologic conditions, and ectopically expressed Gli1 can mimic responses to Shh in certain settings[5–7]. *Gli1*-mutant mice are, however, phenotypically normal[4], whereas *Gli2* mutants exhibit developmental defects in several organ systems[8,9] including skin, which contains hypoplastic hair follicles (R.M. *et al.*, unpublished data). Coupled with the fact that Gli3 is not transcriptionally active in cultured keratinocytes (data not shown), these findings led us to focus specifically on the potential role of Gli2 as an effector of uncontrolled Shh signalling in BCCs.

We overexpressed mouse *Gli2* in transgenic mice under the control of the bovine *K5* promoter, which is active in keratinocytes of the epidermal basal layer and outer root sheath of hair follicles[10]. By three months of age, three of five founders expressing this transgene (*K5–Gli2*) developed multiple skin tumours, which were found on ears, tail, trunk and dorsal aspects of paws (Fig. 1). Tumours on the albino founder exhibited features characteristic of human BCCs: a smooth and shiny surface, translucent or pearly appearance and prominent telangiectases. Ulceration was seen in several lesions on each animal. Many tumours on the agouti and black founders resembled human pigmented BCCs. No tumours exhibited gross evidence of hyperkeratosis, a common feature of squamous cell carcinomas. By breeding additional founders we generated two *K5–Gli2* lines: at present, one has produced an offspring with tumours indistinguishable from those seen in the original founders.

Tumour histology in *Gli2*-overexpressing mice showed similarities to that of human BCCs (Fig. 1*e*,*f*). Tumours were composed of monomorphous cells with scant cytoplasm arranged as nests within the dermis, pigmented tumours contained melanin scattered among tumour cells or in the stroma, keratinocytes at the periphery of some tumour islands were arranged in a palisading pattern and necrotic regions were seen in the centre of some tumours. Mitotic activity was relatively low and invasion of tumour cells into deeper structures was not seen. Like human BCCs (refs 11,12), tumours of *K5–Gli2* mice expressed keratin K17, Bcl-2 and K5 (Fig. 1*g*–*j*); in contrast, K1 and K6 were not present (Fig. 1*k*,*l*).

In situ analysis revealed abundant *Gli1*, *Gli2* and *Ptch* mRNA in tumour cells of *K5–Gli2* mice, but not in overlying epidermis or age-matched control skin

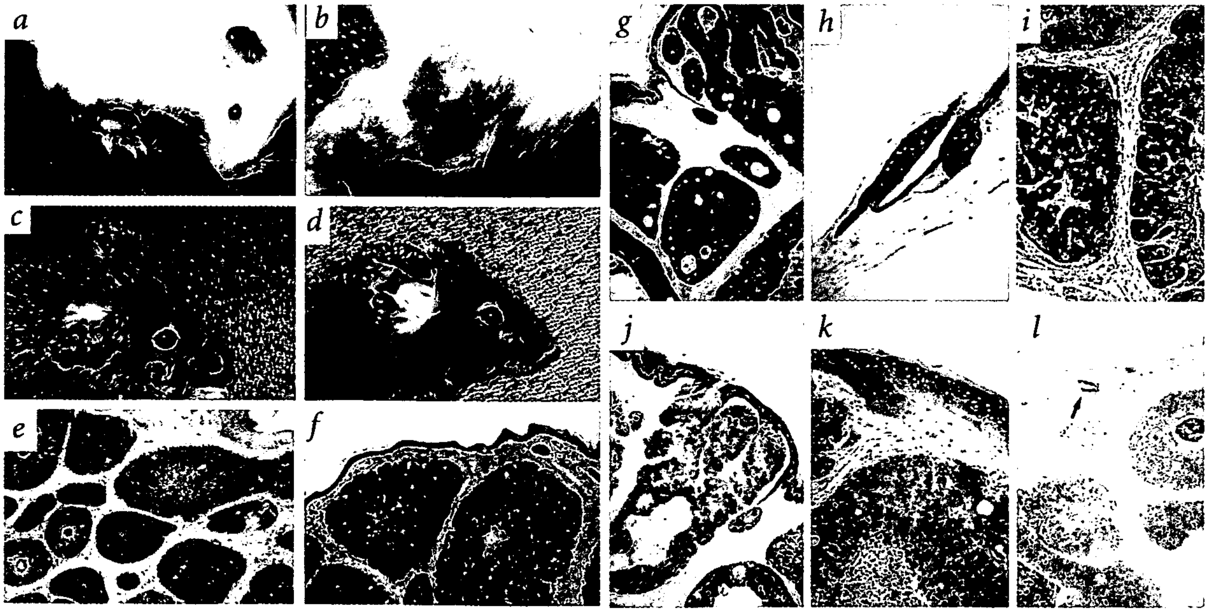

Fig. 1 *K5–Gli2* transgenic mice developed multiple BCCs. Gross appearance (***a***,***b***,***c***,***d***) and histology (***e***,***f***) of tumours on *K5–Gli2* founders. The tumours contained masses of monomorphous cells, with scant cytoplasm filling the dermis. Note the brown-black melanin in pigmented tumours (*e*). Expression of human BCC markers in tumours from *K5–Gli2* mice (*g*–*l*). Keratin K17, expressed in the outer root sheath of hair follicles and human BCCs, was detected in tumours from *K5–Gli2* mice (***g***,***h***). Microscopic tumours occasionally replaced the upper portion of hair follicles (***h***). Bcl-2 (***i***) and keratin K5 (***j***) are expressed in the tumours. Differentiation-specific keratin K1 was detected in suprabasal cells of epidermis, but not tumour cells (***k***). Keratin K6 is expressed in squamous cell tumours but not BCCs, and was not detected in *K5–Gli2* skin tumours (***l***). Note the normal expression of K6 in hair follicle (*l*, arrow). Antibody sources and dilutions available on request. A full-length mouse *Gli2* cDNA with amino-terminal FLAG tag was subcloned into a bovine K5 transgenic cassette. The insert was microinjected into fertilized (C57BL/6xSJL) F_2 eggs and transgenic founders produced using standard procedures. *K5–Gli2* founders were identified using primers for the rabbit β-globin intron.

© 2000 Nature America Inc. • http://genetics.nature.com

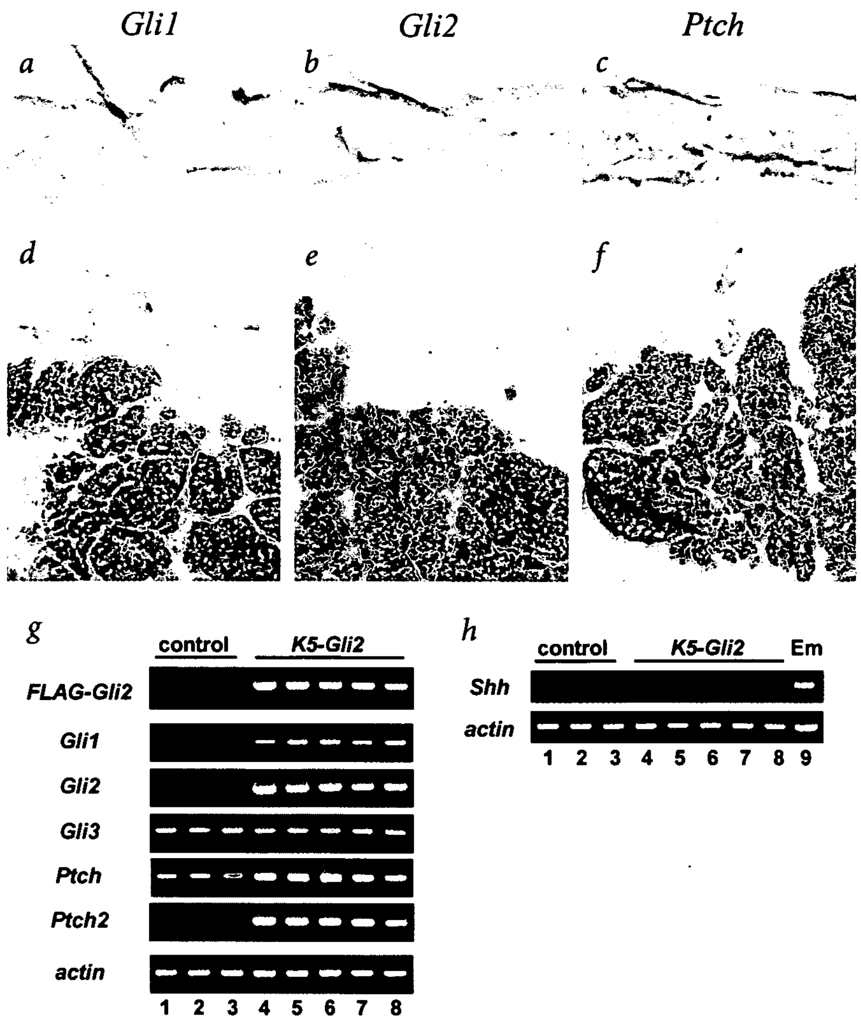

Fig. 2 Upregulation of Shh target genes in skin tumours from *K5–Gli2* transgenic mice. *In situ* analysis[9] of age-matched control skin (***a***,***b***,***c***) and tumours from *K5–Gli2* transgenic mice (***d***,***e***,***f***), revealing upregulation of *Gli1*, *Gli2* and *Ptch* in tumour cells. RT–PCR (ref. 16) of RNA isolated from control skin samples (lanes 1–3) and transgenic tumour samples (lanes 4–8, ***g***,***h***) (primer sequences and PCR conditions available on request) is shown. Amplification using primers to detect mRNA encoding FLAG-tagged Gli2 (*FLAG–Gli2*) confirmed transgene expression in tumour samples. *Gli1*, *Gli2*, *Ptch* and *Ptch2* transcripts are upregulated in tumours relative to control skin. There is a low level of endogenous *Gli2* expression in control skin. *Shh* expression was not increased in *K5–Gli2* transgenic skin tumours (*h*). Em, RNA from E18.5 mouse skin.

(Fig. 2*a–f*); RT–PCR analysis supported these findings (Fig. 2*g*). *Gli2* mRNA is also detected in human BCCs by RT–PCR (Q. Ding *et al.*, unpublished data). *Gli3* expression was similar in tumours and normal skin of control mice, similar to what is observed for human BCCs (ref. 5). *Shh* expression was not detected in tumours (Fig. 2*h*), suggesting that BCCs did not arise indirectly from Gli2-mediated induction of Shh. Our findings show that overexpression of Gli2 in skin results in the activation of multiple Shh target genes, a feature of human BCCs. We propose that irrespective of the genetic alteration eliciting uncontrolled Shh signalling in human BCCs, GLI2 has a central role in the genesis of these tumours.

Constitutive activation of Shh signalling in mouse skin using proximal elements of this pathway produces BCC-like growths detected during late embryogenesis[13,14]. BCCs arise in adult $Ptch^{+/-}$ mice following irradiation[15], but macroscopic skin tumours have not been reported in unirradiated animals. Skin-targeted overexpression of Gli1 reportedly does not give rise to BCCs (A. Oro, pers. comm.). Thus, although *Gli1* is a reliable indicator of Shh pathway activity, and when ectopically expressed can give rise to tumours in frog skin[5], the function of Gli1 in BCC development remains to be established. *K5–Gli2* transgenic mice therefore represent the first practical model of spontaneous BCC in adult animals and will be useful for studying the functional interactions between Shh pathway components and evaluating the efficacy of therapeutic agents targeting this signalling pathway.

Acknowledgements

We thank S. Yuspa, P. Coulombe, D. Bol and J. Jorcano for reagents; L. Lowe, L. Su and T. Johnson for advice on tumour histology; L. Wei and M. Berard for preparing the transgenic mice; and E. Fearon, G. Cotsarelis, S. Egan, S. Morrison and J.T. Elder for constructive comments on the manuscript. C.-c.H. was partially supported by the National Cancer Institute of Canada. A.A.D was supported in part by the University of Michigan Comprehensive Cancer Center (NIH CA46592) and Center for Organogenesis.

Marina Grachtchouk[1], Rong Mo[2], Sandy Yu[2], Xiaoyun Zhang[2], Hiroshi Sasaki[3], Chi-chung Hui[2] & Andrzej A. Dlugosz[1]

[1]University of Michigan Comprehensive Cancer Center and Department of Dermatology, Ann Arbor, Michigan, USA. [2]Program in Developmental Biology, The Hospital for Sick Children, and Department of Molecular and Medical Genetics, University of Toronto, Toronto, Ontario, Canada. [3]Laboratory of Developmental Biology, Institute for Molecular and Cellular Biology, Osaka University, Osaka, Japan. Correspondence should be addressed to A.A.D. (e-mail: dlugosza@umich.edu) or C.-c.H. (e-mail: cchui@sickkids.on.ca).

1. Booth, D.R. *Cancer Metast. Rev.* **18**, 261–284 (1999).
2. Hahn, H. *et al. Cell* **85**, 841–851 (1996).
3. Johnson, R.L. *et al. Science* **272**, 1668–1671 (1996).
4. Matise, M.P. & Joyner, A.L. *Oncogene* **18**, 7852–7859 (1999).
5. Dahmane, N., Lee, J., Robins, P., Heller, P. & Ruiz i Altaba, A. *Nature* **389**, 876–881 (1997).
6. Hynes, M. *et al. Neuron* **19**, 15–26 (1997).
7. Lee, J., Platt, K.A., Censullo, P. & Ruiz i Altaba, A. *Development* **124**, 2537–2552 (1997).
8. Motoyama, J. *et al. Nature Genet.* **20**, 54–57 (1998).
9. Ding, Q. *et al. Development* **125**, 2533–2543 (1998).
10. Ramirez, A., Bravo, A., Jorcano, J.L. & Vidal, M. *Differentiation* **58**, 53–64 (1994).
11. Markey, A.C., Lane, E.B., MacDonald, D.M. & Leigh, I.M. *Br. J. Dermatol.* **126**, 154–160 (1992).
12. Smoller, B.R., van de Rijn, M., Lebrun, D. & Warnke, R.A. *Br. J. Dermatol.* **131**, 28–31 (1994).
13. Oro, A.E. *et al. Science* **276**, 817–821 (1997).
14. Xie, J. *et al. Nature* **391**, 90–92 (1998).
15. Aszterbaum, M. *et al. Nature Med.* **5**, 1285–1291 (1999).
16. Chiang, C. *et al. Dev. Biol.* **205**, 1–9 (1999).

Induction of basal cell carcinomas and trichoepitheliomas in mice overexpressing GLI-1

Mats Nilsson*†, Anne Birgitte Undén*†‡, Darren Krause*, Ulrica Malmqwist*, Karima Raza*, Peter G. Zaphiropoulos*, and Rune Toftgård*§

*Department of Biosciences at Novum, Karolinska Institutet, SE-141 57, Huddinge, Sweden; and ‡Department of Dermatology, Karolinska Hospital, SE-171 76 Stockholm, Sweden

Edited by Bert Vogelstein, Johns Hopkins Oncology Center, Baltimore, MD, and approved January 7, 2000 (received for review October 28, 1999)

Basal cell carcinoma is the most prevalent cancer in the western world, showing a rapid increase in incidence. Activation of the Sonic hedgehog/Patched (PTCH) signaling pathway because of PTCH1 inactivation is a key event in sporadic and familial basal cell carcinoma development in humans and is associated with transcriptional activation of specific target genes, including *PTCH1* itself. These changes are analogous to the situation in *Drosophila* where hedgehog activates the zinc-finger transcription factor Cubitus interruptus, leading to increased transcription of target genes. In the present study, we show that mice ectopically expressing the human Cubitus interruptus homolog GLI-1 in the skin develop tumors closely resembling human BCCs as well as other hair follicle-derived neoplasias, such as trichoepitheliomas, cylindromas, and trichoblastomas. Furthermore, examination of the tumors revealed wild-type *p53* and Ha *ras* genes. These findings firmly establish that increased GLI-1 expression is central and probably sufficient for tumor development and suggest that GLI-1-induced tumor development does not depend on additional *p53* or Ha *ras* mutations.

Genetic studies on patients with nevoid basal cell carcinoma syndrome (NBCCS), which predisposes affected individuals to the development of multiple basal cell carcinomas (BCCs), have led to the identification of inactivating mutations in the human homolog of the *Drosophila* gene *patched* (*PTCH1*) as the defect underlying this syndrome (1, 2). In addition, a number of surveys have provided evidence that mutations in the *PTCH1* locus is a significant cause of sporadic BCCs as well as other hair follicle-derived neoplasias such as trichoepitheliomas (TEs) (3–5). The other common genetic alteration in BCCs is a mutation in the tumor-suppressor gene *p53* (6).

In biochemical assays, Ptch1 has been shown to bind the ligand Sonic hedgehog (Shh) (7, 8). Ptch1 is a transmembrane protein that together with Smoothened (Smoh), a seven-transmembrane protein, forms a receptor complex for Shh (9, 10). Ligand binding results in derepression of signaling from Smoh and subsequently to activation of the transcription factor Gli, the mammalian homolog to *Drosophila* Cubitus interruptus (Ci). Three Ci homologs have been identified in mammals, Gli-1, Gli-2, and Gli-3, which share a highly conserved zinc-finger domain with Ci and are believed to function as the most downstream components in the vertebrate *Sonic hedgehog-Patched* signaling pathway (11, 12). The precise roles played by the three *Gli* genes have not yet been fully defined. *GLI-1* was originally isolated as an amplified gene in a glioma and can transform primary rat cells in cooperation with adenovirus E1A (13). Several lines of evidence suggest a role for Gli-1 in mediating the Shh signal: first, Gli-1 is expressed in cells that are responsive to Shh (14, 15). Second, elevated Gli-1 expression is observed in Shh-treated cells, and third, ectopic expression of Gli-1 in the dorsal midbrain and hindbrain mimics the effects of ectopically expressed Shh (15, 16). Moreover, increased expression of *GLI-1* is observed in human BCCs (17, 18).

BCCs cannot be grown in culture and are not induced in classical mouse skin tumorigenesis experiments. *Ptch1* $+/-$ mice develop medulloblastomas and rhabdomyosarcomas, and recently BCC formation has been reported after UV radiation (19–21). Moreover, transgenic mice overexpressing Shh or a mutated variant of SMOH show epidermal proliferations in late embryonic skin that partially resembles BCC (22, 23). To test the hypothesis that GLI-1 is the downstream effector that drives tumorigenesis, transgenic mice were generated specifically overexpressing GLI-1 in the basal layer of epidermis and outer root sheet of hair follicles. These mice develop several types of spontaneous skin tumors, including BCC, TEs, cylindromas, and trichoblastomas. Furthermore, mutation analysis of the *p53* and Ha *ras* genes, respectively, did not reveal mutations in their hot spot regions, exons 4–8 for *p53* and codons 12, 13, and 61 for Ha *ras*, in any of the tumors examined. This suggests a *p53*- and Ha *ras*-independent mechanism by which GLI-1 induce these tumors in mouse skin.

Materials and Methods

Transgenic Mice. A bluescript KS (−) plasmid (p5′BK5II) containing a 5.2-kb fragment from the bovine keratin 5 (K5) promoter, a 0.6-kb fragment containing the rabbit β-globin intron, and a 1.1-kb fragment containing two 3′ poly(A) signal sequences was obtained from Jose Jorcano (CIEMAT, Madrid). A 3.5-kb fragment containing the full-length human *GLI-1* cDNA was amplified from pGLI-1 K12 (24) by using *GLI-1* specific primers (fwd: 5′-GCGCTAGCATGTTCAACTCGATGACCC-3′, rev: 5′-GCTACGTATTAGGCACTAGAGTTGAGGAA-3′) containing restriction half sites for *Sna*BI and *Nhe*I, respectively. The amplified product was ligated into the *Sna*BI and *Nhe*I sites of the p5′BK5II vector. The construct was verified by sequencing. The transgene was isolated by cutting with *Not*I/*Sal*I. Founder transgenic mice were made by microinjecting the transgene into the pronuclei of fertilized [C57BL/6J × CBA] F_2 oocytes and were genotyped by PCR amplification of sequences specific for the β-globin intron and the human *GLI-1* cDNA respectively from tail genomic DNA. All experiments were performed with mice hemizygous for the transgene, and transgenic mice were always directly compared with nontransgenic siblings. All transgenic mice were generated within the transgenic core facility at Novum/Huddinge hospital.

Immunohistochemical Staining. Tissues used for immunohistochemistry were formalin fixed and paraffin embedded. Before being incubated in 1% H_2O_2 in methanol for 30 min, the paraffin

---

This paper was submitted directly (Track II) to the PNAS office.

Abbreviations: BCC, basal cell carcinoma; RT, reverse transcription; K, keratin; TE, trichoepithelioma.

[†] M.N. and A.B.U. contributed equally to this work

[§] To whom reprint requests should be addressed. E-mail: rune.toftgard@cnt.ki.se.

The publication costs of this article were defrayed in part by page charge payment. This article must therefore be hereby marked "*advertisement*" in accordance with 18 U.S.C. §1734 solely to indicate this fact.

Article published online before print: *Proc. Natl. Acad. Sci. USA*, 10.1073/pnas.050467397. Article and publication date are at www.pnas.org/cgi/doi/10.1073/pnas.050467397

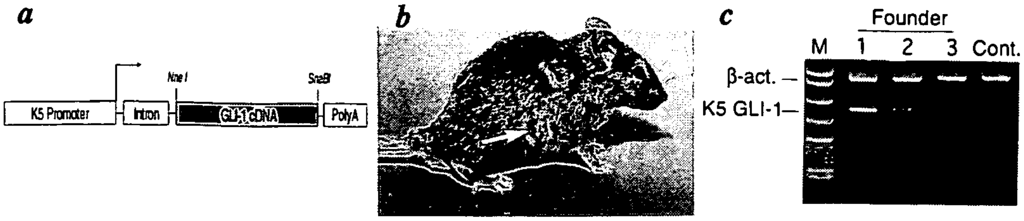

Fig. 1. Generation of transgenic mice. (*a*) Schematic drawing of the *K5 GLI-1* transgene. The transgene contains the bovine K5 promoter, the rabbit β-globin intron, the human *GLI-1* cDNA, and the SV40 poly(A) signal. (*b*) GLI-1 transgenic founder (founder 2) showing a tumor ulceration and the nodule (arrow) on the back. (*c*) RT-PCR analysis of *K5 GLI-1* and β-actin mRNA in dorsal skin of the transgenic founders 1 to 3 (1–3). Sizes of the specific PCR products are 553 bp for β-actin and 370 bp for K5 GLI-1. Lane *M* pBR322-*Msp*I ladder (New England Biolabs).

sections were dewaxed, rehydrated, and submerged in 10 mM citrate buffer while heated in a 97°C water bath, for 20 min. Sections were incubated overnight at +4°C with 1:500 diluted rabbit polyclonal antibodies directed against either mouse K1, K5, K6, or loricrin (all from Berkeley Antibody Company, Berkeley, CA) or 1:200 diluted goat polyclonal antibodies against Gli-1 or Ptch 1 (both from Santa Cruz Biotechnology) or 1:500 diluted rabbit polyclonal antibodies against phosphohistone H3 (Upstate Biotechnology, Lake Placid, NY) or 1:200 diluted mouse monoclonal antibodies against Bcl-2 (Transduction Laboratories, Lexington, KY) or 1:700 diluted rabbit polyclonal antibodies against wild-type p53 (NovoCastra, Newcastle, U.K.). All antibodies were diluted in PBS containing 0.1% BSA. Detection was carried out with the Vectastain Elite Kit (Vector Laboratories) by using rabbit or goat IgG. Sections were washed with PBS before biotinylated secondary antibodies were applied for 1 h at room temperature, followed by extensive rinses and incubation with avidin–biotin immunoperoxidase. Immunohistochemical staining was visualized with 3-amino-9-ethylcarbazole (AEC, Vector Laboratories), and counterstaining was performed with Mayer's hematoxylin.

RNA Isolation and Reverse Transcription (RT)–PCR. Total cellular RNA was isolated from the back skin, containing dermis as well as epidermis, of transgenic and wild-type sibling control mice by using guanidium thiocyanate-phenol-chloroform extraction as described previously (25). RT-PCR was carried out by using the Access RT-PCR system kit (Promega). The RT reaction was performed at 48°C for 45 min by using 1 μg of total RNA. The following primer pairs were used: 5′-TGCTCTTTCTCTCCAGCACCTCGGATC-3′ (sense: corresponding to the vector sequence) and 5′-CAGTGCCCGCTTCTTGGTCAA-3′ (antisense: corresponding to the human *GLI-1* cDNA sequence from 301–327). These transgene-specific *GLI-1* primers yielded a 369-bp PCR product. In the same reaction, β-actin-specific primers giving a 553-bp PCR product were used as an internal control.

Analysis of p53 and Ha *ras* Mutations. Microdissection of 10-μm-thick paraffin sections was performed, and normal cells were separated from tumor cells by using a scalpel. Microdissected tissue was incubated in digestion buffer (10 mM KCl/1.5 mM $MgCl_2$/10 mM Tris, pH 9.0/0.5% Tween 20) containing 200 μg/ml proteinase K at 55°C for 6 h. All microdissected tissue contained >80% tumor cells. Amplification of exons 4–8 of the mouse *p53* gene or exons 1 and 2 of the mouse Ha *ras* gene was performed as follows: 10 μl aliquots of tumor lysate were used for PCR amplification in a 20-μl reaction volume containing 2 μl 10 × reaction buffer without $MgCl_2$ (Promega); 250 μM of each dNTP; 3.2 pmol of each primer; and 0.5 units *Taq* polymerase (Promega). The primers used for amplification of the murine *p53* or Ha *ras* exons and the individual $MgCl_2$ concentrations have previously been described (26, 27). Thirty-five cycles of amplification were carried out, with denaturation at 94°C for 1 min, annealing at 54 or 58°C (*p53*, depending on the exon), or 60°C (Ha *ras*) for 2 min, and extension at 72°C for 2 min. PCR products were purified by using MicroSpin columns (Amersham Pharmacia Biotech) and subjected to sequencing.

Results

Spontaneous Tumor Formation in K5 GLI-1 Transgenic Mice. To examine the effect of deregulated GLI-1 expression in mammalian skin, we generated transgenic mice expressing the human *GLI-1* gene under the control of the bovine K5 promoter (Fig. 1*a*). This K5 promoter fragment has previously been shown to direct transgene expression to the basal cell compartment of stratified squamous epithelia as well as the outer root sheet of hair follicles (28). Three independent K5 GLI-1 transgenic founders were generated, all of which developed tumors within 1–13 wk. In addition to tumor formation, the GLI-1 transgenic mice exhibited failure to thrive and died prematurely at 1 to 6 mo of age. Founder 1 developed a hyperkeratotic tumor on the back within the first week and died at 4 wk of age. Founder 2 showed the first signs of tumor development at 4 wk of age and developed a 1-cm tumor-ulcer at 10 wk of age, and subsequently tumors developed on the back (Fig. 1*b*). The third founder showed the weakest phenotype, because 13 wk passed before tumors developed on the back. RT-PCR analysis of total RNA from dorsal back skin showed *K5 GLI-1* mRNA in all three founders, demonstrating expression of the transgene in these mice (Fig. 1*c*). A summary of the macroscopically detected tumors on each founder is described in Table 1.

Four Different Types of Adnexal Skin Tumors in GLI-1 Overexpressing Mice. Histologic examination of the observed nodules on founder 2 identified two different skin tumors separated by nontumorigenic skin. The first nodule showed a large primitive tumor (Fig. 2*a*). The peripheral layer of these tumor formations showed palisading similar to human BCCs, and the cells had a uniform nonanaplastic appearance (Fig. 2 *a* and *b*). The dermis was completely filled with tumor masses also lined with palisading basaloid cells but with large necrotic areas in the center of the tumor nests. Inside the same tumor islands, abundant amyloid

Table 1. Spontaneous skin tumors in K5 GLI-1 mice

Founder	Macroscopically observed tumors	Tumor site	Age, wk	*p53* status	Ha-*ras* status
1	Trichoepithelioma (1)	Back	1	wt	wt
2	Trichoepithelioma (1)	Back	4	wt	wt
	Trichoepithelioma (1)	Nose	8	–	–
	BCC (1)	Back	10	wt	wt
3	Trichoblastoma (6)	Back	13	wt	wt

Age is in weeks at time of tumor detection. Numbers in parentheses for different tumors indicate the number of each tumor type found. wt, wild type.

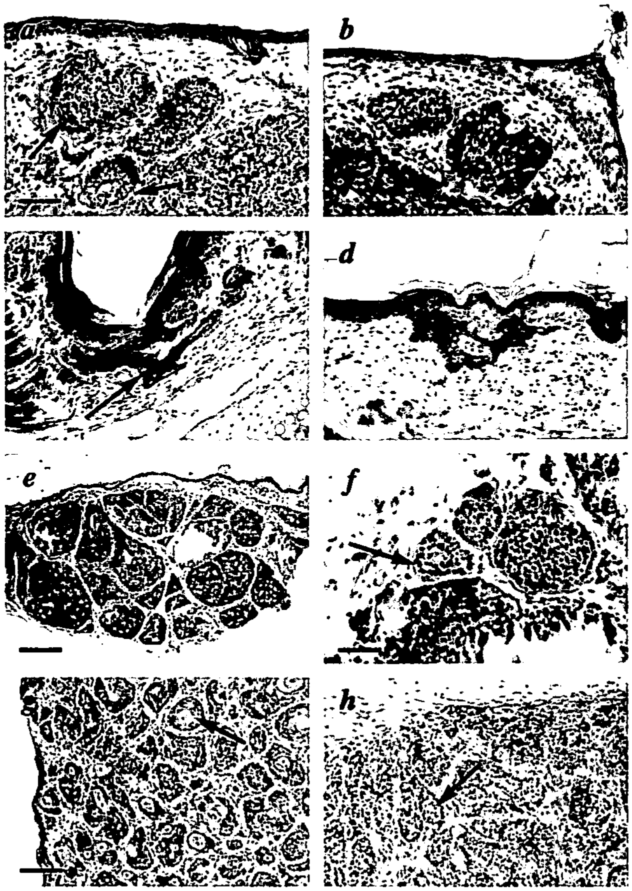

Fig. 2. Histological features of the K5 GLI-1 transgenic skin. (*a*) Nodular BCC from founder 2 with palisading basaloid cells forming tumor nests (T) and retraction space of stroma from tumor islands (R). (*b*) Human nodular BCC. (*c*) Superficial BCC from founder 2 with buds and irregular proliferations of tumor tissue attached to the undersurface of the epidermis (arrow). (*d*) Human superficial BCC. (*e*) Cylindroma from founder 2 with tumor islands forming a jigsaw puzzle. (*f*) The periodic acid/Schiff reagent-positive hyalin membrane surrounding the cylindroma tumor islands (arrow). (*g*) TE from founder 1 with keratinized centers (arrow) surrounded by basophilic tumor cells. (*h*) Trichoblastoma from founder 3 illustrating tumor islands consisting mostly of germinative cells (arrow). Bar = 135 μm (*e*), 54 μm (*a*–*d* and *g*, *h*), and 33 μm (*f*).

was identified, indicating the presence of phagocytosis and apoptosis of tumor cells. Colloid bodies and scattered calcinosis were also observed in this tumor. The stroma was arranged in parallel bundles around the tumor masses with a retraction zone resulting in peritumoral lacuna also seen in human BCCs (Fig. 2*b*). Such retraction zones were observed in some but not all tumor nests. In addition to the nodular BCC observed on the back, several BCCs were found on the nose, including a superficial BCC showing strong resemblance to its human counterpart (Fig. 2 *c* and *d*).

A second type of tumor observed was macroscopically similar to the BCC-like tumor described above but showed different features under the microscope. This tumor consisted of numerous tumor islands of epithelial cells appearing like pieces in a jigsaw puzzle (Fig. 2*e*). The thick hyaline sheath that surrounded the tumor islands like a cylinder was periodic acid/Schiff reagent positive (Fig. 2*f*). All the above characteristics are typical for a cylindroma, and this tumor was consequently classified as a cutaneous cylindroma (29).

A third type of tumor developed on both founder 1 and 2, consisting of large well-circumscribed tumors located in the dermis reaching down to the muscle layer without direct connection with the epidermis. The tumors consisted of multiple tumor nests of epithelial origin all showing horn cysts in the center (Fig. 2*g*). The centers were fully keratinized and surrounded by basophilic tumor cells, similar to the hair matrix cells. These tumors are very similar to human TE, a benign human skin tumor believed to develop from pluripotential epithelial cells in the hair follicle (29).

Six different tumors were examined from founder 3. Histologically, all six tumors were shown to be benign well-circumscribed noduli with a silhouette placed deep in the dermis (Fig. 2*h*). No connection with epidermis was observed, even though the overlying epidermis seemed thickened and hyperplastic. The numerous aggregations consisted mostly of follicular germinative cells arranged in a palisade pattern in the periphery. No keratinizing cysts were observed. These tumors were classified as counterparts to the benign human skin tumor, trichoblastoma (29).

In summary, four different types of skin tumors were found on the K5 GLI-1 mice: BCCs, TE, cylindromas, and trichoblastomas. The tumors described above were macroscopically detected; however, more tumors of similar types were detected when examining additional ($n = 5$) skin samples from these mice (data not shown).

Tumors Show Differentiation Marker Expression Similar to Human BCCs. Terminal differentiation of keratinocytes involves the sequential expression of specific keratins in the basal and spinous layers and loricrin, a component of the cornified envelope, in the granular layer. To determine whether the histologic features seen in the K5 GLI-1 mice are accompanied by an altered pattern of differentiation marker expression, immunohistological analysis was performed. Staining of K5 GLI-1 BCC with antibodies against the basal K5 revealed high expression in the tumor, consistent with the pattern seen in human BCC (Fig. 3*a*) (30). K1, which is expressed only in cells committed to terminal differentiation, was found to be abundantly expressed in the suprabasal layer of the transgenic skin but not in tumor cells (Fig. 3*b*). In addition, loricrin, a major component of the epidermal cornified envelope, showed normal expression in the transgenic stratified epithelia (Fig. 3*c*). Taken together, these findings suggest that the interfollicular epidermal keratinocytes present in the K5 GLI-1 transgenic mice differentiate normally. Analysis of K6 and histone 3, both associated with hyperproliferation, showed abundant expression in tumor cells and in overlaying hyperproliferative epidermis but not in histologically normal epidermis (Fig. 3 *d* and *e*). This observation indicates that, whereas tumor cells and reactive epidermal keratinocytes are actively proliferating, uninvolved epidermal cells proliferate at normal rate.

Increased Expression of GLI-1 Target Genes in Tumor Cells. Human BCCs and TEs consistently overexpress PTCH1 and GLI-1 (5, 17, 18, 31). Furthermore, earlier studies in frogs and mice have shown that ectopic expression of GLI-1 causes increased expression of endogenous Gli-1 and Ptch1 (15, 16, 18). We used immunohistochemical analysis to examine the expression of these genes in transgenic tumors as well as in wild-type skin. Gli-1 was strongly expressed in tumor cells, and expression was also observed in adjacent reactive epidermis, although at a lower level (Fig. 4*a*). Even though the antibody used does not distinguish between the human and murine Gli-1, we interpret the observed difference in signal as reflecting increased expression of the endogenous murine gene because no positive signal was observed in histologically normal epidermis. No Gli-1 expression could be detected in wild-type skin (Fig. 4*b*). Consistent with the Gli-1 expression, increased expression of murine Ptch1 was

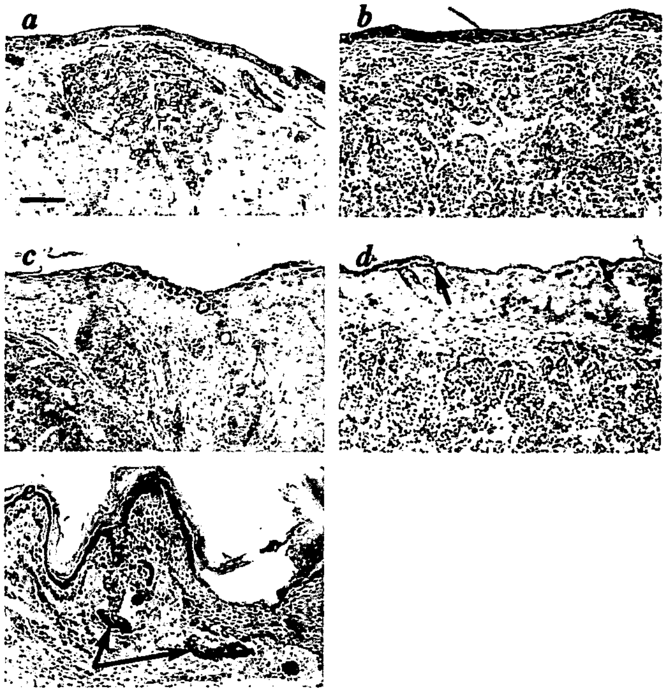

Fig. 3. Expression of marker proteins in the K5 GLI-1 mouse skin. (*a*) Positive immunoreactivity for K5 both in the epidermis and in the tumor cells. (*b*) K1 is expressed in the suprabasal layers of the epidermis but not in the tumor cells. (*c*) The granular layer of the epidermis shows positive immunoreactivity with the loricrin antibody, but the closely located tumor cells are negative. (*d*) Strong expression of K6 in the tumor cells and the overlying hyperproliferative epidermis, whereas the histologically normal epidermis (arrow) is negative. (e) A strong immunoreactivity with phosphohistone 3 (H3) antibodies is seen in the tumor cells (arrows) with a weaker signal in the hyperplastic epidermis. Bar = 54 μm (*a–e*).

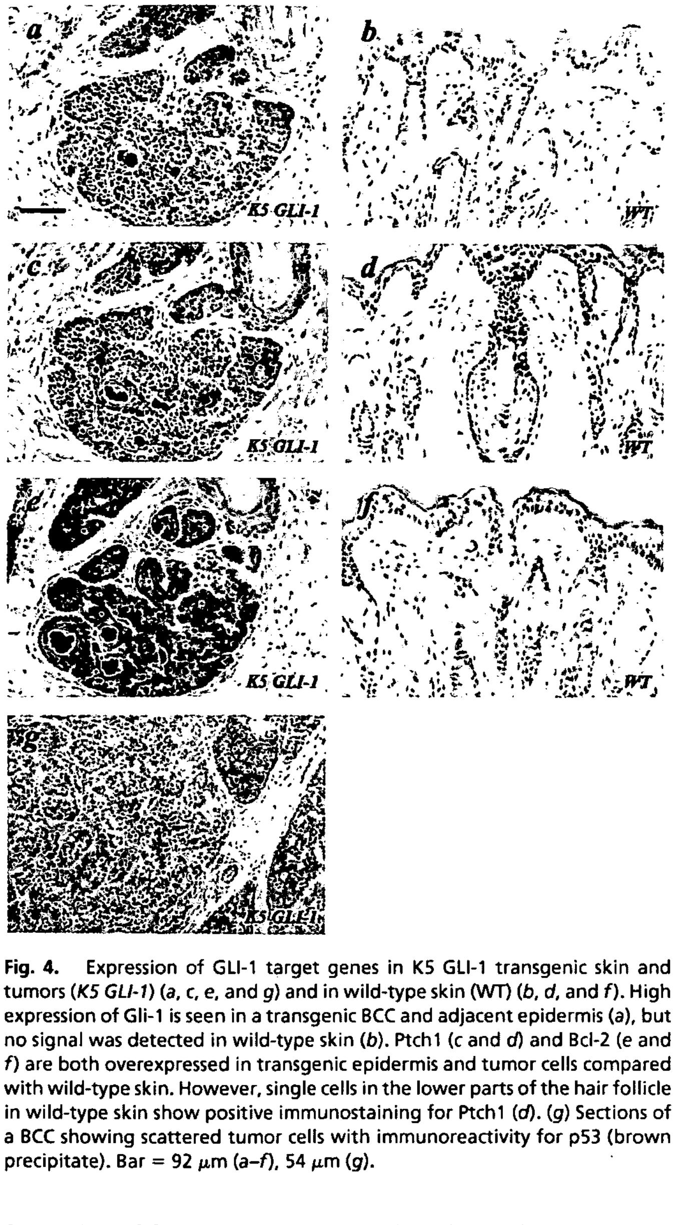

Fig. 4. Expression of GLI-1 target genes in K5 GLI-1 transgenic skin and tumors (*K5 GLI-1*) (*a*, *c*, *e*, and *g*) and in wild-type skin (WT) (*b*, *d*, and *f*). High expression of Gli-1 is seen in a transgenic BCC and adjacent epidermis (*a*), but no signal was detected in wild-type skin (*b*). Ptch1 (*c* and *d*) and Bcl-2 (e and *f*) are both overexpressed in transgenic epidermis and tumor cells compared with wild-type skin. However, single cells in the lower parts of the hair follicle in wild-type skin show positive immunostaining for Ptch1 (*d*). (*g*) Sections of a BCC showing scattered tumor cells with immunoreactivity for p53 (brown precipitate). Bar = 92 μm (*a–f*), 54 μm (*g*).

observed in transgenic skin compared with wild type (Fig. 4 *c* and *d*).

Human BCCs have demonstrated a marked increase in expression of Bcl-2, in contrast to the other common epidermal malignancy, squamous cell carcinoma (30). In the BCC from a K5 GLI-1 transgenic mouse Bcl-2 expression was markedly elevated with no detectable expression in wild-type skin (Fig. 4 *e* and *f*), suggesting a potential role in GLI-1-induced BCC formation.

Wild-Type *p53* and Ha *ras* in Transgenic Skin Tumors. The tumor-suppressor gene *p53* is commonly mutated in most types of human epithelial malignancies, including BCCs (6, 32). The level of p53 protein is low in normal cells; however, increased expression because of stabilization is observed in cells harboring a mutated p53. When analyzing a tumor sample from a K5 GLI-1 mouse for p53 protein expression, a moderately intense dispersed pattern was observed primarily in peripheral cells, suggestive of a possible involvement of p53 in the formation of this tumor (Fig. 4*g*). Similar results were obtained when analyzing additional tumors (n = 3; data not shown). However, direct sequencing of *p53* exons 4–8 after microdissection of this particular BCC did not reveal any mutations (Table 1). Moreover, when the p53 mutation analysis was extended to involve all macroscopically observed tumors (n = 10), no *p53* mutation was found in any tumor. This finding suggests that GLI-1 can drive tumor formation independently of a mutated p53 protein.

Other genes commonly mutated in nonmelanoma skin cancer are members of the *ras* oncogene family, comprised of the N, Ki, and Ha *ras* genes. Mutations in all three *ras* genes have been found in BCCs, with Ha *ras* showing the highest mutation frequency (33). In addition, in patients with nonmelanoma skin cancer, there is a high incidence of Ha *ras* loss of heterozygosity (36% for patients with BCC) in normal-appearing skin (34). These findings suggest a potential involvement of the Ras signaling pathway in BCC development. However, examination of the transgenic mouse tumors (n = 10) for Ha *ras* mutations revealed no mutations in exons 1 and 2, including the hot spot regions codons 12, 13, and 61, suggesting a mechanism whereby GLI-1 induce tumor growth independently of a mutated Ha *ras* gene (Table 1). However, we cannot exclude presence of mutations in other *ras* genes, and further analysis is ongoing to address this issue.

Discussion

In the present study, we have shown that inappropriate expression of the transcription factor GLI-1 is the probable mechanism by which mutations in the SHH-PTCH signaling pathway elicit development of skin tumors. Consistent with this, GLI-1 expression is up-regulated in most human BCCs as well as in medulloblastomas and rhabdomyosaromas appearing in Ptch$^{+/-}$ heterozygous mice (17–20). In addition, ectopic expression of GLI-1 in murine brain or frog epidermis is associated with enhanced proliferation (16, 18). The GLI-1 cDNA used in this study corresponds to the tumor-derived GLI-1 gene originally isolated by Kinzler *et al.* and is hence possibly mutant (16, 24). However, recent functional studies revealed no differences in terms of transactivating ability or potential to interact with SUFUH (suppressor of fused), a known inhibitor of GLI-1, in comparison to GLI-1 cloned from normal tissue (35). Furthermore, the sequence alteration occurs in a region of GLI-1 that is highly variable between different species, indicating that the two forms represent polymorphic variants.

A surprising and very interesting outcome of our study was the development of four different types of skin tumors in K5-GLI-1 mice, in each instance closely mimicking their human counterparts. In the case of BCCs, presence of palisading basaloid cells in the periphery of tumor nests, appearance of retraction spaces, lack of keratinizing centers, as well as expression of Bcl-2, endogenous Gli-1, and Ptch1, are all characteristics typical of human BCCs. Moreover, tumors resembling different histological subtypes like nodular and superficial BCCs were identified. In TEs, advanced follicular differentiation including central horn cysts and rudimentary hair structures combined with lack of retraction spaces were key features. The critical features supporting classification as cylindroma were the jigsaw puzzle arrangement, presence of basaloid cells in the periphery, light-staining cells in the tumor centers, and a periodic acid/Schiff reagent-positive hyalin sheath surrounding the tumor islands. Similarly, the trichoblastomas located in the dermis and penetrance into the subcutaneous fat layer with absence of keratinizing cysts were highly similar to the corresponding human tumor. Consistent with the human situation, no metastasis was observed. Thus, K5-GLI-1 transgenic mice represent a highly relevant experimental model of spontaneous BCC and related skin cancers having the same pathogenetic background as in humans.

In human BCCs, TEs, trichoblastomas, and cylindromas are all classified as adnexal skin tumors with the cell of origin most likely residing in the apocrine/follicular unit, a view supported by a very similar cytokeratin expression pattern in BCC, TE, trichoblastoma, and fetal hair follicles (36). Furthermore, TEs and cylindromas often coexist in patients with the tumor predisposition syndrome hereditary multiple epithelioma (MIM 132700) (37, 38). TE and BCC occur in the multiple familial TE syndrome (MIM 60/606), and trichoblastoma and BCC often develop within a congenital malformation called sebaceous nevus, in which deletions in the *PTCH1* gene region were recently reported (39–41). A link to constitutive activation of the SHH-PTCH1 signaling pathway is clear for BCCs and TEs displaying both PTCH1 mutations and consistent up-regulation of *PTCH1* mRNA in familial as well as sporadic tumors (5, 31). Our finding that all the above tumor types appear in the K5-GLI-1 transgenic mice now suggests that the different predisposing genetic defects converge on activation of GLI-1 expression.

An important question is how overexpression of GLI-1 can result in various tumor phenotypes. We favor the hypothesis that GLI-1 serves as a dose-dependent cell fate/differentiation determinant during hair follicle development and cycling. According to this view, the level of GLI-1 expression underlies the cellular phenotype with a low-level driving proliferation, resulting in trichoblastomas and with higher levels in addition, partly inducing the hair follicle differentiation program yielding BCCs, cylindromas, and TEs. This interpretation is supported by a stronger up-regulation of PTCH1 expression and by inference, GLI-1 expression in human TEs compared with BCCs (5).

As a consequence, the tumors we observe may be regarded as failed attempts to make a hair follicle, a failure because proliferation and hair follicle cell fate is induced in an adnexal progenitor cell within the epithelial compartment without a concomitant recruitment of mensenchymal cells to form a dermal papilla, which can signal back and promote further maturation. Consistent with this interpretation, secretion of Shh by the epithelial placode cells is required for proper papilla formation (42–44), and epithelial outgrowths stimulated by Shh overexpression eventually differentiate into hair follicles (22).

Tumor development is believed to require a number of genetic alterations and is often associated with genetic instability. BCCs are unusual in that they are apparently genetically stable and no precursor lesion has been identified. In humans, p53 mutations occur very frequently in BCCs as well as in patches of morphologically normal skin, especially in UV-exposed areas (32, 45). On the basis of these observations, it has been suggested that p53 mutations are an early and required event in BCC development. Immunohistochemical analysis of p53 expression in K5-GLI-1-induced tumors showed scattered p53-positive cells (Fig. 4*g*) in a pattern previously observed in some human BCCs, suggesting that p53 mutations may be present also in the murine tumors. Surprisingly, direct sequencing of exons 4–8 of p53 in 10 tumors failed to reveal any sequence alterations, supporting the conclusion that development of BCCs or other hair follicle-associated tumors does not absolutely depend on p53 mutations. Consistent with this, there is no reported predisposition for development of BCCs in Li-Fraumeni patients harboring germline p53 mutations or in $p53^{-/}$ mice. However, we can at present not exclude the presence of mutations in other genes involved in the same signaling pathway as p53, such as *p21*$^{\mathrm{waf}}$ and *Mdm2*.

A similar analysis of the Ha *ras* oncogene also failed to reveal any mutations in the transgenic tumors, indicating that GLI-1-induced tumor formation does not depend on secondary Ha *ras* mutations. Again, this observation is consistent with earlier reports describing development of squamous cell carcinomas but not BCCs in mice overexpressing Ha *ras* in epidermal cells (46).

If a single oncogenic event, i.e., GLI-1 expression above a certain threshold, is sufficient to initiate BCC and TE development, then all precursor cells receiving this signal should develop into tumors. In fact, in support of such a view, regions of macroscopically normal dorsal skin from founder 1 having the highest level of transgenic expression when analyzed histologically were found to be filled with tumors in various stages of development, leaving only a few normally appearing hair follicles (data not shown). Fewer tumors in mice with lower expression of the K5-GLI-1 transgene could be explained by not all precursor cells achieving a GLI-1 expression level above the threshold in combination with a slower tumor growth rate. An alternative explanation for a reduced number of tumors could be mosaic transgene expression, sparing potential tumor precursor cells from the expression of GLI-1. In any event, ectopic GLI-1 expression is able to initiate frequent tumor formation originating from hair follicle structures, and these tumors may or may not be associated with secondary genetic hits.

Finally, the observation that GLI-1 is not or is only to a very low level expressed in normal human skin (19) and that there is no apparent phenotype in $\mathrm{Gli}\text{-}1^{-/}$ mice make GLI-1 a promising therapeutic target (47, 48). The availability of a transgenic mouse model for the most common human cancer will make possible detailed mechanistic studies of BCC pathogenesis and development of new therapeutic strategies.

We thank K. W. Kinzler (Program in Human Genetics, The Johns Hopkins University School of Medicine) for the human *GLI-1* cDNA, J. Jorcano for the K5 expression vector, Mari-Anne Hedblad for help with analyzing the tumors, Tobias Skarin and Åsa Bergström for technical assistance, and P. Söderkvist for advice regarding *p53* mutation analysis. This study was supported by grants from the Swedish Cancer Fund, the Swedish Children Cancer Fund, the Swedish Medical Society, the Welander–Finsen Foundation, and Svenska Läkarsällskapet.

1. Johnson, R. L., Rothman, A. L., Xie, J., Goodrich, L. V., Bare, J. W., Bonifas, J. M., Quinn, A. G., Myers, R. M., Cox, D. R., Epstein, E. H., Jr. & Scott, M. P. (1996) *Science* **272**, 1668–1671.
2. Hahn, H., Wicking, C., Zaphiropoulous, P. G., Gailani, M. R., Shanley, S., Chidambaram, A., Vorechovsky, I., Holmberg, E., Undèn, A. B., Gillies, S., *et al.* (1996) *Cell* **85**, 841–851.
3. Aszterbaum, M., Rothman, A., Johnson, R. L., Fisher, M., Xie, J., Bonifas, J. M., Zhang, X., Scott, M. P. & Epstein, E. H., Jr. (1998) *J. Inv. Dermatol.* **110**, 885–888.
4. Gailani, M. R., Stahle-Backdahl, M., Leffell, D. J., Glynn, M., Zaphiropoulos, P. G., Pressman, C., Undèn, A. B., Dean, M., Brash, D. E., Bale, A. E., *et al.* (1996) *Nat. Genet.* **14**, 78–81.
5. Vorechovsky, I., Undèn, A. B., Sandstedt, B., Toftgård, R. & Stahle-Backdahl, M. (1997) *Cancer Res.* **57**, 4677–4681.
6. Hollstein, M., Sidransky, D., Vogelstein, B. & Harris, C. C. (1991) *Science* **253**, 49–53.
7. Marigo, V., Davey, R. A., Zuo, Y., Cunningham, J. M. & Tabin, C. J. (1996) *Nature (London)* **384**, 176–179.
8. Stone, D. M., Hynes, M., Armanini, M., Swanson, T. A., Gu, Q., Johnson, R. L., Scott, M. P., Pennica, D., Goddard, A., Phillips, H., *et al.* (1996) *Nature (London)* **384**, 129–134.
9. Alcedo, J., Ayzenzon, M., Von Ohlen, T., Noll, M. & Hooper, J. E. (1996) *Cell* **86**, 221–232.
10. Murone, M., Rosenthal, A. & de Sauvage, F. J. (1999) *Curr. Biol.* **9**, 76–84.
11. Ruiz i Altaba, A. (1997) *Cell* **90**, 193–196.
12. Ruppert, J. M., Kinzler, K. W., Wong, A. J., Bigner, S. H., Kao, F. T., Law, M. L., Seuanez, H. N., O'Brien, S. J. & Vogelstein, B. (1988) *Mol. Cell. Biol.* **8**, 3104–3113.
13. Ruppert, J. M., Vogelstein, B. & Kinzler, K. W. (1991) *Mol. Cell. Biol.* **11**, 1724–1728.
14. Marigo, V., Johnson, R. L., Vortkamp, A. & Tabin, C. J. (1996) *Dev. Biol.* **180**, 273–283.
15. Sasaki, H., Hui, C., Nakafuku, M. & Kondoh, H. (1997) *Development (Cambridge, U.K.)* **124**, 1313–1322.
16. Hynes, M., Stone, D., Dowd, M., Pitts-Meek, S., Goddard, A., Gurney, A. & Rosenthal, A. (1997) *Neuron* **19**, 15–26.
17. Green, J., Leigh, I. M., Poulsom, R. & Quinn, A. G. (1998) *Br. J. Dermatol.* **139**, 911–915.
18. Dahmane, N., Lee, J., Robins, P., Heller, P. & Ruiz i Altaba, A. (1997) *Nature (London)* **389**, 876–881.
19. Goodrich, L. V., Milenkovic, L., Higgins, K. M. & Scott, M. P. (1997) *Science* **277**, 1109–1113.
20. Hahn, H., Wojnowski, L., Zimmer, A. M., Hall, J., Miller, G. & Zimmer, A. (1998) *Nat. Med.* **4**, 619–622.
21. Aszterbaum, M., Epstein, J., Oro, A., Douglas, V., LeBoit, P. E., Scott, M. P. & Epstein, E. H., Jr. (1999) *Nat. Med.* **5**, 1285–1291.
22. Oro, A. E., Higgins, K. M., Hu, Z., Bonifas, J. M., Epstein, E. H., Jr. & Scott, M. P. (1997) *Science* **276**, 817–821.
23. Xie, J., Murone, M., Luoh, S. M., Ryan, A., Gu, Q., Zhang, C., Bonifas, J. M., Lam, C. W., Hynes, M., Goddard, A., *et al.* (1998) *Nature (London)* **391**, 90–92.
24. Kinzler, K. W., Ruppert, J. M., Bigner, S. H. & Vogelstein, B. (1988) *Nature (London)* **332**, 371–374.
25. Chomczynski, P. & Sacchi, N. (1987) *Anal. Biochem.* **162**, 156–159.
26. Hegi, M. E., Söderkvist, P., Foley, J. F., Schoonhoven, R., Swenberg, J. A., Kari, F., Maronpot, R., Anderson, M. W. & Wiseman, R. W. (1993) *Carcinogenesis* **14**, 803–810.
27. Devereaux, T. R., Foley, J. F., Maronpot, R. R., Kari, F. & Anderson, M. W. (1993) *Carcinogenesis* **14**, 795–801.
28. Ramirez, A., Bravo, A., Jorcano, J. L. & Vidal, M. (1994) *Differentiation (Berlin)* **58**, 53–64.
29. Ackerman, A. B., de Viragh, P. A. & Chongchitnant, N. (1993) *Neoplasms with Follicular Differentiation* (Lea & Febiger, Philadelphia).
30. Markey, A. C., Lane, E. B., Macdonald, D. M. & Leigh, I. M. (1992) *Br. J. Dermatol.* **126**, 154–160.
31. Undèn, A. B., Zaphiropoulos, P. G., Bruce, K., Toftgård, R. & Stahle-Backdahl, M. (1997) *Cancer Res.* **57**, 2336–2340.
32. Pontén, F., Berg, C., Ahmadian, A., Ren, Z. P., Nistér, M., Lundeberg, J., Uhlén, M. & Pontén, J. (1997) *Oncogene* **15**, 1059–1068.
33. Pierceall, W. E., Goldberg, L. H., Tainsky, M. A., Mukhopadhyay, T. & Ananthaswamy, N. (1991) *Mol. Carcinog.* **4**, 196–202.
34. Ananthaswamy, H. N., Applegate, L. A., Goldberg, L. H. & Bales, E. S. (1989) *Mol. Carcinog.* **2**, 298–301.
35. Kogerman, P., Grimm, T., Kogerman, L., Krause, D., Undèn, A. B., Sandstedt, B., Toftgård, R. & Zaphiropoulos, P. G. (1999) *Nat. Cell Biol.* **1**, 312–319.
36. Yamamoto, O. & Asahi, M. (1999) *Br. J. Dermatol.* **140**, 8–16.
37. Puig, L., Nadal, C., Fernandez-Figueras, M. T., Alegre, M. & de Moragas, J. M. (1998) *Am. J. Dermatopathol.* **1**, 56–60.
38. Verhoef, S., Schrander-Stumpel, C. T., Vuzevski, V. D., Temelaars, A., Jansen, L. A., Malfeyt, G. A., Ceelen, T. L., Lindhout, D., Halley, D. J. & van den Ouweland, A. M. (1998) *J. Med. Genet.* **10**, 841–845.
39. Johnson, S. C. & Bennett, R. G. (1993) *J. Am. Acad. Dermatol.* **2**, 322–326.
40. Mehregan, A. H. & Pinkus, H. (1965) *Arch. Dermatol.* **91**, 574–588.
41. Xin, H., Matt, D., Qin, J. Z., Burg, G. & Boni, R. (1999) *Cancer Res.* **8**, 1834–1836.
42. St-Jacques, B., Dassule, H. R., Karavanova, I., Botchkarev, V. A., Li, J., Danielian, P. S., McMahon, J. A., Lewis, P. M., Paus, R. & MacMahon, A. P. (1998) *Curr. Biol.* **19**, 1058–1068.
43. Karlsson, L., Bondjers, C. & Betsholtz, C. (1999) *Development (Cambridge, U.K.)* **126**, 2611–2621.
44. Chiang, C., Swan, R. Z., Grachtchouk, M., Bolinger, M., Litingtung, Y., Robertson, E. K., Cooper, M. K., Gaffield, W., Westphal, H., Beachy, P. A., *et al.* (1999) *Dev. Biol.* **1**, 1–9.
45. Jonason, A. S., Kunala, S., Price, G. J., Restifo, R. J., Spinelli, H. M., Persing, J. A., Leffell, D. J., Tarone, R. E. & Brash, D. E. (1996) *Proc. Natl. Acad. Sci. USA* **24**, 14025–14029.
46. Bailleul, G., Surani, M. A., White, S. C., Barton, S. C., Brown, K., Blessing, M., Jorcano, J. & Balmain, A. (1990) *Cell* **62**, 697–708.
47. Matise, M. P., Epstein, D. J., Park, H. L., Platt, K. A. & Joyner, A. L. (1998) *Development (Cambridge, U.K.)* **125**, 2759–2770.
48. Ding, Q., Motoyama, J., Gasca, S., Mo, R., Sasaki, H., Rossant, J. & Hui, C. C. (1998) *Development (Cambridge, U.K.)* **125**, 2533–2543.

OPEN ACCESS Freely available online PLoS BIOLOGY

Repression of Smoothened by Patched-Dependent (Pro-)Vitamin D3 Secretion

Maarten F. Bijlsma[1*], **C. Arnold Spek**[1], **Danica Zivkovic**[2], **Sandra van de Water**[2], **Farhad Rezaee**[3], **Maikel P. Peppelenbosch**[4]

1 Center for Experimental and Molecular Medicine, Academic Medical Center, University of Amsterdam, Meibergdreef, Amsterdam, Netherlands, 2 Netherlands Institute for Developmental Biology, Hubrecht Laboratory and Centre for Biomedical Genetics, Uppsalalaan, Utrecht, Netherlands, 3 Department of Biochemistry, Academic Medical Center, University of Amsterdam, Meibergdreef, Amsterdam, Netherlands, 4 Department of Cell Biology, University Medical Center Groningen, University of Groningen, Antonius Deusinglaan, Groningen, Netherlands

The developmentally important hedgehog (Hh) pathway is activated by binding of Hh to patched (Ptch1), releasing smoothened (Smo) and the downstream transcription factor glioma associated (Gli) from inhibition. The mechanism behind Ptch1-dependent Smo inhibition remains unresolved. We now show that by mixing Ptch1-transfected and Ptch1 small interfering RNA–transfected cells with Gli reporter cells, Ptch1 is capable of non–cell autonomous repression of Smo. The magnitude of this non–cell autonomous repression of Smo activity was comparable to the fusion of Ptch1-transfected cell lines and Gli reporter cell lines, suggesting that it is the predominant mode of action. CHOD-PAP analysis of medium conditioned by Ptch1-transfected cells showed an elevated 3β-hydroxysteroid content, which we hypothesized to mediate the Smo inhibition. Indeed, the inhibition of 3β-hydroxysteroid synthesis impaired Ptch1 action on Smo, whereas adding the 3β-hydroxysteroid (pro-)vitamin D3 to the medium effectively inhibited Gli activity. Vitamin D3 bound to Smo with high affinity in a cyclopamine-sensitive manner. Treating zebrafish embryos with vitamin D3 mimicked the *smo*$^{-/-}$ phenotype, confirming the inhibitory action in vivo. Hh activates its signalling cascade by inhibiting Ptch1-dependent secretion of the 3β-hydroxysteroid (pro-)vitamin D3. This action not only explains the seemingly contradictory cause of Smith-Lemli-Opitz syndrome (SLOS), but also establishes Hh as a unique morphogen, because binding of Hh on one cell is capable of activating Hh-dependent signalling cascades on other cells.

Citation: Bijlsma MF, Spek CA, Zivkovic D, van de Water S, Rezaee F, et al. (2006) Repression of smoothened by patched-dependent (pro-)vitamin D3 secretion. PLoS Biol 4(8): e232. DOI: 10.1371/journal.pbio.0040232

Introduction

Signal transduction of the morphogen hedgehog (Hh) is highly unusual, with many features unique to this signalling system, many of which are only partly understood [1]. For instance, Hh signalling is mediated by two membrane proteins: patched (Ptch1) and smoothened (Smo). The former is a 12-pass transmembrane protein [2,3] resembling the Niemann-Pick disease type C1 (NPC1) protein (which is involved in cholesterol trafficking and has a pump function); the latter is a seven-pass transmembrane protein that resembles a G protein–coupled receptor [4]. In the absence of the inhibitory receptor Ptch1 (or in the case of a specific mutation rendering Ptch1 dysfunctional), Smo is constitutively active and leads to the activation and nuclear translocation of its downstream transcription factor glioma associated (Gli). Under normal physiological circumstances, the activation of the signalling pathway is caused by binding of Hh to Ptch1, resulting in the internalisation of Ptch1 and, consequently, the alleviation of the inhibitory effect of Ptch1 on Smo [5,6]. The exact mechanism behind Ptch1 inhibition of Smo, however, remains unclear [7].

Similarities in the phenotypes of humans with inherited disorders of sterol biosynthesis (Figure 1A, lathosterolosis and Smith-Lemli-Opitz syndrome [SLOS]) and the phenotypes seen with mutations in the Hh signalling pathway have led to the suggestion that cholesterol-synthesizing enzymes may somehow be involved in Ptch1-dependent Smo inhibition [1]. Sterol content has been found to be crucial to a cell's responsiveness to Hh, independent of proper Hh sterolation [8], suggesting that sterol—or more specifically cholesterol—levels are pivotal to a cell's ability to respond to Hh, rather than to the accumulation of a specific inhibitory metabolite.

Academic Editor: Matthew Scott, Stanford University, United States of America

Received September 29, 2005; **Accepted** May 8, 2006; **Published** July 18, 2006

DOI: 10.1371/journal.pbio.0040232

Copyright: © 2006 Bijlsma et al. This is an open-access article distributed under the terms of the Creative Commons Attribution License, which permits unrestricted use, distribution, and reproduction in any medium, provided the original author and source are credited.

Abbreviations: 7-DHC, 7-dehydrocholesterol; BSA, bovine serum albumin; CHOD-PAP, cholesterol oxidase peroxidase-amidopyrine; CMV, cytomegalovirus; DMEM, Dulbecco's Modified Eagle Medium; FCS, fetal calf serum; FPLC, fast performance liquid chromatography; Gli, glioma associated; HDL, high-density lipoprotein; Hh, hedgehog; HMG-CoA, 3-hydroxy-3-methylglutaryl coenzyme A; hpf, hours post fertilisation; Ihh, Indian hedgehog; ISH, in situ hybridisation; LDL, low-density lipoprotein; MEF, mouse embryonic fibroblast; mGli, mutant Gli binding site; NPC1, Niemann-Pick disease type C1; PBS, phosphate buffered saline; Ptch1, patched; RLU, relative light unit; Shh, Sonic hedgehog; siRNA, small interfering RNA; SLOS, Smith-Lemli-Opitz syndrome; Smo, smoothened; VLDL, very-low-density lipoprotein

* To whom correspondence should be addressed. E-mail: m.f.bijlsma@amc.uva.nl

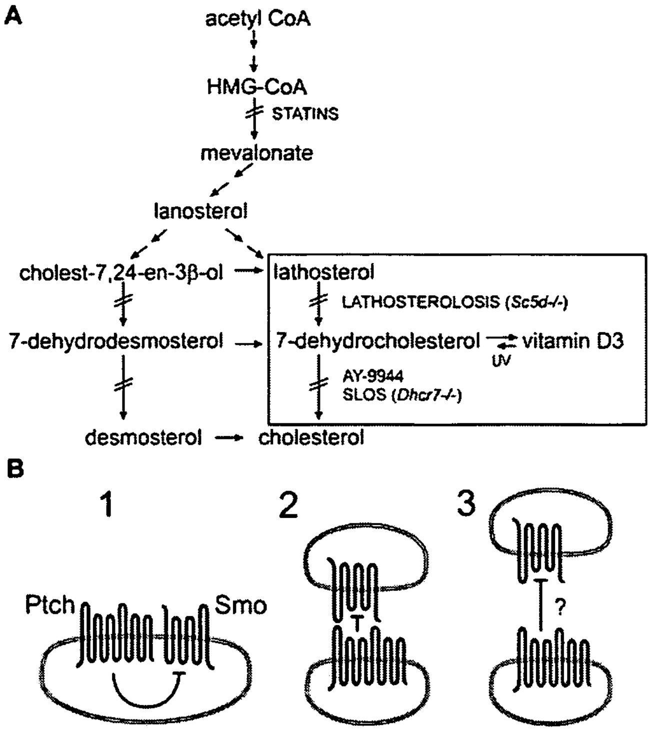

Figure 1. Cholesterol Synthesis and Possible Modes of Action of Ptch1

(A) Shown is a schematic representation of cholesterol synthesis. Boxed are lathosterol and 7-DHC, cholesterol precursors known to accumulate in lathosterolosis and SLOS patients, respectively. Mutations in or genetic loss of sterol C5-desaturase *(Sc5d)* cause stacking of lathosterol, whereas dysfunction of 7-DHC reductase *(Dchr7)* or the addition of its synthetic inhibitor AY-9944 causes accumulation of 7-DHC. The conversion of 7-DHC to vitamin D3 (cholecalciferol) is mediated by UV light. Statins, like pravastatin, inhibit HMG-CoA reductase, the enzyme that forms mevalonate.

(B) Shown are three possible models for the inhibitory action of the Hh receptor Ptch1 on Smo. (1) A cell-autonomous mode of action, in which direct binding of Ptch1 inhibits Smo. (2) An intracellular inhibitory action, mediated by direct binding of Ptch1 to Smo. (3) The model in which Ptch1 pumps an inhibitory small molecule that is capable of Smo-repression intercellularly (as well as intracellularly; not shown).

DOI: 10.1371/journal.pbio.0040232.g001

Figure 1B depicts the proposed possible modes of Ptch1 action on Smo. Because Ptch1 and Smo do not unambiguously show physical association and because Ptch1 can inhibit Smo substoichiometrically, direct binding of Ptch1 to Smo as shown in Figures 1B, columns 1 and 2, seems an unlikely mechanism of inhibition [9]. Ptch1 shares high homology (for instance, a sterol-sensing domain) with NPC1, a protein involved in cholesterol trafficking [10], as well as with various (prokaryotic) pump proteins. Also, several small molecules with homology to cholesterol that act as Hh pathway antagonists have been identified [11–13]. Cyclopamine, a well-known antagonist of Smo, has been widely used for assessing the effects of Hh pathway inhibition in several model systems (for example, in [14]). Consequently, it has been anticipated that in the absence of Hh, Ptch1 translocates a small molecule resembling cholesterol across the membrane, acting as a Smo antagonist. This hypothesis is summarized in Figure 1B, column 3.

A consequence of the proposed "pump" model for Ptch1 is that the action of Ptch1 should be non-cell autonomous. We set out to test this prediction, and we established that Hh activates its signalling cascade by inhibiting Ptch1-dependent secretion of the 3β-hydroxysteroid (pro-)vitamin D3. These data provide fundamental new insight into the molecular mechanisms by which Hh exerts its action in pathophysiology.

Results

A Model System for Measuring Ptch1-Dependent Smo Inhibition

An experimental system allowing the study of intercellular inhibitory actions of Ptch1 on Smo should fulfill four requirements: (1) cells must be capable of sustaining Ptch1 expression, (2) expressed Ptch1 must be functionally active, (3) the inhibition of Gli activity should be Smo-mediated, and (4) endogenous Hh should not be a contributing factor. To set up a model system for studying Ptch1-dependent inhibition, C3H/10T1/2 fibroblasts, which are cells extensively used for Hh research, were transfected with an 8× Gli-binding site luciferase construct [15] together with Ptch1, Smo, Smo and Ptch1, or Gli1.

Overexpression of Ptch1 drove cells into apoptosis (unpublished data, consistent with [16]), possibly a reflection of the function of Ptch1 as a so-called dependence receptor. To overcome this problem, we performed experiments in the presence of 20 µM caspase inhibitor zVADfmk. Under these conditions, transfection with a Ptch1 expression construct led to efficient overexpression of Ptch1 as detected by Western blot (Figure 2A). Transfection of Ptch1 effectively inhibited transactivation of the Gli reporter in the presence of overexpressed Smo (Figure 2B). The Ptch1-insensitive mutant SmoM2 [11,17] was not inhibited by Ptch1 cotransfection and showed a high basal Gli activity. Ptch1 transfection in the absence of Smo overexpression yielded no inhibition below control values, which has been described previously [18]. This finding suggests the presence of high basal Ptch1 levels and indicates the specificity of Ptch1 inhibition acting through Smo in our system. The inhibitory effect of the high basal Ptch1 levels could be overcome by the addition of 1 µg/ml recombinant N-terminal Sonic hedgehog (Shh) for 6 h, as can be seen from the high reporter activity upon stimulation (Figure 2B). Addition of 1 µg/ml 5E1 Shh-blocking antibody [19] could counteract the stimulation by Shh. Because Smo and Gli overexpression were capable of increasing transactivation of the Gli reporter despite the presence of a caspase inhibitor, our experimental system is a valid readout for Smo-mediated Gli activity.

The requirement for Smo overexpression to respond to Ptch1 inhibition and the high responsiveness to exogenously added Shh suggest that endogenous Hh production is not a major factor in our setup, although others have shown mRNA for Indian hedgehog (Ihh) and Shh in C3H/10T1/2 cells [20,21]. To exclude Hh protein excretion by our C3H/10T1/2 cells as a contributing factor in our model system, we performed Western blot analysis on Shh-spiked medium and medium from fibroblast cell culture. The cells did not excrete Hh protein (Figure 2C). As can be seen, the detection limit was about 5 ng/ml, which was not reached in the (4× concentrated) medium, indicating that the Hh concentration in the medium was less than 1.25 ng/ml, a concentration too low to evoke a response [22]. Reprobing the blot for Ihh did not yield a signal for the medium either.

Ptch1 Can Inhibit Smo in a Non–Cell Autonomous Fashion

To assess the ability of Ptch1 to act upon Smo on another cell, we used a "mix-and-match" approach (as schematically shown in Figure 3A), in which two populations of cells are mixed. The donor population expresses Ptch1 at different levels (using an overexpression construct or small interfering RNA [siRNA]) that could act on reporter cells with a constitutively active Hh pathway (reporter cells: Smo receptor overexpressed and a Gli-luciferase reporter). We mixed reporter cells with vector, Ptch1, Ptch1 siRNA and scrambled control siRNA transfectants. Cell populations were detached by EDTA treatment, mixed, and replated. By using two fluorescent tracers for labelling the cell populations, the capability of this procedure to obtain a homogenous mixture could be assessed. Figure 3A shows that combining two cell populations yields evenly mixed cells with intimate cell-cell contacts (micrograph). When Gli reporter cells were mixed with Ptch1- overexpressing cells in these mix-and-match experiments, a significant reduction in Smo-mediated Gli activation could be seen compared with control. This inhibition could not be diminished by addition of 1 μg/ml 5E1 Hh-blocking antibody (Figure 3A), again demonstrating that endogenous Hh is not a contributing factor in our experimental setup. This is important, specifically because the presence of Hh in the medium would increase reporter activity. As Ptch1 scavenges Hh from the medium, medium of Ptch1-overexpressing cells would contain lower Hh levels than would control or Ptch1 siRNA-transfected cells. The reduction in reporter activity as consequence of such scavenging would mask the action of a potential inhibitory molecule. The addition of 1 μg/ml recombinant Shh, which should inhibit Ptch1 present in these experiments, was able to abolish the inhibition conferred by Ptch1. Mixing reporter cells with Ptch1 siRNA-transfected cells increased Smo-dependent reporter activity (Figure 3A, blue bars), demonstrating that the inhibition is Ptch1 dependent and again suggests that C3H/10T1/2 cells have a significant basal level of Ptch1 activity. Showing opposite effects of Ptch1 siRNA versus DNA excludes any overexpression artefacts from responsibility for the observed non–cell autonomous effect. To exclude cell-specific artefacts, the procedures were also performed with MDA-MB-231 breast tumour cells, which had even higher levels of endogenous PTCH1 and SMO than the C3H/10T1/2 fibroblasts (Western blot, unpublished data). Indeed, using these cells yielded similar but more pronounced effects, as did the C3H/10T1/2 cells (Figure 3A, hatched bars).

To determine the maximal inhibition Ptch1 confers in a cell-autonomous fashion—that is, the extent to which Ptch1 can inhibit Smo on the same cell—we mixed and fused the two previously described cell populations. PEG1500 induced efficient cell fusion, which was evident from blended staining of PEG1500-treated cells and the multinucleated cells (procedure and micrographs shown in Figure 3B, left panel). Fusion of reporter cells with Ptch1-overexpressing cells again showed a reduction in Gli activation, similar to that observed in the mix-and-match experiments (Figure 3A). The reduction in reporter activity was of the same magnitude as that obtained in the mixing experiments. Therefore, we conclude that Ptch1 inhibition of Gli reporter activity in our system is mediated mainly intercellularly.

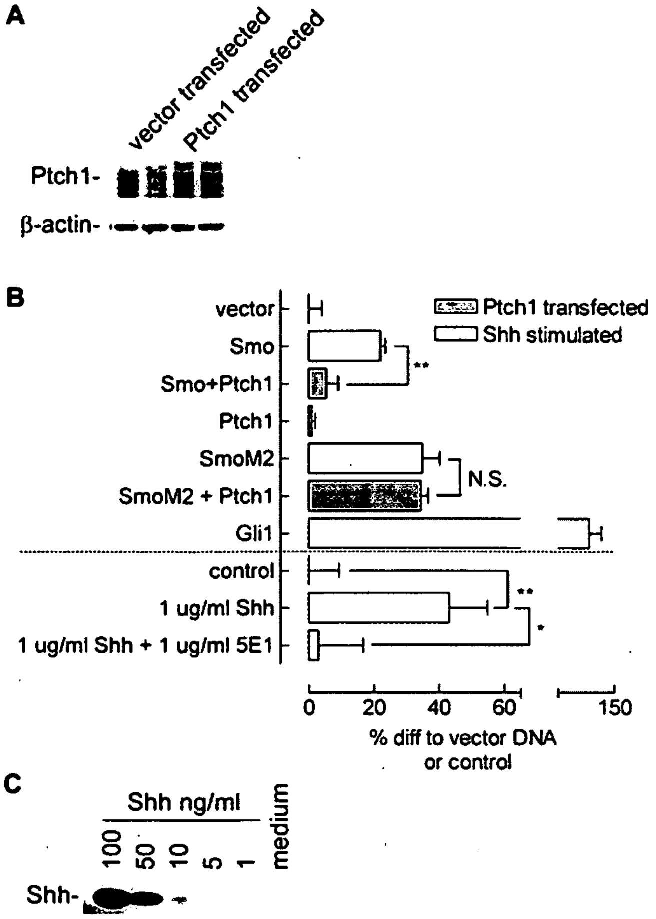

Figure 2. Confirmation of Functionality of Constructs and Model System Used

(A) Transfection of Ptch1 expression construct in C3H/10T1/2 fibroblasts increased Ptch1 expression over basal expression, as seen on Western blot. Actin levels remained unaltered; cells were lysed 24 h post transfection.

(B) C3H/10T1/2 cells are sensitive to Hh pathway components as indicated by Gli reporter activity when pathway components are expressed: Smo increased Hh pathway activity as determined by Gli reporter luciferase assay. Cotransfection of Ptch1 suppressed Smo-induced Gli activation. Transfection of Ptch1 in the absence of Smo overexpression did not decrease Gli activity below control levels. Shh stimulation (1 μg/ml for 6 h, 16 h post transfection) and transfection of a Gli1 expression construct showed highest reporter activity, as expected. Addition of 1 μg/ml Shh-blocking antibody 5E1 reduced Shh-mediated activation of Gli reporter activity. The Ptch1-insensitive mutant SmoM2 showed a high basal activity that could not be diminished by cotransfecting Ptch1, as expected. Cells were transfected and lysed after 24 h. Values shown are relative light unit (RLU) values corrected for an internal CMV Renilla standard, expressed as percent increase relative to vector (pcDNA 3.1-) transfection or control stimulation. Depicted is the mean ± SEM. ($n = 4$; *, $p < 0.05$; **, $p < 0.01$).

(C) Shh concentration in medium is below the detection limit (5 ng/ml) of Western blotting. Medium was spiked with decreasing concentrations of recombinant Shh, and blotted along with a 4× concentrated medium sample obtained from C3H/10T1/2 fibroblasts (incubated for 16 h at a volume-to-surface ratio identical to the mix-and-match and medium transfer experiments).

DOI: 10.1371/journal.pbio.0040232.g002

The specificity of the observed inhibitory action of Ptch1 acting through Smo was assessed by using the Ptch1-insensitive SmoM2 mutant, as previously shown in Figure 2B. As can be seen in Figure 3C, SmoM2-transfected reporter cells are no longer sensitive to mixing with Ptch1-over-

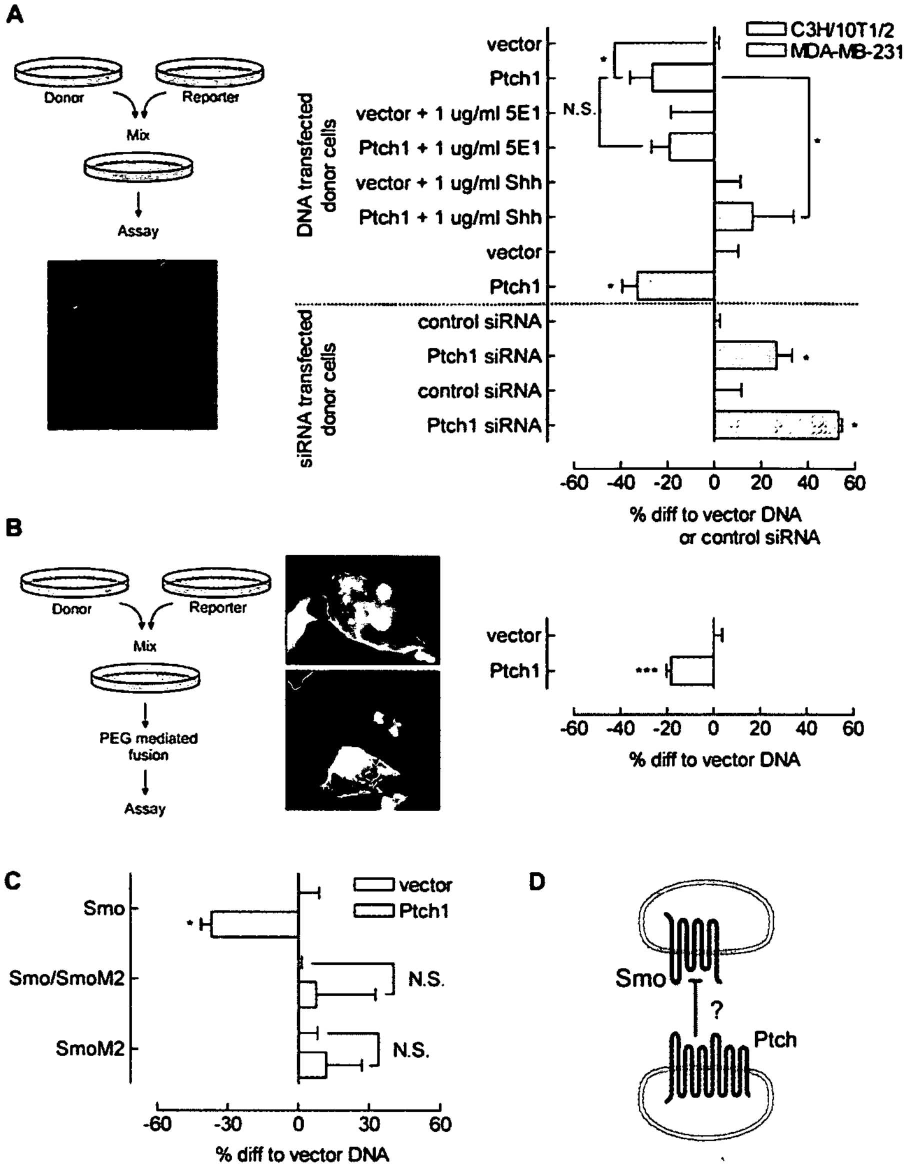

Figure 3. Ptch1 Inhibits Smo Intercellularly

(A) Detaching and mixing of two populations of fluorescently labelled cells resulted in a homogenous mixture with intimate cell–cell contacts. The procedure is summarized in the left panel. Original magnification is 400×. Intercellular capacity of Ptch1 to inhibit Smo was assessed by mixing reporter cells overexpressing Smo and a Gli reporter with Ptch1-overexpressing donor cells. The observed decrease in Gli reporter activity could not be inhibited by the addition of 1 μg/ml 5E1 Shh-blocking antibody. Exogenously added Shh (1 μg/ml) was capable of abolishing the Ptch1-mediated inhibition. Transfecting donor cells with Ptch1 siRNA reversed the inhibitory effect (blue bars). MDA-MB-231 breast carcinoma cells (hatched bars) showed a response similar to the C3H/10T1/2 fibroblasts'. Donor cells were transfected, washed (16 h post transfection), mixed with reporter cells, and lysed after 6 to 8 h. Shown are RLU values corrected for an internal CMV Renilla luciferase control, expressed as percent differences relative to control-transfected donor cells (vector DNA or scrambled control siRNA). ($n \geq 4$; *, $p < 0.05$; ***, $p < 0.005$). Depicted is the mean ± SEM.

(B) Fusion of reporter cells with Ptch1 overexpressing donor cells showed a decrease in Gli reporter activity comparable in magnitude to the inhibition observed in mixed cells. Right panel: treating fluorescently labelled cells with PEG1500 4 h after mixing resulted in multiple nuclei per cell and composite cell colours, indicating successful cell fusion. Magnification is 1,000×. Statistics and incubation times are as in (A).

(C) To assess the specificity of Ptch1 acting on Smo, reporter cells expressing the Ptch1-insensitive mutant SmoM2 (as indicated on the *y*-axis) were mixed with donor cells. The loss of inhibition indicates the specificity of Ptch1 acting through Smo in the mix-and-match setup. Statistics and incubation times are as in (A).

(D) Shown is a model for the proposed intercellular action of Ptch1 inhibition following the results obtained in the mix-and-match experiments.

DOI: 10.1371/journal.pbio.0040232.g003

expressing donor cells, even when cotransfected with wild-type Smo. These findings led us to suggest the model for Ptch1 action as depicted in Figure 1B, column 3, and Figure 3D, in which Ptch1 on one cell is capable of specifically inhibiting Smo on another cell, to act non–cell autonomously.

Non–Cell Autonomous Ptch1-Dependent Smo Inhibition Is Carried Out by a Medium-Borne Factor

The intercellular Ptch1-mediated inhibition of Smo as identified in the mix-and-match experiments may be conferred by either an inhibitory molecule secreted or translocated by Ptch1 or by diffusion of a cytosolic mediator through tight junctions. The latter possibility is less likely, because it would result in a merged fluorophore signal in the mixed cell population, which was not observed (Figure 3A). Indeed, important support for the possibility that Ptch1 secretes a Smo inhibitory molecule into the medium was obtained from experiments in which medium conditioned on Ptch1-transfected cells was transferred to reporter cells in which Gli activity was assayed (procedure schematically shown in Figure 4A, left panel).

By using this experimental setup, we found that medium conditioned on Ptch1-transfected cells exerted a strong inhibitory effect on Gli activation as compared with medium conditioned on control-transfected cells (Figure 4A). This inhibition could not be blocked by the addition of 1 μg/ml Shh or 5E1 to the reporter cells. The inability of Shh to prevent Ptch1-conditioned, medium-dependent inhibition of Smo activity is expected, because the transferred medium does not contain donor cells expressing Ptch1 on which Shh should exert its action, and the presence of the medium-borne factor in the Ptch1-conditioned medium shortcuts the function of endogenous Ptch1 in the reporter cells. Using MDA-MB-231 cells in this setup, similar results were obtained (Figure 4A, hatched bars). As for the mix-and-match experiments, medium conditioned on Ptch1 siRNA-transfected cells increased Smo-dependent reporter activity in both cell lines. Medium conditioned on mouse embryonic fibroblasts (MEFs) from *Ptch1* knockout mice [23] showed a distinct deficiency in their capacity to inhibit Smo compared with medium conditioned on wild-type (*Ptch1*$^{+/+}$) MEFs (Figure 4, pink bars). This inhibitory effect could again not be conferred to reporter cells transfected with the Ptch1-insensitive SmoM2. The opposite effects, as observed with Ptch1 DNA transfection versus either Ptch1 siRNA transfection (blue bars) or genetic Ptch1-deficient MEFs, exclude transfection artefacts on the donor cells as the potential cause of the observed effects. Overall, these findings suggest that Ptch1 transfers a molecule to the medium that inhibits Smo activity. Medium conditioned on Ptch1-overexpressing MDA-MD-231 cells could inhibit Gli activity in C3H/10T1/2 cells and vice versa (unpublished data), suggesting that the inhibitory factor is not species-specific, at least not among mammals.

Using serum-free medium, we could confer no inhibitory action of Ptch1-conditioned medium on reporter cells (Figure 4A). Serum-free medium contains no lipoproteins, which implies an important role for lipoproteins in conveying the inhibitory signal from cell to cell. Alternatively, serum-free medium also lacks lipids, which could stress the necessity for lipids supplied in the medium for Hh responsiveness [8]. However, serum-free conditions for 8 h (the incubation time in our experiments) do not deplete a cell's cholesterol metabolism, arguing in favour of a role for lipoproteins in communicating the inhibitory signal.

Ptch1-Dependent Secretion of 3β-Hydroxysteroids

The conditioned media were subjected to fast performance liquid chromatography (FPLC)-coupled cholesterol oxidase peroxidase-amidopyrine (CHOD-PAP) analysis, a technique that analyzes 3β-hydroxysteroid content. The Ptch1-conditioned medium was found to be enriched with 3β-hydroxysteroids relative to medium conditioned by control cells (Figure 4B and 4C; quantification of FPLC profiles as mM total 3β-hydroxysteroid). Judging from the retention profile, these 3β-hydroxysteroids were present on low-density lipoprotein (LDL) particles and, to a lesser extent, on very-low-density lipoprotein (VLDL). High-density lipoprotein (HDL) 3β-hydroxysteroid levels remained constant in all conditions. Medium incubated on cells transfected with siRNA for Ptch1 was virtually devoid of LDL-associated 3β-hydroxysteroids. This correlation between modified Ptch1 levels and the accumulation of 3β-hydroxysteroid molecules in the medium suggests that Ptch1 translocates or pumps these 3β-hydroxysteroids into the medium and thereby transfers the Smo inhibitory activity.

3β-Hydroxysteroids Are Necessary for Ptch1-Dependent Smo Inhibition

In the presence of pravastatin, a 3-hydroxy-3-methylglutaryl coenzyme A (HMG-CoA) reductase inhibitor that abrogates the biosynthesis of the 3β-hydroxysteroid precursor mevalonate (Figure 1A), LDL-associated 3β-hydroxysteroid (named LDL-C on axis) levels were substantially reduced (Figure 4C), and, correspondingly, reduced Gli inhibition was observed in Ptch1-overexpressing reporter cells as shown in Figure 4D. Conversely, the 3β-hydroxysteroid precursor mevalonate strongly increased LDL-associated 3β-hydroxysteroids and Ptch1-mediated inhibition of Gli transactivation.

If the observed effects of steroid synthesis modifiers on Gli activation are Smo-specific, Hh responses mediated by Ptch1 (but not those by Smo) should remain unaffected. The endocytosis of Ptch1 is such a Smo-independent response to Hh [3,4]. By using [3H]-sucrose as a tracer [24], we observed no effect of 1 mM pravastatin on Hh-mediated endocytosis (Figure 4E), and thus the effects of steroid-synthesis inhibitors are Smo-specific. The above-mentioned reporter data, however, are not from medium transfer experiments, and the inhibition or stimulation of cholesterol synthesis and the concomitant effects on Gli activity do not unequivocally prove the contribution of sterol biosynthesis to the intercellular action of Ptch1.

Using *Dhcr7*$^{-/-}$ and *Sc5d*$^{-/-}$ MEFs to Identify the Inhibitory Compound

The paradoxical phenotype of SLOS patients, in which diminished Hh signalling is accompanied by an accumulation of the sterol 7-dehydrocholesterol (7-DHC; see Figure 1A), led us to hypothesize that 7-DHC might be a Smo inhibitor. To test this hypothesis, we used MEFs [8] from mice genetically deficient for 7-DHC reductase (*Dhcr7*$^{-/-}$), because these cells stack 7-DHC. To confirm the specificity of 7-DHC as Smo inhibitor, we also used sterol C5-desaturase (*Sc5d*$^{-/-}$) MEFs that stack the precursor of 7-DHC (lathosterol) and contain little or no 7-DHC. Indeed, as shown in Figure 5A, *Dhcr7*$^{-/-}$ MEFs had a significantly reduced Gli activity as compared with *Sc5d*$^{-/-}$ MEFs. In addition, the Smo-inhibitory potential of *Dhcr7*$^{-/-}$ MEF-conditioned medium was much higher than that of *Sc5d*$^{-/-}$ MEF-conditioned medium, as shown in the medium transfer experiment depicted in Figure 5A. In addition to stacking a specific metabolite, both MEFs are equally incapable of sterol synthesis. Our data therefore argue against reduced sterol levels as being responsible for the observed Smo inhibition. Overall, these data strongly suggest that 7-DHC or a Dhcr7-independent metabolite of 7-DHC have an inhibitory action on Smo.

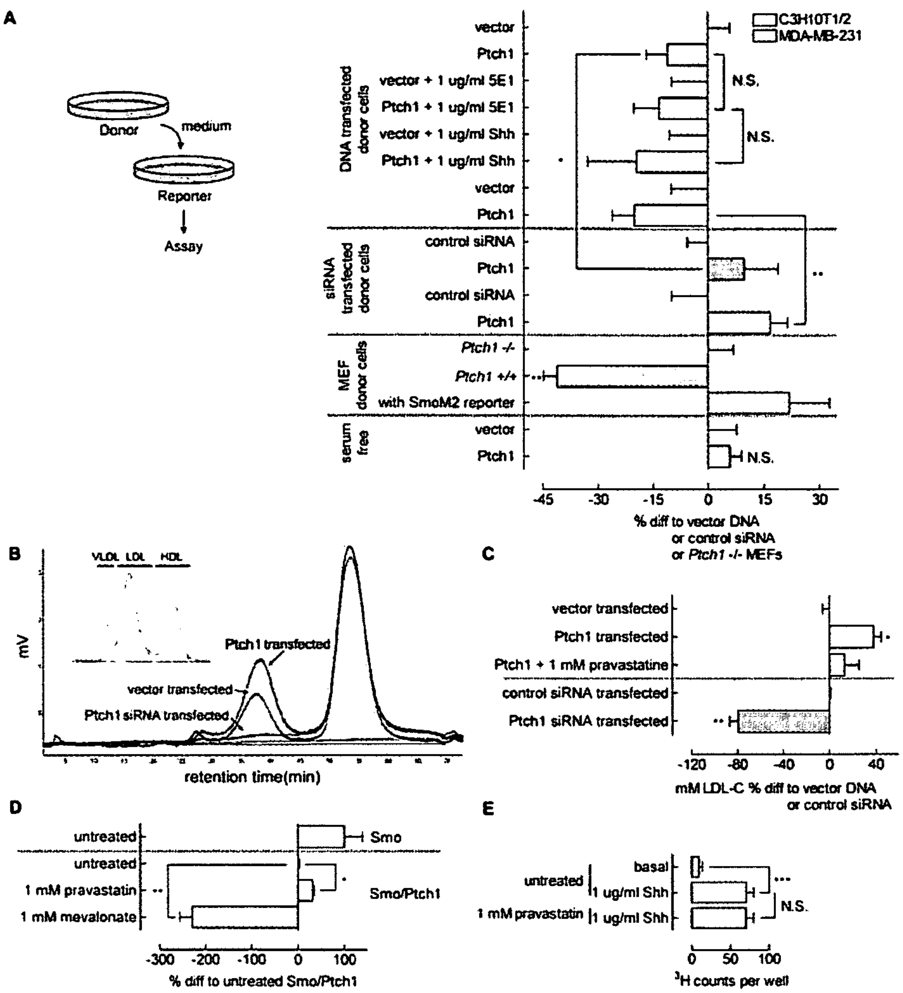

Figure 4. Ptch1 Secretes Smo-Inhibitory 3β-Hydroxysteroids

(A) The left panel shows a schematic representation of the medium transfer experiments, in which medium was incubated on (transfected) donor cells and subsequently transferred to reporter cells. Right panel: intercellular Smo inhibition by Ptch1 is carried by the medium. Medium conditioned by control-, Ptch1-, or Ptch1 siRNA-transfected (C3H/10T1/2, solid bars, and MDA-MB-231, hatched bars) cells was transferred to Gli reporter cells. The same inhibitory action for Ptch1 was found as in the mix-and-match experiments. Neither 5E1 blocking antibody nor recombinant Shh addition to the reporter cells could diminish the inhibitory potential of the conditioned media. Medium conditioned on wild-type (*Ptch1*$^{+/+}$) MEFs showed a pronounced inhibitory effect on reporter cells as compared with *Ptch1* knockout (*Ptch1*$^{-/-}$) MEF-conditioned medium. Gli activity in reporter cells transfected with SmoM2 was not inhibited by *Ptch1*$^{+/+}$ MEF-conditioned medium. In the absence of serum, Ptch1 transfectant conditioned medium did not contain the inhibitory activity. Incubation times are as in Figure 3B. Values shown are RLU values corrected for an internal CMV Renilla standard and expressed as percent difference to control-transfected donor cells. Depicted is the mean ± SEM. ($n \geq 4$; *, $p < 0.05$; **, $p < 0.01$; medium Ptch1-transfected compared with medium Ptch1 siRNA-transfected).

(B) Vector, Ptch1, and Ptch1 siRNA transfectant-conditioned media investigated with FPLC-coupled CHOD-PAP analysis shows loading of 3β-hydroxysteroids on lipoproteins by control cells. Medium conditioned by Ptch1-transfected cells shows a strong increase in 3β-hydroxysteroids, mainly in the LDL fraction. Ptch1 siRNA transfection abolishes 3β-hydroxysteroid loading on LDL. The inset shows the lipid standard FCS containing VLDL, LDL, and HDL. Medium was incubated on cells for 16 h. Shown are typical profiles.

(C) Shown is quantification of the LDL peaks, expressed as mM. LDL-C shows the Ptch1-induced increase, a reduction by HMG-CoA reductase inhibitor pravastatin treatment, and the abolition by Ptch1 siRNA transfection of 3β-hydroxysteroid loading on LDL ($n = 3$; *, $p < 0.05$; **, $p < 0.01$).

(D) Pravastatin-inhibited Ptch1 action on Smo-driven Gli reporter activity, whereas the addition of the cholesterol precursor mevalonate enhanced this inhibition. Cells were transfected, and, after 16 h, pravastatin or mevalonate was added for 6 to 8 h. Depicted is the mean ± SEM. ($n = 4$; *, $p < 0.05$; **, $p < 0.01$).

(E) Hh-induced endocytosis is not inhibited by 1 mM pravastatin ($n = 24$; ***, $p < 0.005$). Cells were stimulated with 1 μg/ml Shh for 1 h, and preincubated with 1 mM pravastatin or control for 6 h.

DOI: 10.1371/journal.pbio.0040232.g004

To assess whether Ptch1 uses 7-DHC to inhibit Smo, we performed medium transfer experiments with Ptch1 (or Ptch1 siRNA)-transfected *Dhcr7*$^{-/-}$ and *Sc5d*$^{-/-}$ MEFs as donor cells. If Ptch1 would indeed pump 7-DHC, Ptch1 overexpression or knockdown in the *Sc5d*$^{-/-}$ MEFs should show no effect on Smo inhibition. As shown in Figure 5B, the *Sc5d*$^{-/-}$ MEFs were severely hampered in their ability to transfer Ptch1 action to the medium, because neither Ptch1 DNA nor siRNA transfectants differed from control transfectants in their ability to inhibit Smo on reporter cells. The *Dhcr7*$^{-/-}$ MEFs, however, were well capable of translating Ptch1 expression levels to differential inhibitory action on reporter cells. UVB treatment of *Dhcr7*$^{-/-}$ MEF-conditioned media, which catalyzes the reaction from 7-DHC to vitamin D3, increased the Ptch1 effect on reporter cells, raising the tantalising option that Ptch1 uses vitamin D3 to inhibit Smo.

Vitamin D3 Is Sufficient for Smo Inhibition

From the experiments described above, we hypothesized that the addition of synthetic 7-DHC or vitamin D3 would inhibit Gli activity in reporter cells as well. Indeed, as can be seen from Figure 6A, 7-DHC was capable of inhibiting Smo, but was not nearly as potent as its derivative, vitamin D3. This fits the observation that UV treatment enhanced the inhibitory potential of Ptch1-conditioned medium (Figure 5B). The addition of the 7-DHC reductase inhibitor AY-9944 [25] successfully enhanced the effect of vitamin D3 treatment but was also capable of inhibiting Smo by itself, possibly by causing accumulation of endogenously synthesized 7-DHC or by acting as a 7-DHC mimetic. The magnitude of inhibition conveyed by either the transfer of Ptch1 transfectant–conditioned medium or Ptch1 cotransfection were both smaller than that of vitamin D3. In addition, inhibition conferred by vitamin D3 was stronger than that of 10 µM cyclopamine. The finding that AY-9944 was not a necessity for inhibitory action excludes a role for sterol deprivation in this model (Figure 1A), because the exogenously added 7-DHC or vitamin D3 can be readily metabolized by these (wild-type) fibroblasts to produce downstream sterols.

Shown in Figure 6B is a dose-dependent response of reporter cells to vitamin D3 for 6 h. In agreement, the level of inhibitory N-terminal Gli3 protein increased accordingly, as quantified from Western blot. This digestion product of Gli3 originates from proteolysis in the SuFu/Fu complex present in Hh pathway inactive cells and is considered the repressor form [26]. To exclude cytotoxic artefacts of vitamin D3, we measured cell viability by MTT reduction. Only at very high (1 mM) concentrations of vitamin D3 could we could observe a slight decrease in cell viability. Using SmoM2-transfected reporter cells, Gli reporter inhibition occurred only at 100 µM vitamin D3, and below that concentration, no inhibition could be observed. This is very similar to the impaired but not absent response of SmoM2 to cyclopamine [11].

To exclude Gli-independent effects of vitamin D3 from being responsible for the observed reporter inhibition, we used a panel of various luciferase reporter constructs. As can be seen in Figure 6C, interferon-stimulated response element (pISRE), TATA-like promoter (pTAL), nuclear factor–kappa B (pNF-κB), and mutant Gli binding site (mGli) luciferase reporter constructs were not significantly inhibited by the addition of 10 µM vitamin D3 for 6 h, whereas reporter activity of a TATA-like promoter–luciferase construct was increased. Thus, the inhibitory effect of vitamin D3 on Gli reporter activity appears to be a genuine effect of Smo-dependent signalling.

Figure 6D shows Gli reporter inhibition by vitamin D3 in the cell lines C3H/10T1/2 and MDA-MB-231 previously used in the mix-and-match and medium transfer experiments. Both showed a marked inhibition in reporter activity after treatment with 10 µM vitamin D3. $Ptch1^{-/-}$ MEFs also responded to vitamin D3. Because these cells have no Ptch1, any artefacts of vitamin D3 by interference with Ptch1 action rather than Smo activity can be excluded.

A consequence of our model in which vitamin D3 or a very similar molecule mediates Ptch1 action on Smo (Figure 6E) is that exogenously added vitamin D3 should overrule any effect of Hh on Ptch1. To confirm this, we stimulated stable Gli-luciferase transfectants (Shh-LIGHT II) overnight with 10 µM vitamin D3 and/or 200 ng/ml Shh. What is apparent from Figure 6F is that in the presence of vitamin D3 reporter activity could not be increased by the addition of Shh, confirming our hypothesis.

Scatchard Analysis Reveals Vitamin D3 Binding to Smo

To assess possible binding of vitamin D3 to Smo, we used a yeast strain *(Pichia pastoris)* transformed with Smo. The expression of Smo could be induced by the addition of methanol to the growth medium (kind gift of Dr. I. Mus-Veteau [27]). We chose this approach for two reasons: first, to our knowledge there is no vitamin D3 receptor in *P. pastoris;* second, baseline (or background) levels of Smo in noninduced *P. pastoris* are negligible.

First we confirmed the successful induction of Smo expression by Western blot using a Smo antibody as shown in Figure 7A. We then set out to perform a Scatchard analysis

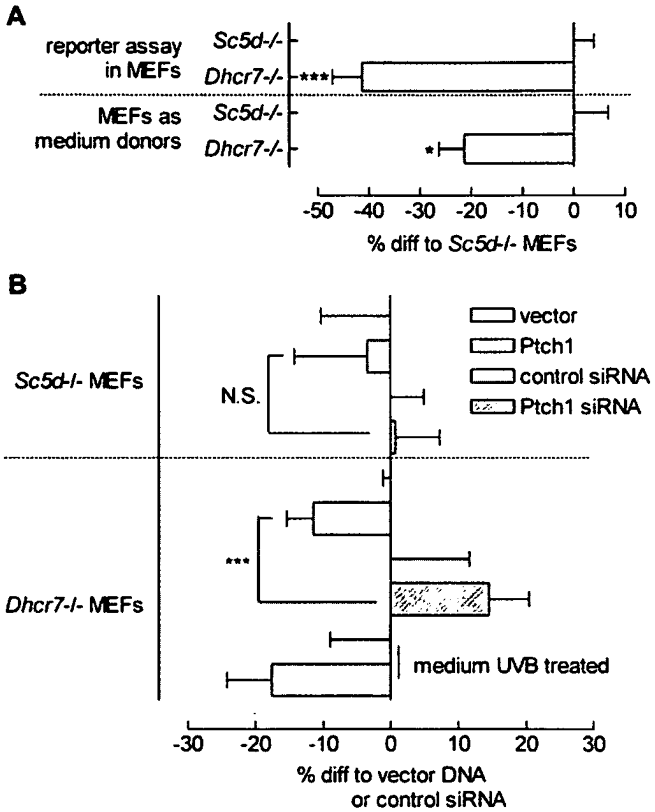

Figure 5. Differentially Modulated Ptch1 Action in $Dhcr7^{-/-}$ and $Sc5d^{-/-}$ MEFs

(A) Basal Gli reporter activity measured in MEFs either deficient for Sc5d or Dhcr7 shows that the stacking of 7-DHC (in the $Dhcr7^{-/-}$ MEFs) lowers Gli activity in the mutant cells compared with lathosterol stacking in the $Sc5d^{-/-}$ MEFs. Transfer of the conditioned media to reporter cells (indicated as "MEFs as medium donors") shows that the inhibitory potential of the $Dhcr7^{-/-}$ MEFs is medium-borne. Media were incubated on donor MEFs for 16 h and transferred to reporter cells for 6 to 8 h. ($n \geq 4$; *, $p < 0.05$; ***, $p < 0.005$).

(B) Medium transfer of Ptch1, Ptch1 siRNA, or control-transfected $Sc5d^{-/-}$ and $Dhcr7^{-/-}$ MEFs shows that cells stacking lathosterol but lacking 7-DHC ($Sc5d^{-/-}$ MEFs) are not able to translate different Ptch1 levels to an inhibitory action on reporter cells. The $Dhcr7^{-/-}$ cells were able to properly convey an inhibitory signal when transfected with Ptch1 or, inversely, show a diminished inhibitory potential upon *Ptch1* siRNA transfection. UVB treatment of Ptch1 transfectant medium (2 h) amplified the inhibitory action. Media incubations and statistics are as in (A).

DOI: 10.1371/journal.pbio.0040232.g005

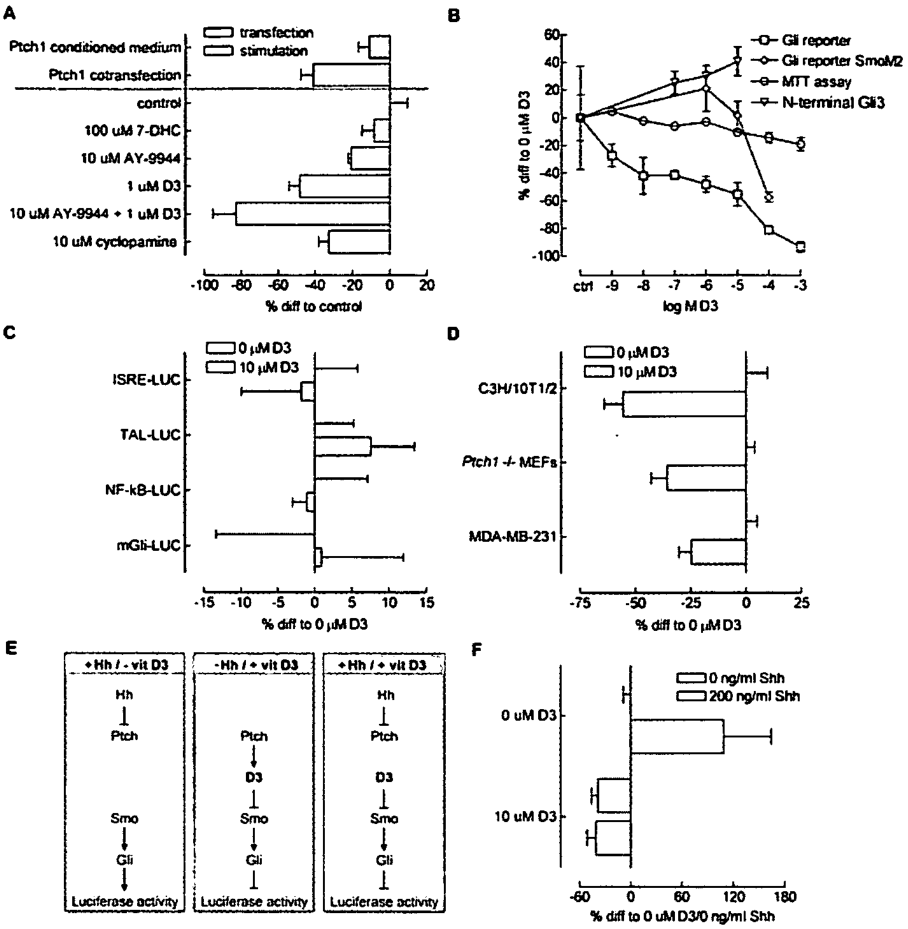

Figure 6. Analysis of Vitamin D3 as a Specific Smo Antagonist

(A) Shown are the Gli reporter inhibitions by 7-DHC, AY-9944, a Dhcr7 inhibitor, vitamin D3, and a combination of the latter two. Also shown is the inhibition that can be conferred by the well-known Smo antagonist cyclopamine and the previously observed effects for Ptch1 transfectant conditioned medium as well as Ptch1 cotransfection (data taken from Figure 4B and Figure 2B, respectively). Cells were stimulated with the various compounds for 6 h (16 h past transfection), except for the cotransfection, which was lysed after 24 h ($n \geq 4$).

(B) A range of concentrations of vitamin D3 was tested for inhibition of Gli reporter activity (also in SmoM2-transfected cells), MTT viability assay, and N-terminal repressor form Gli3 levels. Cells were stimulated with vitamin D3 for 6 h before lysis. For the reporter assays, RLU values were corrected for an internal CMV Renilla standard and expressed as percent difference to control stimulated cells ($n = 4$). The MTT assays shown were raw absorption data expressed as percent difference to control stimulated ($n = 8$); MTT agent was added for 3 h. N-terminal repressor form Gli3 was determined by quantifying ECL signal from Western blot and corrected for β-actin ($n = 3$). Depicted is the mean ± SEM.

(C) Gli specificity of the inhibitory effect of 10 μM vitamin D3 was assayed by using a panel of luciferase reporter constructs, one of which was a mGli reporter (mGli-LUC). Cells were stimulated for 6 h with vitamin D3, and the luciferase activity was assayed; values were calculated from RLU values corrected for an internal CMV Renilla standard and expressed as percent difference to control stimulated cells ($n \geq 4$). Depicted is the mean ± SEM.

(D) Different cell types share the inhibitory response to vitamin D3 on Gli activity. C3H/10T1/2 and MDA-MD-231 cells were used earlier in the mix-and-match and medium transfer experiments. *Ptch1*$^{-/-}$ MEFs served as a control for any possible effects of vitamin D3 on Ptch1 function. Cells were stimulated for 6 h, and the luciferase activity was assayed,; values are RLU values corrected for an internal CMV Renilla standard and expressed as percent difference to control stimulated cells ($n = 4$). Depicted is the mean ± SEM.

(E) Proposed mechanism of vitamin D3 action. First panel: in the presence of Hh, Ptch1 is inactive and does not inhibit Smo. The Hh pathway is active, and Gli activity can be measured in a reporter assay. Second panel: in the absence of Hh, Ptch1 is active and uses vitamin D3 to inhibit Smo. The pathway is inactive, and low Gli activity is measured. Third panel: in the presence of Hh as well as exogenous D3, Smo is inhibited independently of Ptch1, and Hh can no longer elicit a Gli response.

(F) Confluent Shh-LIGHT II stable Gli reporter transfectants were stimulated with 10 μM vitamin D3 and/or 200 ng/ml Shh overnight in the presence of 0.5% FCS. Luciferase activity was assayed; values are RLU values corrected for an internal CMV Renilla standard and expressed as percent difference to control stimulated cells (0 μM vitamin D3; 0 ng/ml Shh). In the presence of vitamin D3, Shh is no longer able to induce reporter activity. $n = 4$; depicted is the mean ± SEM.

DOI: 10.1371/journal.pbio.0040232.g006

[24] with heterologous competition by cyclopamine. Cyclopamine is a ligand for Smo, and this enabled us to distinguish the observed competition from any background by non-specific binding or specific binding to a vitamin D3 receptor (although it is not known to exist in these cells). As can be seen from Figure 7B, [3H]-D3 was not capable of specific binding to non–methanol induced *P. pastoris* (BMGY), whereas after methanol induction (BMMY), specific binding of [3H]-D3 was observed that was subject to competition by cyclopamine. Cyclopamine replaced [3H]-D3 with an apparent dissociation constant K_d of 2 nM in this heterologous assay, a higher affinity than the earlier reported 20-nM affinity of cyclopamine [28]. Nevertheless, these results show that vitamin D3 has the potential to bind Smo at the same site

as cyclopamine, indicating that vitamin D3 is indeed a physiological ligand for Smo.

Vitamin D3 Treatment Mimics the *smo*$^{-/-}$ Phenotype in Zebrafish

To test the action of vitamin D3 in a developmental in vivo model system, we continuously incubated zebrafish embryos starting between 32- and 64-cell stage in 1.2 mg/ml sonicated vitamin D3. We used sonication as described for 7-DHC [29], but did not use a stabilizing reagent. The vitamin D3 treatment phenocopied to a great extent the *slow muscle omitted (smu)* mutant phenotype [30], which has been identified as the zebrafish ortholog of *smo* [31,32].

One of the most striking features of the *smo*$^{-/-}$ phenotype is the U-shaped somites in contrast to the sharply defined chevron (V)-shaped somites of wild-type embryos. The vitamin D3–treated embryos showed these disrupted somites (as indicated by arrow 1 in Figure 8A) at the developmental stages shown. Of the treated animals, approximately 75% ($n =$ 30 embryos in six individual experiments) showed this somite phenotype as well as the typical responses as listed below. Quantification of the somite angle was performed, measuring the angle between the dorsal and ventral portions of the individual somites while positioning the apex of the angle on the horizontal myoseptum (Figure 8B, top panel). In properly shaped somites, this angle was relatively sharp, whereas in vitamin D3–treated embryos, somites were kidney-shaped, displaying a shallow angle (Figure 8B). The ventrally curved body that is characteristic of *smo*$^{-/-}$ zebrafish embryos was also observed upon vitamin D3 treatment. The horizontal myoseptum was malformed (Figure 8A; see also Figure 1B of [32]). Another aspect of the *smo*$^{-/-}$ phenotype is the aberrant extension of the yolk tube, resulting in a shorter and thicker yolk tube; this was also clearly noticeable in the vitamin D3–treated embryos (indicated by arrow 2 in Figure 8A; compare to Figure 1A of [32] and Figure 4 of [31]). Although motoneurons have been described to be missing in *smo*$^{-/-}$ animals [32], we observed no apparent difference in touch response between control and vitamin D3 animals. To our knowledge not previously reported, it appeared that the dorsal midbrain was more prominent in the treated embryos versus controls, resembling the prominent dorsal midbrain in *smo*$^{-/-}$ embryos (indicated by arrow 3 in Figure 8A; compare to Figure 1 of [32] and Figure 4 of [31]). Also, note the similarity of the treated embryo shown at 18 h with regard to a reduced trunk, possibly caused by increased cell death as shown for *smo* mutants (indicated by arrow 4 in Figure 8A; compare to Figure 8B of [33]).

To assess the specificity of vitamin D3 action on the Hh pathway, we used molecular markers specific for Hh pathway activity in zebrafish. The protein Engrailed is a marker for muscle pioneers in normal development, and as development advances, it is also expressed in the cells surrounding the muscle pioneers [34]. In zebrafish embryos with an abrogated Hh signalling, muscle pioneers fail to differentiate and Engrailed is totally absent [31,35–37]. No Engrailed staining of muscle pioneers (indicated by arrow in Figure 8, panel labelled 4D9) or surrounding cells was observed in vitamin D3–treated embryos, suggestive of inhibition of Hh signalling by vitamin D3. In the control-treated animals, staining of muscle pioneers as well as ventrally located cells in the somites was observed. Expression of *ptc1* as determined by in situ hybridisation (ISH) (Figure 8A, *ptc1*) showed a marked reduction of transcript levels in the vitamin D3–treated animals. Because ptc1 is not only the primary receptor for the Hh pathway but also a transcriptional readout of Hh activity [32,37], the attenuated expression seen in the treated animals confirms that vitamin D3 specifically inhibits the Hh pathway. Another marker previously described to be indicative of Hh pathway activity is slow muscle fibre orientation and number in the somites. In *smo*$^{-/-}$ zebrafish, slow muscle fibres are fewer and malformed [30,31]. Shown in Figure 8 (panel marked F59) is the disturbed pattern and number of slow muscle fibres after vitamin D3 treatment, reminiscent of *smo*$^{-/-}$ zebrafish embryos. The use of the abovementioned molecular markers confirms that the effects of vitamin D3 on zebrafish embryo morphology are indeed due to reduced Hh pathway activity.

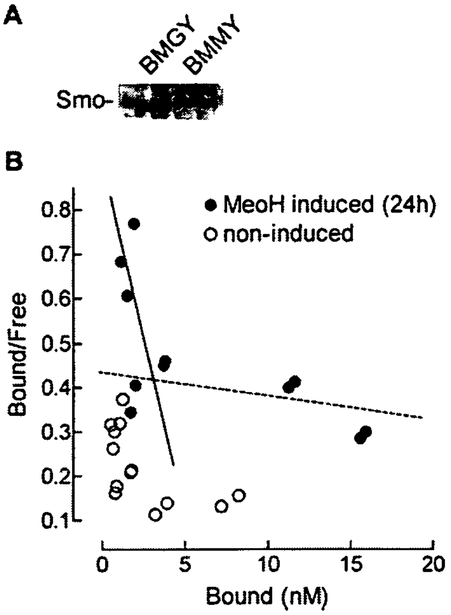

Figure 7. Scatchard Analysis of Vitamin D3 Using Smo-Expressing *P. pastoris*

(A) 24 h methanol induction (buffered methanol-complex medium; BMMY) of Smo-transformed *P. pastoris* yielded successful Smo expression as shown by Western blot analysis with an antibody directed against Smo.

(B) Scatchard analysis of heterologous competition with cyclopamine representing the binding of [3H]-D3 to Smo-expressing (solid circles, MeOH induced) and nonexpressing (open circles, noninduced) yeast strains. The solid line indicates the induced high-affinity binding, whereas the dotted line indicates nonspecific low-affinity binding. Scatchard analysis and fitting was performed as described earlier [53].

DOI: 10.1371/journal.pbio.0040232.g007

At later stages, we observed a subtle cardiac edema, and all treated embryos died after 5 d of vitamin D3 treatment, a feature again similar to the *smo*$^{-/-}$ phenotype (Figure 8C). Although we found the eyes to be relatively ventrally positioned throughout various developmental stages (Figure 8C), no absolute cyclopia was observed. However, cyclopia is not an unambiguous hallmark of the *smo*-deficient phenotype [31–33].

Because nearly all of the typical *smo*$^{-/-}$ phenotypic features were also prominently present in vitamin D3–treated zebrafish embryos and the molecular markers used all pointed to a defective Hh signalling, we conclude that the in vivo action of

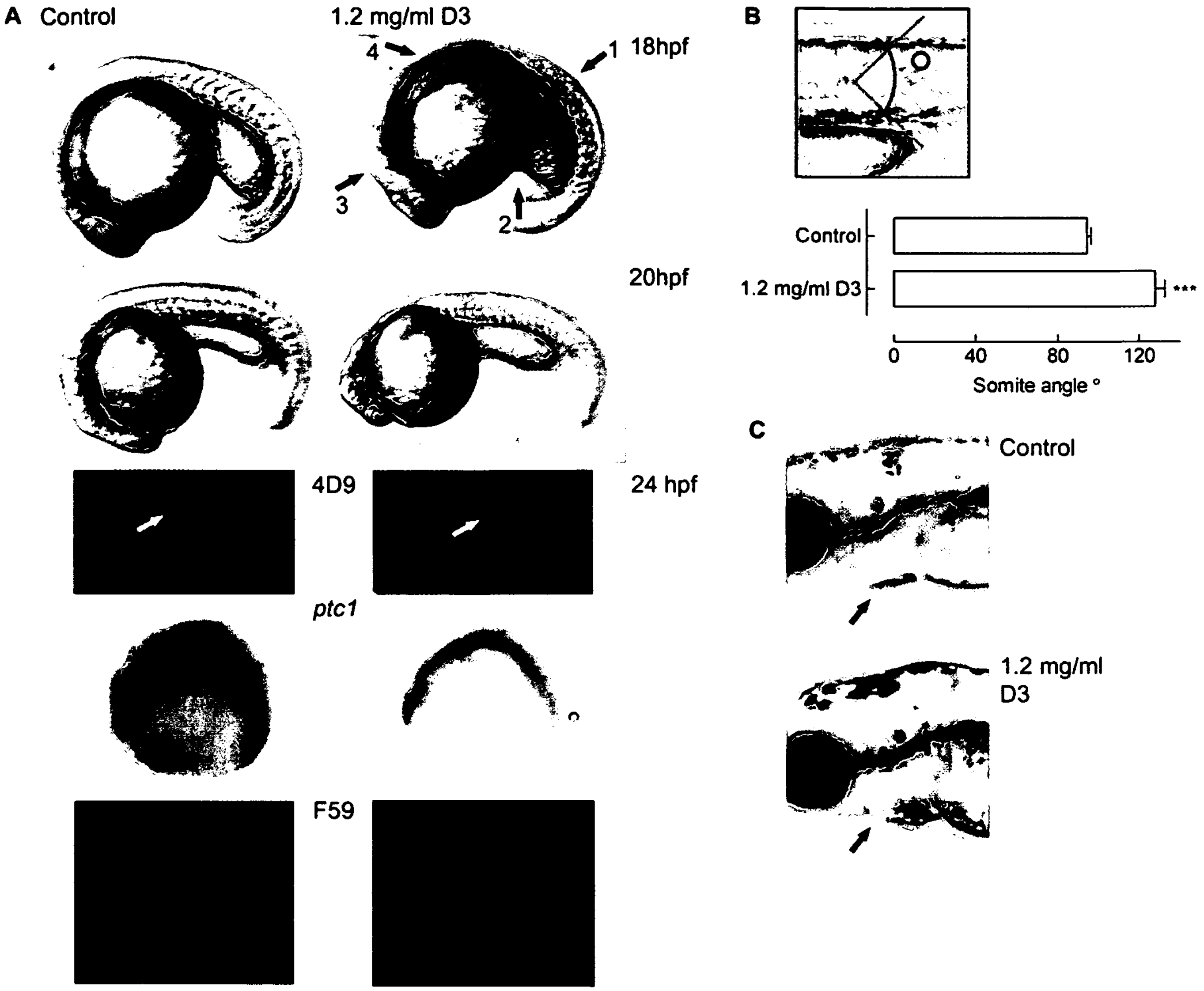

Figure 8. Effects of Vitamin D3 on Developing Zebrafish Embryos

(A) Fertilized zebrafish eggs were dechorionated and placed in buffer containing 1.2 mg/ml sonicated vitamin D3, starting the continuous incubation between the 32- and 64-cell stages. At the different developmental stages (as indicated), the embryos were analysed, revealing persistent somite malformations, a ventrally curved body, poorly developed myoseptum, an aberrant extension of the yolk tube, a prominent dorsal midbrain, and a reduced trunk. The wild-type Engrailed staining (4D9) of muscle pioneers and surrounding cells in control-treated animals was not observed upon vitamin D3 treatment. ISH for *ptc1* mRNA showed a strongly reduced signal in vitamin D3–treated animals compared with controls. Staining with the F59 antibody revealed that slow muscle fibres were disturbed in number and orientation in the treated animals.

(B) At 18 hpf, embryos were photographed in detail and somite angles were determined (as shown in top panel). The measurement was taken of an individual somite between dorsal and ventral portions of the vertical myoseptum for corresponding somites between the wild-type and vitamin D3–treated embryos. Shown are the mean angles (±SEM; $n = 3$) of wild-type control- and vitamin D3–treated embryos.

C) Detail of 4-dpf embryo. Note the slightly enlarged pericardial cavity in vitamin D3–treated animals. The orientation of all images is a lateral view, anterior to the left.

DOI: 10.1371/journal.pbio.0040232.g008

vitamin D3 on embryonic development is due to a specific inhibitory effect on Smo.

Discussion

In the present study, we investigated the molecular mode by which Ptch1 represses Smo activity. By mixing Ptch1-expressing cells with cells expressing Smo and a Gli reporter, we were able to show that Ptch1 is capable of non-cell autonomous repression of Smo. This non-cell autonomous repression is carried by the extracellular medium, because medium conditioned by Ptch1-transfected cells was capable of inhibiting Gli reporter activity as well. Conversely, medium conditioned by cells transfected with Ptch1 siRNA (so lacking endogenous Ptch1 expression) elevated Gli reporter activity significantly above medium that was conditioned by control cells, demonstrating that Ptch1 overexpression is not a prerequisite for observing this cell non-autonomous repression of Smo by Ptch1. Mixing Ptch1-overexpression cells with cells expressing Smo and Gli reporter produced inhibition of Gli reporter activity to approximately the same extent as fusing these cells, showing that this non-cell autonomous repression of Smo by Ptch1 is of roughly similar potency compared to intracellular Smo repression by Ptch1. This result suggests that this intercellular repression constitutes an important physiological mechanism. In this context, it is important to note that Hh quenching was not a major contributing factor in our experimental system, because Hh-neutralising antibodies do not interfere with Ptch1-dependent intercellular repression of Smo and we were not able to detect Hh release by the cells.

Conditioning medium with Ptch1-transfected cells led to the appearance of a 3β-hydroxysteroid in this medium, suggesting that this compound is increasingly translocated into the medium as a consequence of elevated Ptch1 expression. These results are concordant with the observation that Smo antagonists bear structural similarities to steroids [12] and the high homology of Ptch1 to the NPC1 protein, which has cholesterol trafficking and pump functions [10], as well as to various prokaryotic pump proteins. These homologies gave rise to the suggestion that, in the absence of Hh, Ptch1 pumps a compound out of the cell that binds to and inhibits Smo, and the data from this study confirm this model. Transfection of Ptch1 siRNA abolished deposition of this 3β-hydroxysteroid into the medium when compared to control-transfected cells, showing that 3β-hydroxysteroid translocation is not an artefact of Ptch1 overexpression, but that endogenous Ptch1 expression levels are sufficient to sustain detectable 3β-hydroxysteroid translocation. This 3β-hydroxysteroid translocation seems important for the intercellular repression of Smo by Ptch1, because in the presence of 3β-hydroxysteroid synthesis inhibitors Ptch1 was no longer capable of repressing Smo, whereas artificial stimulation of 3β-hydroxysteroid biosynthesis by using mevalonate supplementation enhanced the inhibitory potential of Ptch1 on Smo.

The 3β-hydroxysteroid responsible for intercellular repression of Smo is most likely the (pro-)vitamin D3 (that is, either 7-DHC or its metabolite vitamin D3) or a highly similar molecule. Fibroblasts derived from animals genetically incapable of synthesizing these 3β-hydroxysteroids (*Sc5d*$^{-/-}$) do not sustain intercellular repression of Smo by Ptch1, whereas fibroblasts that have a genetic defect leading to increased (pro-)vitamin D3 production (*Dhcr7*$^{-/-}$) show exaggerated intercellular repression of Smo by Ptch1. Exogenous addition of vitamin D3 was more efficient in inhibiting Gli reporter activity than the established Smo antagonist cyclopamine. SmoM2, which has a reduced sensitivity towards cyclopamine, showed diminished sensitivity to vitamin D3 as well. In Scatchard assays, cyclopamine and vitamin D3 competed for Smo binding, suggesting that both compounds have an identical binding site on Smo. Scatchard analysis using the precursor 7-DHC as a competitor revealed a 10-fold lower affinity for Smo than did vitamin D3 or the hydroxylated (active) form of vitamin D3 (unpublished data). Treatment of *Danio rerio* embryos with vitamin D3 phenocopied most of the aspects of the *smo*$^{-/-}$ phenotype in zebrafish. These findings strongly suggest that Ptch1 translocates either vitamin D3, a related molecule, or possibly a precursor that is subsequently metabolised in the extracellular medium that acts as a Smo antagonist.

Our findings shed light on the puzzling biochemical basis of SLOS, in which accumulation of 7-DHC (Figure 1A) accompanies a reduced cholesterol content and a seemingly decreased Hh signalling [38]. Previously, the SLOS phenotype has been mimicked by using AY-9944 [25], which inhibits 7-DHC reductase (Figure 1A), leading to the accumulation of its substrate. This result suggests that this molecule mediates Hh inhibition. Treatment of patients with a cholesterol-rich diet, however, has been successful, and statin treatment does not seem to alleviate the symptoms, suggesting that the lack of cholesterol is the culprit [38,39]. Others have been able to counteract the effect of 7-DHC stacking in experimental settings by exogenously adding cholesterol [40], confirming that AY-9944 merely inhibits synthesis of cholesterol needed for proper Hh processing. Although these findings seem to preclude the stacking of a specific metabolite to be responsible for the SLOS phenotype, it has become clear that the clinical phenotype correlates best with the ratio of 7-DHC to cholesterol levels in patient plasma rather than the levels of cholesterol alone. Also, the treatment of infants with cholesterol is arguably too late an intervention, because most of the Hh patterning events are completed in utero. Our experiments show that even in the absence of AY-9944, addition of vitamin D3 strongly inhibits Hh signalling. This inhibition is stronger than Ptch1 cotransfection and Ptch1-transfectant conditioned medium, and we therefore conclude that the stacking of 7-DHC is responsible for the SLOS phenotype.

Very relevant to this manuscript and the abovementioned studies are the findings of Cooper et al., who found that reduced sterol levels impair a cell's responsiveness to Hh [8]. By using fibroblasts from mice genetically deficient for the enzymes involved in lathosterolosis (Sc5d) and SLOS (Dhcr7) and by depleting lipids and sterols from the medium, they showed that sterol levels were crucial to a cell's responsiveness to Hh. By analyzing the Hh protein in these cells under the various conditions, they could demonstrate proper Hh maturation, thereby excluding improper Hh sterolation as the cause of SLOS. They did not, however, hypothesize an inhibitory role for excess cholesterol precursors. We explain our hypothesis and findings in light of their results: by genetic and/or medium condition causes, steroid synthesis is seriously impaired in cells in their experiments. As a result, 7-DHC levels will drop, leaving Ptch1 devoid of substrate. Without substrate to pump or translocate, Ptch1 is "paralysed", and addition of Hh will not exert an effect, explaining the reduced responsiveness. Hh responsiveness does not equal pathway activity, and the absence of Ptch1 substrate will diminish responsiveness but not pathway activity. Because both cell lines share the inability to properly synthesize cholesterol, and because we find a differential inhibitory potential on Smo, we conclude that sterol content alone cannot account for Ptch1-mediated Smo inhibition, and we suggest that the effects found by other groups take place elsewhere in the Hh signalling pathway. In our system, LDL seems to be a prerequisite for the diffusion of the inhibitory molecule, and, recently, a similar requirement has also been found for the distribution of Hh itself [41].

Although the present study clearly demonstrates that Ptch1 can inhibit Smo in an intercellular fashion, we have not addressed whether such intercellular action of Ptch1 on Smo is relevant for Hh action in vivo. Vitamin D3 is highly hydrophobic and is not expected to diffuse very far in the aqueous environment that surrounds cells. We observed that in the absence of LDL as a carrier for the hydrophobic Smo inhibitor, intercellular repression of Smo activity was undetectable. Hence, although Ptch1 exports (pro-)vitamin D3, it might act on Smo on the same cell (and thus function cell autonomously) or, depending on the cell's surroundings, on Smo on adjacent cells (and thus function non-cell autonomously). Nevertheless, the expression of Ptch1 and Smo is often discordant, with Ptch1 expression being in the vicinity of Smo-expressing cells, without complete colocalisation [42,43]. We observed that in cardiac nerve branch ganglia, Smo and Ptch1 colocalise in the bronchial cartilage and epithelium, but not in the ganglion itself. In the ganglion, a pronounced staining for Ptch1 can be seen, whereas Smo staining is observed in only the adjacent cells. These findings are suggestive for intercellular signalling actually occurring in vivo (MF Bijlsma, unpublished data). In contrast with these findings are earlier reported experiments by Briscoe et al. [44] in which a Hh uninhabitable form of Ptch1 (Ptch1$^{\Delta loop2}$) was evaluated with respect to its effects on Hh signalling in *Drosophila melanogaster* and *Gallus gallus* embryogenesis. The results obtained in this study suggest that the border of Ptch1$^{\Delta loop2}$ expression more or less corresponds with the boundary of Hh-induced gene expression. Thus, it would appear that in these experimental systems, a Smo-inhibitory, vitamin D3–like ligand has not much capacity to diffuse over multiple cell layers. We therefore suggest that the action of Ptch1 can be cell autonomous or non–cell autonomous in various in vivo situations, perhaps dependent on the presence or absence of molecules that can carry the hydrophobic ligand over larger distances and subsequently present this molecule to Smo.

Recently it was demonstrated that Hh-bound Ptch1 could titrate the inhibitory action of the abovementioned Ptch1$^{\Delta loop2}$. Furthermore, Hh-bound Ptch1 allowed Smo signalling to occur even in the presence of a Ptch1 form that is incapable of binding Hh [45]. This observation is inconsistent with a model in which Ptch1 serves to translocate a Smo-inhibitory molecule out of the cell, because in this model, Ptch1 action would depend on the amount of unliganded Ptch1, not the amount of liganded Ptch1. Casali and Struhl provide as a possible explanation for the titration effect that liganded and unliganded Ptch1 compete for access to Smo: Ptch1 acts as a multimer in which binding of Hh to any of the subunits blocks the action of the complex, or liganded and unliganded Ptch1 exert counteracting catalytic activities. Only the latter explanation seems consistent with the data presented in this study; the other explanation requires Ptch1 to function in a cell-autonomous fashion. Hence, it is possible that unliganded Ptch1 translocates a Smo inhibitor to extracellular medium, whereas Hh-bound Ptch1 would transport this inhibitor to the cytosol. Alternatively, Hh-bound Ptch1 is internalized, and it is possible that in this process it cointernalizes the Ptch1$^{\Delta loop2}$ protein, especially if both proteins would localize to the same plasma membrane compartment—for example, lipid rafts. Support for this notion might be deduced from the strong Hh-dependent endocytosis we observed in the present study, suggesting that endocytosis is indeed a major cellular response to Hh binding to Ptch1. But further studies are needed to address the exact mode by which wild-type Ptch1 impairs Ptch1$^{\Delta loop2}$ function.

Activation of the Hh pathway is, under certain conditions, associated with the development of cancer, especially in the upper digestive tract [46,47] and in basal cell carcinoma in the skin, where this disease is linked to mutations in Ptch1 [48–51]. Intercellular action of Ptch1 will allow this molecule to exert its action as a tumour suppressor, on not only the Ptch1-expressing cell but also neighbouring cells that may have acquired inactivating mutations of Ptch1, making this mode of Ptch1-dependent Smo inhibition especially attractive with respect to tumour suppression. Thus, it will be interesting to investigate whether intercellular repression of Smo by Ptch1 actually contributes to tumour suppression in vivo. Experiments addressing this possibility are currently in progress.

Materials and Methods

Constructs/siRNA used. Mouse Ptch1 (a generous gift of Dr. M. P. Scott) was cloned into the pcDNA 3.1(–) vector (Invitrogen, Carlsbad, California, United States). Human SMO (referred to as Smo) cDNA (Image Consortium/RZPD, Berlin, Germany) was cloned into the pcDNA 3.1(+) vector. The Gli1 cDNA is in pcDNA1 (a generous gift of Dr. A. Ruiz i Altaba). The Gli-reporter δ51-LucII was kindly provided by Dr. H. Sasaki, as was the mutant binding site variant (mGli). The NF-κB, ISRE, and TAL luciferase constructs were from Clontech Laboratories (Mountain View, California, United States). The internal control cytomegalovirus (CMV) promoter-driven Renilla luciferase vector was from Promega (Madison, Wisconsin, United States). SmoM2 in pRK7 was obtained from Genentech (South San Francisco, California, United States). The Ptch1 (#63908) and scrambled control siRNA were from Ambion (Austin, Texas, United States).

Western blotting. Transfected cells were lysed in Laemmli buffer and brought onto SDS-PAGE gels. After electrophoresis, protein was transferred onto Immobilon-PVDF membranes (Millipore, Billerica, Massachusetts, United States). Membranes were blocked in 5% bovine serum albumin (BSA) (Sigma-Aldrich, St Louis, Missouri, United States) in TBS/0.1% Tween-20 (TBST) for 1 h. Goat polyclonal α-Ptch1 antibody G-19, α-Smo C-17, α-Gli3 N-terminal N-19, α-Shh N-19, or α-Ihh I-19 (Santa Cruz Biotechnology, Santa Cruz, California, United States) were diluted to 1:500 in 3% BSA in TBST, and membranes were incubated overnight. Goat polyclonal α-actin I-19 (Santa Cruz Biotechnology) was diluted to 1:1000 in 3% BSA in TBST. After 1 h incubation in 1:1000 α-goat HRP-conjugated secondary antibody (DakoCytomation, Glostrup, Denmark), blots were imaged using LumiLight Plus enhanced chemiluminescence substrate (ECL) (Roche, Basel, Switzerland) on a GeneGnome chemiluminescence imager (Syngene, Cambridge, United Kingdom).

Mix-and-match procedure. Mouse mesenchymal fibroblasts (C3H/10T1/2 from American Type Culture Collection CCL-226, Manassas, Virginia, United States) were grown in Dulbecco's Modified Eagle Medium (DMEM) (Cambrex, East Rutherford, New Jersey, United States) containing 10% fetal calf serum (FCS) (Cambrex). Human MDA-MB-231 breast carcinoma cells (American Type Culture Collection HTB-26) were grown in L-15 Leibovitz medium (Cambrex) with 10% FCS. Cells were grown to approximately 70% and transfected with either Ptch1 or Smo and the Gli luciferase reporter in combination with a CMV-Renilla luciferase internal standard using Effectene (Qiagen, Hilden, Germany) according to routine procedures. Ptch1 and scrambled control siRNA were transfected using RNAiFect (Qiagen) following the supplied protocol. Transfected cells were treated with o-methylated 20 μM zVADfmk (Sigma-Aldrich) to neutralize the apoptotic effects of Ptch1. After 16 h, cells were washed three times with phosphate buffered saline (PBS), detached by 2 mM EDTA (Sigma-Aldrich) in PBS, resuspended in DMEM with 10% FCS, and pipetted three times through a 40-μm cell strainer (BD Biosciences, San Jose, California, United States) into a tube to allow a homogenous mixture. Equal volumes of reporter and donor cells were mixed thoroughly and subsequently transferred to 24-well plates. After 6 h (4 + 2 h for the fusion protocol), cells were lysed with passive lysis buffer as provided by Promega, and luciferase activity was assayed according to the Promega Dual-Glo Luciferase Assay System (Promega) protocol on a Lumat Berthold LB 9501 Luminometer (Berthold Technologies, Bad Wildbad, Germany). Each firefly luciferase value was corrected for its cotransfected CMV-driven Renilla luciferase standard to correct for transfection efficiency or dilution effects. Recombinant N-terminal Shh was obtained from R&D Systems (Minneapolis, Minnesota, United States) and dissolved in PBS with 0.1% BSA. The 5E1 Shh-blocking antibody was from the Developmental Hybridoma Bank (Iowa City, Iowa, United States).

Fluorescent tracking of cells. Cells were grown to approximately 70% confluence in DMEM containing 10% FCS and washed with PBS to remove serum. CellTracker Green CMFDA or Orange CMTMR (Molecular Probes, Eugene, Oregon, United States) were diluted to 5 µM in serum-free DMEM and added to cells for 45 min, the medium was aspirated, and fresh medium containing 10% FCS was added. Cells were detached and mixed as described above. After 16 h, cells were fixed in 3.7% formaldehyde overnight or mixed as described above and subsequently fixed. For fluorescent staining of nuclei, cells were washed with PBS/0.1% Triton X-100 (PBST) and incubated in 200 ng/ml DAPI (Roche) in PBST for 1 h. Before microscopy, cells on cover slips were washed briefly in PBS, placed upside-down on another cover slip if imaged on a Leica TCS SP II confocal laser scanning microscope (Leica Microsystems, Wetzlar, Germany), or placed on an object glass when imaged on a Zeiss Axioskop (Carl Zeiss, Oberkochen, Germany).

Cell fusion. After fluorescent labelling (1 h) or transfection (16 h), cells were mixed, medium was aspirated, and cells were washed with PBS. Prewarmed PEG 1500/HEPES (pH 7.4) 50% (Roche) was added to the cells for 90 s, after which the cells were washed three times with PBS. Fresh medium was added, and after 2 h, cells were either lysed with passive lysis buffer and assayed for luciferase activity or fixed for microscopy after 8 h.

Medium transfer experiments. Donor and reporter cells were transfected for 16 h, after which the donor cells were washed extensively to wash out any remaining transfection complexes and supplied with fresh medium for 6 h. Medium was transferred to reporter cells for 6 to 8 h, after which cells were lysed and assayed for luciferase activity (according to manufacturer's protocol). The mutant MEFs were grown in complete DMEM supplemented with 15% FCS and nonessential amino acids (Sigma).

CHOD-PAP–coupled FPLC. Steroid levels in the main lipoprotein classes (VLDL, LDL, and HDL) were determined using high-performance gel filtration chromatography. The system contained a PU-980 ternary pump with an LG-980-02 linear degasser, FP-920 fluorescence, and UV-975 UV/VIS detectors (Jasco, Tokyo, Japan). An extra P-50 pump (Pharmacia Biotech, Uppsala, Sweden) was used for in-line CHOD-PAP enzymatic reagent (Biomerieux, Marcy l'Etoile, France) addition at 0.1 ml/min. 60 µl from each sample was subjected to size-exclusion chromatography to determine whether there is a relationship between Ptch1 expression and medium 3β-hydroxysteroid levels using a Superose 6 HR 10/30 (Pharmacia Biotech) column with Tris-buffered saline (TBS) (pH 7.4) at a flow rate of 0.31 ml/min with in-line fluorescence and UV detection on the Jasco system with CHOD-PAP assay described above. Commercially available lipid plasma standards were used for total cholesterol pattern analysis (SKZL, Nijmegen, Netherlands).

Endocytosis assay. Cells on 24-well plates were grown to 70% confluence and treated with no or 1 mM pravastatin for 6 h. Subsequently, 200 nCi of [3H]-labelled sucrose (Amersham Pharmacia Biotech, Freiburg, Germany) was added per well. Cells were stimulated with either 1 µg/ml Shh or solvent control (0.1% BSA/PBS) for 1 h. After washing, cells were lysed in 1% Nonidet P-40 and the lysate was transferred to 4 ml of scintillation fluid and activity was determined on a Packard Tri-Carb scintillation counter (PerkinElmer, Wellesley, Massachusetts, United States). Values were corrected for solvent control treated cells on ice.

Stimulation experiments. Cells transfected with the Gli-luciferase reporter were stimulated for the indicated times and concentrations with the following: cyclopamine (Biomol, Plymouth Meeting, Pennsylvania, United States), AY-9944 (Calbiochem, San Diego, California, United States), vitamin D3, or 7-DHC (Sigma).

MTT assay. Cells were seeded in flat-bottom 96-well plates and treated with the indicated concentrations of vitamin D3 for 6 h. During the last 3 h, 0.5 mg/ml thiazolyl blue tetrazolium bromide (MTT) was added. After incubation, supernatant was discarded, cells were lysed in 50 µl of 40 mM HCl in isopropanol, and absorbance was measured at 570 nm in a Benchmark Plus Microplate Spectrophotometer (Bio-Rad, Hercules, California, United States).

***P. pastoris* culture.** The Smo-transformed *P. pastoris* strain was a kind gift from Dr. I. Mus-Veteau. Culture of yeast and induction of Smo expression was performed as described [27].

Scatchard analysis. Scatchard analysis was performed on intact cells as described earlier for [52,53]. After 24 h growth in methanol- or glycerol-complex medium, *P. pastoris* strains were washed with PBS and diluted to the same OD_{600}. Subsequently, aliquots of cells were labelled for 1.5 h at 4 °C in PBS containing 1.66 nM of [3H]-labelled vitamin D3 (Amersham Pharmacia Biotech) and eight different concentrations of unlabelled cyclopamine, 7-DHC, vitamin D3, or hydroxylated vitamin D3 (Sigma-Aldrich). The reaction was stopped by washing four times with ice-cold PBS. The bound radioactivity was determined by transferring the washed pellets to 4 ml of scintillation fluid, and activity was determined on a Packard Tri-Carb scintillation counter (PerkinElmer). In each experiment, each condition was performed in duplicate. In general, Scatchard plots on intact cells show considerable nonspecific low-affinity binding of [3H]-vitamin D3. Therefore, Scatchard plots were fitted according to a one- or two-site model, as appropriate. The observed points of noninduced yeast were a satisfactory fit with a one-site (low affinity) model, whereas two affinity sites could be distinguished in the induced *P. pastoris.*

Animals. Wild-type zebrafish *(D. rerio)* were kept and bred according to standard protocols. 1- to 1.5-h post fertilisation (hpf) embryos were dechorionated following 2 mg/ml pronase treatment for 1 min followed by extensive rinsing. 1.2 mg/ml vitamin D3 was added to HEPES buffered Ringer's solution and sonicated on ice for 3 min; control buffer was also sonicated. Suspension temperatures were equilibrated and added to the embryos.

ISH and immunofluorescence. After treatment, embryos were fixed in 4% paraformaldehyde/PBS, and ISH was carried out as described [54] using a *ptc1* probe synthesized according to [55]. The 4D9 and F59 antibodies were obtained from the Developmental Hybridoma Bank and used as previously described [56].

Supporting Information

Accession Numbers

The Entrez Protein (http://www.pubmedexpress.nih.gov/entrez/query.fcgi?db=Protein) accession numbers for the genes and gene products discussed in this paper are Gli1 (BAA85004), NPC1 (AAB63373), Ptch1 (NP_032983), and Smo (AAH48091).

Acknowledgments

We thank Dr. Sander Diks for advice concerning cell transfection, and Dr. Leon Tertoolen for advice on cell fusion. We are indebted to Drs. H. Sasaki and A. Ruiz i Altaba for their kind provision of constructs. Dr. F. D. Porter kindly provided the *Dhcr7*$^{-/-}$ and *Sc5d*$^{-/-}$ MEFs. We are especially grateful to Dr. Matthew Scott for his generous donation of the *Ptch1* construct as well as the *Ptch1* knockout and wild-type MEFs. The *P. pastoris* strain was a kind gift from Dr. I. Mus-Veteau.

Author contributions. MFB, CAS, and MPP conceived and designed the experiments. MFB, CAS, DZ, SvdW, FR, and MPP performed the experiments and analyzed the data. MFB, CAS, and MPP wrote the paper.

Competing interests. The authors have declared that no competing interests exist.

Funding. This work was supported by the STW Technology Foundation.

References

1. Bijlsma MF, Spek CA, Peppelenbosch MP (2004) Hedgehog: An unusual signal transducer. Bioessays 26: 387–394.
2. Ingham PW, Taylor AM, Nakano Y (1991) Role of the Drosophila patched gene in positional signalling. Nature 353: 184–187.
3. Marigo V, Davey RA, Zuo Y, Cunningham JM, Tabin CJ (1996) Biochemical evidence that patched is the Hedgehog receptor. Nature 384: 176–179.
4. van den Heuvel M, Ingham PW (1996) smoothened encodes a receptor-like serpentine protein required for hedgehog signalling. Nature 382: 547–551.
5. Denef N, Neubuser D, Perez L, Cohen SM (2000) Hedgehog induces opposite changes in turnover and subcellular localization of patched and smoothened. Cell 102: 521–531.
6. Incardona JP, Gruenberg J, Roelink H (2002) Sonic hedgehog induces the segregation of patched and smoothened in endosomes. Curr Biol 12: 983–995.
7. Hooper JE, Scott MP (2005) Communicating with Hedgehogs. Nat Rev Mol Cell Biol 6: 306–317.
8. Cooper MK, Wassif CA, Krakowiak PA, Taipale J, Gong R, et al. (2003) A defective response to Hedgehog signaling in disorders of cholesterol biosynthesis. Nat Genet 33: 508–513.
9. Taipale J, Cooper MK, Maiti T, Beachy PA (2002) Patched acts catalytically to suppress the activity of Smoothened. Nature 418: 892–897.
10. Davies JP, Chen FW, Ioannou YA (2000) Transmembrane molecular pump activity of Niemann-Pick C1 protein. Science 290: 2295–2298.
11. Taipale J, Chen JK, Cooper MK, Wang B, Mann RK, et al. (2000) Effects of oncogenic mutations in Smoothened and Patched can be reversed by cyclopamine. Nature 406: 1005–1009.

12. Incardona JP, Gaffield W, Kapur RP, Roelink H (1998) The teratogenic Veratrum alkaloid cyclopamine inhibits sonic hedgehog signal transduction. Development 125: 3553–3562.
13. Frank-Kamenetsky M, Zhang XM, Bottega S, Guicherit O, Wichterle H, et al. (2002) Small-molecule modulators of Hedgehog signaling: Identification and characterization of Smoothened agonists and antagonists. J Biol 1: 10.
14. van den Brink GR, Bleuming SA, Hardwick JC, Schepman BL, Offerhaus GJ, et al. (2004) Indian Hedgehog is an antagonist of Wnt signaling in colonic epithelial cell differentiation. Nat Genet 36: 277–282.
15. Sasaki H, Nishizaki Y, Hui C, Nakafuku M, Kondoh H (1999) Regulation of Gli2 and Gli3 activities by an amino-terminal repression domain: Implication of Gli2 and Gli3 as primary mediators of Shh signaling. Development 126: 3915–3924.
16. Thibert C, Teillet MA, Lapointe F, Mazelin L, Le Douarin NM, et al. (2003) Inhibition of neuroepithelial patched-induced apoptosis by sonic hedgehog. Science 301: 843–846.
17. Xie J, Murone M, Luoh SM, Ryan A, Gu Q, et al. (1998) Activating Smoothened mutations in sporadic basal-cell carcinoma. Nature 391: 90–92.
18. Murone M, Rosenthal A, de Sauvage FJ (1999) Sonic hedgehog signaling by the patched-smoothened receptor complex. Curr Biol 9: 76–84.
19. Ericson J, Morton S, Kawakami A, Roelink H, Jessell TM (1996) Two critical periods of Sonic Hedgehog signaling required for the specification of motor neuron identity. Cell 87: 661–673.
20. Wu X, Walker J, Zhang J, Ding S, Schultz PG (2004) Purmorphamine induces osteogenesis by activation of the hedgehog signaling pathway. Chem Biol 11: 1229–1238.
21. Shea CM, Edgar CM, Einhorn TA, Gerstenfeld LC (2003) BMP treatment of C3H10T1/2 mesenchymal stem cells induces both chondrogenesis and osteogenesis. J Cell Biochem 90: 1112–1127.
22. Pepinsky RB, Zeng C, Wen D, Rayhorn P, Baker DP, et al. (1998) Identification of a palmitic acid-modified form of human Sonic hedgehog. J Biol Chem 273: 14037–14045.
23. Goodrich LV, Milenkovic L, Higgins KM, Scott MP (1997) Altered neural cell fates and medulloblastoma in mouse patched mutants. Science 277: 1109–1113.
24. Peppelenbosch MP, DeSmedt M, ten Hove T, van Deventer SJ, Grooten J (1999) Lipopolysaccharide regulates macrophage fluid phase pinocytosis via CD14-dependent and CD14-independent pathways. Blood 93: 4011–4018.
25. Repetto M, Maziere JC, Citadelle D, Dupuis R, Meier M, et al. (1990) Teratogenic effect of the cholesterol synthesis inhibitor AY 9944 on rat embryos in vitro. Teratology 42: 611–618.
26. Ruiz i Altaba A (1999) Gli proteins encode context-dependent positive and negative functions: Implications for development and disease. Development 126: 3205–3216.
27. De Rivoyre M, Bonino F, Ruel L, Bidet M, Therond P, et al. (2005) Human receptor Smoothened, a mediator of Hedgehog signalling, expressed in its native conformation in yeast. FEBS Lett 579: 1529–1533.
28. Chen JK, Taipale J, Cooper MK, Beachy PA (2002) Inhibition of Hedgehog signaling by direct binding of cyclopamine to Smoothened. Genes Dev 16: 2743–2748.
29. Gaoua W, Chevy F, Roux C, Wolf C (1999) Oxidized derivatives of 7-dehydrocholesterol induce growth retardation in cultured rat embryos: A model for antenatal growth retardation in the Smith-Lemli-Opitz syndrome. J Lipid Res 40: 456–463.
30. Barresi MJ, Stickney HL, Devoto SH (2000) The zebrafish slow-muscle-omitted gene product is required for Hedgehog signal transduction and the development of slow muscle identity. Development 127: 2189–2199.
31. Corbit KC, Aanstad P, Singla V, Norman AR, Stainier DY, et al. (2005) Vertebrate Smoothened functions at the primary cilium. Nature 437: 1018–1021.
32. Varga ZM, Amores A, Lewis KE, Yan YL, Postlethwait JH, et al. (2001) Zebrafish smoothened functions in ventral neural tube specification and axon tract formation. Development 128: 3497–3509.
33. Chen W, Burgess S, Hopkins N (2001) Analysis of the zebrafish smoothened mutant reveals conserved and divergent functions of hedgehog activity. Development 128: 2385–2396.
34. Hatta K, Bremiller R, Westerfield M, Kimmel CB (1991) Diversity of expression of engrailed-like antigens in zebrafish. Development 112: 821–832.
35. Wilbanks AM, Fralish GB, Kirby ML, Barak LS, Li YX, et al. (2004) Beta-arrestin 2 regulates zebrafish development through the hedgehog signaling pathway. Science 306: 2264–2267.
36. Wolff C, Roy S, Ingham PW (2003) Multiple muscle cell identities induced by distinct levels and timing of hedgehog activity in the zebrafish embryo. Curr Biol 13: 1169–1181.
37. Woods IG, Talbot WS (2005) The *you* gene encodes an EGF-CUB protein essential for Hedgehog signaling in zebrafish. PLoS Biol 3: e66. DOI: 10.1371/journal.pbio.0030066
38. Waterham HR (2002) Inherited disorders of cholesterol biosynthesis. Clin Genet 61: 393–403.
39. Kelley RI, Herman GE (2001) Inborn errors of sterol biosynthesis. Annu Rev Genomics Hum Genet 2: 299–341.
40. Gaoua W, Wolf C, Chevy F, Ilien F, Roux C (2000) Cholesterol deficit but not accumulation of aberrant sterols is the major cause of the teratogenic activity in the Smith-Lemli-Opitz syndrome animal model. J Lipid Res 41: 637–646.
41. Panakova D, Sprong H, Marois E, Thiele C, Eaton S (2005) Lipoprotein particles are required for Hedgehog and Wingless signalling. Nature 435: 58–65.
42. Sacedon R, Varas A, Hernandez-Lopez C, Gutierrez-deFrias C, Crompton T, et al. (2003) Expression of hedgehog proteins in the human thymus. J Histochem Cytochem 51: 1557–1566.
43. Koebernick K, Hollemann T, Pieler T (2001) Molecular cloning and expression analysis of the Hedgehog receptors XPtc1 and XSmo in *Xenopus laevis*. Mech Dev 100: 303–308.
44. Briscoe J, Chen Y, Jessell TM, Struhl G (2001) A hedgehog-insensitive form of patched provides evidence for direct long-range morphogen activity of sonic hedgehog in the neural tube. Mol Cell 7: 1279–1291.
45. Casali A, Struhl G (2004) Reading the Hedgehog morphogen gradient by measuring the ratio of bound to unbound Patched protein. Nature 431: 76–80.
46. Thayer SP, di Magliano MP, Heiser PW, Nielsen CM, Roberts DJ, et al. (2003) Hedgehog is an early and late mediator of pancreatic cancer tumorigenesis. Nature 425: 851–856.
47. Berman DM, Karhadkar SS, Maitra A, Montes De Oca R, Gerstenblith MR, et al. (2003) Widespread requirement for Hedgehog ligand stimulation in growth of digestive tract tumours. Nature 425: 846–851.
48. Fan H, Oro AE, Scott MP, Khavari PA (1997) Induction of basal cell carcinoma features in transgenic human skin expressing Sonic Hedgehog. Nat Med 3: 788–792.
49. Oro AE, Higgins KM, Hu Z, Bonifas JM, Epstein EH Jr., et al. (1997) Basal cell carcinomas in mice overexpressing sonic hedgehog. Science 276: 817–821.
50. Gailani MR, Stahle-Backdahl M, Leffell DJ, Glynn M, Zaphiropoulos PG, et al. (1996) The role of the human homologue of Drosophila patched in sporadic basal cell carcinomas. Nat Genet 14: 78–81.
51. Johnson RL, Rothman AL, Xie J, Goodrich LV, Bare JW, et al. (1996) Human homolog of patched, a candidate gene for the basal cell nevus syndrome. Science 272: 1668–1671.
52. Bloemers SM, Verheule S, Peppelenbosch MP, Smit MJ, Tertoolen LG, et al. (1998) Sensitization of the histamine H1 receptor by increased ligand affinity. J Biol Chem 273: 2249–2255.
53. Pynaert G, Grooten J, van Deventer SJ, Peppelenbosch MP (1999) Cysteinyl leukotrienes mediate histamine hypersensitivity ex vivo by increasing histamine receptor numbers. Mol Med 5: 685–692.
54. Thisse C, Thisse B, Schilling TF, Postlethwait JH (1993) Structure of the zebrafish snail1 gene and its expression in wild-type, spadetail and no tail mutant embryos. Development 119: 1203–1215.
55. Concordet JP, Lewis KE, Moore JW, Goodrich LV, Johnson RL, et al. (1996) Spatial regulation of a zebrafish patched homologue reflects the roles of sonic hedgehog and protein kinase A in neural tube and somite patterning. Development 122: 2835–2846.
56. Bader D, Masaki T, Fischman DA (1982) Immunochemical analysis of myosin heavy chain during avian myogenesis in vivo and in vitro. J Cell Biol 95: 763–770.